Title
Elucidating the Effects on Proteome Regulation under Caloric Restriction

Author
Palacios, Hector Hugo

Publication Date
2020

Peer reviewed|Thesis/dissertation

Elucidating the Effects on Proteome Regulation under Caloric Restriction

By

Hector H Palacios

A dissertation submitted in partial satisfaction of the

requirements for the degree of

Doctor of Philosophy

in

Metabolic Biology

in the

Graduate Division

of the

University of California, Berkeley

Committee in charge:

Professor Marc K. Hellerstein, Chair
Professor Hei Sook Sul
Professor Nicholas Ingolia

Fall 2020

Abstract

Elucidating the Effects of Proteome Regulation Under Caloric Restriction

by

Hector H Palacios

Doctor of Philosophy in Metabolic Biology

University of California, Berkeley

Professor Marc K. Hellerstein, Chair

Cellular energy homeostasis contributes to normal cell growth, functioning as a biological checkpoint of life. There have been numerous genes and metabolic pathways known to regulate the energy status of the cell, and how they contribute to cellular maintenance is of great interest; Caloric Restriction (CR) takes advantage of these metabolic pathways, retarding the aging process by slowing down the metabolic rate. However, despite the many studies on cellular energy homeostasis, much work still needs to be done.

Many of the applications of CR in various organisms have established life-extending benefits by regulating age-related diseases through convergent mechanisms. In fact, a number of signaling pathways, as well as master regulator proteins, act through these mechanisms to interact and regulate protein expressions. CR, as well as other lifespan extending interventions such as rapamycin treatment and inhibition of insulin growth factors, are subject to translational regulation. Increased caloric intake and obesity related comorbidities, in turn, can also work through these pathways to induce translation and cause disease, indicating the role of protein synthesis in health and disease is of great importance.

Stable isotope-labeling proteomics are a powerful strategy that enable the assessment of proteome-wide dynamic fluxes in energy regulating biological interventions such as CR and mimetics. Using mass spectrometric (MS) strategies has afforded scientists a never before seen understanding of how proteome dynamics stand at the center of phenotype, physiologic adaptation, and disease pathogenesis. Through this approach, researches have been able to measure protein synthesis and turnover rates, both for targeted proteins an unbiased screening.

In this dissertation, I present a thorough review of our current understanding of metabolic pathways in the context of lifespan extension interventions like CR. I also discuss the underlying principles for measuring protein dynamics, focusing on metabolic labeling with $^{2}H_2O$ (heavy water) combined with tandem MS analysis of mass isotopomer abundances. Next, I demonstrate its application in four separate studies. First, I use $^{2}H_2O$ labeling in CR mice in a time-course to identify whether the

protein turnover rate slowdown occurs immediately, gradually, or within a discreate time period. Next, I explore separately whether two potential CR mimetics, exercise and metformin administration, are able to slow down the fractional synthesis rate of proteins in a manner comparable to CR. Finally, I discuss a potential CR modulator in Nitric Oxide, a short-lived bioactive molecule known to be induced under CR conditions and reduced during aging and disease. Overall, the work reported in this dissertation demonstrates how global proteome dynamics require NO for proper regulation, CR mimetics influence the proteome in similar mode, aerobic exercise has very different effects and CR effects on proteome fluxes are activated within a narrow and discrete time period.

Dedication

This dissertation is dedicated to my family – my parents Yvonne and Hector Palacios and my siblings Yvette and Giselle. My nieces Natalie (Aleli) and Madi and my brother-in-law Eben.

Los quiero mucho

"I was never more certain of how far away I was from my goal than when I was standing right beside it."

-Ethan Hawke – *Vincent Freeman*

"Who of you by worrying can add a single hour to your life?"

-Luke 20:25

Table of Contents

List of Abbreviations

CR	Caloric Restriction
MS	Mass spectrometer
LC	Liquid Chromatography
GC	Gas Chromatography
^2H_2O	Heavy water
D_2O	Deuterium Oxide
PKA	Protein kinase A
C	Caenorhabditis
Gbp	Gigabasepair
WNPRC	Wisconsin National Primate Research Center
CVD	Cardiovascular disease
NIA	National Institute on Aging
NIH	National Institutes of Health
EE	Energy expenditure
mTOR	Mammalian target of rapamycin
ROS	Reactive oxygen species
OXPHOS	Oxidative phosphorylation
NO	Nitric oxide
OLETF	Otsuka Long-Evans Tokushima Fatty
SA β–gal	Senescence-associated βgalactosidase
pRB	Retinoblastoma
AMPK	AMP-dependent/activated protein kinase
EMT	Epithelial-mesenchymal transition
ACC	Acetyl CoA carboxylase
PTC	Primary proximal tubular cells
PPARα	Peroxisome proliferator-activated receptor-α
AKT	Protein kinase
PI3K	Phosphoinositide 3-kinase
IRS	Insulin receptor substrate
HK	Hexokinase
PFK-1	Phosphofructokinase-1
PIP2	Phosphatidylinositol 4,5-bisphosphate
TSC	Tuberous sclerosis complex
Rheb	RAS homologue enriched in brain
ERK1/2	Extracellular-signal-regulated kinase 1/2
S6K1	Ribosomal protein S6 kinase
4E-BP1	4E-binding protein 1
CDK	Cyclin-dependent kinase
BDNF	Brain-derived neurotrophic factor
ULK1	Unc-51-like autophagy activating kinase 1
Nampt	Nicotinamide phosphoribosyltransferase
PGC-1α	Proliferator-activated receptor gamma coactivator 1-alpha
AML	Acute myeloid leukemia
FKBP12	FK506-binding protein
RCC	Renal cell carcinoma

Acyl-CoA	Acetyl-coenzyme A
MEC	Mammary epithelial cells
eIF2α	Eukaryotic initiation factor 2 alpha
GSK3β	Glycogen synthase kinase 3 beta
SIRT	Sirtuin
NAD+	Nicotine adenine dinucleotide
KDAC	NAD+-dependent lysine deacetylases
1C	One-carbon
ETC	Electron transport chain
EX	Aerobic exercise
FXS	Fragile X syndrome
COX-IV	Cytochrome oxidase subunit IV
Mt	Mitochondrial
LPS	Lipopolysaccharide
Cytc	Cytochrome C
NHEJ	Non-homologous end joining
CTX	Cyclophosphamide
SHMT1	Hydroxymethyltransferase
DTT	Dithiothreitol
TCEP	Tris(2-carboxyethyl)phosphine
PMSF	Phenylmethylsulfonyl fluoride
T	Tween 20
BCA	Bicinchoninic acid
ACSM	American College of Sports Medicine
SAC	Sacrification
Ad lib	Ad libitum
WPAS	Within proteome absolute synthesis
CMA	Chaperone-mediated autophagy
ETC	Electron transport change
LAMP-2A	Lysosomal associated membrane protein type 2A
HSC70	Heat shock cognate 70 kDa
HSP7C	Heat shock cognate 71 kDa
FSR	Fractional synthesis rate
ITT	Insulin tolerance test
GTT	Glucose tolerance test
IP	Immunorecipitation
RER	Respiratory exchange ratio
SR	Sarcoplasmic reticulum
ARI	Arginase I
ASL	Arginosuccinate Lyase
CPS	Carbamoyl-phosphate synthase
ASS	Argininosuccinate synthase
AST	Aspartate aminotransferase
OC	Ornithine carbamoyltransferase
NOS	Nitric oxide synthase
GDH	Glutamate dehydrogenase
OAA	Oxaloacetate

CHAPTER ONE: Calorie Restriction: Current Understandings

1. INTRODUCTION

Regulation of energy homeostasis contributes to balanced cell growth, a key aspect of metabolic biology. In chapter one, I review how a decrease in caloric intake without malnutrition, henceforth understood and referred to as CR, leads to altered metabolic pathways that increase lifespan and improve health. I also discuss various lifespan extending interventions that interact with CR, and how they deregulate proteome balance by suppressing its synthesis rates.

Dramatic energy changes require coping mechanisms in order to manage metabolism for optimal substrate control. During chronic CR, the metabolic flexibility of the cell allows for the deactivation of nutrient sensors and the activation of energy status sensors [1]. CR acts on numerous signaling pathways to regulate growth, oxidative stress response, damage repair, inflammation, autophagy, and significantly proteostasis [2,3], leading to the slowdown of the aging process [4–6]. These pathways then have the capacity to exert an analogous and combinatorial regulatory effect on aging by modulating protein synthesis [5,7] through effectors of suppression [7,8] and maintenance [9,10]. In here, I will discuss the various aspects of cell metabolism regulated under CR and its mimetics. We will first discuss the major pathways regulated under these interventions. We then discuss the intersecting role of these pathways to protein regulation. Along the way, we consider the major role of global protein regulation to human health and disease.

2. CELL METABOLISM UNDER CR

2.1. CR: The fountain of youth

The ancient Greek historian Herodotus talked of a society that lived during the first millennium BC in what is now modern-day Somalia. These people were said to be very special, as most lived to be one hundred and twenty years old and beyond. In their land there was also a unique fountain, which they claimed, provided them their exceptional longevity. The water had uncommon properties that gave it the texture of oil on the skin and the scent of violets. Their diet was also quite peculiar - they ate roasted meat and drank only milk [11]. In these writings, Herodotus fascinatingly conceptualizes not only the idea of the fountain of youth but perhaps one of the first links between diet, nutrition and longevity.

Over a century ago, Rous published one of the first scientific observations on the health benefits of CR through his experimentations on the impact of underfeeding laboratory animals on transplanted and induced tumors [12,13]. Almost a decade later, a group led by Osborne *et. al.* described one of the first evidence of lifespan extension in a murine model. They reported that although female rats were fed a uniform experimental diet, those experiencing stunting lived much longer - up to 40 months of age [14]. Interest in growth rates and longevity soon followed [5]. However, it was not until 1935 that McCay et al. linked extended lifespan with CR by showing that 40% food restriction in rats throughout their life doubled their lifespan [15]. Since then, many reports on the effects of CR on longevity have been reported [16]. For example, Fischer 344 rats under 60% CR initiated at 6 months of age were reported to have a markedly

increased in lifespan [17]. Another report using a murine model demonstrated the effects of CR starting in middle age (12- to 13-month-old mice) and concluding that the restricted diet group had 20% increased maximum lifespan [18].

While murine models demonstrated early and powerful evidence on the effects of CR and longevity, many other experimental models have been put to the test [5]. A successful approach to lifespan studies has been the use of short-lived organisms like *Saccharomyces cerevisiae* (commonly referred to as yeast). In this system, lifespan can be extended by limiting glucose or by reducing the activity of the glucose-sensing cyclic-AMP-dependent kinase (PKA) [19,20]. In genetic studies, it has been shown that ageing in yeast is regulated by SIR2, with its overexpression extending lifespan and its deletion shortening it [21]. Aging yeast cultured under CR conditions (0.2% glucose) lived significantly longer than yeast undergoing chronological aging under non-CR (2% glucose) [22].

Another short-lived model is *Caenorhabditis (C.) elegans*, with which various strategies have been approached to induce CR effects. In general, bacterial food deprivation has been used as a means of inducing CR, and transient CR has been shown to confer long-term benefits including stress resistance and increased longevity [23]. The addition of resveratrol to the medium has also been show to extend life-span [24], and even gradients of bacterial concentrations have been explored [25]. Indeed, the capacity to vary the nutrient regimes of CR in this model have been shown to result in increased longevity to various degrees. An effect believed to be mediated through nutrient-sensing systems [24–26].

First reported in 1971, the quantitative effects of CR on *Drosophila melanogaster* have been demonstrated, with adult flies maintained on an *ad-libitum* but diluted diet living longer than the controls [27]. This is an interesting approach as flies are usually kept on an agar-based media that can be manipulated to combine different nutrients like yeast, sugar or molasses, cornmeal, and other carbohydrates [28–30]. Interestingly, Staats *et. al*. [31] used a diet based on sucrose, corn meal, and yeast supplemented with resveratrol to study longevity and concluded that the resveratrol did not affect lifespan nor other longevity-associated markers. It should be noted that CR associated longevity in flies has been connected with changes in the ratio of consumed protein relative to carbohydrates [30] as well as genes that modulate stress resistance [32–34]. Genetic studies on flies have shown that longevity increases as a result of the over-expression of genes involved in stress response such as the chaperone *hsp70* [35,36] and insulin-modulating gene *tequila* [37].

Rodents are another shorter-lived species that is most commonly used as a model organism in human disease research [38] and one of the most widely used mammalian research models overall. The use of mice as the prototypical organisms to study human biology is further based on the genetic and physiological similarities between the species [39]. The mouse genome is only about 14% smaller than the human genome (~2.5 Gigabasepair [Gbp] compared with 2.8 Gbp) [40] and encodes a similar number of genes (~30,000 compared with ~25,000 in humans) [36,40].

The beneficial effects of CR on lifespan and age-related diseases have also been reported for longer-lived species, including rhesus monkeys (Macaca mulatta) at the Wisconsin National Primate Research Center (WNPRC) [41,42]. In this study, a moderate CR regimen (30%) slowly introduced to adults (7-14 years of age) lowered the incidence of aging-related deaths. They observed improved outcome in three major age-related conditions: neoplasia, cardiovascular disease (CVD), and glucoregulatory impairment. Many of the benefits observed came from decreases in blood insulin and glucose, which decreased the development of insulin resistance and diabetes. They also saw improved outcome from risk factors for atherosclerosis, lower T3 levels and metabolic rate, decreased oxidative damage and inflammatory markers (TNFα, IL-6, C-reactive peptide). The rhesus monkeys also have delayed senescence of the immune system, decreased loss of gray matter (suggested as a marker for brain atrophy), and decreased cancer rates [41,42].

In a conflicting study at the National Institute on Aging (NIA), young and older rhesus monkeys under a CR regimen were reported to not have improved survival outcomes [43]. This was in stark contrast with the study at the WNPRC, which had previously reported an improved survival under CR (30%) initiated in adult rhesus monkeys (7–14 years) [41–43]. The NIA study performed CR (25%) and showed beneficial health effects but not survival. Possible explanations suggested are from the differences in the studies, where the composition of the diets utilized was significantly different (**Table 1-1**). Other possibilities are that at the NIA, the controls were not fed ad libitum. The animals also had greater genetic diversity by mixing groups from India and China and some of their monkeys had also previously been used in military research. At the NIA, the monkeys were also kept in small cages and the females (both the control and CR) died before the males [43].

Grey mouse lemurs (Microcebus murinus) are lemurid primates reported to live up to 15 years. In a study by Pifferi *et.al.* [44], they exposed mouse lemurs to CR (30%) and observed a 50% increase in lifespan (median survival from 6.4 to 9.6 years). This was also accompanied by reduced age-associated diseases and improved brain white matter but significantly not grey matter.

The CR effects on lifespan in humans has been somewhat inconclusive, as experiments in longer-living organisms like humans and other primates are more difficult to conduct. Nevertheless, some positive outcomes have been glanced in different studies. For example, the Vallejo study [45,46] tested the effects of CR without malnutrition in nonobese humans by an alternate day feeding approach in 120 men. Half of the participants in the control group were ad libitum, while the other half underwent CR (~35%) by receiving an average of 1500 kcal per day for 3 years. Redman, in a follow up review, observed that while the initial report was short, post hoc analyses on hospital admissions rates revealed a decrease of approximately 50% on the CR group [45].

One of the larger trial efforts was the Phase 1 Comprehensive Assessment of the Long-Term Effects of Reducing Intake of Energy (CALERIE) studies, sponsored by the US National Institutes of Health (NIH). The randomized, controlled trial tested the effects of 2 years of CR on metabolism in more than 200 healthy, non-obese adults [47–

[49]. In a clinical report by Redman *et.al*. [45,50], they used 53 non-obese human subjects (34 CR and 19 control) to test the effects of endocrine mediators and energy expenditure (EE) on a CR diet over 2 years. They showed that under CR (15%), subjects had a weight loss of 8.7 kg compared to controls who gained 1.8 kg. Furthermore, the CR group had an EE (measuring during sleep or over 24 hours) of approximately 80–120 kcal/day. This was reported to be lower than expected on the basis of weight loss, indicating sustained metabolic adaptation over the course of the trial [50].

Of note, there has been great interest in understanding centenarian populations. A well-documented group in this category is found in the Japanese island of Okinawa. Centenarians represent a rare phenotype, appearing in ~10 to 20 per 100,000 persons in most industrialized nations. However, in Okinawa centenarians appear as high as ~40 to 50 per 100,000 persons in Okinawa [51]. The Okinawans have a unique identity, dialect, social organization and religion, as well as dietary habits [51,52], whose nutritional cues are considered as a mild and consistent CR (~10%–15%) [53,54].

While CR has many positive effects that lead to similarly positive outcomes, it is important to mention some of the negative effects described. Of note is the increased hunger and temperament effects like aggression, lethargy and anxiety observed in the rhesus monkeys [43]. In various organisms there is also suggested diminished libido and fecundity though this has been contested [55]. CR has also been shown to exhibit adverse effects on certain organs and systems, including immunosuppression [56]. However, a study on the effect of CR (2 years duration) on mood, quality of life, and sexual function in healthy nonobese adults observed that those under CR had significantly improved mood, reduced tension, and improved general health and sexual drive as well as improved sleep [57].

Many efforts have been made to tease out the modulatory effects of CR on health and lifespan. This has proved an immense challenge, however, since experimental models have not always been appropriate and contradictory outcomes have been reported.

Dietary Ingredients	NIA Study	WNPRC Study
Source	Natural	Purified
Proteins	Various (wheat, soy, corn)	Lactalbumin
Antioxidants	Flavanoids	No
Essential Fatty Acids	ω3 Fatty Acids	No
Oil	Fish, wheat, corn	Corn
Carbohydrates	Wheat, corn	Corn starch, sucrose
Vitamin Supplements	Controls supplemented	Controls not supplemented

Table 1-1. Summary of differences in diet between the NIA and WNPRC non-human primate CR studies.

2.2. The role of CR on aging

Understanding how the rate of aging can be manipulated makes establishing a connection between CR and lifespan extension of great interest. Studies on CR have

yielded results of increased maximal lifespan by up to 50% [44]. This brings to question how we can slow down human aging through CR by modulating the underlying molecular mechanisms in order to develop therapeutic interventions (eg. drugs and nutrients) to mimic CR.

There are many theories on how aging and age-related diseases come to be **(Table 1-2)** [58]. Indeed, the complex process of biological aging, as an intrinsic feature of living beings, is the result of genetic and, to an extent, environmental factors and time. However, it is the cellular aspects (free radicals, apoptosis & proteostasis, and telomeric) that have gained increased attention in the field of aging research in recent years. The *free radical theory of aging* is a hypothesis that postulates the accumulation of oxidative damage as a cause for aging and disease [59,60]. Denham Harman conceived the first iteration of the free radical theory of aging in 1956 [61], basing the theory on the presupposition that lifespan is dependent on metabolic rate [61,62]. However, his hypothesis has since fallen out of favor [62,63]. Nevertheless, oxidative stress has been shown to be associated with aging and age-related diseases, including cancer [62,64,65], neurodegeneration [62,66,67], CVD [62,68,69], and diabetes [62,70]. In this regard, it is known that during aging the body undergoes a decline in mitochondrial function associated with the production and accumulation of reactive oxygen species (ROS). This, in turn, has been suggested to be in part responsible for the decline in cellular performance [71]. During mitochondrial oxidative phosphorylation (OXPHOS), ROS are produced. These are particularly associated with damage to DNA, lipids and proteins [13].

Various investigations have reported reductions in steady-state oxidative damage to proteins, lipids, and DNA in animals under CR conditions [72]. In a study using mitochondria from liver tissue of male Brown Norway rats under CR, assessment of hydrogen peroxide measurement concluded that CR resulted in a decrease in the production rate of ROS. Furthermore, this decrease was attributed to a reduction in protonmotive force in mitochondria from the CR animals [73,74]. Another study was set to determine the effects of CR (30% reduction from free intake) on mitochondrial ROS production, UCP2, and the nitric oxide (NO)-cGMP pathway in the cardiovascular tissues of type II diabetic Otsuka Long-Evans Tokushima Fatty (OLETF) rats. The authors determined that mitochondrial ROS production and UCP2 expression significantly decreased in the heart and aorta of the CR group, further demonstrating that CR significantly improved the NO-cGMP pathway via normalizing ROS generation in OLETF rats [75].

Detractors of the free radical theory of aging have claimed that this theory has limitations as it often remains uncertain if these are a cause or consequence of the aging process and do not explain the possibility of inherent failure from biological process as the source of the damage observed [76]. Another consideration is that many genetic interventions (such as the tissue specific removal of antioxidants) leading to overall enhanced oxidative damage have a moderate to negligible effect on lifespan [77]. In this regard, a study on the effects of CR on mitochondrial function, showed that CR (55% of control food intake) on male Brown-Norway rats yielded no significant changes in ROS production [73].

Recently, it was suggested that ROS signaling played an important role in cell senescence and organismal aging [78,79]. In this regard, *cellular senescence* was first explained in 1961 by Hayflick and Moorhead as a way to define the phenomenon of limited proliferation capacity in cultured human fibroblasts [80,81]. It was observed that cellular senescence came from an acute loss of replicative competence through the reticence of the proliferative capacity of cells [82]. In addition, this was restricted to just proliferation-competent cells [81]. More recently, this phenomenon has been better understood as replicative senescence, and believed to be caused by telomere erosion [82]. Considering that telomeres are specialized DNA-protein structures composed of several kilobases (kb) of simple repeats (TTAGGG)n located at the ends of chromosomes [83,84], the length of telomeres has been suggested as an accurate predictor of the replicative ability of cells and the reduction in the number of repetitions is believed to cause cell senescence [82]. The limited replicative capacity in both mitotic and postmitotic cells, may therefore be a manifestation of aging at the cellular level [85,86].

As an irreversible form of long-term cell-cycle arrest, cellular senescence is caused by excessive intracellular or extracellular stress that can lead to cellular damage [83]. Senescence can also be triggered under various conditions: oxidative stress, telomere damage/shortening, DNA damage, mitochondrial dysfunction, chromatin disruption, and inflammation [87,88]. These can then lead to the permanent growth arrest of the cell through the activation of specific signaling pathways that lead to senescence regulation.

Tumor-suppressor pathways are of particular interest as activators of autophagy and senescence regulation [89,90], epigenetic dysregulation, and oncogene activation [83,91–93]. Of these, the p53-p21 and $p16^{INK4a}$–retinoblastoma (pRB) are the two essential pathways responsible for the replicative arrest during senescence [82]. Interestingly, both p53 and $p16^{INK4a}$ are the most commonly mutated genes in cancer. A study using The Cancer Genome Atlas (TCGA) Pan-Cancer database (a landmark cancer genomics program sponsored by the NIH), determined that the most frequently mutated gene in the Pan-Cancer cohort was p53 (42% of samples), further showing the mutations predominate in serous ovarian (95%) and serous endometrial carcinomas (89%) [94]. In addition, $p16^{INK4a}$ has been observed in 25–70% of all human cancers [95,96], and its upregulation has been detected in early stage cancer cells, and thus is associated with better prognosis [95].

A main inducer of senescence is cellular damage. Because of this, it has been suggested that CR might prevent senescence by precluding the damage from occurring. For example, CR has been shown to upregulate antioxidant defense mechanisms through the increase of sirtuins, induction of transcription factors like FoxO1 [82] or enhanced immune response [97]. In this regard, a study on short term dietary restriction in middle-aged mice showed decreased abundance of senescent cells in hepatocytes and enterocytes. Associating a decrease in cumulative oxidative stress markers through γH2AX (DNA damage) and PCNA (replication), with senescence-associated βgalactosidase (SA β–gal) as an improvement in telomere maintenance without increased telomerase activity [98]. In regard to immune response, a study of cell immunity on rhesus primates set out to test the impact of CR on T cell senescence. It

demonstrated that CR effected a marked improvement in the maintenance and/or production of naive T cells and the consequent preservation of T cell receptor repertoire diversity [99]. CR can also protect cellular deterioration by decreasing oxidative stress and inflammation, or repairing/eliminating already present damage, for example by increasing autophagy [100–102] and regulating cell death [103].

Apoptotic cell death is a protective mechanism to remove cells with DNA damage or diseased cells that might interfere with normal functioning, or eliminate cells at the end of their functional lifespan [104]. Apart from the ability to induce autophagy, CR and CR mimetics such as resveratrol, are capable of modulating the expression of pro- and anti-*apoptotic factors* [105]. This is significant, as the role of apoptosis is critical for organ and tissue morphogenesis, development, and even senescence [106]. Apoptosis is a conserved homeostatic programmed process for cell death that also participates in the etiology of several human diseases including cancer, neurodegenerative, and autoimmune disorders [107] and possibly even aging.

Functionally, one of the earliest molecular markers of apoptosis is the externalization of cell membrane phosphatidylserine. When phosphatidylserine is exposed, it can function as a signal to nearby macrophages to engulf the dying cell. The earliest noticeable changes of apoptosis are the shrinkage of the cell and karyopyknosis (shortening of the nucleus and chromatin). What follows is an orchestrated fragmentation of the nucleus and chromatin called karyorrhexis, followed by cell membrane blebbing, and ultimately leading to the budding of the cell into a series of membrane-bound structures called apoptotic bodies [108]. Macrophages then engage through phagocytosis, where the apoptotic bodies are further broken down in phagolysosomes for recycling.

The apoptotic process is not known to induce the immune response because no cellular materials are released into the interstitial space, and the engulfing cells do not release inflammatory cytokines [109]. This is of significance for the disease process and in particular cancer. Studies have revealed that cancerous cells inhibit cytochrome C-mediated apoptosis by supplying sufficient glutathione to keep cytochrome C in a reduced and inactive state [110]. The production of NADPH has also been linked to enhanced cancer cell survival and indeed the suppression of apoptosis; NADPH is required for the synthesis of glutathione, which protects cells from redox stress, thus promoting resistance to apoptosis [111,112]. Aging is further associated with an inhibited apoptotic response [108]. For example, in human adipose mesenchymal stem cells, aging was shown to decrease the expression of apoptotic genes while increasing the expression of senescence-related genes [113]. In mice, bone marrow mesenchymal stem cells had decreased expression of both cell cycle and apoptotic genes during aging [114].

The effects of CR on apoptosis have also been explored with mixed results. In one study of CR (40% reduction) in 6-month-oldmale Fischer 344 rats, cytoplasmic histone-associated DNA fragment analysis showed no changes in DNA fragmentation levels (indicative of apoptosis) in tissues like kidney [115]. Interestingly, another study on kidney function using younger (12-) or older (24-month-old) rats revealed protein expression levels of a pro-apoptotic Bax protein increased in the older rats, while an anti-apoptotic protein, Bcl-2, was reduced in the aged rat kidney. Furthermore,

cytosolic cytochrome C level was significantly increased in the aged kidney. However, these age-related changes were reversed by CR [116].

Countless studies have attempted to explain the concept of aging, aligning their efforts with any number of theories in an effort to understand what is behind this process that culminates in death. The many levels explored, from cellular to systemic, are a commendable effort that can allow us to glance deeper into human mortality. CR has been used to help in this task, providing insights into how lifespan extension modulates the aging process.

Level	Theory	Description
Evolutionary	Mutations	Mutations affecting the health of elderly populations are not selected against.
	Somatic	Somatic cell maintenance is maintained for reproductive success.
	Pleiotropic	Genes beneficial at early life cycles become deleterious during aging.
Molecular	Genetic	Gene expression regulation dictates the aging process.
	Codon	mRNA translation fidelity declines with age.
	Dysdifferentiation	Gene expression regulation is impaired by accumulative damage over time.
Cellular *	Telomere	Aging phenotypes result from increased frequency of senescence
	Free radical	Oxidative damage of lipids, proteins and DNA from free radicals.
	Apoptosis	Programmed cell death.
Systemic	Endocrine	Alterations of the endocrine control system over time.
	Immunologic	Decline of immune function with age.
	Metabolic	Fixed amount of metabolic potential.

* Discussed in text

Table 1-2. Summary of the various theories of aging and their description.

3. METABOLIC PATHWAYS OF CR

While the mechanisms accounting for the decline in cellular function remain enigmatic, pathways that stand out during aging are metabolic in nature [117–119] and involved in cell maintenance through catabolic and anabolic processes [120]. Fundamental metabolic pathways **(Figure 1)** such as glycolysis, fatty acid oxidation, amino acid oxidation, lipogenesis, and ketogenesis are also altered in aging [119], so elucidating the resulting deregulation is at the core of understanding lifespan extension and CR. In here, I will address two reciprocally regulated key enzyme complexes that have received attention in control of aging and CR: 1) the nutrient and hormone sensing mammalian target of rapamycin (mTOR) complex 1 (C1) and 2) the AMP-dependent/activated protein kinase (AMPK).

3.1. Energy signaling under CR

CR is an intervention that alters the energy status of the cell and is sensed by the energy regulating AMPK [121]. As a heterotrimeric kinase with one catalytic subunit (α) and two regulatory subunits (β & γ), this protein responds to energy usage, inhibiting various cellular responses that require energy expenditure while promoting catabolic processes to generate ATP [122]. In order to answer to the energy availability of the cell, AMPK monitors changes in the ratios of AMP:ATP and ADP:ATP which then bind to the γ subunit. This leads to the phosphorylation of the α subunit on an activating loop at Thr^{172} by upstream kinases like LKB1 [122,123]. On the other hand, the β subunit contains an evolutionary conserved carbohydrate binding domain, which allows

AMPK to interact with glycogen particles [124]. The resulting activation of AMPK works to restore energy balance by inhibiting anabolic processes [125].

While the main upstream kinase in most cell types on the AMPK signaling pathway is the LKB1/STRAD/MO25 complex, its constitutive activation is inhibited by phosphatases under basal conditions [126]. In *Drosophila*, the expression of LKB1 and the AMPK substrate acetyl CoA carboxylase (ACC-1) are conserved [127], and overexpressing LKB1 has been shown to extend lifespan [128]. In this regard, a recent study showed that overexpression of AMPK in muscle and abdominal fat body extended lifespan, and that supplementation of adenosine could modulate the beneficial effects of CR [129].

The activation of AMPK affects many metabolic pathways conducive to catabolism to restore ATP levels by promoting glycolysis and fatty acid oxidation, as well as by increasing mitochondrial content and the use of mitochondrial substrates as an energy source [125,126]. The ability of AMPK to reprogram metabolism has therefore been a focus of interest as a therapeutic avenue for the treatment of several metabolic diseases [130]. In this regard, a recent study used siRNA to deplete AMPK in a renal fibrosis model of chronic kidney disease, which is characterized by reduced glomerular filtration rate that mainly affects the aging population. Using high glucose to induced senescence and epithelial-mesenchymal transition (EMT) in human primary proximal tubular cells (PTCs), the authors observed markers of cellular senescence and inactivation of AMPK signaling markers associated with EMT, which were alleviated upon induction with CR mimetics like resveratrol and metformin [131].

Under low energy conditions, starvation hormones like Fgf21 [132] are upregulated in response to CR in tissues like liver and secreted into plasma [133]. Through a signaling cascade, this leads to a rapid phosphorylation of downstream pathway components, including the MAPK cascade [134] and leading to the activation of AMPK [135] . This has been of great interest, as Fgf21 is also a direct target gene of the peroxisome proliferator-activated receptor-α (PPARα) [136,137], a regulator for CR-induced lipolysis. Exploring its neuroprotective effects in ApoE knockout mice under CR, Rühlmann *et.al*. [138] observed that Fgf21 played an important role in adaptation to metabolic states by improving cognitive performance through Morris water maze test and higher synaptic plasticity by immunohistochemical analysis of PSD95-positive (synapse associated) neurons.

3.2. Nutrient signaling under CR

AMPK is highly regulated by upstream signals, making it a master regulator of energy homeostasis in the cell [122], and a coordinator of growth and metabolism in eukaryotes in both specialized tissues and at the whole body level [130]. In this regard, AMPK interplays with the serine/threonine kinase AKT (or protein kinase B or PKB)/phosphoinositide 3-kinase (PI3K)/mTOR signaling pathway through the inhibition of the kinase activity of mTOR. This regulation is a well-studied link between CR and lifespan extension [54], as mTOR acts as an autophagy repressor in opposition to the pro-autophagic effects of CR [9,139,140].

The activity of mTOR can be regulated through the constitutive activation of PI3K signaling components through the PI3K-PKB/AKT pathway - a highly conserved and tightly controlled multistep process [141]. Activated cell membrane receptors directly stimulate class 1A PI3Ks bound via their regulatory subunit or adapter molecules such as the insulin receptor substrate (IRS) proteins [141]. When insulin binds to its receptor, it initiates a sequence of phosphorylation events that lead to activation of the catalytic activity of PI3K, a lipid kinase that coordinates the intake and utilization of glucose, and mTOR, a kinase downstream of PI3K that stimulates transcription and translation [142]. These can also directly stimulate levels of glucose uptake and general metabolism through increased expression and localization of the glucose transporter GLUT1 to the plasma membrane and through increasing the activity of hexokinase (HK), phosphofructokinase-1 (PFK-1), and phosphofructokinase-2 (PFK-2) [143–146]. PI3K is also known to phosphorylate phosphatidylinositol 4,5-bisphosphate (PIP2) to phosphatidylinositol 3,4,5- triphosphate (PIP3), which then activates AKT [147]. In this regard, AKT plays numerous important biological roles within the cell and within the context of CR it was previously shown that PI3K and AKT transcripts were significantly down-regulated in human skeletal muscle under CR [148].

Indeed, the PI3K/mTOR signaling pathway plays key roles in regulating many cellular processes like cellular metabolism, cel cycle progression, proliferation, growth, autophagy, and significantly protein synthesis [149–151]. Activation of PI3K recruits AKT via its pleckstrin homology domain [149]. Upon activation, AKT involves the phosphorylation of the tuberous sclerosis complex (TSC) 2 subunit, an essential controller of mTORC1. Inhibition of TSC2 then leads to the accumulation of GTP-bound RAS homologue enriched in brain (Rheb), whose activity is inhibited by the heterodimer complex of TSC1 and TSC2 [152]. Indeed, TSC1/2 is a mediator of mTORC1 through many upstream signals from growth factors, such as insulin and insulin growth factor (IGF-1), which stimulate the PI3K and RAS pathways. The effector kinases of these pathways, including AKT, extracellular-signal-regulated kinase 1/2 (ERK1/2), and ribosomal protein S6 kinase β-1 (S6K1), directly phosphorylate and inactivate the TSC1/TSC2 complex, leading to the activation of mTORC1 [152]. Indeed, the activation of mTORC1 signaling via downstream targets including p70S6K and eukaryotic translation initiation factor 4E-binding protein 1 (4E-BP1) [153] are fundamental in protein translation events.

The activation of AKT regulates cell growth through its effects on the TSC1/TSC2 complex and mTOR signaling [154]. AKT also contributes to cell proliferation via phosphorylation of the cyclin-dependent kinase (CDK) inhibitors p21 and p27, and is a major mediator of cell survival through direct inhibition of pro-apoptotic proteins like Bad or inhibition of pro-apoptotic signals generated by transcription factors like FoxO1 [155]. In this regard, evidence has shown CR to be a powerful autophagy inducer in various metabolic tissues like liver [156]. In rat skeletal muscle, CR (40%) decreased the content of phosphorylated mTOR, S6K1, pS6K1, FoxO3a, and ubiquitinated proteins [157]. Similar results were also observed in senile mice, where mTOR and S6K1 protein activation and mTOR and S6K1 mRNA were significantly lower in the CR group [158]. In the brain, the activity of mTOR and its upstream brain-derived neurotrophic factor (BDNF)/PI3K/AKT signaling was decreased with aging and CR ameliorated the observed age-related cognitive deficits [159].

3.3. Regulators of energy and nutrients

AMPK and mTOR signaling pathways **(Figure 2)** participate in nutrient-sensing in order to control cell activity. Their complex regulatory dynamic has unique responses to macromolecules that coordinate cell behavior. Importantly, crosstalk between these key pathways is essential for cellular response to nutrients. Therefore, understanding how CR is involved in their modulation can be hypothesis generating in the context of benefits in cell metabolism, energy homeostasis and aging [44].

Considering AMPK as a key energy sensor, it has the ability to transcriptionally reprogram the cell and metabolically adapt to external cues [126]. Genetic evidence has suggested that AMPK is required for many of the adaptations triggered by CR, including lifespan extension. Similarly, AMPK activation impacts on mitochondrial metabolism and on the activity of the FoxO, sirtuins and mTOR signaling pathways, all linked with CR [126,160]. Since CR triggers activation of AMPK, this event then promotes the TSC complex (through phosphorylation) to impose its inhibition on mTOR- unc-51-like autophagy activating kinase 1 (ULK1) signaling through Rheb, leading to facilitated autophagy and autophagy flux [161].

The role of AMPK as a primary sensor has been of great interest. It has been shown that it can control insulin sensitivity upon CR in skeletal muscle through regulating phosphorylation of the mTOR−S6K1−IRS-1 signaling pathway and activation of the nicotinamide phosphoribosyltransferase (Nampt)-SIRT1 axis in transgenic mice [162]. Another group demonstrated that after 11 months of CR, there was activation of the AMPK-SIRT1-peroxisome proliferator-activated receptor gamma coactivator 1-alpha (PGC-1α) axis in C57Bl/6J mice [163]. Furthermore, by targeting AMPK in dopamine neurons in a Parkinson's disease mouse model, Bayless *et.al.* [164] demonstrated a novel way in which CR maintains neuronal activity through CR-induced increases in plasma ghrelin. This is of particular interest since aging is associated with attenuated ghrelin signaling [165].

In the context of disease, inducing mTORC1 activity has been shown to be constitutively activated in some forms of malignant cancers, such as primary acute myeloid leukemia (AML) cells [166], therefore representing a major target for drug development in these malignancies. Many mTOR kinase inhibitors fully suppress protein synthesis and induce apoptosis [167,168]. For example, the mTORC1 pathway is rapamycin-sensitive and controls protein translation through the phosphorylation of 4E-BP1 in many experimental models [149].

The story of mTOR could be said to begin in 1964, when a Canadian expedition set sail to a remote volcanic island in the South Pacific Ocean. This island, located in the Polynesian Triangle, was called Rapa Nui (also known as Easter Island or *Isla de Pascua*). The expedition had the aim of collecting soil samples with the goal of identifying novel antimicrobial agents. In bacteria isolated from one of these samples, scientists discovered a compound with notable antifungal, immunosuppressive, and antitumor properties [169,170].

Further analysis of this compound, named rapamycin after its site of discovery (clinically known as sirolimus), revealed it as a bacterial macrolidic metabolite whose mode of action involved the formation of a gain-of-function complex with the peptidyl-prolylisomerase 12 kDa FK506-binding protein (FKBP12) [171] to inhibit signal transduction pathways required for cell growth and proliferation [170,172].

Initially, the interest on rapamycin was for its antifungal properties, so it was not until the 1990s that its immunosuppressive and antiproliferative properties in mammalian cells were discovered [170]. In fact, the first mTOR inhibitor in clinical use was rapamycin, which was used as an immunosuppressant drug given after transplant surgeries. Known also as sirolimus, this macrolide was approved in the United States in 1999 for prophylaxis of rejection in renal transplantation patients [173].

Temsirolimus, a rapamycin derivative, was subsequently developed and approved for the treatment of renal cell carcinoma (RCC) [174]. Similarly, Everolimus was developed as an oral mTOR inhibitor used in the treatment of neuroendocrine tumors [175] and also approved for use in post-menopausal women with breast cancer [88,176]. These agents, called "rapalogues", exert their effect mainly as allosteric inhibitors of mTORC1. However, since they only inhibit the mTORC1 complex, their use has been associated with negative feedback regulatory mechanisms and other mechanisms of resistance, causing paradoxical activation of AKT and proliferative effects via other downstream targets [177].

As an amino acid sensor, mTOR has been suggested as a mediator of CR [178]. The high activity of mTORC1 is involved in translation dysregulation during aging [179] and deletion of S6K homologue SCH9 in yeast or depletion of TOR (*let-363*) [180] or RAPTOR (mTORC1 protein member; *daf-15*) by RNA interference (RNAi) in *C. elegans* [181,182] extends life span in both models. It is therefore possible that rapalogues mimic the effects of CR on healthy life extension. However, the extent of the mechanistic overlap between both interventions remains incompletely understood. A study by Choi *et.al.* [183] on yeast compared the impact of CR and rapamycin on cellular metabolic status and showed how both regimens maintained intracellular ATP and enhanced mitochondrial capacity through the chronological aging process of this model. and showed enhanced mitochondrial capacity. However, while CR severely reduced the level of energy storage molecules including glycogen and lipid droplets, rapamycin did not elucidate such as response. Furthermore, rapamycin boosted the production of enzymes responsible for the breakdown of glycogen and lipid droplets, leading the authors to suggest their mechanism of action, at least in part, is by regulating distinctive pathways [183].

4. REGULATION OF TRANSLATION DURING CR

The cost of protein synthesis is a central part of cell metabolism, being also intimately linked with the rate of cell division [184]. Protein turnover is one of the main metabolic processes by which functional proteins are preserved and damaged proteins are removed. The maintenance of proteostasis could therefore be a marker of cellular status and function by which the cell guides regulatory processes for maintenance. Hence, when considering that the translational control is a regulated process, any

signal or intervention able to affect global changes in the translational capacity of the cell is of great interest. Therefore, understanding how CR improves health and extends lifespan by modulating protein turnover rates could in fact provide important insights in the development of interventional and preventative strategies against age-related diseases.

4.1. Cellular capacity for translation during CR

Energy-driven signaling systems are integral for the capacity of the cell to maintain homeostasis. This reveals the question of how easy it is for translation rates to change, a query that comes with many layers of intricacy. For example, flux pathways such as phosphorylation, s-nitrosylation and ubiquitination are capable of modifying the assembly of proteins to a degree [185–187]. Fasting and starvation can also lead to a slowdown in protein synthesis rates and activation of autophagy [188]. In fact, numerous regulators of CR are involved in protein synthesis, putting translation at the center of cell function due to its high economic cost for cellular resources to maintain normal cellular physiology [7,189].

In terms of energy expenditure, protein biosynthesis demands a very large portion of the available resources during cellular proliferation. Indeed, translation by ribosomes has been estimated to cost the cell approximately half of the available energy in rapidly growing bacteria, and around a third of the available energy in dividing mammalian cell [190,191]. The significant energy budget associated with protein synthesis makes it a key step for regulating diverse cellular functions. Being so intimately linked to energy and nutrition, protein synthesis is therefore a primary target of CR research [192]. It could then be considered that while the mechanisms involved in delay of aging remain poorly understood, it is possible that translation is a key aspect altered under CR through a modulation in the rates of protein synthesis and even cell proliferation. For example, CR in rodent models greatly reduces global protein replacement rates in liver and muscle [7,193] and cell proliferation rates in keratinocytes, liver cells, T-lymphocytes, prostate epithelial cells and mammary epithelial cells (MECs) [194,195].

Some ways by which the cellular capacity for translation is assessed involve the polysome association of mRNAs as a reflection of active translation [196–198]. Polysome profiling was developed to infer the translational status of a specific mRNA species or to analyze a subset of mRNAs actively translated in a cell [198]. In this respect, an analysis of protein translation through polysome-associated mRNAs could yield interesting inferences into the role of CR in proteostasis. Experiments in mice have revealed that <1% of transcripts in mouse livers are differentially abundant in polysomes under CR. However, when taking into account time of feeding in the context of circadian rhythms, a large differential of up to 10% was detected between the control and CR. The study suggested that CR strongly reprograms translation as a reflection of feeding patterns through lipid metabolism by modulating long-chain acetyl-coenzyme A (Acyl-CoA) [199]. Looking at adaptive changes in gene expression through transcriptome and translatome analysis of *C. elegans* under CR revealed an increase in transcription of muscle regulatory and structural genes while 3′ UTR editing and intron retention increase under CR and was correlated with diminished translation [200].

4.2. The role of global protein synthesis rates in CR metabolism

The nature of every living system is to fight against entropy to maintain life. In a highly regulated contrivance, the conservation of order through the synthesis and breakdown of proteins is a favorable tool for survival. However, it often comes at the cost of energy expenditure regardless of energy status, repair mechanism errors and its byproducts or even the unintended activation of signaling systems that respond to sudden alterations in the cellular environment. Indeed, it is generally accepted through observations that abrupt alterations to the cellular homeostasis can be detrimental to survival. However, we can usually expect that a proper response is often strong enough to maintain cellular homeostasis. For example, when a natural (eg. immune response) or xenobiotic (eg. drugs such as metformin) intervention elicits a positive response, it is capable of offsetting the cellular regulatory mechanisms and steer the cell to alter its translational capacity.

In respect to translation, this is a fundamental biosynthetic reaction whose regulation determines cell fate temporally and spatially. Since protein synthesis and cell growth are tightly coupled, the dysregulation of translation is a common mechanism underlying pathologies from unrestrained growth in cellular transformation to tumor development [201]. Indeed, re-tuning of the aberrant translation status by translation inhibitors is an attractive strategy for tumor treatment [202,203]. It has been suggested that the translation capacity of the cell can change during CR and increased protein synthesis has even been proposed as a mechanism of lifespan extension during CR [204,205]. However, observations on protein turnover rates have yielded conflicting data. For example, an early study measuring *in vivo* protein synthesis in CR mice showed no significant changes during acute feeding. Nevertheless, they observed a decrease in liver mitochondrial protein synthesis under CR [193].

As addressed earlier in this chapter, there is a critical role for the AKT/PI3K/mTOR signaling pathway in regulating diverse cellular functions and has even been suggested as an important therapeutic target for the treatment of human disease through regulation of cancer cell growth, survival, motility, and metabolism [206]. Generally, phosphorylation of 4E-BP1 and p70S6K by mTOR are essential for protein synthesis and hypertrophy in muscle [207]. AKT can promote protein synthesis by inhibiting glycogen synthase kinase 3 beta (GSK3β), impeding its inhibitory action on protein synthesis [208]. Another consideration is that protein synthesis requires sufficient and appropriate amino acid availability, and amino acid deprivation induces the phosphorylation of eukaryotic initiation factor 2 alpha (eIF2α), thereby impeding translation initiation [209]. A significant study on CR in humans using muscle biopsies from the deltoid and vastus lateralis showed that during severe energy deficit, pSer9-GSK3β levels were reduced, turning the skeletal muscle towards anabolic effects. Other observed effects were associated with the changes in lean mass and serum insulin, testosterone, and cortisol concentrations. Metabolically, the Akt/mTor/p70S6K pathway and total eIF2α were unchanged. Interestingly, total 4E-BP1 and Thr37/464E-BP1 were higher [210].

Another aspect of CR is that it can directly and indirectly activates sirtuins (SIRTs), which are nicotine adenine dinucleotide (NAD+)-dependent lysine deacetylases (KDACs) and play central roles during aging and autophagy [205]. It is possible that

SIRT1 and AMPK may engage in a positive feedforward loop to amplify the response to CR, opposing the frequency by which AKT/PI3K/mTOR signaling contributes to protein synthesis.

Due to various cellular events, such as cell growth, exacting a high protein synthesis demand, there is an increased effort in understanding how biological systems adjust their global protein translational capacity according to resource bioavailability. It has been considered that the protein translational capacity is determined by mRNA expression and the efficacy of ribosomes. The tight coordination between protein translation processes with mRNA transcription is therefore assumed to ensure efficient cell growth and upkeep. Efforts to monitor protein synthesis rates at the global level have mainly relied on pulsed metabolic labeling followed by two-dimensional gel electrophoresis, or more recently by MS [211–213], where pulse labeling with stable isotopes has been used to measure protein turnover rates. Nevertheless, these methods have not been effective in directly providing information about translation rates [213].

While relative changes in synthesis rates for the same protein are attainable [214], absolute rates are more difficult to evaluate. Additionally, the precision of pulsed metabolic labeling is limited by requirement for nutrient shifts, a fundamental effect of CR. Using expression profiling to determining global mRNA levels (e.g. high-density microarrays or RNA-seq) have not reported significant regulation events to be present at the level of translation [192]. For example, a report using RNA-seq in cerebral cortex from rats subjected to CR did not observe global changes in gene expression but more specific towards neuroprotection [215]. This pattern was also observed in a multi-tissue single-cell transcriptomic atlas for aging, where CR was observed to ameliorate aging-related accumulation of pro-inflammatory cells in various tissues [216].

5. MIMETICS OF CR

CR has proven to be the most robust intervention to impart and maintain health in a large array of experimental models. However, application of CR to complex organisms like primates and humans has been both impractical and inconclusive. Therefore, identifying better interventions that elucidate the advantageous mechanisms and effects as CR can be key to develop treatment strategies to extend health and lifespan in humans.

Compounds, or even interventions, that provide the physiological benefit of CR without restricting calories is of great interest. Taking advantage of this beneficial effects through pharmaceutical compounds could be a fundamental for the reduction of age-related diseases that permeate the world at large. The most widely studied compounds believed to be mimetics of CR are rapamycin, resveratrol and metformin. In addition, attention has been given to the exercise as a paradigm of CR as it can invoke similar physiological signatures involving pathways associated with stress responses and mitochondrial homeostasis [217–219].

Resveratrol, a component of red wine, has been an interesting target of aging research. Considered as an antioxidant, resveratrol is known to involve the sirtuin system [220]. Sirtuins are highly conserved enzymes whose activity involves the NAD+ dependent

deacetylase and/or mono ADP ribosyltransferase. A long line of evidence has linked sirtuins in the aging process, and data has inferred very positive results in its effective attenuation of several diseases. Nevertheless, the efforts to study sirtuin activators has been contentious [221].

Rapamycin has been explored in the context of fractional synthesis rates. Mean hepatic proteome replacement rates were modestly but significantly reduced after rapamycin treatment [7]. In fact, the overall observation of rapamycin effects on proteome regulation have been, while consistent, not very dramatic. Another study on 10 weeks of 14 ppm rapamycin treatment reported just a ~13% reduction in hepatic protein replacement rates in mice [189]. This has left metformin and exercise as potential CR mimetics in the context of proteome dynamics we will discuss here.

5.1. Metformin as a CR mimetic

Metformin is a biguanide drug used for over 45 years to treat type 2 diabetes. In humans, Metformin has been demonstrated to enhance insulin sensitivity and suppress gluconeogenesis, preventing the deleterious effects of this devastating disease. Surprisingly, the molecular mechanisms that underlie its function remain to be understood. In this regard, it has been theorized that Metformin acts as a CR mimetic, as both conditions are known to regulate many shared pathways [222].

Metformin function as a glucose sensitizer is thought to come from the inhibition of hepatic gluconeogenesis, possibly through a decrease in cytosolic ATP:ADP ratios [223]. Another aspect of metformin comes from its anti-cancer properties [224], where it has been observed to attenuate tumor growth through the activation of SIRT1 and AMPK while inhibiting AKT and mTOR [225,226]. perhaps through its interaction with the electron transport chain (ETC) complex I [223,227,228]. In this regard, it is suspected that Metformin decreases oxygen consumption and mitochondrial membrane potential in hepatocytes, where it singularly affects the respiratory chain complex I [223].

One-carbon (1C) metabolism comprises a series of interlinking metabolic pathways that include the methionine and folate cycles that are central to cellular function, providing 1C units (methyl groups) for the synthesis of DNA, polyamines, amino acids, creatine, and phospholipids [229]. The relationship between energy and 1C metabolism is extremely sensitive to food intake. Metformin activity has provided a link to overlapping factors where organismal bioenergetics remodel 1C metabolism. Indeed, Metformin not only inhibits mitochondrial complex 1, but modulates the metabolic response to nutrient intake through folate metabolism which could represent direct effects on some of the hallmarks of tissue aging [230]. By increasing the contribution of 1C DNA methyltransferases from folate stores, Metformin is suspected to induce AMPK-sensed energetic responses capable of reprogramming the DNA methylation machinery [231].

Due to their role in regulating cellular energy levels, AMPK and mTORC1 stand out as key regulators of metabolism that are respectively activated and inhibited in acute response to cellular energy depletion. Metformin has been shown to robustly inhibit mTORC1 in mouse liver tissue and primary hepatocytes, preventing hepatocyte protein synthesis in a manner that is largely dependent on its ability to suppress mTORC1

signaling [232]. A recent study of Fragile X syndrome (FXS) linked metformin treatment to decrease *de novo* protein synthesis rates in FMRP-deficient human neurons. This has been of great interest, as the loss of FMRP has been shown to lead to elevated protein synthesis and is thought to be a major cause of the synaptic plasticity and behavioral deficits in FXS. It is suspected that the increase in protein synthesis results in part from abnormal activation of key protein translation pathways downstream of ERK1/2 and mTOR signaling [233]. Another potential pathway for the effect of metformin comes through the v-ATPase-Ragulator lysosomal pathway [222] which could coordinate mTORC1 and AMPK, two hubs governing metabolic programs. An experiment in *C. elegans* demonstrated that both v-ATPase-mediated TORC1 inhibition and v-ATPase-AXIN/LKB1-mediated AMPK activation contribute to the lifespan extension effect of metformin [234].

5.2. Exercise as a CR mimetic

Physical activity increases health span and life expectancy in human epidemiological correlations [235]. In this regard, exercise and CR result in an overlapping phenotypic outcome in terms of mitochondrial function and oxidative metabolism, reduction of ROS, DNA stability and even autophagy. Even though exercise and CR affect energy intake (at least in some individuals) and expenditure in a diametrically opposite manner, the shared regulation of a number of phenotypic changes in skeletal muscle and potentially other tissues could underlie the similar health benefits of both interventions. Importantly however, are the effects on muscle and cardiovascular function as well as body weight and energy metabolism observed after exercise and CR [4,236].

Because of its central role in the oxidation of fuels, skeletal muscle mitochondria is an important aspect of aerobic exercise (EX), a condition of increased whole body energy flux characterized by general cellular fitness and healthy aging [237–242]. It was first demonstrated more than 4 decades ago that EX training promotes skeletal muscle mitochondrial biogenesis and enhances the capacity for glucose and fatty acid oxidation [243]. EX training is frequently prescribed for the treatment of chronic diseases including type 2 diabetes, insulin resistance, sarcopenia, CVD, and cancer [244,245]. A wealth of data demonstrate that EX increases mitochondrial mass, mitochondrial DNA (mtDNA) content, OXPHOS enzyme activity, and maximal ATP production [246–248]. These adaptations contribute to an increase in basal metabolic rate and an increase in calorie consumption [249], and skeletal muscle plays a major role as an energy-consuming tissue in animals and undergoes significant structural and metabolic adaptations in response to altered contractile activity and nutrient availability [1].

Dietary CR, in contrast to EX, causes a reduction in basal metabolic rate and body temperature [250], and delays the onset of many age-related diseases, including type 2 diabetes, hypertension, CVD, and cancer [244,251]. Importantly, as reported earlier, CR extends mean and maximal lifespan in diverse species, including yeast [252], worms [253], flies [254], murine animals [255], and nonhuman primates [256–258], consistent with increases in cellular fitness. It has been proposed that CR retards the rate of aging in part by reducing steady-state levels of mitochondrial oxidative stress and oxidative damage to mtDNA [259,260].

Although both CR and exercise have similar beneficial effects on general health, it is not known though whether similar mechanisms promote these effects. It is well accepted that EX training promotes muscle mitochondrial biogenesis [239,243,261–266]. Despite the reduced basal metabolic rate, it has been proposed that CR also induces mitochondrial biogenesis. Nisoli et al. reported that 30% CR for 3 months increased mitochondrial biogenesis in mice, as evidenced by increased mtDNA, increased cytochrome c (Cytc) protein, increased cytochrome oxidase subunit IV (COX-IV) protein, and increased mRNA expression of key mitochondrial markers [267]. Soon after, it was reported that CR induced the proliferation of mitochondria with reduced membrane potential and mtROS production rate [268], increased oxidative capacity [237] and increased expression of key mitochondrial markers [269]. In humans, Civitarese showed that 6 months of 25% CR resulted in a ~35% increase in muscle mtDNA content [270].

Multiple investigators, however, have reported data in opposition to the hypothesis that CR results in increased mitochondrial biogenesis. Hancock et al. reported that 30% CR in rats had no effect on the expression of key respiratory chain protein complexes associated with mitochondrial biogenesis, the expression levels of 6 key mitochondrial markers, the coordinately regulated GLUT4 transporter, or CS activity in the brain, muscle, liver and heart [271]. Similarly, Sreekumar *et. al* found that reduced calorie intake in rats had no impact on muscle mitochondrial ATP production or CS activity [272].

Recently, lifelong CR in mice was shown to prevent the age-related loss of oxidative capacity without increasing mitochondrial abundance [273]. Taken together, these results argue that total mitochondrial content and oxidative capacity are unaffected by CR in multiple tissues, contrary to other reports supporting CR-induced mitochondrial biogenesis. Indeed, these conflicting results may be in part due to the reliance on surrogate markers like mRNA, and static protein concentrations. Mitochondrial biogenesis and degradation are inherently kinetic processes and mRNA and protein concentration may not be accurate metrics.

6. OTHER POTENTIAL CR MODULATORS

As the world's elderly population surges at an accelerated pace, it presents several public health challenges. In this regard, CR has been linked to lifespan extension and preserved cellular homeostasis. Recently, a meta-omics renaissance has changed the way the mechanisms of aging and disease are studied. An interesting link between nutrition and human health is the host-microbiome interaction. It has been observed that dietary regimens have incredible implications to the health of an organism, and these effects are reflective of the gut microbiome to a great degree. This has brought to the forefront great interest into understanding how the microbiome changes through dietary interventions like CR and how the remodeling of the microbiome guides the host.

6.1. Host-Microbiome Interactions during CR

From the efforts of the meta-omics renaissance, we have learned a paradigm in which the essential role of microbial communities to human health can be modulated through nutrition. Furthermore, the elucidation of host-microbiome processes through meta-

omics studies depend heavily on the identification of novel biomolecules and requires our ability to assign them specific functions in terms of enzymes and small molecules.

In light of these requirements, great interest has been placed on MS methods as a means of expanding the understanding of how CR leads to lifespan extension through the regulation of the gut microbiome. The identification of bacteria through reliable genomic technologies in conjunction with novel MS methods to detect changes in polymers like metabolites has several advantages over classical experimental methods.

The use of 16S rRNA gene sequences to study bacterial phylogeny and taxonomy has been by far the most common housekeeping genetic marker and a mainstay of sequence-based bacterial analysis for decades [274,275]. This approach has been of particular important in the identification of bacteria with unusual phenotypic profiles, rare bacteria, slow-growing bacteria, and uncultivable bacteria among others [276]. Not only has it provided insights into etiologies of infectious disease, but it also helps clinicians in choosing antibiotics and in determining the duration of treatment and infection control procedures. Indeed, rapid and reliable identification of bacterial pathogens directly from patient samples is required for optimizing antimicrobial therapy [277].

Although sequencing of the 16S rRNA gene is a common approach, species identification and discrimination is not always achievable for bacteria as their 16S rRNA genes have sometimes high sequence homology [277]. Unlike 16S rRNA sequencing, shotgun metagenomic sequencing is capable of reading the whole genomic DNA in a sample. This approach has been used to reveal the functional potential of a microbial population, being successfully applied to investigate microbial diversity, adaptation, evolution, and function [278]. On the other hand, metatranscriptomes (total RNA-based) has been shown to represent a more clear picture of microbial composition divergence [279]. In this regard, metatranscriptomics seem to avoid potential biases caused by mRNA enrichment and allow simultaneous use of rRNA for generation of compositional profiles [279,280]. Therefore, combining metatranscriptomic and metagenomic methods can potentially allow for a better link between the microbiome with host phenotypes [279].

The mammalian gastrointestinal tract harbors a complex community of over 100 trillion microbial cells that can influence host physiology, nutrition, metabolism, and immune function. Indeed, these microorganisms are suspected to be responsible for a number of functions within an organism through byproducts such as fermentation of macronutrients and have been reported to contribute to variation in the health of an organism [279]. The intestinal microbiota can influence the whole-body metabolism by affecting energy balance [281–283]. However, the microbial signals that guide the mechanisms and functional alterations causing the observed phenotypic and morphological changes that regulate energy homeostasis during CR, remain poorly understood [284].

Profiling of the microbiota composition in the cecum and feces by 16S rRNA gene sequencing from mice under CR (30% reduction) revealed a significant increase in Lactobacillaceae and Erysipelotichaceae and a decrease in other Firmicutes families,

as well as increased Bacteroidaceae and Verrucomicrobiaceae, the latter represented by *Akkermansia muciniphila* [284]. This was in line with previous studies that showed that CR had a unique gut microbiota dominated by potentially beneficial bacteria such as *Lactobacillus spp* in mice [285] and Fisher 344 rats [286]. In addition, metagenomics analysis identified decrease system modality of DNA metabolism in feces upon CR, while an increase of the Arabinose Sensor and Transport after was observed in both secum and feces. Another system of interest shared in both samples and decreased upon CR was the Cell Wall and Capsule, a system that includes the biosynthesis of lipopolysaccharide (LPS), known to be positively correlated with host BW and insulin resistance [284,287].

The dysbiosis of gut microbiota has been proven to be associated with several intestinal diseases, such as inflammatory bowel disease and colorectal cancer, as well as some systematic diseases such as diabetes and neurological diseases [288]. Further studies on using 16S rRNA gene sequencing on CR models have been done to explore such pathologies. In this regard, mucositis can be induced by immunosuppressants during chemotherapy such as Cyclophosphamide (CTX) and is seen in up to 50% of cancer patients [289]. This in turn is believed to cause at disruption of the gut microbiota that can lead to severe intestinal complications. A recent study observed the effects of CR on CTX-induced mucositis. CR mice showed significantly less mucositis in response to CTX, including lower intestinal permeability, less bacterial translocation, higher number of epithelial stem cells, and less epithelium damage [290].

Indeed, experimental animal models of CR have been demonstrated to induce changes of the intestinal microbiota composition, regardless of fat content and/or exercise [286]. Metabolomic studies on dietary compounds and phytochemicals that may modulate bacterial abundance within the gut have suggested dietary interactions with microbiome composition are able to alter host metabolism [291].Another approach to understand the role of CR in health is metabolomics - the measurement of hundreds of small molecule metabolites, their precursors, derivatives, and degradation products [292]. In human plasma samples of male subjects under CR, metabolomic analysis revealed distinct metabolomic signature associated with acute CR characterized by a shift in energy usage from carbohydrate to fat utilization with increased lipolysis and β-fatty acid oxidation [292]. Further metabolomic (metabonomic) approaches on the effects of CR have yielded interesting results. For example, studies in dogs and monkeys revealed that CR was associated with changes in urinary bacterial metabolites, suggesting a potential connection among the gut microbiota, CR and aging [285,293,294].

Metaproteomic profile studies on rat gut microbiota after CR revealed an induction of changes, such as a reduction of the Firmicutes/Bacteroidetes ratio and an expansion of lactobacilli. Furthermore, expression changes of the microbial enzymes responsible for short-chain fatty acid biosynthesis were observed by which CR boosted propionogenesis and limited butyrogenesis and acetogenesis [295].

7. CONCLUSION

Metabolic regulation, an emerging hallmark of aging, is a clear focus of research today with the goal of developing treatments targeted not only to extend health but increase

lifespan. It has been shown that during aging, there are multifarious alterations to metabolic pathways, from mutational heterogeneity causing cancer, to protein dysregulation. From well-understood nutrient-sensing proteins, such as AMPK and mTOR, to insufficiently understood processes, such as maintenance of proteostasis, aging's impact on the metabolic landscape is wide-ranging and still poorly understood. Working to understand the variety of metabolic variations in the context of aging will pave the way for a more comprehensive understanding of the different iterations of age-related diseases and enable the development of therapies with to improve quality of life.

A fuller understanding of interventions with implications in lifespan extension will allow for more nuanced treatments targeting specific alterations. Some of these steps are already being taken, particularly in the realm of CR, the most robust intervention to extend health and lifespan in numerous animal models. Current efforts focus on understanding how CR creates an array of metabolic adaptations. Such efforts are spurred by the discovery of increased anti-aging activity upon maintenance of proteins and increased expression of immunoprotective genes among others. In addition, new perspectives on how CR modulates health and lifespan extension hold promise for novel therapies through CR mimetics. By targeting the deleterious effects of aging, it is hoped that CR, through its intrinsic metabolic alterations, can open new avenues in therapeutics. As our understanding of aging's metabolic landscape expands, however, an increasing number of targets arise, and with the aim to effectively understand how each contributes to improvements in quality of life, it is necessary to reach for all possible experimental tools. Perhaps one of the most fruitful - yet rather underutilized - approaches is to investigate the natural protein flux dynamics as a way to understand how the cell "thinks." Previously, researchers have lacked efficient assays to measure protein dynamics, but the meta-omics era has provided viable options for deciphering molecular identities in complex samples. Several interventions mentioned in here, such as metformin administration and exercise, have been integral to our understanding of metabolic alterations under CR. Cellular energy adaptation is a particularly persuasive example of the power of CR, as it has linked various lifespan extension interventions, such as rapamycin administration, with CR regulated pathways. In order to continue understanding how age-related diseases can be prevented, investigation into CR, its targets and mimetics must continue to be pursued.

This chapter serves to underscore the importance of researching CR's metabolic alterations. However, I recognize that the current state of knowledge is vastly incomplete – though an enzyme may be implicated with the response of CR, such as AMPK, simply increasing its activity can produce a number of negative physiological effects, specially under disease conditions [296,297]. As the field continues to develop, our understanding of CR's metabolic implications is expanding beyond the simplistic, singular cause-and-effect relationships and yes-or-no effects as exemplified by the opposing effects of CR in the lifespan of rhesus monkeys observed between the NIA and WNPRC studies discussed earlier. Though a broad approach to answering a scientific query is necessary, a more in-depth understanding will become necessary to effectively create preventative outcomes to diseases.

8. FIGURES

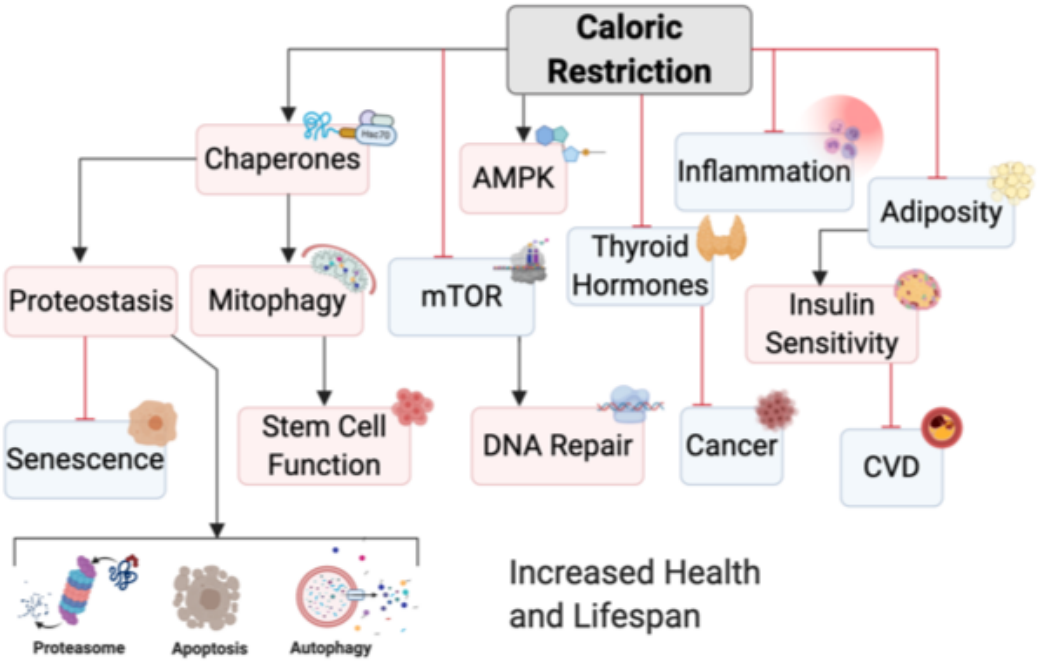

Figure 1. CR effector pathway linked to increased health and lifespan.

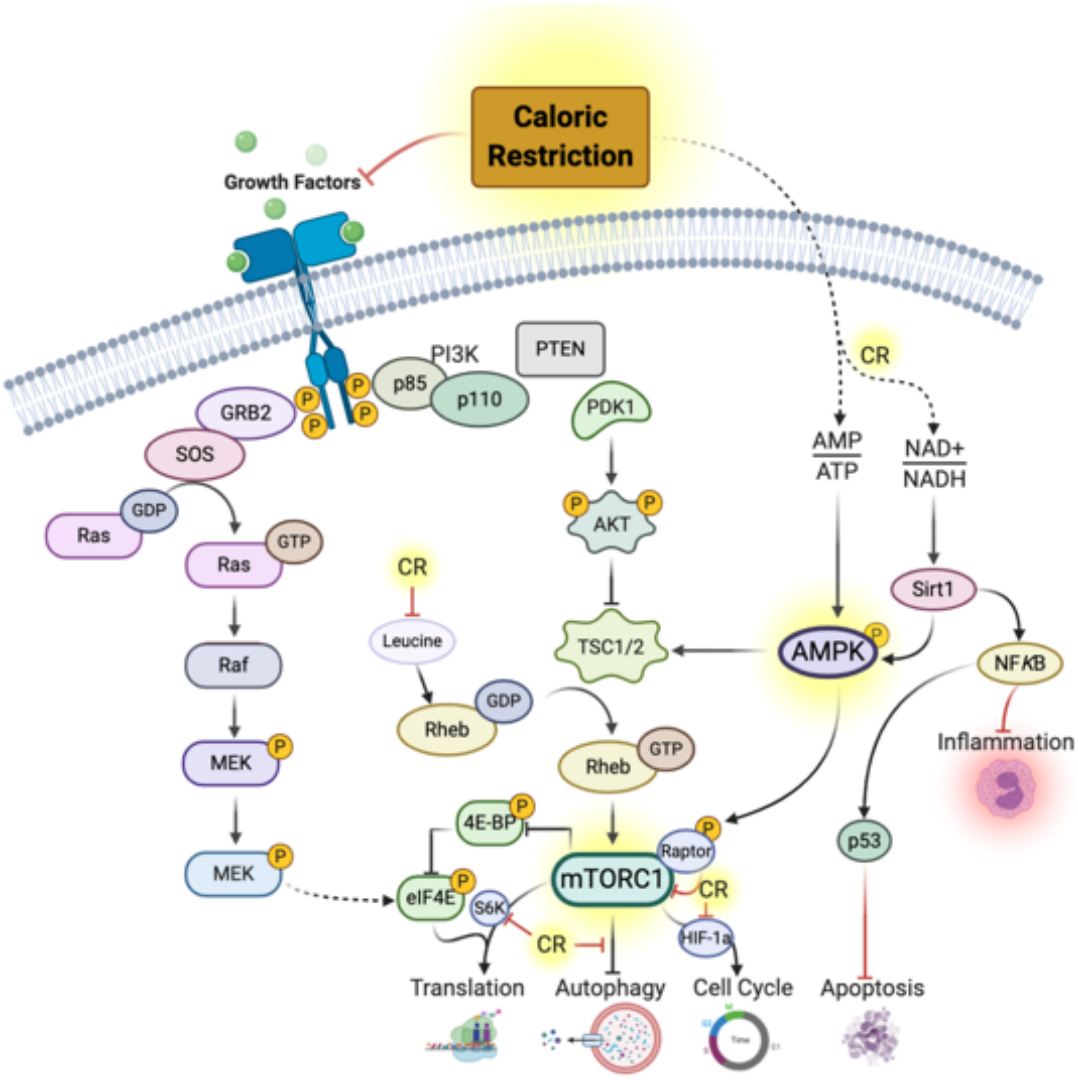

Figure 2. Mammalian energy-sensing pathways implicated in CR. A complex crosstalk exists between the energy-sensing pathways in mammals. The complexes of mTORC1 and AMPK are regulated by CR. AMPK is activated at low ATP levels while mTORC1 is inhibited under low energy conditions.

CHAPTER TWO: *In Vivo* Proteome-Wide Measurement of Protein Kinetics Using Metabolic Labeling

1. INTRODUCTION

As discussed in Chapter One, CR has many levels of complexity and as such requires new investigative approaches. Numerous regulators of CR are involved in protein synthesis. In fact, protein translation is at the center of cell function and its high energy demand is a primary focus within the scope of CR. This brings to attention the need for understanding how translational control, as a regulated process, can be altered under lower caloric intake that shifts the translational capacity or transcripts selected by the cell. However, our capacity to measure dynamic changes in complex samples had been very limited in part due to a lack of experimental methods that can allow the measurement of molecular fluxes at a large scale. Here we explore proteome dynamics by MS as an observability method by which global protein fluxes can be measured through stable isotope labeling in conjunction with proteomics.

2. PROTEOME DYNAMICS

In 1961, Dintzis published his seminal paper on the assembly of peptide chains during translation of mRNA. He showed that protein synthesis happens sequentially from N-terminus to C- terminus [298]. Since then, great efforts have been placed to study protein synthesis. The dogma of gene expression as a master regulator of protein translation has resulted in the general view that transcript levels represent a metric of protein synthesis. This view has allowed mRNA levels to be widely accepted for decades as a direct marker of protein synthesis. However, recent quantitative and genome-wide analyses revealed a larger contribution of translational regulation to the final output of proteins in cells than previously thought [192,299–301]. Indeed, although the biochemical fundamentals of protein synthesis have been well studied in great detail *in vitro*, monitoring protein synthesis *in vivo* has been a demanding task. Thus, diverse approaches have to be developed in order to explore the translational status of cells.

Most biomolecules are composed of hydrogen, carbon, nitrogen, oxygen, and sulphur. It is known that the natural isotopes of these elements occur with different probabilities [302–304], and in some experiments the relative abundances of an element's isotopes can be manipulated by using a technique known as stable isotopic labeling [305]. The relative abundances of isotopes determine a molecule's isotopic distribution, which can be measured experimentally using a MS. The elemental composition of the measured element can then be compared and identifying within a library of known compounds sharing the unique signature of the underlying molecule. The isotopic distribution allows for the prediction of masses and abundances of the isotopes for a given formula **(Figure 1)**. In this example, an amino acid like alanine, under natural abundance, will have an isotopic distribution at an exact center of mass m/z of ~72.1 which can be visualized through a fine-grained (high-resolution) isotopic distribution based on a polynomial-based algorithm. The mass intensity under natural abundance of alanine can be distributed as 96.1% M0, 3.64% M1, and 0.25% M2. However, when the charge state of a molecule changes through positive charges as the number of added hydrogen ions (eg. ^{2}H: 2) increases, it changes the elemental composition of the molecule. In the case of alanine, the isotopic distribution at the exact center of mass m/z in the 2+ charge state shifts to ~36.6. Considering the measured precursor pool enrichment as 10% (p = 0.1) influences the charge distribution where 86.5 % M0,

1.29% M1, 0.06 % M2, and 0.003% M3. More complex molecules like di- or polypeptides will have a different isotopic distribution. In the case of alanyl-tryptophan, the isotopic distribution of the exact center of mass m/z is ~258.3 under natural abundance. But when the charge from ^{2}H is considered for this di-peptide, the isotopic distribution centers around the mass m/z of ~129.7.

3. EXPERIMENTAL APPROACH

In order to deal with biological complexity, the aim has been to change the way information is viewed towards a systems approach. To aid in this, high-throughput and quantitative exploration can be done through MS. Using proteomics, the presence and/or concentration of a large number of individual proteins in a sample can be measured. Looking at dynamics can then reveal the synthesis and breakdown rate of molecules and in essence elucidate the molecular fluxes through pathways. Therefore, merging these two concepts towards dynamic proteomics fits the criteria of elucidating biological complexity. Through this approach, protein dynamics can be explored through the measurement of the kinetics of many hundreds to thousands of peptides within a complex sample.

The combining of non-radioactive stable isotope labeling with the brilliance of tandem MS can create a powerful approach to understand protein fluxes **(Figure 2)**. In this example, a stable isotopically enriched precursor like heavy water ($^{2}H_2O$, D_2O, or deuterated water) is administered to an organism like a mouse. Maintaining the concentration of $^{2}H_2O$ at ~5% of the total body water will then allow for the deuterium to incorporate into every biological process which requires hydrogen during its synthesis. After a labeling period, the tissues and samples must be collected. Within the sample of interests, proteins can then be processed and amended through cleanup methods like in-gel separation. Afterwards, they can then be trypsin digested. Running the thousands of peptides generated on an LC/MS/MS can then allow for its identification, telling the investigator the identity of the protein from which the peptide came from.

Looking at the pattern of labeling **(Figure 3)** can then tell its functional information such as the synthesis and breakdown rates. Under non-labeling conditions (p=0%), each biomolecule has a natural abundance isotope pattern with a signature. When introducing labeling (eg. p=25%), such as deuterium, into the system it creates a perturbation pattern that we can then interpret through informatics by mass isotope distribution analysis. The concept of mass isotopomer distribution has been applied for the measurement of biosynthesis and turnover of polymers [306] through increases in abundances of isotopic isomers under experimental conditions. This results in the enrichment of specific isotopologues in the metabolic product in contrast to its natural abundance. The deconvolution of the mass intensities from the isotopomer enrichment is essential to understanding its distribution [307]. This can be achieved by comparison of statistical distributions predicted from binomial or even multinomial expansion to the pattern of excess isotopomer frequencies observed in the measured polymer.

4. CONCLUSION

Quantification of mass isotopomer distributions in peptides is a powerful tool to estimate fractional synthesis rates of individual proteins through a labeling period. Unlike traditional proteome techniques which are static in nature, this approach provides information regarding their active synthesis and breakdown during the labeling period, in essence turning the information into biological fluxes of living systems. Advantages of this approach include the fact that changes in isotopomer abundances are not really sensitive to changes in protein yield or recovery during collection and preparation. As such, these methods provide an internalized system for measurements irrespective of differences in protein abundances between samples.

.

5. FIGURES

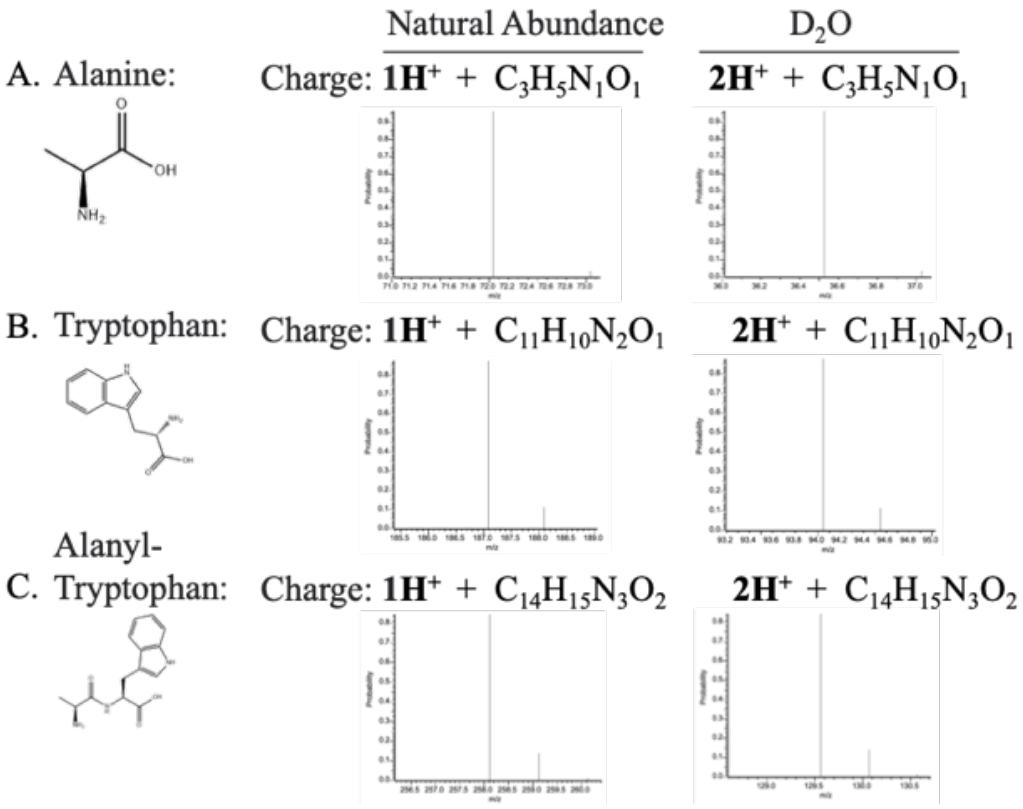

Figure 1. Molecular Isotopic Distribution. Elemental composition of molecular amino acids under natural abundance or with ^{2}H incorporation is shown here through a polynomial based method. **(A)** Alanine is shown at two different charge states and its isotopic distribution mass (Da) is represented at its expected center of mass m/z. **(B)** Tryptophan is shown at two different charge states and its isotopic distribution mass (Da) is represented at its expected center of mass m/z. **(C)** Alanyl-tryptophan is shown at two different charge states and its isotopic distribution mass (Da) is represented at its expected center of mass m/z.

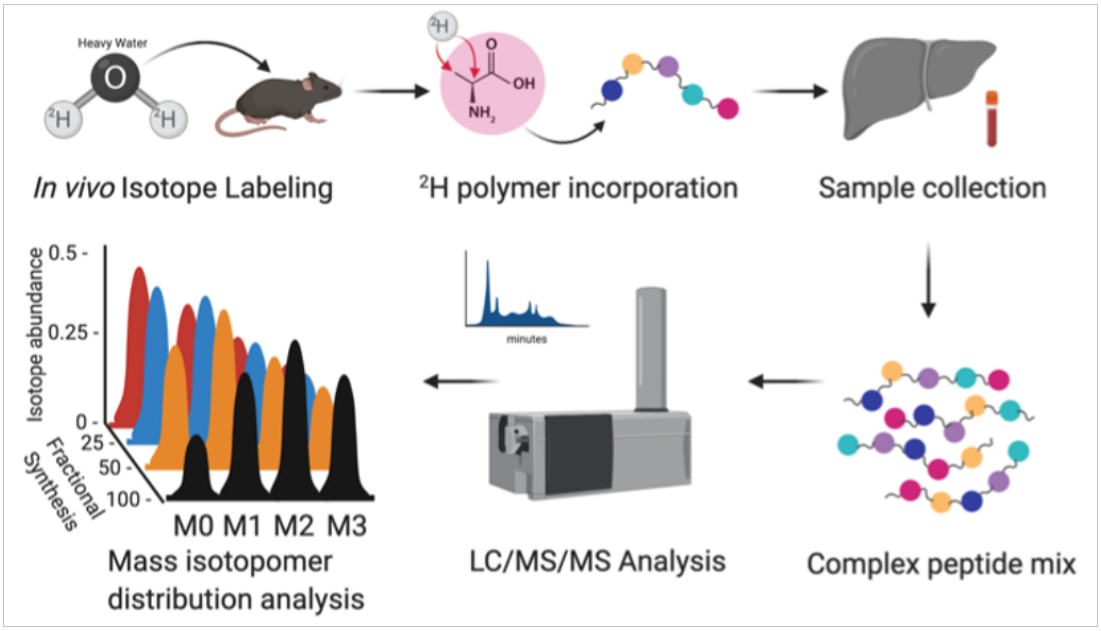

Figure 2. Experimental approach for measurement of *in vivo* protein dynamics across the global proteome.

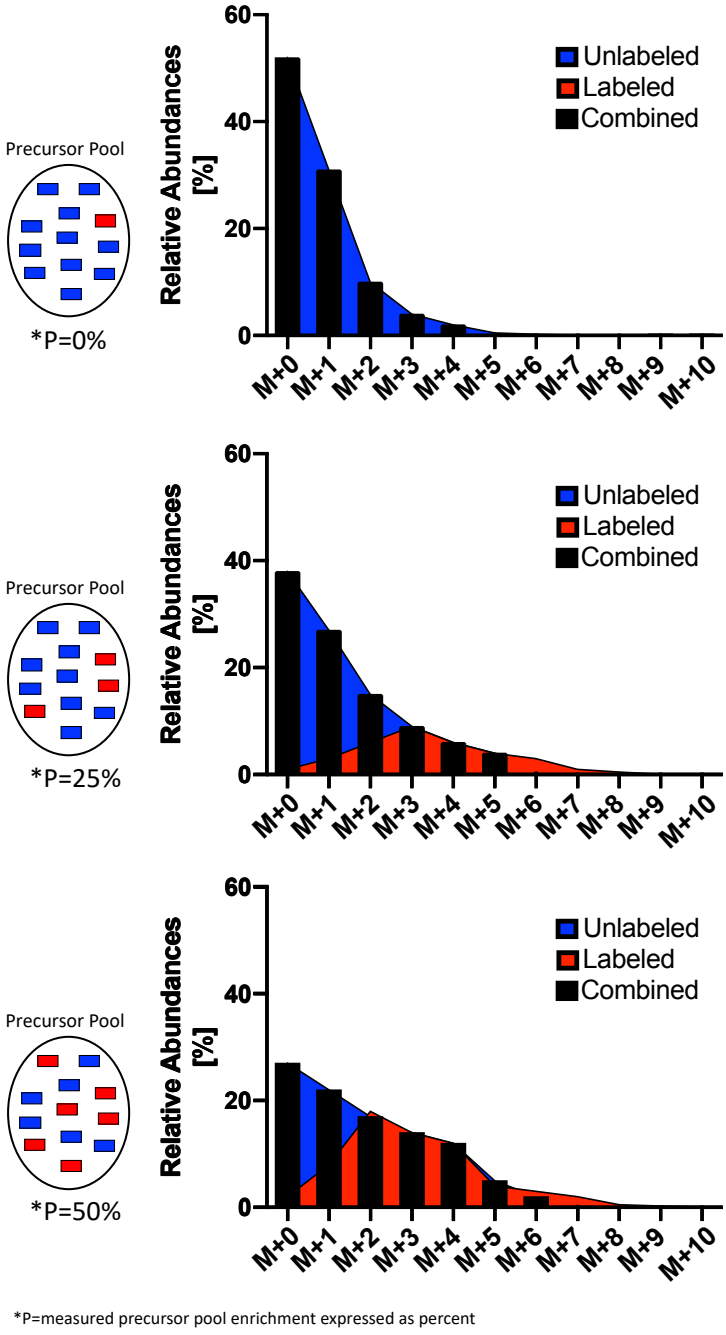

Figure 3. Stable isotope label incorporation in polymers at different *p* with resulting isotopomer relative abundances. *p* = the measured precursor pool enrichment expressed as percent.

CHAPTER THREE: Time-Course of Proteome Turnover Rate During Calorie Restriction in Mice Reveals a Discrete Transition Period and no Correlation with Gene Expression

1. INTRODUCTION

CR is one of the most robust interventions to maintain health and extend lifespan in murine models. Considering that the mouse is a warm-blooded mammal with many similarities to humans, including the genome level (discussed in Chapter One), murine models are widely popular experimental models. However, there are several considerations that need to be taken into account when interpreting experimental results during CR, and variabilities in a number of factors can change their interpretation. The role of gender, strain, and even level of CR can influence the outcome. An elegant study by Mitchell *et.al.* proved this point by comparing the role of strain and sex on the lifespan of mice on varying degrees of CR. They compared male and female C57Bl/6J and DBA/2J mice under either a 20% or 40% CR intervention starting at 6 months of age and for the remainder of their lives. They reported that in C57Bl/6J mice, 20% CR significantly improved survival, with a mean lifespan extension of 40.6% (the longest lifespan extension at 190 weeks of age). in females and 24.4% in males [308].

Another factor that can become confounding in age-related research is the age of the experimental animals. In mice, the juvenile period spans from 0.5 to 4 weeks of age, followed by puberty until they are ~10 weeks old. Adulthood is then considered between ~10 to 64 weeks followed by a reproductive period of senescence [309]. Age is also closely related with occurrence and development of disease, and timing of CR in mice has been shown to impact phenotype [310]. Typically, mice used in studies are ~6-8 weeks old which is considered within the age of puberty [309]. In CR studies, there has been broader discretion for the timing of CR. In this regard, a seminal work on lifespan extension showed that among groups of mice in different levers of CR and starting at ~4 weeks of age, the degree of CR was directly related to the reduction in body weight and the increase in average and maximal life spans. However, when CR was started at ~52 weeks, the lifespan was also extended, although to a lesser, suggesting a primary role for CR during the developmental period [311,312].

The length of intervention is another variable that changes considerably between studies when trying to elucidate the CR response. For example, a study using male 21-week-old C57Bl/6J mice placed them on a low CR (12%) for 10 week [313]. Another experiment subjected mice to CR starting at 14 weeks, though the time they remained on the diet varied from about 6.5-23 months [314]. Therefore, defining not just what entails a short-term CR intervention and how it can be distinguished from longer-termed CR duration but its effects in the organism is important [315]. In this regard, it has been suggested that the benefits of CR occur rapidly upon initiation, and the experimental literature usually classifies these as “short-term” studies. On the other hand, “long-term” studies are traditionally those that span the lifespan of the animal model [316]. However, short-term interventions of CR in mice are difficult to define because of the lax use of this term. In addition, extrapolation to human interventions will surely be more relevant with interventions that are not life-long.

In a study of CR in mice, Mahoney *et.al.* restricted C57Bl/6J’s for 3 weeks, choosing that length of time because it reduced body weight by approximately 15–20% [317]. However, Robertson *et.al.* modeled weight changes and suggested that a ~25% decrease could happen after a week of CR [316]. Even shorter CR interventions in murine models

have been done with positive results, such as 2 weeks of CR (30%) in C57Bl/6J improving survival and kidney function following renal ischemia reperfusion injury [318].

Longer interventions have also been describes as short-term, such as 4 weeks of CR being sufficient to ameliorate age-related alterations in DNA methylome [319]. Indeed, the length of 4 weeks has also been suggested to improve non-homologous end joining (NHEJ) efficiency under CR (40%) [320]. Another study looking at the metabolic effects of CR in Ins2-/- mice, used either 8 or 10 weeks of CR and classified this experiment as short-term [321]. Boldrin *et.al.* further defined CR length of intervention as short (2.5 month) longer term (8.5 and 18.5 months) [322]. Furthermore, short-term CR has also been described for experiments where mice underwent CR from 3 until 15 months of age [323,324], expanding the range in which the literature defines short-term CR from ~3 weeks up to 12 months of intervention. Last for these considerations are the graded effect of CR over time. The most common metrics observed are phenotypic and behavioral such as body weights, insulin and glucose tolerance tests, body composition, and performance tests which can be measured throughout the course of the experiment with minimal invasion [99,217,308]. Body temperature, for example, was shown to have a gradual decline [325].

The manner in which CR has been implemented in longevity experiments is variable, with numerous variables changing between studies. From age and strain to time of feeding and composition of the diet. Since implementation of feeding paradigms over the lifetime is logistically difficult, finding a commonality like a biomarker is essential to the implementation of CR in different experimental models. A consistency within all parameters could be the model in which alterations in protein synthesis and proteostasis functions to establish health and lifespan extension. As discussed in Chapter One, numerous models of lifespan extension indeed are characterized by reduced signal or expression of protein synthesis machinery. Accordingly, the goal here was to test the hypothesis that reduced fractional synthesis rates of proteins across the global proteome is a biomarker of lifespan extension in mice that is induced over a discrete and narrow timeframe between days 25 and 32 of CR and no correlation with changes in mRNA levels.

2. RESULTS

Here, we elaborate on our prior observation [7,194,326] that CR leads to a marked slowdown of proteome replacement rates in the liver with the goal of understanding the time-course of reduction in proteome-wide protein synthesis rates during CR. After an acclimatation period and starting at 6±1 weeks of age, mice were single caged and underwent CR (30% less food intake than control/week) for 0 (no CR), 9, 14, 20, 25, 27, 28, 29, 30, 31, 32, 40, 42, 73, or 170 days. ^2H_2O labeling was for the 4-5 days before SAC **(Figure 3-1A)**. To determine whether the global slowing of protein turnover develops gradually or discretely at a specific timepoint during CR, we combined metabolic labeling by ^2H_2O of hepatic proteins with tandem mass spectrometric analysis of mass isotopomer abundances in peptides in C57Bl/6J mice (n=120) under CR at serial timepoints.

The most commonly measured parameter for CR is a reduction in body weight. Mice were weighed at regular intervals throughout the experimental timeframe **(Figure 3-1B)** and a significant reduction in body weight ($p<0.05$) was observed within a week of the start of the experiments. Plasma glucose levels (mg/dL) **(Figure 3-1C)** under fasting for 4-6 hours in both Con and CR were then assessed over time. The data show a relatively rapid effect of CR on glucose sensitivity, one of the markers of CR on health span.

For *in vivo* stable isotope labeling in conjunction with mass spectrometry, analysis was done at each time-point in our time-course to determine the time evolution of proteome-wide reduction in protein synthesis rates. The stable isotope tracer used in this experiment was heavy water (^2H_2O). ^2H_2O was given IP to immediately raise the body water to ~5% enrichment and then as 8% ^2H_2O in the drinking water to maintain the ~5% ^2H_2O enrichment body water enrichment during the labeling period [7,194,326]. Because the hydrogens or protons in solvent water are used in almost all biological reactions and processes, including entry into C-H bonds during intermediary metabolism and synthesis of non-essential amino acids and transamination of essential amino acids [305,326], this allows ^2H to be incorporated covalently into newly synthesized polymers such as polypeptides. Because stable peptides and proteins once formed do not exchange hydrogen in covalent C-H bonds with solvent water [305], this labeling approach tags only proteins that were newly synthesized during the period of label exposure.

Through this approach, we measured *in vivo* hepatic proteome-wide dynamics of individual proteins by quantifying the rate of incorporation of deuterium from heavy water into proteins, as previously described [326]. After the period of labeling (4-5 days), liver samples were collected, and the complex peptide pool recovered after trypsin hydrolysis of the mixture of unlabeled and labeled proteins was run by LC-MS/MS analysis. Peptide identification was carried out by protein informatics and isotope incorporation was analyzed by mass isotope distribution analysis (MIDA) to calculate flux rates of each peptide that passed analytic criteria [305,306,326]. Peptides were rolled up into their parent protein and the mean value was used to calculate replacement rate of the parent protein [7,194]. The hepatic proteomic analyses **(Figure 3-2)** were conducted in C57Bl/6J male mice with the onset of CR (30%) intervention starting at 6 or 7 weeks of age. The number of identified proteins with measurable kinetic values varied among experiments from 96 proteins in the lowest set to 269 in the highest **(Figure 3-2)**. The protein turnover rates under CR were compared to their matched *Ad lib* control and each protein was considered as upregulated when fractional synthesis rates [FSR] was higher in CR or downregulated when FSR is lower in CR **(Figure 3-2)**. Only proteins for which kinetic values were measurable in both CR and AL groups were used in comparisons.

There were generally modest or no apparent changes in the number of proteins with a slower turnover rate under CR between days 0 and 25 of intervention **(Figure 3-3A through 3-3B)**. Strikingly, however, what followed was a dramatic slow-down in the rate of protein synthesis in the CR group that reached 75- 85 % of proteins measured by days 30 to 32 **(Figure 3-3A through 3-3B)**. The slow-down became evident though it was somewhat variable in the daily measurements that we carried out between days 25 and 30. This slow-down was then maintained through the measured timepoints between

days 40 to 170, with between ~75-85% of the proteins slowed down at all timepoints **(Figure 3-3A through 3-3B)**. When a cut-off value of greater than 10% higher or lower FSR was used, the transition between days 25 and 32 became even more striking (**Figure 3-2**). Before day 25, fewer than 20% of measured proteins achieved this cut-off of 10% higher FSR than in controls, but by days 30 – 32, about 60% of proteins measured achieved this 10% higher FSR cut-off value.

We used a sequence enrichment analysis approach using genome-wide expression profiles [327] to look for significant changes in proteome dynamics between days 25 and 30. We were able to identify sets of genes that are enriched in four main datasets (Hallmark, gene ontologies v7, KEGG, and Reactome). This approach allowed us to consider not only gene ontologies but the changes in gene expression of all genes belonging to the dataset. We observed that at 25 days of CR, 104 out of the 210 datasets showed "upregulation", or higher replacement rates, for the gene set collections found in the databases used. Of this, 10 gene sets were significantly enriched at an FDR < 0.25 **(Figure 3-4A)** in which proteolysis, apoptosis and cytokines stood out as potential proteostasis modulators. In comparison, an almost identical fraction of 106 out of 210 data sets were higher in the Con group and none were significant by any stringent statistical analysis. At day 30 of CR, only 19 out of the 210 data sets used for analysis were upregulated in the CR group and none were statistically significant by sequence enrichment analysis whereas 191 out of 210 data sets used for analysis were downregulated under CR and of these 6 were significantly enriched at nominal ($p<0.05$) value **(Figure 3-4B)**, in which OXPHOS processes stood out. Ranked list correlation profiles of FSR values at day 25 **(Figure 3-4A)** revealed an equal distribution of up and downregulated data sets that shifted to almost an all-downregulation of ontologies at day 30 **(Figure 3-4B)**. Looking at the "leading-edge" allowed us to determine which subsets of genes contributed the most to the enrichment signal of a given gene set's leading edge (core enriched). Our analysis of genes enriched within the datasets revealed various proteins involved in proper protein folding (HSP90AB1, HSP90B1, HSPA9, and PDIA3) to be significantly regulated at day 25 **(Figure 3-4A)**. The leading edge analysis of genes enriched at day 30 **(Figure 3-4B)** showed increased expression of the enzyme serine hydroxymethyltransferase (SHMT1) which has a key role in one-carbon metabolism and control of cell proliferation [328]. A notable shift, however, was a decrease of HSP90B1 as previously observed [329].

To obtain a comprehensive view of gene expression during CR in the final time point that showed a lack of observable inhibition of global protein FSR, we performed RNA-seq on hepatic RNA after 25 days of CR **(Figure 3-5A)**. The experiment yielded 15,082 genes after filtering out low-quality reads. Gene Sequence Enrichment Analysis was then used to analyze leading edge genes within gene overlaps. The two biggest overlaps observed **(Figure 3-5A)** were between OXPHOS signal with mitochondria complex I biogenesis, and translation signals with NMD signals. Further data characterization was performed using gene enrichment scores to define some of the major biological themes **(Figure 3-5A)** within an enrichment map including clusters of either up- or downregulated groups. Of note was that no downregulated genes were observed in any particular biological theme. Nevertheless, a number of gene clusters for eukaryotic translation and respiratory electron transport were observed.

A similar approach was done for gene expression during CR in the initial time-point with a high level of inhibition of protein FSR. We performed RNA-seq on hepatic RNA after 30 days of CR **(Figure 3-6A through 3-6C)**. The experiment yielded 15,239 genes after filtering out low-quality reads. Gene Sequence Enrichment Analysis was then used to analyze leading edge genes within gene overlaps. The two biggest overlaps observed **(Figure 3-6B)** were consistent with what we observed at day 25 between OXPHOS signal with TCA Cycle signal, and translation signals (and 43S cap formation) with Slit and Robos signals. Of note is that slits are highly conserved glycoproteins that are secreted to regulate several processes like neuronal axon guidance, cell proliferation, cell migration, and vascularization, via binding to Robo receptors [330]. Further data characterization was performed using gene enrichment scores to define some of the major biological themes **(Figure 3-6C)** within an enrichment map including clusters of either up- or downregulated groups. Of note was that, unlike day 25 where no downregulated genes were observed, we saw four clusters decreased of which two (interferon alpha and interferon beta signaling) play a fundamental role in immunity. In addition, a large cluster of genes for translation initiation and TCA cycle were observed.

In order to understand if there were uniquely regulated genes between days 25 and 30 of CR, we sorted the genes by those with a log2(FC) $\geq$ 0.1 between control and CR. Using that cutoff, we then compared overlapping genes in both timepoints and represented them by Venn diagram **(Figure 3-7A through 7-3B)**. Considering the genes not overlapping at day 30, we then analyzed them through systems-level datasets [331]. The metascape gene analysis revealed several pathways uniquely upregulated at day 30 **(Figure 3-7A)** of which the AMPK signaling pathway stood out (this is discussed in Chapter 5, where we test the effects of metformin). Uniquely downregulated gene analysis **(Figure 3-7B)** further confirmed a decrease of protective gene signals.

It is well understood that long-term CR leads to lifespan extension and preserved cellular homeostasis. Indeed, many studies on CR have focused on its life-long effects through lifespan studies. However, an important question on the effects of CR is whether this intervention generates its functional benefits at the onset of restriction, through a progressive accumulation of metabolic alterations, or even across a discrete time period along the length of interventions. At the beginning of CR, the organism can be considered, in general, under a newly imposed semi-fasting state [332]. What follows can be contemplated as an integrated series of metabolic adaptations where the organism begins to respond to the newly established energy economy. However, the point in which we can distinguish the biologic onset of objectively measurable biochemical or molecular changes is not known – as most studies vary in onset of experiment and length (from months to life-long in murine models, as discussed earlier).

An important broad observation is that most studies applying CR in mice have required month-long interventions to see a biological response when looking beyond the body weight and related changes that happen very early on. This observation may have important implications into how CR is studied. In this regard, one of the most conserved molecular phenotype in disease states is the signature of protein synthesis [333]. In our hands, CR in rodents results in dramatic reductions in global protein synthesis rates. But these observations had previously been made mainly in mice under CR for months or near-lifetime exposure to CR (e. g. 14 months [7]).

If CR is able to remodel the metabolic profile of an organism earlier, then there may be no need to maintain animal under CR for such long periods of time unless the question is age-related. Similarly, if the effects of CR are gradual and progressive, then we need to delineate the time over which the changes are sufficient to be measurable or robust enough to be significant. However, if there is a discrete timepoint at which CR becomes functional, we can take advantage of that knowledge to explore the actual pathways being altered and apply that knowledge in the development of therapeutic interventions. In these series of CR experiments where strain, sex, age, and diet were kept consistent, we have tried to tackle the difficult question of how and when CR begins to induce it characteristic long-term biochemical and molecular changes.

Our data reveal a surprisingly narrow and reproducible period over which CR slows down the turnover rate of hepatic proteins. This phenotype became evident within a discrete time-period between days 25 and 32 of intervention. These changes are then maintained long after the initial observation of hepatic protein replacement rate slow-down. The question of what the signals and metabolic events are that induce this striking transition between days 25 to 32 of CR opens new avenues for research.

As discussed previously, there is an implicit and rarely tested dogma in which gene expression is taken to be the key regulator of protein translation and therefore a reliable indirect marker of protein synthesis rates. To test this assumption and understand if the FSR values observed under CR are regulated at the transcriptional level we compared our identified protein turnover rates with their gene expression **(Figure 3-8A through 3-8B)**. The FSR values and gene expression results were compared by their log2(FC) between control and CR. At day 25 of CR **(Figure 3-8A)**, we observed an almost even split between gene expression and protein FSRs going the same direction (i.e. 46.8%in which both data types were either increased or decreased by CR). Binomial distribution analysis (2-tailed p: 0.38) showed no significance or a direct correlation between changes in gene expression and protein FSR. Interestingly, at day 30 of CR **(Figure 3-8B)** a larger difference in expression of the two types of data was observed, where 65% of genes and their corresponding FSRs had divergent directional changes in expression effects induced by CR. To further explore the hypothesis that translation regulation is not gene dependent, we tested the protein levels of the P70 S6 kinase (p70S6K) **(Figure 3-8C)**. The phosphorylation of this kinase is activated by a signaling pathway that includes mTOR, and is required for cell growth and G1 cell cycle progression [334]. We saw hints of decreased synthesis rate of this kinase at day 25, however at day 30 we saw a more dramatic inhibition of its activity. Gene expression showed no difference between day 25 and 30.

As a way to explore our observations of differential gene expression related to immunity between day 25 (**Figure 3-4A**; higher gene expression for cytokines under CR) and day 30 (**Figure 3-6C**; lower expression of interferon clusters under CR) we then focused on cytokine expression at the protein level **(Figure 3-9A)**. We performed a profiled array of cytokines through an immunoassay. Of note was that while at day 25 there was an overall increase in cytokines under CR **(Figure 3-9B)**, this was the opposite at day 30 of CR which matched our gene expression analysis. In this instance,

gene expression matches protein content and paralleled the CR effects on protein fluxes of changing during a discrete time period.

3. CONCLUSIONS

An important question that is often hard to answer is how long it takes for a particular intervention to incuse a complex phenotypic response. Having a critical or potentially causal biochemical marker of the broad phenotype can be a great help in this effort, as we show here using the striking slowing of proteome-wide protein turnover rates during CR. If a discrete time-period of induction is identified, a second important question may then become possible to explore: the underlying signals and molecular mechanisms by which this transition occurs. The data presented here show a functional way in which we may be able to understand both when and how CR exposure can induce beneficial effects.

Through proteome dynamics, we were able to make powerful inferences into the period over which CR induces an important functional change. *A priori*, the possible outcomes could be a rapid or immediate reduction on induction of CR in the liver proteome (e.g., days), a gradual reduction over time, or a sudden onset of reductions in either a predictable or unpredictable manner. Here, we demonstrate that during the early stages of CR (between days 9 and 25) there are no significant changes in the FSR of proteins between control and CR. However, over a *discrete time period* we observed a dramatic shift to slower protein turnover rates (starting on days 27-32). This signature remained or became more marked during the later points (days 43-170). This demonstrates for the first time that ~30 days is enough to elucidate proteome wide remodeling of hepatic proteins and that the period immediately leading up to day 25 -32 may be particularly informative for exploring the signals underlying this long-term adaptation.

As discussed earlier, the concept that gene expression is a reasonably accurate metric and driver of protein synthesis and expression is implicitly accepted by many investigators who use mRNA expression as a surrogate marker [335,336]. In order to understand if the sudden shift in protein turnover rates was due to transcriptional or message level control, RNA-Seq was performed at days 25 and 30. Of significance was that while CR increased the half-lives of most of the hepatic proteins between days 25 and 30, this did not occur at the transcriptional level where only a fraction of the genes had a log2(FC)>0.1. When matching the gene expression with their corresponding protein FSR, the discrepancy was even more pronounced, with most genes having almost no distinguishable expression changes when compared to their protein FSRs. At day 25 n equal proportion of genes had variations in expression that were in the same direction as their cognate protein FSR. However, at day 30 there was a wide divergence between direction of gene expression and protein FSR variations.

While little or no direct correlation between gene expression and their protein FSR could be seen, it is clear there is a unique role for gene expression in the biology of CR. Our gene expression changes were analyzed through a stringent statistical analysis through GSEA and Metascape, in which we were able to observe transcriptome drivers. Of note were that in both the transitional CR timepoints (day 25 and day 30), translational gene clusters were highly upregulated, together with energy generating

genes. Interestingly, further interrogation of the data set revealed several pathways uniquely upregulated at day 30 of which AMPK signaling stood out. Our data illustrates here the potential for a flux proteomics approach in providing insight for a complex physiologic adaptation model such as CR and one of the first indications shown to date that the effects of CR may not come uniquely or primarily from transcriptional level modulation.

Although it is clear that mRNA levels were not the primary drivers for protein FSR changes, they can still play a fundamental role in the adaptations of CR. For two observations of significant changes in the gene expression data – an increase in immune response genes at day 25 and a reduction at day 30 in cytokine genes – measurements of protein concentrations paralleled the changes in mRNA levels.

Taken together, these data show that the proteome-wide slowing of protein fluxes which is characteristic of long-term CR as well as other lifespan extending interventions [7] occurs over a strikingly discrete time-period after induction of CR in mice. Moreover, the changes in protein fluxes are not paralleled by changes at the mRNA level. These findings open the possibility of identifying key cellular and organismal signals that underlie this important phenotypic adaptation, by exploring changes before and during a discrete transitional time-period.

4. METHODS

Mice, animal husbandry, diets, feeding regimens and duration of heavy water (^2H_2O) labeling. All mice were maintained were maintained under temperature- and light-controlled conditions (12h:12h light-dark cycle, lights on at 0700h and off at 1900h).

CR Model. For the *in vivo* study, 6-7-week-old male C57Bl/6J mice (Jackson laboratory, Bar Harbor, ME) were used. All mice were housed individually. Mice were randomly assigned to one of the following two groups: ad libitum-fed (AL) or CR. Mice in the AL group were provided unrestricted access to the NIH41 diet (Diet# 58YP, TestDiet, St. Louis, MO). Due to excessive powdering of the NIH41 diet, which prohibited the accurate measurement of food intake in the AL group, mice in the CR group were provided with enough NIH41-fortified diet (Diet# 5TPD, TestDiet, St. Louis, MO) to achieve a 30% reduction in body weight relative to the AL group mean by weekly adjustments. Mice in the CR group were then provided with enough NIH41-fortified diet to maintain a body weight that was ~75% of the AL group mean for the duration of the study. Therefore, the CR mice in this study were effectively on a 30% CR diet. CR mice were provided with food daily at 1200hr. All mice in this study were kept on their diets for a total of 9 to 170 days. The body weight of each mouse was measured at least three times per week and all mice were labeled with heavy water 4-5 days before SAC. The in vivo hepatic proteomics approach presented here for the CR model were based on a previous publication from our group [326].

Heavy water labeling protocol. To measure rates of *in vivo* protein replacement, mice were labeled with an intraperitoneal injection of 100% ^2H_2O at the times specified in Figure 3-1A 4-5 days prior to the end of each study. Mice were then provided free

access to 8% heavy water as drinking water for the remainder of the studies, as previously described [194].

Blood, plasma and tissue collection. Upon completion of each study, mice were anesthetized under 3% isoflurane and blood was collected via cardiac puncture, followed by cervical dislocation and tissue collection. Following centrifugation of blood, plasma was collected and stored at -80°C. Upon dissection, the liver was cut into several small pieces (~20-100mg), which were flash frozen in liquid nitrogen.

Measurement of ^2H_2O enrichment in body water. Enrichment of ^2H_2O in body water (blood) was measured via chemical conversion to tetrabromoethane as previously described [326]. Body water ^2H_2O enrichment values (p) were used to calculate the fractional synthetic rate (*f*) of peptides as detailed in a subsequent section.

Preparation of liver samples for LC-MS/MS proteomic analysis. Frozen livers from AL and CR mice labeled with heavy water were prepared and treated as previously described [326]. Frozen livers from AL and CR mice labeled with heavy water were homogenized in ~500ul lysis buffer (10mM Tris-base, 150mM NaCl, 1% NP-40, 0.1% SDS, 0.5% sodium deoxycholate, 1mM dithiothreitol (DTT), 1mM phenylmethylsulfonyl fluoride (PMSF), 7.5ug/mL leupeptin, 1.0ug/mL pepstatin, 2.0ug/mL aprotinin and 1 Phosphatase Inhibitor Cocktail (Roche Applied Science, Indianapolis, IN) per 10mL buffer, pH ~7.5) using a stainless steel bead and a TissueLyserII (Retsch, Newtown, PA) set at 30hz for 1min. Tissue homogenates were sonicated in a sonication water bath for 1min and then centrifuged at 10,000 rcf at 4°C for 10min followed by supernatant collection. Protein concentrations were determined by bicinchoninic acid (BCA) assay (Pierce, Rockford, IL). 100-250ug aliquots of protein from these homogenates were uniformly reduced via incubation in 4.8mM tris(2-carboxyethyl)phosphine (TCEP) and SDS-PAGE sample loading buffer for 10min at 70°C. The reduced samples were then alkylated via incubation in 14.3mM iodoacetamide for 1hr in the dark at room temperature. Tryptic peptides from all protein homogenates were prepared as previously described [326].

LC-MS/MS analysis. Trypsin-digested peptides were analyzed on either an Agilent 6520 or 6550 Q-TOF (quadrupole time-of-flight) mass spectrometer with 1260 Chip Cube nano ESI source (Agilent Technologies, Santa Clara, CA). Peptides were separated chromatographically using a Polaris HR chip (Agilent #G4240-62030) consisting of a 360nL enrichment column and a 0.075 x 150 mm analytical column, each packed with Polaris C18-A stationary phase with 3 μm particle size. Mobile phases were (A) 5% v/v acetonitrile and 0.1% formic acid in deionized water and (B) 95% acetonitrile and 0.1% formic acid in deionized water. Peptides were eluted at a flow rate of 350 nL/min during an 18 min nano LC gradient (2% B at 0 min, 5% B at 0.5 min, 30% B at 10 min, 50% B at 13 min, 90% B at 13.1-18 min, 2% B at 18.1 min; Stop time: 32 min). Each sample was analyzed twice, once for protein/peptide identification in data-dependent MS/MS mode. Acquisition parameters were: MS/MS acquisition rate = 6 Hz MS and 4 Hz MS/MS with up to 12 precursors per cycle, MS acquisition rate = 0.9 Hz (6520 QTOF) or 0.6 Hz (6550 QTOF), ionization mode = positive electrospray; capillary voltage = 1980 V; drying gas flow = 9 L/min (6520 QTOF) or 11 L/min (6550 QTOF); drying gas temperature = 290 °C; fragmentor = 360

V; skimmer = 45 V; maximum precursor per cycle = 12; scan range = 100-1700 m/z (MS), 50-1700 m/z (MS/MS); isolation width (MS/MS) = medium (~4 m/z); collision energy (V) = -4.8+3.6 (precursor m/z/100); active exclusion enabled (exclude after 1 spectrum, release after 0.12 min); charge state preference = 2, 3, >3 only, sorted by abundance; TIC target = 25,000; reference mass = 922.009798 m/z (6520 QTOF) or 1221.990637 m/z (6550 QTOF). Acquired MS/MS spectra were extracted and searched using Spectrum Mill Proteomics Workbench software (version B.04.00 released Feb 2012, Agilent Technologies, Santa Clara, CA) and a UniProtKB/Swiss-Prot mouse protein database (16,612 proteins, UniProt.org, release 2013_05). Data files were extracted with the following parameters: fixed modification = carbamidomethylation of cysteine, scans with same precursor mass merged by spectral similarity within tolerances (retention time +/- 10 sec, mass +/-1.4 m/z), precursor charge maximum z = 6, precursor minimum MS1 S/n = 10, and 12C precursor m/z assigned during extraction. Extracted files were searched with parameters: enzyme = trypsin, species = Mus musculus, fixed modification = carbamidomethylation of cysteine, variable modifications = oxidized methionine + pyroglutamic acid + hydroxylation of proline, maximum number of missed cleavages = 2, minimum matched peak intensity = 30%, precursor mass tolerance = 10 ppm, product mass tolerance = 30 ppm, minimum number of detected peaks = 4, maximum precursor charge = 3. Search results were validated at the peptide and protein levels with a global false discovery rate of 1%. Proteins with scores greater than 11.0 were reported, and a list of peptides with scores greater than 6 and scored peak intensities greater than 50% was exported from Spectrum Mill and condensed to a non-redundant peptide formula database using Microsoft Excel. This database, containing peptide elemental composition, mass, and retention time was used to extract MS spectra (M0-M3) from corresponding MS-only acquisition files with the Find-by-Formula algorithm in Mass Hunter Qualitative Analysis software (version B.05.00, Agilent Technologies, Santa Clara, CA). MS spectra were extracted with parameters: extracted ion chromatogram integration by Agile integrator; peak height > 10,000 counts; include spectra with average scans > 12% of peak height; no MS peak spectrum background; unbiased isotope model; isotope peak spacing tolerance = 0.0025 m/z plus 12.0 ppm; mass and retention time matches required; mass match tolerance = +/- 12 ppm; retention time match tolerance = +/- 0.8 min; charge states z = +2 to +4; chromatogram extraction = +/- 12 ppm (symmetric); EIC extraction limit around expected retention time = +/- 0.6 min.

Proteome dynamics (fluxs) calculations. Data from individual biological samples were filtered to exclude protein measurements with fewer than two peptide spectra measurements per protein. Details of fractional replacement calculations were described previously [326]. Briefly, in-house software was developed to calculate the peptide elemental composition and curve fit parameters for predicting isotope enrichments of peptides in newly synthesized proteins based on precursor body water enrichment (p) and the number (n) of amino acid C-H positions per peptide actively incorporating H and ^{2}H from body water. Incorporation of ^{2}H into tryptic peptides decreases the relative proportion of M0 within the overall isotope envelope spanning M0–M3. Fractional synthesis was calculated as the ratio of excess %M0 (EM0) for each peptide to the maximal absolute EM0 possible at the measured body water enrichment. Data handling was performed using Microsoft Excel templates, with input of precursor body water enrichment for each subject, to yield FSR data at the protein level. Data from individual

biological samples were filtered to exclude protein measurements with fewer than two peptide spectra measurements per protein. FSR data at individual time points (weeks) are reported as a cumulative value (percentage of protein newly synthesized over the entirety of the labeling period).

RNA-Sequencing. Total RNA was isolated from mouse livers using RNeasy Micro Kit from Qiagen (Hilden, Germany). RNA Quantity was determined using a Qubit (TM) fluorometric assay and quality was determined using Eukaryote Total RNA Pico (Agilent Bioanalyzer 2100). The library preparation and sequencing were done on a single lane (Illumina HiSeq4000) at 100bp pair-end (PE) reads and performed at the Vincent J. Coates Genomics Sequencing Laboratory at University of California (UC), Berkeley. The raw sequencing files were processed with CASAVA 1.8.2 (Illumina) to generate fastq files. We first obtained read quality reports by using the FastQC tool (http://www.bioinformatics.babraham.ac.uk/projects/fastqc/), which gave us overall high-quality scores. The fastq files were then uploaded onto the Galaxy project portal (https://usegalaxy.org/) [337]. The reads were then mapped to the mouse reference genome (mm10) using the Burrows-Wheeler Aligner (BWA) module. Differential gene expression of RNA-seq was determined using DESeq2 [338].

Western Blots. p70 S6 kinase antibody (#9202) was obtained through Cell Signal. Mouse livers were lysed in CST lysis buffer containing 20 mM Tris pH 7.5, 150 mM NaCl, 1 mM EDTA, 1 mM EGTA, 1% Triton X-100, 2.5 mM pyrophosphate, 50 mM NaF, 5 mM β-glycero-phosphate, 1 mM Na_3VO_4, 50 nM calyculin A (EMD Millipore), and protease inhibitors (Roche). Lysate was incubated on a rotator at 4°C for 30 min, and insoluble residue was subsequently removed with a centrifugation at 14,000 rpm for 10 min. Protein samples were normalized to a single concentration between 1 and 2 mg/mL. Proteins were separated by SDS/PAGE and transferred to nitrocellulose membranes with the iBlot system (Invitrogen). Blots were blocked with 5% BSA in Tris-buffered saline containing Tween 20 (TBST) solution for 1 h at RT and then washed with TBST. The blots were probed overnight at 4°C with primary antibodies diluted in 5% BSA in TBST according to manufacturer's instructions. Following washes with TBST, the blots were incubated in the dark for 1 h at RT with secondary antibodies (Rockland). Blots were visualized using a ChemiDoc MP (Bio-Rad Laboratories, Inc.).

Cytokine array. Proteome profiler mouse XL Cytokine Array ARY028 (R&D Systems) was used to detect change in level of cytokines in liver lysates. All reagents, kits and chemicals, unless otherwise stated, were used according to the manufacturers' instructions. Other chemicals unless specified were purchased from Sigma-Aldrich.

Statistical analyses. Data were analyzed using GraphPad Prism software (version 9.0) (La Jolla, CA, USA), InfernoRDN (https://omics.pnl.gov/software/infernordn) windows application (version 1.1), Gene set enrichment analysis, GSEA software, and Molecular Signature Database (MSigDB) [327] (http://www.broad.mit.edu/gsea/), and Real Statistics Resource Pack (http://www.real-statistics.com/free-download/real-statistics-resource-pack/) in Excel (version 16).

This work used the Vincent J. Coates Genomics Sequencing Laboratory at UC Berkeley, supported by NIH S10 OD018174 Instrumentation Grant.

5. FIGURES

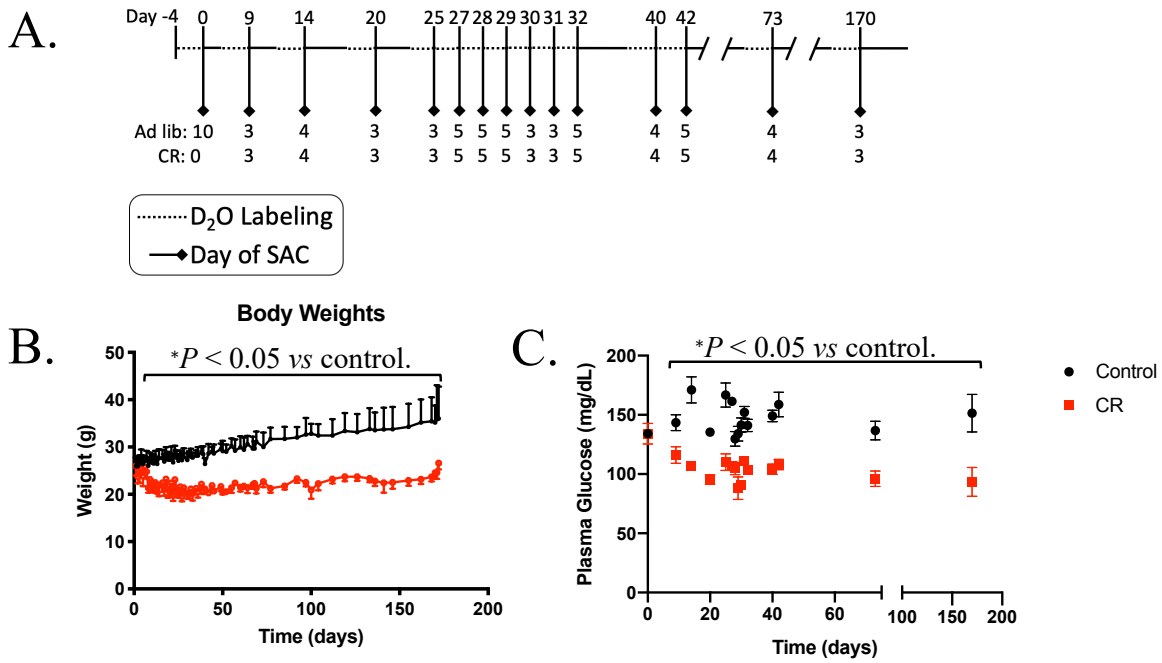

Figure 3-1. Experimental Data. (A) Schematic of experimental timepoints. Male C57Bl/6J mice starting at 6±1 weeks of age underwent CR (30% less than control/week) between 1 to 170 days. Mice were labeled with $^{2}H_2O$ by IP 4-5 days before sacrification (SAC) and body water enrichment was maintained with 8% $^{2}H_2O$ in drinking water. **(B)** Animal parameters were used to establish physiological effects under CR. Male C57Bl/6J mice (*n=120)* of similar age (6±1 weeks) were single-caged and split into ad-lib and CR. Mice were weighed at regular intervals throughout the experimental period. **(C)** Plasma levels of glucose from mice fasted for 4-6 hours for both Con and CR. Data are mean ± SEM, (n = 3-5 for all experiments). ∗P < 0.05 vs control.

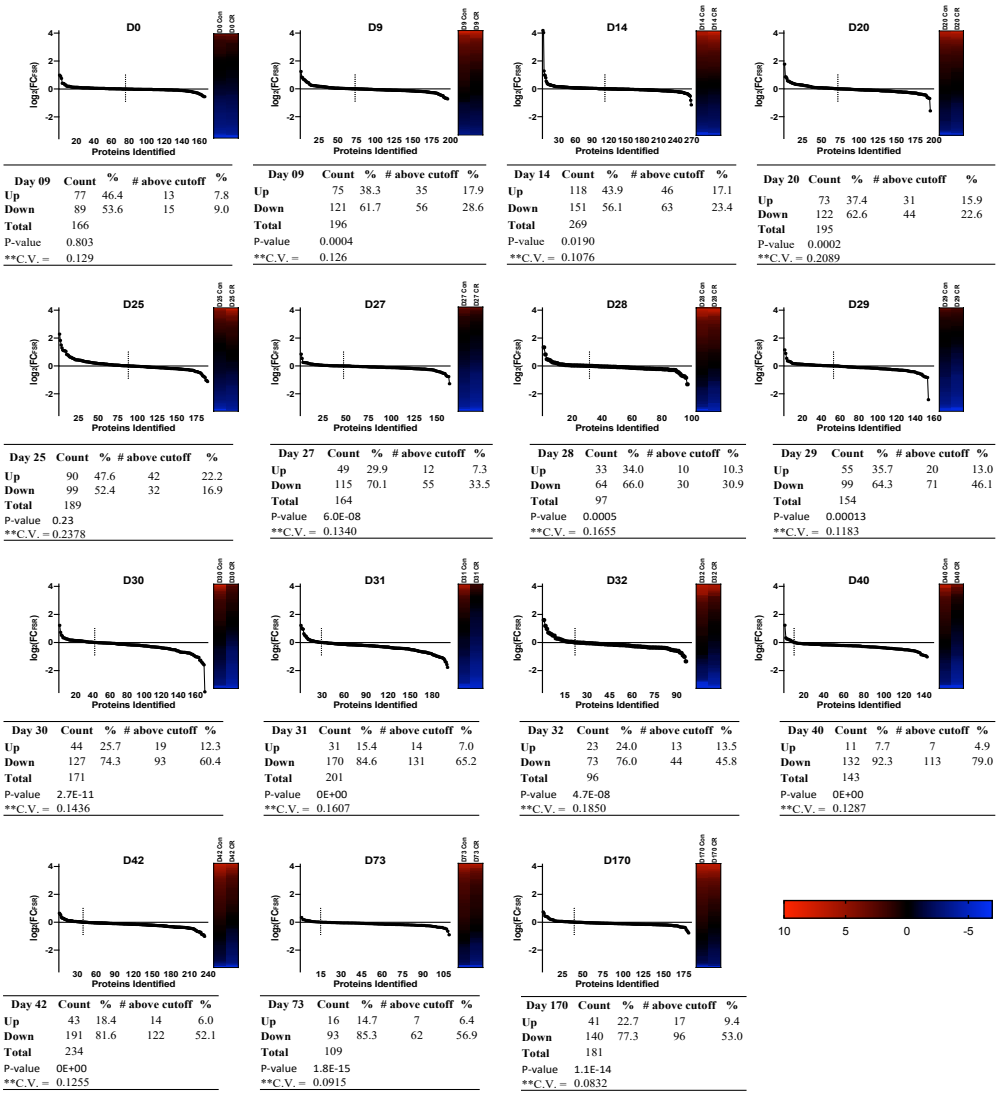

Day 09	Count	%	# above cutoff	%
Up	77	46.4	13	7.8
Down	89	53.6	15	9.0
Total	166			
P-value	0.803			
**C.V. =	0.129			

Day 09	Count	%	# above cutoff	%
Up	75	38.3	35	17.9
Down	121	61.7	56	28.6
Total	196			
P-value	0.0004			
**C.V. =	0.126			

Day 14	Count	%	# above cutoff	%
Up	118	43.9	46	17.1
Down	151	56.1	63	23.4
Total	269			
P-value	0.0190			
**C.V. =	0.1076			

Day 20	Count	%	# above cutoff	%
Up	73	37.4	31	15.9
Down	122	62.6	44	22.6
Total	195			
P-value	0.0002			
**C.V. =	0.2089			

Day 25	Count	%	# above cutoff	%
Up	90	47.6	42	22.2
Down	99	52.4	32	16.9
Total	189			
P-value	0.23			
**C.V. =	0.2378			

Day 27	Count	%	# above cutoff	%
Up	49	29.9	12	7.3
Down	115	70.1	55	33.5
Total	164			
P-value	6.0E-08			
**C.V. =	0.1340			

Day 28	Count	%	# above cutoff	%
Up	33	34.0	10	10.3
Down	64	66.0	30	30.9
Total	97			
P-value	0.0005			
**C.V. =	0.1655			

Day 29	Count	%	# above cutoff	%
Up	55	35.7	20	13.0
Down	99	64.3	71	46.1
Total	154			
P-value	0.00013			
**C.V. =	0.1183			

Day 30	Count	%	# above cutoff	%
Up	44	25.7	19	12.3
Down	127	74.3	93	60.4
Total	171			
P-value	2.7E-11			
**C.V. =	0.1436			

Day 31	Count	%	# above cutoff	%
Up	31	15.4	14	7.0
Down	170	84.6	131	65.2
Total	201			
P-value	0E+00			
**C.V. =	0.1607			

Day 32	Count	%	# above cutoff	%
Up	23	24.0	13	13.5
Down	73	76.0	44	45.8
Total	96			
P-value	4.7E-08			
**C.V. =	0.1850			

Day 40	Count	%	# above cutoff	%
Up	11	7.7	7	4.9
Down	132	92.3	113	79.0
Total	143			
P-value	0E+00			
**C.V. =	0.1287			

Day 42	Count	%	# above cutoff	%
Up	43	18.4	14	6.0
Down	191	81.6	122	52.1
Total	234			
P-value	0E+00			
**C.V. =	0.1255			

Day 73	Count	%	# above cutoff	%
Up	16	14.7	7	6.4
Down	93	85.3	62	56.9
Total	109			
P-value	1.8E-15			
**C.V. =	0.0915			

Day 170	Count	%	# above cutoff	%
Up	41	22.7	17	9.4
Down	140	77.3	96	53.0
Total	181			
P-value	1.1E-14			
**C.V. =	0.0832			

Figure 3-2. Time-course of reduction in proteome-wide protein fractional synthesis rates (FSR) during long-term CR. Data represent multiple experiments on which C57Bl/6J male mice underwent CR for different lengths of time with heavy water labeling for the 4-5 days prior to each time point. Livers were collected and the proteome was analyzed by LC-MS/MS and the FSR (turnover rates) were calculated by MIDA, as described in Methods. Heatmaps represent the *z-score* of the FSR between control and CR for each timepoint: each group was averaged and sorted from highest to smallest value and graphed as a double-gradient heatmap. The dot graph shows the log2(FC) of CR vs control FSR. Dots represent individual proteins identified by LC-MS. Tables show the binomial distribution significance between upregulated (higher FSR) or downregulated (lower FSR) proteins in CR vs control and also show the number and percent of proteins that reached a cut-off value of 10% higher or lower FSR than in controls. Vertical dotted line shows the dividing line separating faster (left) and slower (right) FSRs.

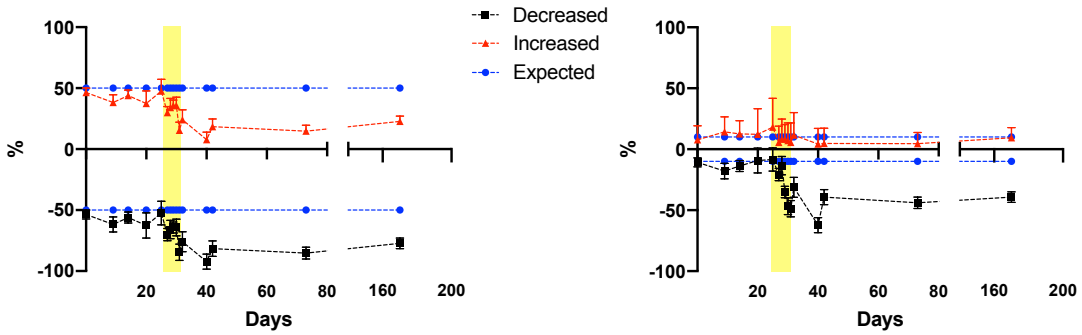

Figure 3-3. Identifying the timeframe of protein turnover rates by binomial distribution test. (A) Proteins in each timepoint and under CR were compared to their control and sorted by the percentage of proteins whose turnover was either higher (faster replacement rate) or lower (slower replacement rate). **(B)** Proteins in each timepoint are sorted by Coefficient of Variation (CV = SD/mean). CV was determined for the Control group and the average was used as a 'cutoff' to determine variations within the control group to represent the percentage of proteins with more than one CV above or below controls. Yellow line represents the period (days 25 – 30) where a significant shift in replacement rate is observed.

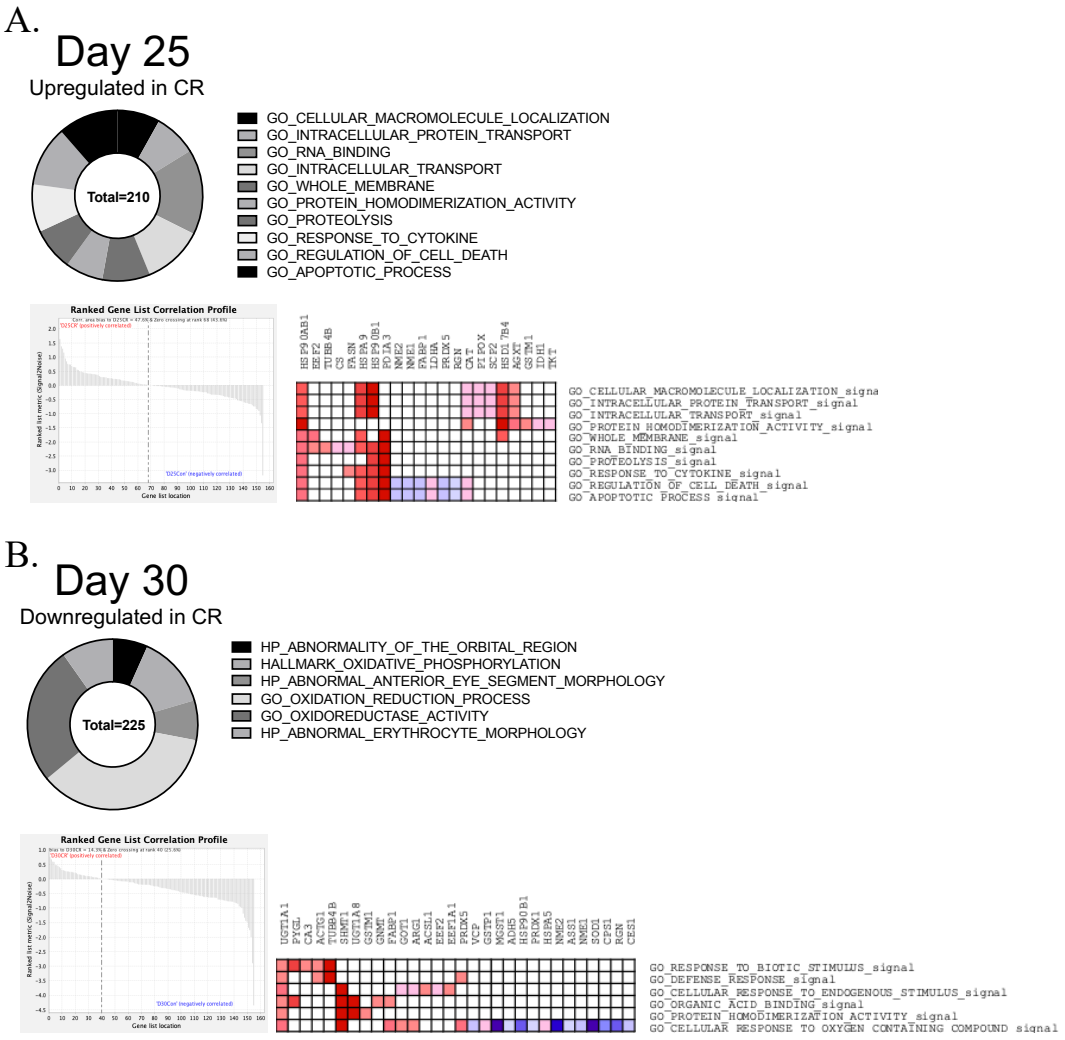

Figure 3-4. Sequence Enrichment Analysis of Protein FSR values at days 25 and 30 of CR. This data represents the sequence enrichment analysis of gene expression profiling. **(A)** Data from day 25 of CR. 104 out of 210 datasets tested were enriched in the CR group and are represented as a fraction of the total number of genes included in each dataset. Of these, 10 datasets were significantly enriched at a FDR < 0.25 and 106 out of 210 datasets were upregulated in the Con group. However, no data sets were significantly enriched. A ranked gene list correlation profile for FSR expressions showed the distribution of FSR values and assigned as positive (CR group) and negative (Con group) for the correlation. Heatmap shows a representation of leading-edge between gene sets (top) present as an overlap within gene sets that can suggest phenotype driving genes. **(B)** Data from day 30 of CR showed that 19 out of 210 datasets were enriched in the CR group. However, no datasets were significant. 191 out of 210 data sets were upregulated in the control group. 6 out of 210 datasets were significantly enriched nominal p <0.05. A ranked gene list correlation profile for FSR expressions showed the distribution of FSR values between positive (CR group) and negative (Con group) correlation. Heatmap shows the leading-edge between gene sets (top) that could be gene drivers.

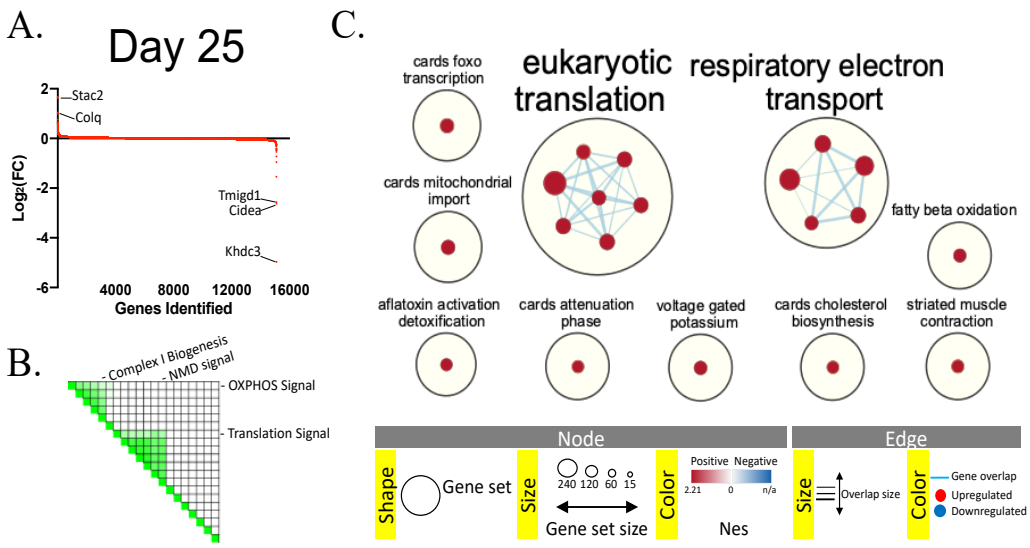

Figure 3-5. Gene Regulation based on mRNA levels at day 25 of CR. RNA-Seq from mouse livers. **(A)** Over 15,000 genes were identified by RNA-Seq and sorted from increased to decreased expression as log2(Fold Change) between the control and CR. **(B)** Leading edge analysis among gene sets. Color intensity is used to show the overlap between subsets, the darker the color, the greater the overlap between the subsets. Specifically, the intensity of the cells for 'translation signal' with 'NMD signal' and 'OXPHOS signal' with 'Complex I biogenesis' were correlated the strongest. **(C)** Gene enrichment scores defining the major biological themes were annotated in Cytoscape enrichment mapper. Clusters of similar pathways are represented where each node signifies one specific dataset. The yellow circles represent the annotation with related pathways. generate an Enrichment map including clusters of similar pathways.

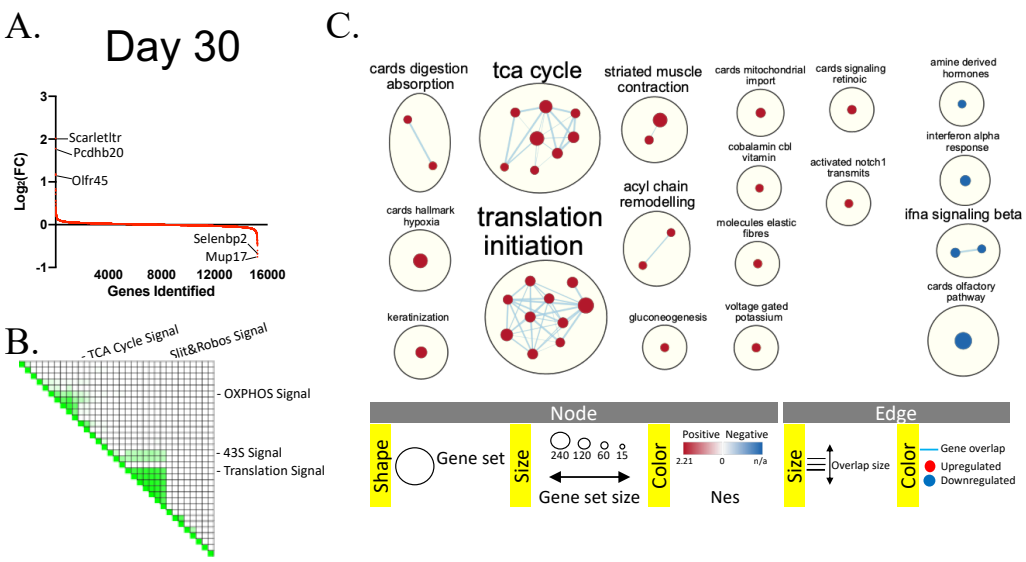

Figure 3-6. Gene Regulation based on mRNA levels at day 30 of CR. RNA-Seq from mouse livers. **(A)** Over 15,000 genes were identified by RNA-Seq and sorted from increased to decreased expression as log2(Fold Change) between the control and CR. **(B)** Leading edge analysis among gene sets. Color intensity is used to show the overlap between subsets, the darker the color, the greater the overlap between the subsets. Specifically, the intensity of the cells for 'translation signal' and '43S signal' with 'Slit&Robos signal' and 'OXPHOS signal' with 'TCA Cycle signal' were correlated the strongest. **(C)** Gene enrichment scores defining the major biological themes were annotated in Cytoscape enrichment mapper. Clusters of similar pathways are represented where each node signifies one specific dataset. The yellow circles represent the annotation with related pathways. generate an Enrichment map including clusters of similar pathways.

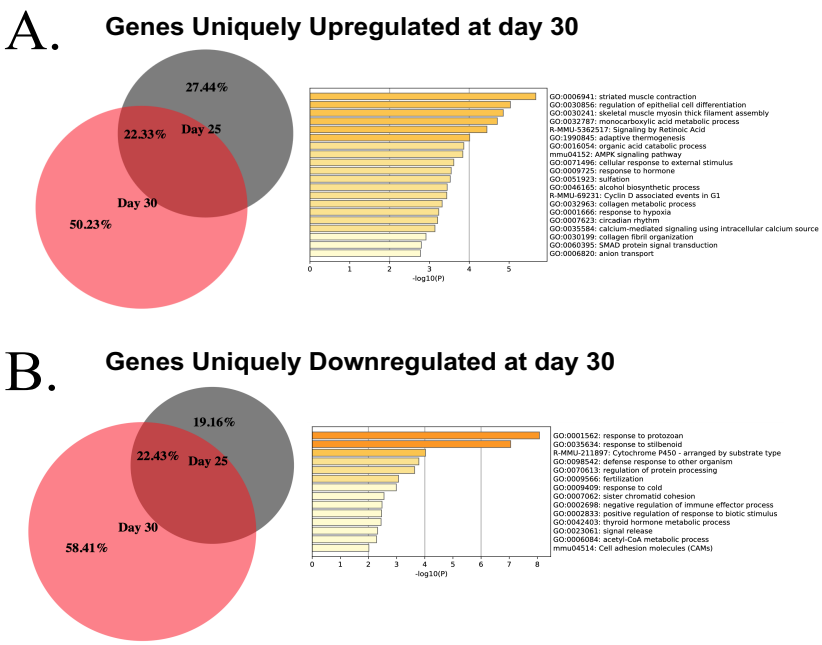

Figure 3-7. Gene Expression Changes. (A) Venn Diagram and gene ontology of genes uniquely upregulated at day 30. The cutoff was considered within the change in their log2(FC) ≥ 0.1 between control and CR for both day 25 and 30. Genes that did not overlap at day 30 were then analyzed by MetaScape to generate functional annotation. **(B)** Venn Diagram and gene ontology of genes uniquely downregulated at day 30. The cutoff was considered within the change in their log2(FC) ≥ 0.1 between control and CR for both day 25 and 30. Genes that did not overlap at day 30 were then analyzed by MetaScape to generate functional annotation.

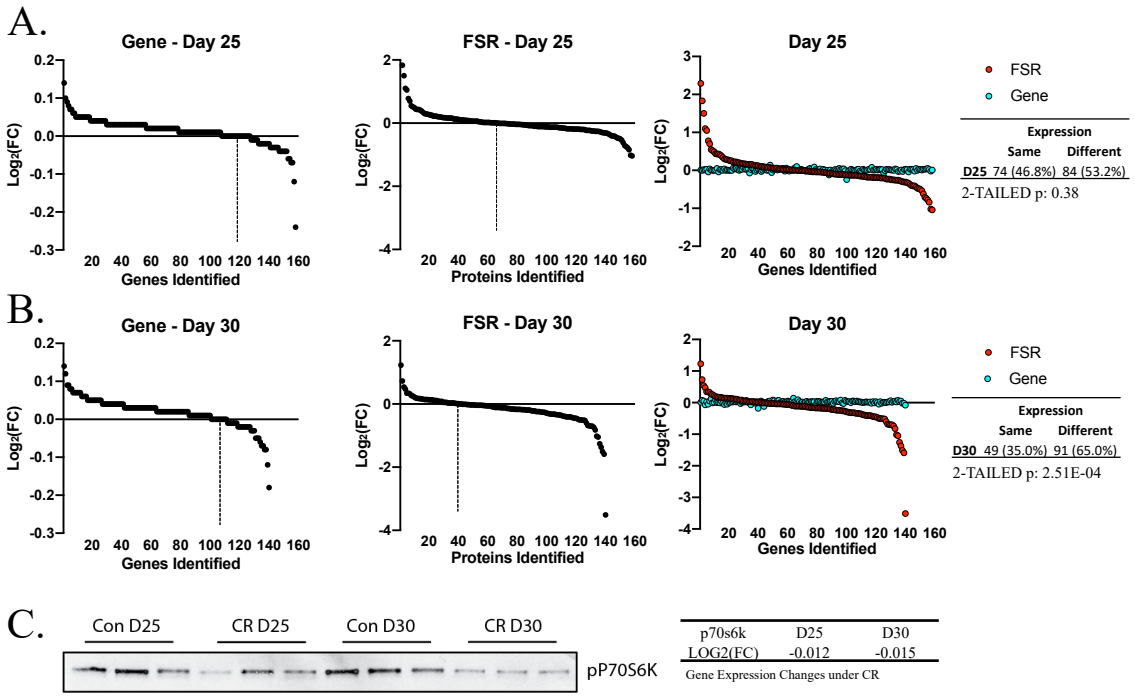

Figure 3-8. Protein FSR and Gene Expression Compared. Protein FSRs and Gene expression comparison for day 25 **(A)** and day 30 **(B)**. Only proteins also identified in the genomic dataset were included in the comparison and shown in this figure. Graphic lines in black were sorted from highest to lowest fold change for FSR or gene expression. Graphs in color were sorted from highest to lowest fold-change for FSR as a way to compare gene expression to protein FSR. Table represents the number of genes and protein FSRs with either the same or different direction for expression pattern. Table shows statistics as determined by binomial distribution 2-TAILED P values. Vertical dotted line shows the dividing line separating faster (left) and slower (right) values compared to controls. **(C)** Liver protein expression analysis of pP70S6 Kinase as a marker of active protein translation and compared to gene expression of p70S6 Kinase as the fold change to the age-matched control.

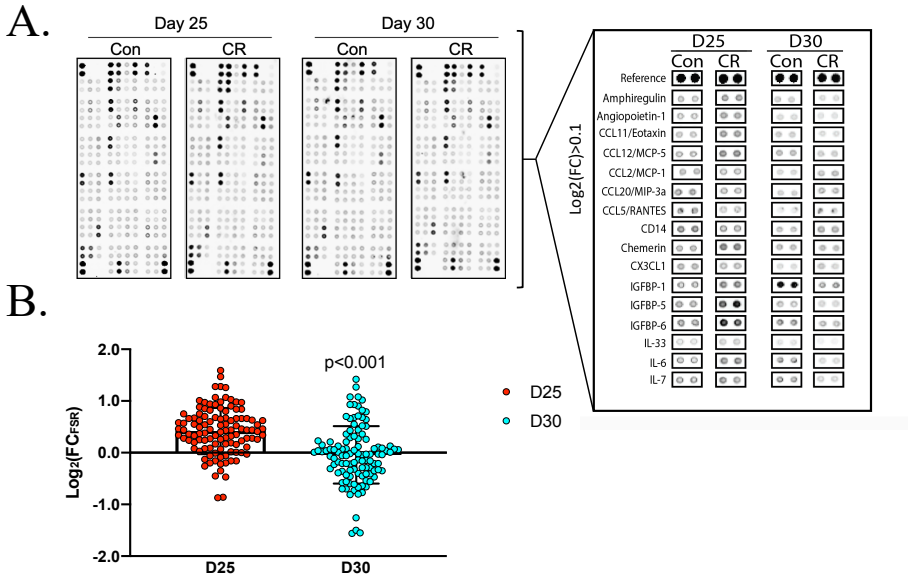

Figure 3-9. Cytokine Array Expression. (A) Protein lysates from mouse livers between Con and CR for days 25 and 30 were extracted for immunoblot analysis for a cytokine array. Each protein was quantified by densitometry (pixel intensity on ImageJ). The average of the densitometry analysis was then compared between the CR and Control groups and represented as the Log2(FC). **(B)** Representative comparison of the cytokine array for proteins with a log2(FC) >0.1. Table represents the number of genes and protein FSRs with either the same or different expression pattern. Two-way ANOVA for column factor expressed as: $P < 0.05$

CHAPTER FOUR: Different Effects of CR and Exercise on Skeletal Muscle Mitochondrial Biogenesis and Global Protein Synthesis Rates

1. INTRODUCTION

Aging is an timepoint in life when protein damage [339] and metabolic imbalances that lead to loss of muscle mass and strength often occur [340], yet little is known about how to prevent these deleterious effects. CR is a lifespan extension intervention considered to be the most effecting rejuvenating treatment known so far [341]. In addition, as discussed in chapter one, exercise has been suggested to be a CR mimetic.

Both CR and EX have been shown to lead to physiological changes such as lower body weight, and to protect against the age-related diseases [342–344], although different effects on extension of maximal life-span in rodents has been reported [345]. It is widely accepted that EX leads to mitochondrial biogenesis [346–348]. Mitochondrial biogenesis due to EX has been quantified and shown to increase in multiple studies [346–348], and importantly, is consistent with increased metabolic rate associated with EX. In contrast, long-term 40% CR results in changes in metabolism that achieve a stable body composition at lower body mass and lower energy expenditure [349]. CR has been reported to increase mitochondrial biogenesis rates [204,350,351] but this observation is more controversial in light of the lower basal metabolism, total energy expenditure and calorie availability. In addition, given that EX increases lean muscle mass and metabolic rate while CR reduces total body mass and metabolic rate, it seems surprising that skeletal muscle mitochondrial biogenesis has been reported to occur in both interventions.

Directly comparing the synthesis rates and abundances of cytoplasmic and mitochondrial proteins across the muscle proteome in mice could be of great benefit in understanding the biology behind both EX and CR. This can be achieved through *in vivo* $^{2}H_2O$ (heavy water) labeling, LC-MS/MS analysis and label-free quantitative proteomics. An effective approach is through forced treadmill exercise training as a model of EX that is well-established model to increase mitochondrial biogenesis. Through this approach, it is possible to explore which interventions lead to significantly increased turnover rates (decreased the half-lives) or decreased turnover rates (increased the half-lives) of major muscle protein families such of contractile fiber, cytoskeletal, glycolytic, mitochondrial and sarcoplasmic reticulum proteins. Possible observations could be also derived through the changes in cellular and mitochondrial protein abundances compared with sedentary (SED) control mice, where the hypothesis of increased mitochondrial absolute protein synthesis rates through EX can be studied.

The American College of Sports Medicine (ACSM) defines EX as any activity that uses large muscle groups, can be maintained continuously and is rhythmic in nature [352,353]. While regular physical activity is known to improve CVD associated morbidity and mortality, the optimal duration, frequency, and intensity of exercise remains unclear [354]. Exercise training procedures should therefore take into account intensity, modality of exercise, frequency, and duration. Basing these on exercise classifications such as dynamic[355,356], and exhaustion or fatigue testing [357].

2. RESULTS

In here, we compare how long-term (14 months on 40% CR) and progressive EX affect muscle biology and potentially protect against age-related disease by measuring the synthesis rates, half-lives and content of proteins across the global proteome in skeletal muscle of mice. In particular, we explore how short-term (2-weeks on 30%) and daily exhaustion EX affect muscle biogenesis.

We have previously described a liquid chromatography mass spectrometry (LC/MS/MS) technique measuring the synthesis rates and half-lives of proteins across the global proteome in tissues and body fluids [194,326]. This technique involves *in vivo* metabolic labeling of newly synthesized proteins with $^{2}H_2O$ (heavy water) followed by the measurement of the isotope patterns and relative abundances of thousands of individual trypsin-generated peptides by LC-MS/MS **(Figure 4-1)**. We have previously used this "dynamic proteomics" approach to measure the *in vivo* synthesis and degradation rates of hundreds of proteins in the liver of CR mice [7,194,326] and in skeletal muscle of exercised humans [358]. We have also shown that individual proteins within multi-protein complexes often have very similar turnover rates, including complexes within the mitochondria [359]. In generating an entire mitochondrion, more than 1000 specific proteins must be synthesized [360]. Therefore, if the cell is modulating the rates of mitochondrial biogenesis or degradation, we should see it reflected in the turnover rates of many proteins within our data as a direct representation of mitochondria biogenesis.

It is important to note that in both EX and CR experiments, we compared the differences in mitochondrial protein kinetics relative to age matched controls. Healthy 18-month old male mice from the NIA CR colony and age-matched controls were used. These animals have been maintained on a CR diet for 14 months, which ensures that we are measuring the proteome dynamics and mitochondrial protein kinetics in animals that are at steady state and are experiencing the well describe CR-dependent benefits [7,194]. The CR animals weighed significantly less than the controls (SED) but gained weight during the study, confirming that they were healthy and at a metabolic steady state **(Figure 4-2E)**.

For the EX group, mice were placed into a progressive increase in exercise regimen **(Figure 4-2A through 4-2B)**. Mice were first acclimated to the rodent treadmill at low speed for the first 10 min followed by timed increases up to 30 mins. After acclimation, a low intensity level (level 1) regimen was performed for the first five days in which the average speeds were increased. The next step was an increase in intensity (level 2) between days 6-10 where the time was extended to a 50 min run. Then, a high-performance course (level 3) was performed for days 11-14 with an increase in both time and intensity. Level 3 was repeated for 14 days by avoiding acclimation and increased steps (level 4) to establish a constant exercise dataset. The diet and labeling planning **(Figure 4-2C)** for CR was set to restrict caloric intake by 40% and label the proteome at specific time-points. The EX-group weighed significantly less than sedentary control mice (SED) at all time points and weighed 12% less at the conclusion of the training protocol (26.5±0.6 g vs. 30.2±1.7 g, $p<0.001$) **(Figure 4-2D)**.

Long-term CR also resulted in lower body weight; CR mice weighed significantly less than AL controls at the beginning of the experiment and throughout the $^{2}H_2O$ labeling period ($p<0.001$ at all time points). CR mice weighed 29% less than AL animals at the

conclusion of the experiment (26.5+1.0 vs. 35.8+5.0, p<0.001) **(Figure 4-2E)**. EX mice consumed an average of 4.2 g/day (represented by level 4 group) and SED mice consumed an average of 4.3 g/day. CR mice were energy restricted by 40% throughout the study; CR mice ate 3.0 g of food daily, and AL mice consumed an average of 5.0 g per day **(Figure 4-2F)**.

To analyze the effects of EX and CR on global muscle protein turnover, we measured the synthesis rates of 7550 peptides between EX and SED animals. Following application of the stringent filtering criteria for acceptance of protein synthetic measurements previously described [194,326], the synthesis rates of 174 proteins found in EX animals and SED animals were calculated **(Figure 4-3A)**.

Exercised animals exhibited higher mean overall FSR (73% higher, 2-tailed p < 0.0001) with values being higher by >10% (FC>0.1) for 56.3% out of the 73% proteins with higher mean. Of the 27% with a lower mean FSR, only 19.5% were lower by >10% (FC>0.1). For muscle turnover rates under CR, we measured the fractional synthesis rates of 9560 peptides, resulting in 209 proteins observed in both AL and CR **(Figure 4-3B)**. In contrast with EX, CR exhibited lower global FSR by >10% (78% lower, 2-tailed p < 0.0001) compared with AL Only 5% of proteins showed higher FSR (FC>0.1), with 17% showing no significance (FC<0.1).

We then determined the gene ontology of significantly altered proteins identified in our global analysis through the DAVID informatics database [361,362]. Proteins were grouped into five main ontologies **(Figure 4-4A)** by their highest level of significance: mitochondrial proteins, sarcoplasmic reticulum (SR) proteins, cytoskeletal proteins, contractile fiber proteins, and glycolytic proteins. A linear correlation showed that EX significantly increased the FSR of proteins in all groups (above the line) except contractile fiber and glycolytic proteins. For CR ontological analysis **(Figure 4-4B)**, the group assignation by highest level of significance was: mitochondrial proteins, antioxidant proteins, cytoskeletal proteins, contractile fiber proteins, and glycolytic proteins. A linear correlation showed significantly lower values of FSR after CR in mitochondrial proteins, cytoskeletal proteins, contractile fiber proteins, and glycolytic proteins.

Through quantitative proteomics, we also determined the change in protein pool size (abundance) of EX and CR relative to age matched control using label free quantitative proteomics. EX mice **(Figure 4-5A)** exhibited significantly higher pool size for many ontologies, with the strongest effect on mitochondrial and cytoskeletal proteins. Pool size was overall higher in mitochondrial proteins by 13% in EX mice (n=95, p<0.001), and cytoskeletal proteins by 26% (n=40, p<0.001). Similar to exercise training, CR mice **(Figure 4-5B)** showed significantly higher pool sizes of proteins across many categories with the strongest effect on mitochondrial proteins. Mitochondrial protein abundance was higher by 14% (n=109, p<0.001), while cytoskeletal protein abundance was greater by 18% (n=30, p<0.01). Of interest was that there were no differences in glycolytic protein pool size for both interventions **(Figure 4-5A through 4-5B)**.

Next, we determined within proteome absolute synthesis (WPAS) rates of individual proteins. Exercise trained mice **(Figure 4-6A)** exhibited significantly higher WPAS

rates of many protein classes, including 38% higher values for mitochondrial proteins (n=50, p<0.001), 41% higher for cytoskeletal proteins (n=21, p<0.01), and 62% higher values for glycolytic proteins (n=17, p<0.05). Mitochondrial proteins were markedly affected by exercise training. In contrast, CR mice **(Figure 4-6B)** did not significantly alter WPAS rates for proteins involved in mitochondrial metabolism, cytoskeletal proteins, nor glycolytic proteins.

Based on the experimental results above, we then examined whether similar effects could be repeated in a different paradigm through a commonly used anaerobic or exhaustion EX approach, where the progression of aerobic exercise capacity by increasing intensity levels is not applied. This EX was applied as a training routine instead of a performance test [217] and done alongside a short-term (2 weeks) CR (30%) group in aged matched C57Bl/6J mice. Of note, the effects of EX and CR on global muscle protein turnover were compared for 104 common proteins **(Figure 4-7A through 4-7B)** shared between Con, CR and EX. During EX **(Figure 4-7A)**, animals did not exhibit an excess fraction with higher global FSR (52%) in contrast to the first EX group. In contrast, under CR **(Figure 4-7B)** we again observed globally that 81% of muscle proteins had a lower FSR, and 68% of those proteins had a FC>0.1.

We then looked at gene set enrichment analysis of the FSR (% per day) values for Con, CR, and EX. The top 2 ($p < 0.5$) enrichment phenotypes for enrichment under treatment condition were evaluated **(Figure 4-8A)**. Of note was that under EX, core enriched proteins matched through the GO database showed upregulation of EX proteins in NADH metabolic process. On the Reactome database we observed core enrichment of a number of proteins under glucose metabolism. Downregulated under EX we observed abnormality of connective tissue and actin cytoskeleton ontologies. Similar to the EX analysis approach, CR proteins **(Figure 4-8B)** were most enriched under the regulation of cell death and, interestingly, abnormality of coordination. On their downregulation, we observed ATP metabolic processed and carbohydrate catabolic processes. Interrogating the FSR (% per day) data for mitochondria-related ontologies through the same enrichment analysis, we observed **(Figure 4-9)** an obvious downregulation of proteins under CR that was more modest under EX.

Through quantitative proteomics, we determined the change in protein pool size (abundance) of EX and CR relative to controls. EX mice **(Figure 4-10A)** exhibited significantly higher pool size for many ontologies, with the strongest effect on actin binding and the electron transport change (ETC). Downregulated pathways, in contrast were involved in carbohydrate derivatives and the anchoring junction. For CR **(Figure 4-10B)**, of note was an increase in the pool size of some classes of proteins. Ontologies observed with higher relative concentration under CR were involved in apoptotic process and muscle contraction. Downregulated pathways were involved in secretion and, interestingly, mitochondria envelope. Following up on specific mitochondria and muscle ontologies **(Figure 4-11)** by enrichment analysis showed downregulation of a number of proteins under both exhaustion exercise and its age-matched CR for proteins involved in muscle spasm. No obvious change in pool size was observed for proteins involved in cellular respiration.

Next, we determined WPAS rates for CR **(Figure 4-12B)** and exhaustion EX **(Figure 4-12A)**. While no obvious global changes were observed under EX, core-enriched pathways were seen on NADH metabolic process and glucose metabolism. Downregulated pathways were observed for abnormality of connective tissue and actin of the cytoskeleton. CR resulted in significantly higher WPAS rates of some protein classes, including pathways core-enriched for regulation of cell death and abnormality of coordination. Downregulated under CR were pathways for ATP metabolism and contractile fibers. Following the interest on muscle and mitochondria proteins we observed **(Figure 4-13)** EX having a more modest decrease in many proteins involved in myogenesis and the mitochondrion. On the other hand, CR noticeably decreased the WPASR of both, in contrast with the overall increase in global WPASR.

Lastly, plasma **(Figure 4-14A)** was analyzed for lipid and insulin content. Insulin levels were significantly lower under CR ($p<0.05$) but not in the exhaustion EX group. Plasma triglyceride levels were significantly decreased for both groups. The FSR of trigyceride-palmitate, triglyceride-glycerol and their relation to DNL (fatty acid synthesis from carbohydrates) showed no significant changes. Enrichment analysis showed cardiovascular abnormalities under CR **(Figure 4-14B)**, so we then tested heart DNA turnover rates (a measure of cell proliferation [7,326]) and saw trends but no significant decrease in cell proliferation of heart.

These data indicate that EX increases the fractional synthesis and the pool size of mitochondria proteins leading to an overall increase in WPAS rates. CR on the other hand decreases the FSR while increasing the pool size leading to a decrease in WPAS rates. These results were validated under short-term CR and to a lesser extent during exhaustion exercise.

3. CONCLUSION

To compare the effects of EX and CR on mitochondrial protein synthesis rates, half-lives and concentrations in mice, we used an LC-MS/MS approach with *in vivo* heavy water labeling. We report that EX and CR have different effects on the muscle mitochondrial dynamic proteome. EX was tested in two paradigms, 1) Aerobic training over time, which is shown to increase the WPAS rates (based on combination of individual protein FSR and abundance quantitation) and increases both the rate of protein turnover and the mitochondrial protein pool size. 2) Exhaustion only module leading to anaerobic exercise resulted in modest increases in WPAS rates when compared to aerobic training. During CR, on the other hand, two lengths of intervention were applied, 1) Long term CR which increases mitochondrial protein pool size in skeletal muscle not by increasing mitochondrial protein synthesis rates but instead through a reduction in mitochondrial protein degradation rates (prolonged half-lives). 2) Short-term CR decreased WPASR had no noticeable changes in pool size.

Because there are no external concentration references necessary for FSR measurement, many studies assume homeostasis during the period of the measurement [7,326,358,363–365]. We used the measurement of relative protein pool size within the proteome to correct for any effects of either intervention on protein expression and composition. The calculation of WPAS rates provides a comparison of protein synthesis and degradation

rates in the face of changes in relative protein expression within the muscle proteome. The WPAS calculation requires a measurement of protein pool size (concentration), which was performed here by using label-free mass spectrometric quantitation [7]. We measured relative protein concentration within the proteome for each protein in the experimental group versus the control group. As expected, EX resulted in higher concentrations of many proteins including mitochondrial proteins. Interestingly we observed that CR also resulted in some significantly higher mitochondrial protein concentrations, in agreement with previous studies [237,267] but that this increase in pool size is due to lower turnover (lower FSR), not higher synthesis rates. The WPAS rates showed that the mass of mitochondrial protein synthesized per unit of time (reflecting mitochondrial biogenesis) was unchanged in CR compared to controls, whereas WPAS rates were significantly higher in EX than in controls.

Our results show that during CR the muscle reduces mitochondrial protein turnover or replacement rates (increasing half-lives) concomitantly with an increase in mitochondrial protein pool size. This result exemplifies the general principle that direct kinetic measurements are required to explain changes in pool size [7,194,326]. The higher muscle mitochondrial protein pool sizes in CR mice were not due to increased rates of synthesis, but can instead be explained by slower mitochondrial protein degradation rates or mitophagy, i.e., prolonged half-lives.

Taken in context of the lower body weight, lean body mass and energy flux in CR mice compared to AL controls [240,241,366–370], these findings are consistent with CR inducing a conservation program that includes reducing the rate of mitochondrial protein degradation in skeletal muscle, resulting in an increase relative mitochondrial content. Whether mitochondria comprising, on average, older proteins that are more efficient oxidatively and reduce production of partial oxidation products, as has been proposed as a mechanism of the health benefits for CR [341,371], is an interesting question that is raised by our findings.

This study has some limitations. As previously noted, exercise training will likely cause new cells to be produced and cell size to increase, meaning that the tissue may have more total protein content. We did not calculate total muscle mass or whole-body mitochondrial protein synthesis here, however but rates relative to other proteins in the muscle proteome.

Taken more broadly, Chapter Four shows that EX training and CR alter mitochondrial protein kinetics differently. Exercise induces mitochondrial biogenesis, manifested by mitochondrial higher protein synthesis rates and pool sizes rates in comparison with SED mice. In contrast, CR does not induce higher rates of new protein synthesis in muscle mitochondria (mitochondrial biogenesis) but causes a relative increase in mitochondrial protein content through reduced protein degradation rates, i.e. longer half-lives. The addition of protein turnover measurements to static proteomics here brings new insights into metabolic control. By classifying both the protein synthesis rates and pool sizes of related protein groups, a critical dimension of understanding into the regulation of protein homeostasis was added.

4. METHODS

Exercise Training. Eight-week old male C57Bl/6 mice (n=12) were purchased from Charles River (Wilmington, MA), and were randomly divided into the exercise training group (EX, n=6) or the sedentary group (SED, n=6). Eight-week old male C57Bl/6J mice (n=4) were purchased from (Jackson laboratory, Bar Harbor, ME) for the level 4 study. Following one week of acclimation, EX animals were trained on an Exer3/6 treadmill (Columbus Instruments, Columbus, OH) for a total of 3 weeks (5 sessions per week). The exercise period was divided into four levels of increasing speed and duration **(Figure 4-2A)**, while level 4 was designed as an exhaustion only experimental approach by inducing only level 3 throughout the experiment. Animals in both groups were provided unrestricted access to the AIN-93M diet (Bio-Serv). Body weights and food intake were recorded approximately every 4 days during the training period. Animals were labeled with ^2H_2O following the third week of EX training and sacrificed 3-4 days later.

Calorie Restriction. Male C57Bl/6 mice which had been calorie restricted for 14 months (n=12) and age-matched AL controls (n=12) were purchased from the NIA Caloric Restricted Mouse Colony via Charles River (Wilmington, MA). Animals in the CR group were fed 3.0 grams of the NIH-31/NIA fortified diet at 5pm daily, and animals in the AL group were provided unrestricted access to the NIH-31 diet **(Figure 4-2C)**. Animals were sacrificed following 0.4, 1, 4, 8, 15 or 32 days of heavy water labeling. Body weight and food intake were monitored on a weekly basis, and at the time of euthanasia.

Euthanasia. Animals were anesthetized with isoflurane and euthanized by cardiac puncture. All experiments were performed under the approval of the Institutional Animal Care and Use Committees of the University of California at Berkeley.

Measurement of ^2H enrichment in body water. Animals in each group were labeled with an intraperitoneal injection of 100% ^2H_2O saline (0.35mL/10 g body weight), and provided with 8% ^2H_2O drinking water for the remainder of the study to maintain body ^2H_2O enrichments of approximately 5%, as described previously [372]. Measurement of ^2H_2O enrichment in body water was done from whole blood samples using a Liquid Water Isotope Analyzer (Los Gatos Research, Mountain View, CA) after a 1:300 dilution and distillation as previously described [373].

Muscle Protein Isolation and In-Gel Trypsin Digestion. Bilateral soleus and triceps muscles were harvested from mice at the time of euthanasia, and immediately snap frozen on liquid nitrogen until further analysis. Tissue protein was isolated by homogenization in RIPA buffer containing PhosStop phosphatase inhibitor cocktail (Roche, Indianapolis, IN), 1mM DTT, 7.5ug/mL leupeptin, 1ug/mL pepstatin, 2ug/mL aprotinin, 1mM PMSF in isopropanol, and 100nM nicotinamide using a TissueLyser (Qiagen, Germantown, MD), followed by centrifugation at 10,000g for 10 minutes at 4 ^oC. The supernatant containing soluble proteins was used for the analysis. Protein from prepared homogenates was uniformly reduced by incubation in 10 mM DTT and SDS-PAGE sample loading buffer for 10 min at 70°C. The reduced samples were then alkylated by incubating in 15 mM iodoacetamide for 1 hour at room temperature in the dark. Proteins were then fractionated by SDS-PAGE. Using in-gel molecular weight

markers, each sample was divided into molecular weight regions and trypsin digested at 37ºC (Trypsin Gold, Promega, Madison, WI). In each experiment, 5 gel bands were analyzed by LC-MS/MS, corresponding to a molecular weight range of 20-80kDa.

LC/MS Analysis and Protein Turnover Calculations. Trypsin-digested peptides were analyzed on an Agilent 6520 QTOF (quadrupole time-of-flight) mass spectrometer with 1260 Chip Cube nano ESI source (Agilent Technologies, Santa Clara, CA). Peptides were separated chromatographically using a Polaris HR chip (Agilent #G4240-62030) consisting of a 360 nL enrichment column and a 0.075 x 150 mm analytical column, each packed with Polaris C18-A stationary phase with 3 µm particle size. Mobile phases were (A) 5% v/v acetonitrile and 0.1% formic acid in deionized water and (B) 95% acetonitrile and 0.1% formic acid in deionized water. Peptides were eluted at a flow rate of 350 nL/min during a 18 min LC gradient (2%B at 0 min, 5%B at 0.5 min, 30%B at 10 min, 50%B at 13 min, 90%B at 13.1-18 min, 2%B at 18.1 min; Stop time: 32 min). Each sample was analyzed twice, once for protein/peptide identification in data-dependent MS/MS mode and once for peptide isotope analysis in MS-only mode. Acquisition parameters were: MS/MS acquisition rate = 6 Hz MS and 4 Hz MS/MS with up to 12 precursors per cycle, MS acquisition rate = 0.9 Hz, ionization mode = positive electrospray; capillary voltage = -1980 V; drying gas flow = 4 L/min; drying gas temperature = 290 °C; fragmentor = 170 V; skimmer = 65 V; maximum precursor per cycle = 20; scan range = 100-1700 m/z (MS), 50-1700 m/z (MS/MS); isolation width (MS/MS) = medium (~4 m/z); collision energy (V) = -4.8+3.6*(precursor m/z/100); active exclusion enabled (exclude after 1 spectrum, release after 0.12 min); charge state preference = 2, 3, >3 only, sorted by abundance; TIC target = 25,000; reference mass = 922.009798 m/z. Acquired MS/MS spectra were extracted and searched using Spectrum Mill Proteomics Workbench software (version B.04.00, Agilent Technologies, Santa Clara, CA) and a UniProtKB/Swiss-Prot mouse protein database (UniProt.org, release 2012_02). Data files were extracted with the following parameters: fixed modification = carbamidomethylation of cysteine, scans with same precursor mass merged by spectral similarity within tolerances (retention time +/- 10 sec, mass +/-1.4 m/z), precursor charge maximum z = 6, precursor minimum MS1 S/N = 10, and 12C precursor m/z assigned during extraction. Extracted files were searched with parameters: enzyme = trypsin, *Mus Musculus*, fixed modification = carbamidomethylation of cysteine, variable modifications = oxidized methionine + pyroglutamic acid + hydroxylation of proline, maximum missed cleavages = 2, minimum matched peak intensity = 30%, precursor mass tolerance = 10 ppm, product mass tolerance = 30 ppm, minimum detected peaks = 4, maximum precursor charge = 3. Search results were validated at the peptide and protein levels with a global false discovery rate of 1%. Proteins with scores greater than 11.0 were reported and a list of peptides with scores greater than 6 and scored peak intensities greater than 50% was exported from Spectrum Mill and condensed to a non-redundant peptide formula database using Excel. This database, containing peptide elemental composition, mass, and retention time was used to extract MS spectra (M0-M3) from corresponding MS-only acquisition files with the Find-by-Formula algorithm in Mass Hunter Qualitative Analysis software (version B.05.00, Agilent Technologies, Santa Clara, CA). MS spectra were extracted with parameters: EIC integration by Agile integrator, peak height > 10,000 counts, include spectra with average scans > 12% of peak height, no MS peak spectrum background, unbiased

isotope model, isotope peak spacing tolerance = 0.0025 m/z plus 12.0 ppm, mass and retention time matches required, mass match tolerance = +/- 12 ppm, retention time match tolerance = +/- 0.8 min, charge states z = +2 to +4, chromatogram extraction = +/- 12 ppm (symmetric), EIC extraction limit around expected retention time = +/- 1.2 min. Details of FSR calculations and data filtering criteria were described previously [305,326]. Briefly, in-house software was developed to calculate peptide elemental composition and curve fit parameters for predicting isotope enrichments of peptides in newly synthesized proteins based on precursor body water enrichment (*p*) and the number (n) of amino acid C–H positions per peptide actively incorporating ^{1}H and ^{2}H from body water. Incorporation of ^{2}H into tryptic peptides decreases the relative proportion of M0 within the overall isotope envelope spanning M0-M3. Fractional synthesis was calculated as the ratio of excess %M0 (EM_0) for each peptide compared to the maximal absolute EM_0 possible at the measured body water enrichment. Data handling was performed using Microsoft Excel templates, with input of precursor body water enrichment for each subject, to yield fractional replacement rate (FSR) data at the protein level. The kinetics data were filtered to exclude protein measurements with fewer than two peptide isotope measurements per protein. Following LC-MS/MS measurement of peptide spectra, we used five stringent selection criteria to remove low confidence kinetic data: (a) peptide signal intensity must be more than 30,000 counts, (b) RMS error for unlabeled peptide mass isotopomer abundance measurements must be less than 1.5% compared with natural abundance, (c) observation of the parent protein in at least 2 mice per experimental group, (d) a coefficient of variation of the one-phase exponential association curve fit less than 30%, and (e) an r^2 curve fit value greater than 0.7 **(Figure 4-1)**. Since all animals in the EX group were labeled for 3 days, the latter two curve-fit criteria were not applied.

Label Free Quantitative Proteomics. The signal intensities of unlabeled peptides were log2 transformed and mean centered to account for small variations in sample loading and instrument variability. A Pearson cross correlation matrix was then created as a visual quality control step in order to examine peptide-level intra-group and inter-group variability. Peptides were then rolled up into their parent proteins, using the top 30% most intense peptides. Proteins containing only a single peptide were eliminated from further analysis. A second Pearson cross correlation matrix was then created as a visual quality control step in order to examine protein-level intra-group and inter-group variability, followed by a principal component analysis (PCA) to examine protein-level clustering. The signal intensities of both experimental groups were normalized against their age-matched control group means. All label free calculations, plots and analysis were performed using Inferno for Proteomics 1.0b (formerly known as DAnTE, developed and distributed by the *Pacific Northwest National Laboratory (PNNL).*

Calculation of Within Proteome Absolute Synthesis (WPAS) Rates. Protein FSR was calculated using the rate constant (k) calculated from curve fitting fractional synthesis values (f) vs. time (t) according to a single pool, monoexponential model: $f=1-e^{(-kt)}$, so that $k=[-\ln(1-f)]/t$, where $t^{1/2}=\ln(2)/k$. The label free normalized signal intensity quotient (Q) was calculated for each protein by correcting individual signal intensities against the control group mean. The WPAS rate is a quantitative metric that combines fractional synthesis and relative pool size changes. WPAS for a given protein was determined by multiplying the fractional synthesis rates and label free values

together: WPAS=k*Q. Our calculation of WPAS rate of individual proteins represents the mass of newly synthesized proteins within a proteome.

Insulin. To determine glucose level, blood samples were taken by venipuncture. To quantify insulin level, plasma was obtained after ON fasting and spun at 14,000 rpm for 5 min to pellet blood cells and supernatant transferred to a fresh tube and placed on dry ice and stored at -80C until use. Insulin in plasma were measured by ELISA kits (Crystal Chem Inc., Downers Grove, IL) using manufactures instructions.

DNL. Mice under the exhaustion EX group were tested by their plasma. We measured DNL of palmitate and synthesis of the glycerol moiety of plasma triglyceride as previously described [374]. In short, body ^2H_2O enrichments were measured by using isotope-ratio mass spectrometry (IRMS) (Metabolic Solutions); average enrichments were 5±1.00% of plasma water. Deuterium incorporation into TG-palmitate was determined by using gas chromatography–mass spectrometry (GC-MS) on an Agilent 6890N GC gas chromatograph coupled to a 5975 MS detector and 7683B injector (Agilent Technologies). Enrichments were determined by selective ion monitoring for their respective m/z under electron ionization, and the percentage of newly made TG-palmitate and TG-glycerol were calculated through MIDA.

Statistics. Protein synthesis rates (k) were modeled using a nonlinear monoexponential biosynthetic model, $f = 1- e^{kt}$ within a mixed-effects statistical model which accounted for the variability in mean peptide counts calculated for each protein as well as the correlation among measurements from the same animals. Reported rates and signifcance levels are based on the mixed model. Tests of the within ontological group treatment effects on FSR assess the difference between rates calculated from mean peptide counts from the control and experimental animals and correspond to tests on fixed effects coeffcients for treatment. Analyses were conducted using R (version 3.1.2). Data were analyzed using GraphPad Prism software (version 9.0) (La Jolla, CA, USA), InfernoRDN (https://omics.pnl.gov/software/infernordn) windows application (version 1.1), Gene set enrichment analysis, GSEA software, and Molecular Signature Database (MSigDB) [327] (http://www.broad.mit.edu/gsea/), and Real Statistics Resource Pack (http://www.real-statistics.com/free-download/real-statistics-resource-pack/) in Excel (version 16).

Gene Ontology Analysis. Gene annotation, gene ontology and biochemical pathway information were obtained from the Database for Annotation, Visualization and Integrated Discovery (DAVID) v6.7 from the National Institute of Allergy and Infectious Diseases (NIAID), at the National Institutes of Health (NIH) [375,376]. In-house software was developed and used to query, compile and statistically analyze gene ontology data, accessed programmatically from DAVID.

5. FIGURES

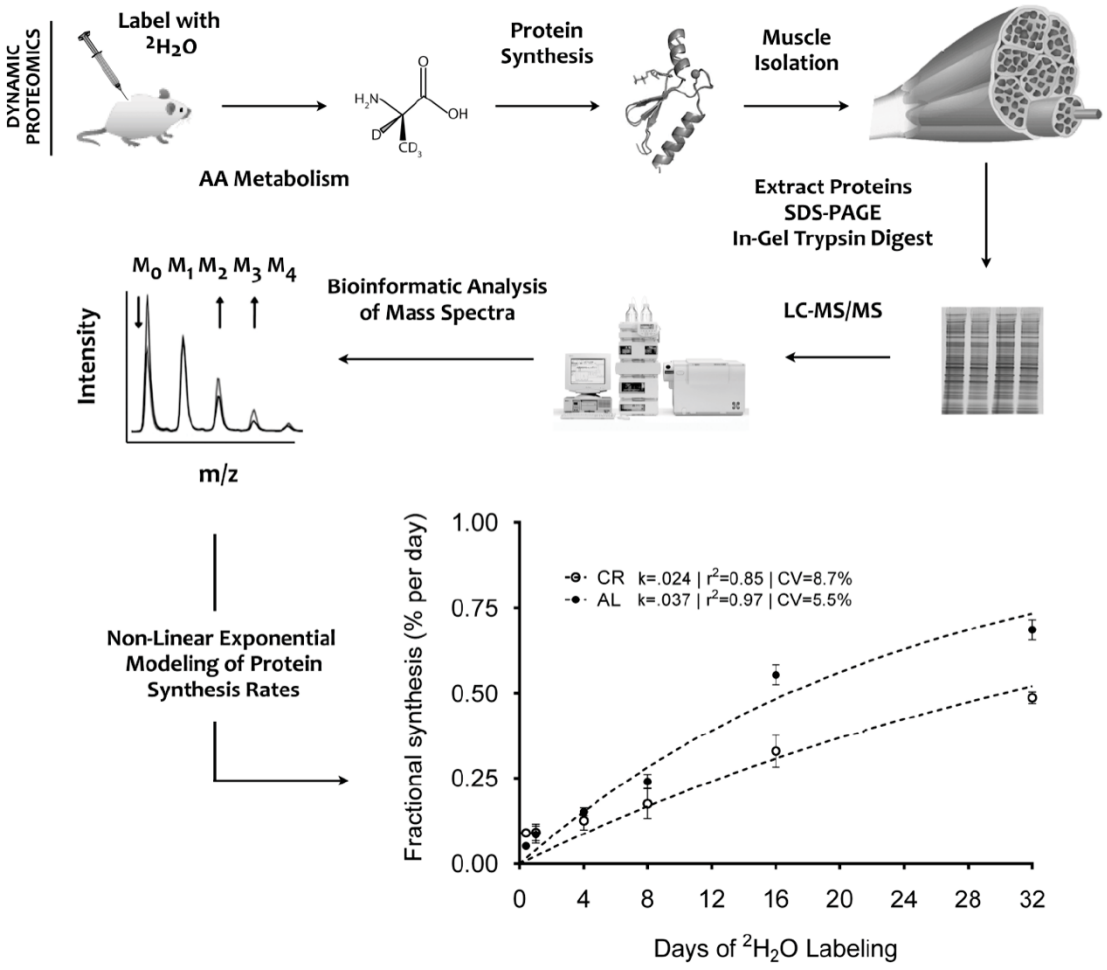

Figure 4-1. Dynamic proteomics experimental workflow. Dynamic proteomics measurements were performed by labeling rats with ^2H_2O (intraperitoneal bolus followed by 8% ^2H_2O in drinking water) to achieve a body water ^2H_2O enrichment of 5%, to allow metabolic labeling of newly synthesized proteins. Muscle isolation, SDS-PAGE protein separation, in-gel trypsinization, and LCMS analysis were performed following 12 hours, 2 days and 5 days of labeling. Dynamic proteomics measurements were performed by analysis of the change in peptide isotope abundance, and quantitative proteomics measurements were performed by label-free analysis. A representative curve-fit for a protein in the CR intervention is shown, filtered according to the following criteria: (a) at least 2 peptides per protein, (b) protein must be identified in at least 2 time points (c) a %CV of the exponential curve fit less than 30%, (d) r^2 value of the protein curve fit greater than 0.7. The rate constant *(k)* in the experimental group was then compared against the rate constant *(k)* in the control group. Only proteins that were altered by a minimum of 10% were considered different than age-matched controls.

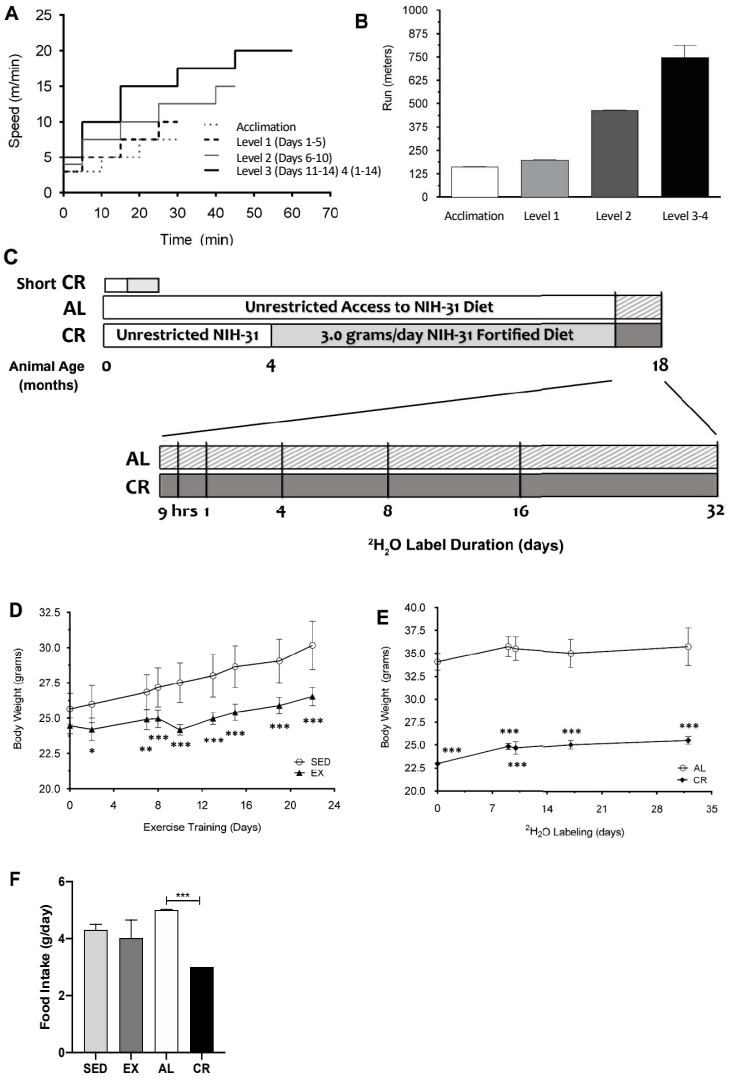

Figure 4-2. EX training protocol and calorie restriction (CR) regimen. (A) EX mice were trained on a rodent treadmill for a total of 3 weeks, at 5 sessions per week. The training protocol was divided into four levels of increasing speed and duration (acclimation, level 1, level 2 and level 3). **(B)** The total distance run during a single exercise session showed a stepwise increase with each level of increasing difficulty. **(C)** CR mice were fed the NIH-31/NIA fortified diet at 5pm daily, and AL mice were provided unrestricted access to the NIH-31 diet. **(D)** Body weight was significantly decreased in EX mice in comparison with SED control mice at all time points after the start of the intervention. **(E)** CR mice weighed significantly less with a stable difference compared to AL control mice throughout the duration of ^2H_2O labeling. **(F)** Food intake was measured for all groups. Data for EX group represents level 4 animals. CR were maintained on a 40% calorie restricted regimen vs. AL control mice from months 4-18 of life. CR mice were fed 3.0 grams of the NIH-31/NIA fortified diet at 5pm daily, and AL mice were provided unrestricted access to the NIH-31 diet. Significance was calculated by a student's t-test vs. age-matched controls (*, $p<0.05$; **, $p<0.01$; ***, $p<0.001$).

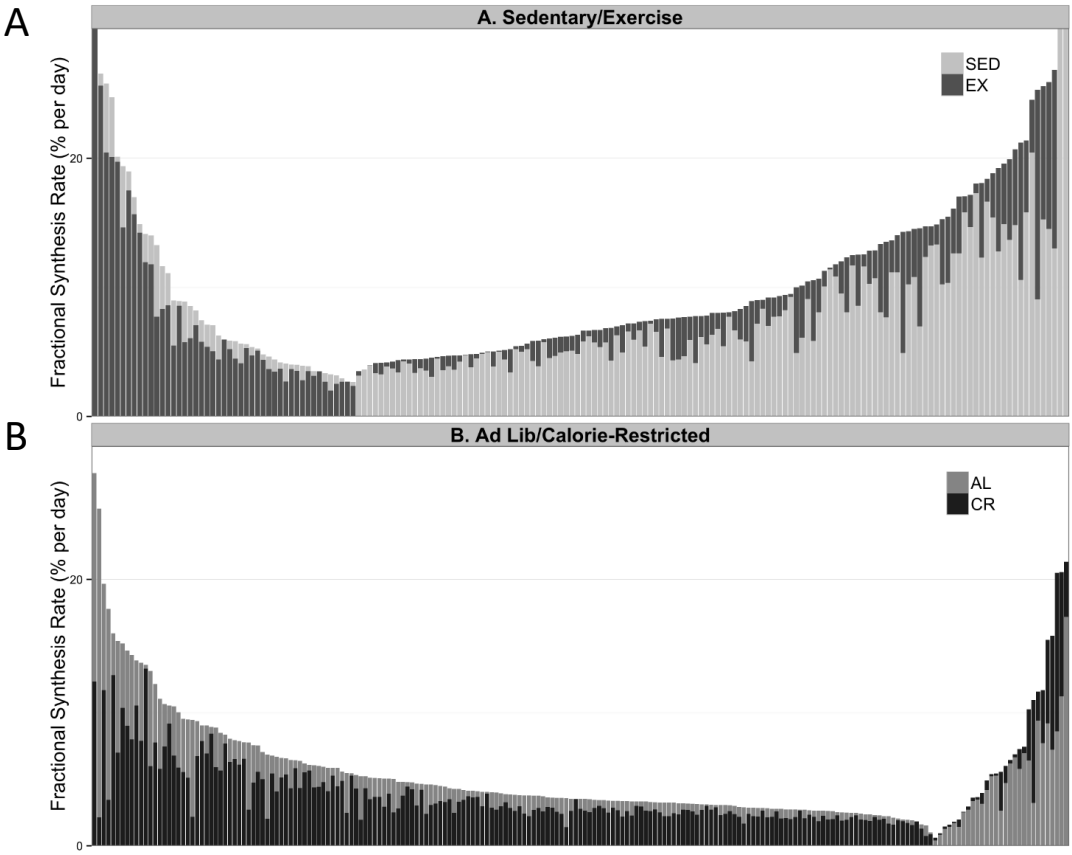

Figure 4-3. Differential effects of calorie restriction on global muscle protein turnover rates. Stacked bars represent the FSR of individual proteins in the experimental and control groups. **(A)** Of the 174 proteins common to the exercise and sedentary samples, exercised mice exhibited higher values of FSR by at least 10% for 56.3% of proteins (n = 98) lower values of FSR by at least 10% for 19.5% proteins (n = 34) and < 10% difference in FSR for the remaining 24.1% of proteins (n = 42). **(B)** Of the 209 proteins common to the CR and sedentary samples, CR mice exhibited lower values of FSR for 77.5% proteins by at least 10% (n = 162), higher values of FSR by at least 10% for 9.1% of proteins (n = 19) and< 10% difference in FSR for the remaining 13.4% of proteins (n = 28). 3 proteins with FSR over 40% were truncated within panel for simplicity of presentation **(A)** (Q61838, Q00898, P29699).

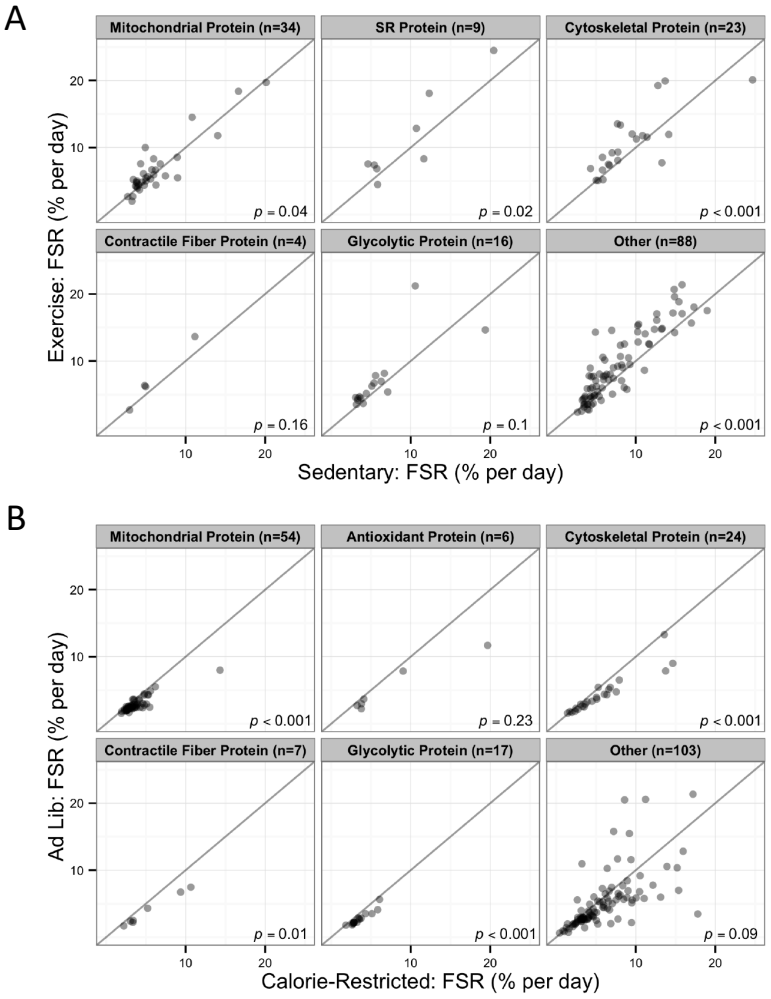

Figure 4-4. EX training increases and CR decreases global muscle protein turnover across many ontologies. (A) Plotted against the line of unity for each individual protein, exercise trained mice exhibited significantly higher protein FSR values across many ontologies including mitochondrial, sarcoplasmic reticulum, and cytoskeletal proteins. Proteins with FSR above 25% were omitted (2 from SR panel, 2 from cytoskeletal panel, 17 from other panel). **(B)** Plotted against the line of unity, CR mice exhibited significantly lower protein FSR values across many ontologies including mitochondrial, cytoskeletal, contractile fiber, and glycolytic proteins. Proteins with FSR above 25% were omitted from the plot. Reported p-values derived from the mixed model assess the within-ontological-group difference in FSR comparing control and intervention.

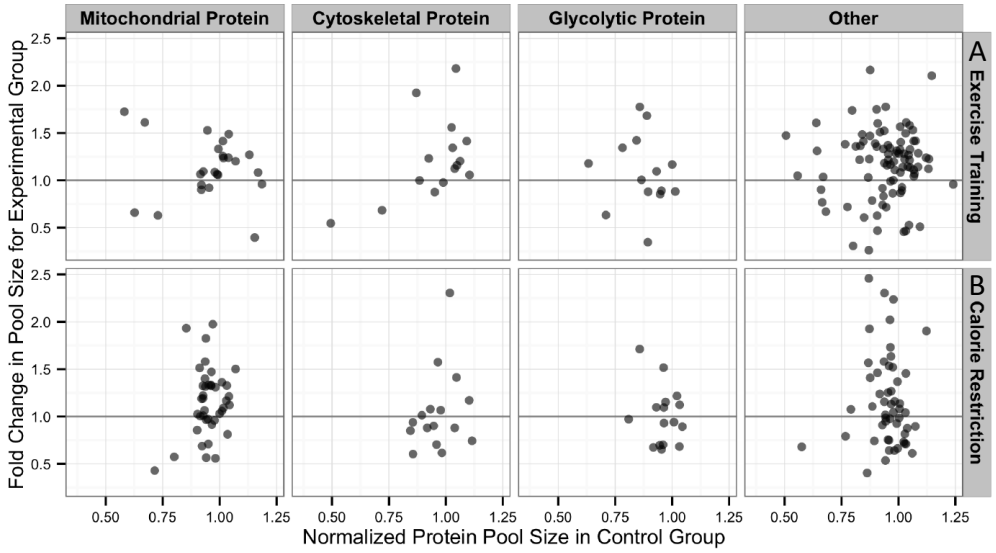

Figure 4-5. EX Training and CR increase global and mitochondrial protein pool size. Median fold difference in protein pool size for experimental group versus median normalized protein pool size in the control group. Protein pool sizes were higher in response to EX training **(A, top panels)** and CR **(B, lower panels)** for mitochondrial and cytoskeletal proteins.

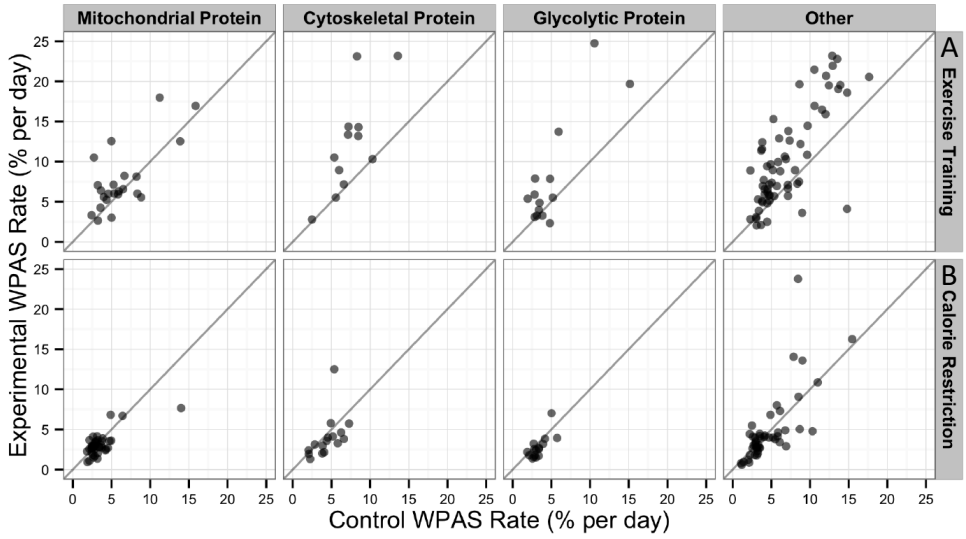

Figure 4-6. Protein WPAS rates are increased in EX but not in CR. WPAS rates for proteins observed in exercise training vs. sedentary animals **(A, top panels)** and CR vs. ad lib animals **(B, lower panels)**; plotted against the line of unity. Points above the line of unity indicate that the WPAS rate for a given protein is higher in the experimental intervention animals than in the control animals. Most points fall above the line in the top panel indicating WPAS rates are higher for proteins in exercised trained animals compared to control animals; the points cluster around the line in the bottom panel, indicating that WPAS rates are similar for proteins in CR and ad lib animals. Proteins with WPAS rates above 25% are not included in the plot.

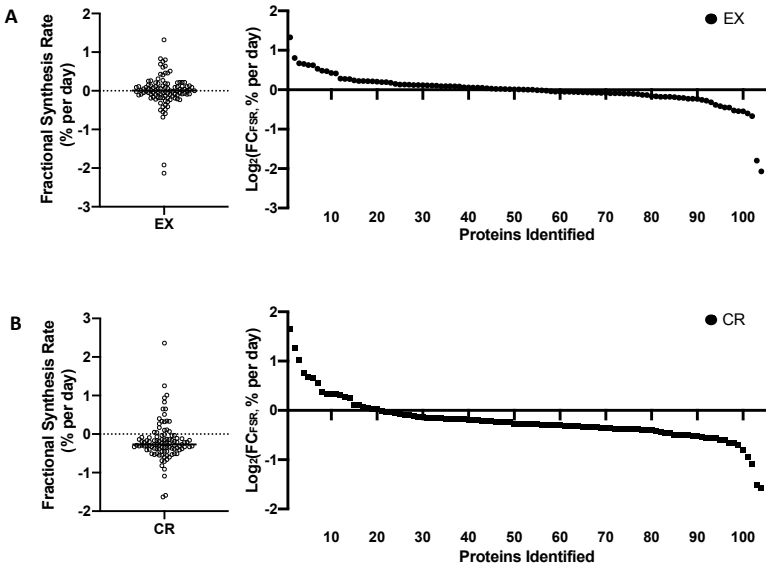

Figure 4-7. Protein FSRs in Skeletal Muscle Are Lower than Controls in CR but not in exhaustion EX. (A) Fractional synthesis rates for proteins observed in EX vs. Con and **(B)** CR vs. Con; plotted as the logarithmic fold change. Points above the line (point 0) represent upregulated proteins (shorter half-lives). Under exhaustion, FSR values are not changed. Under CR condition there was a significant decrease in FSR values (increased half-lives).

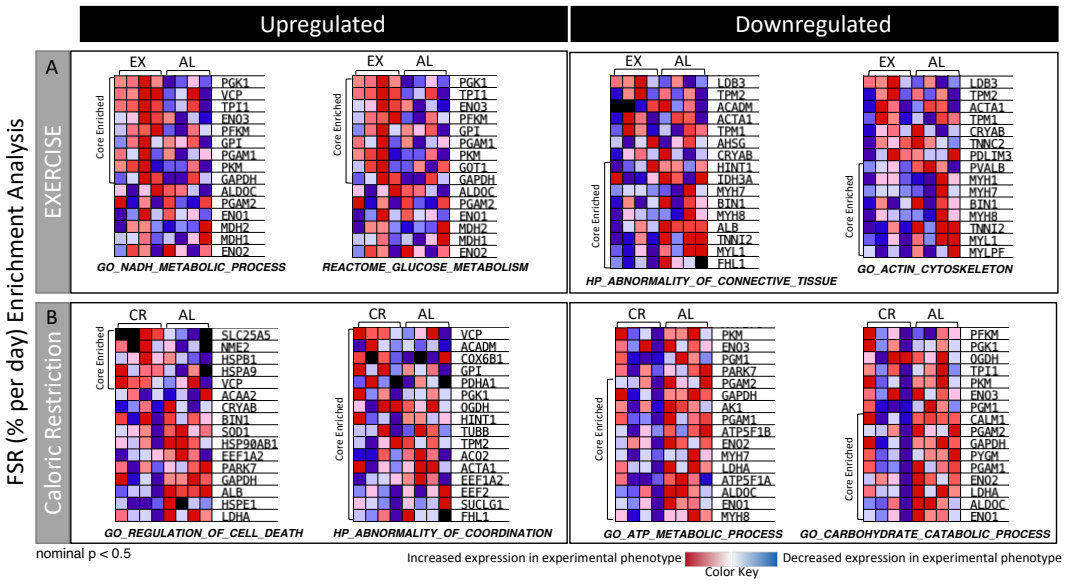

Figure 4-8. Effects of age-matched CR and exhaustion EX on skeletal muscle FSR. An expression data set sorted by correlation with phenotype was used. The corresponding heat map was generated by the maximum enrichment score (ES) ran through a series of datasets. The ES scores were sorted by a rank order of *N* genes according to their correlation to their expression profile. The top ontological of the datasets used (GO, HP, Hallmark, Reactome) led to the most significant pathways observed by functional enrichment analysis of these top bins by EX **(A)** and CR **(B)** phenotypes. A nominal p<0.5 was used as our selection cutoff for the top ontological pathways.

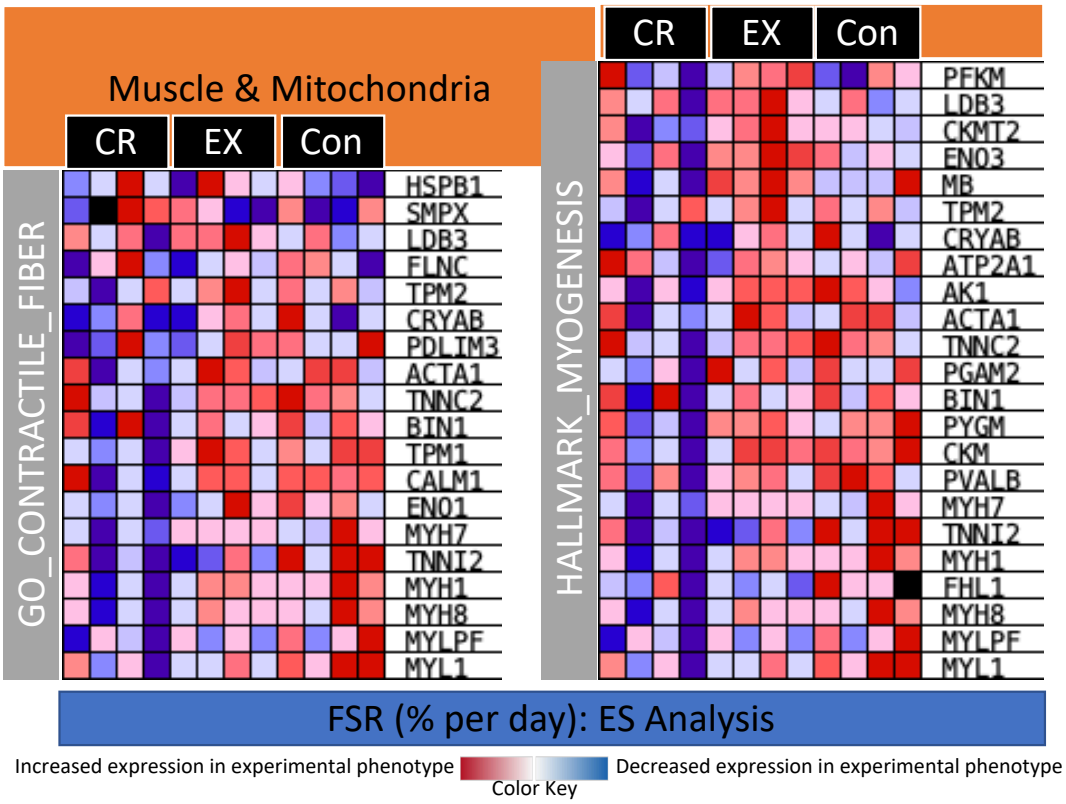

Figure 4-9. Effects of age-matched CR and exhaustion EX on mitochondria and muscle FSR. An expression data set sorted by correlation with phenotype through enrichment analysis was used to compare the effects of intervention on muscle and mitochondria of ontological related pathways.

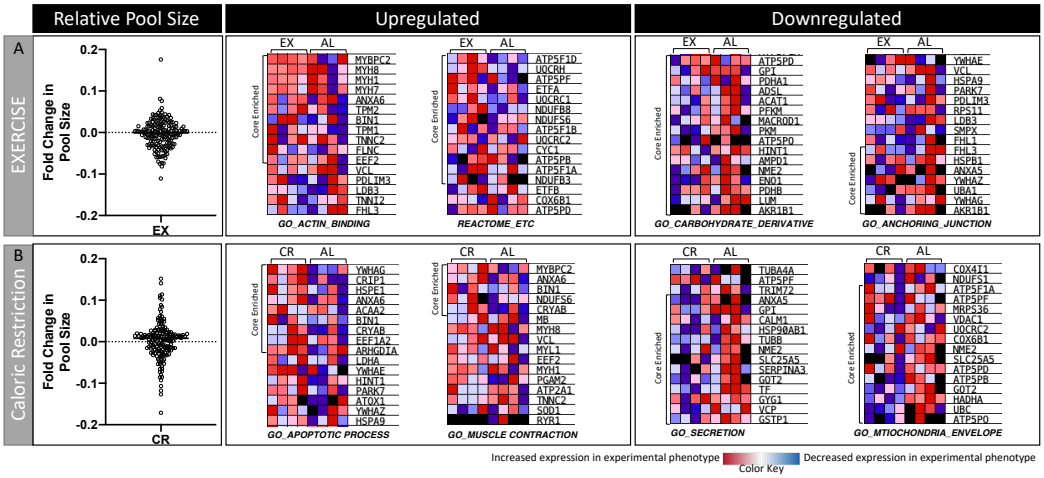

Figure 4-10. Effects of age-matched CR and exhaustion EX on the relative pool size of proteins. EX **(A)** and CR **(B)** comparisons of pool sizes of proteins compared to control. Pool size of CR had a greater fold change than EX on all proteins identified. Ontological analysis by enrichment of comparable proteins by ontology are shown.

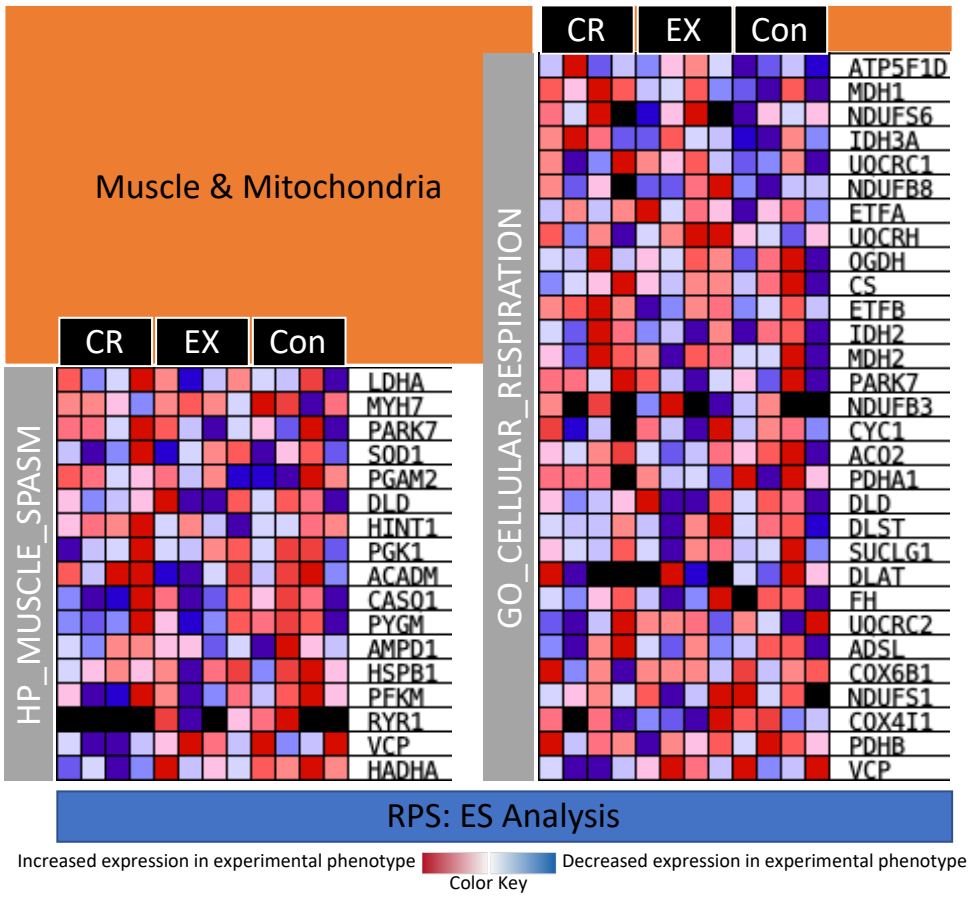

Figure 4-11. Effects of age-matched CR and exhaustion EX on mitochondria and muscle relative pool size. An expression data set sorted by correlation with phenotype was used to compare the effects of intervention on muscle and mitochondria of ontological related pathways.

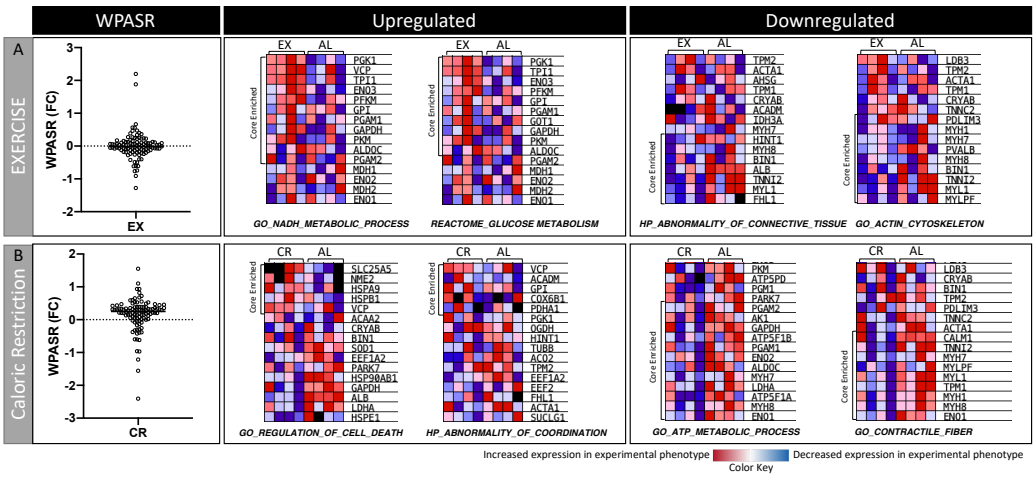

Figure 4-12. Effects of age-matched CR and exhaustion EX on the WPAS rate. EX **(A)** and CR **(B)** comparisons of reveal that CR has a higher global WPASR of proteins compared to control.

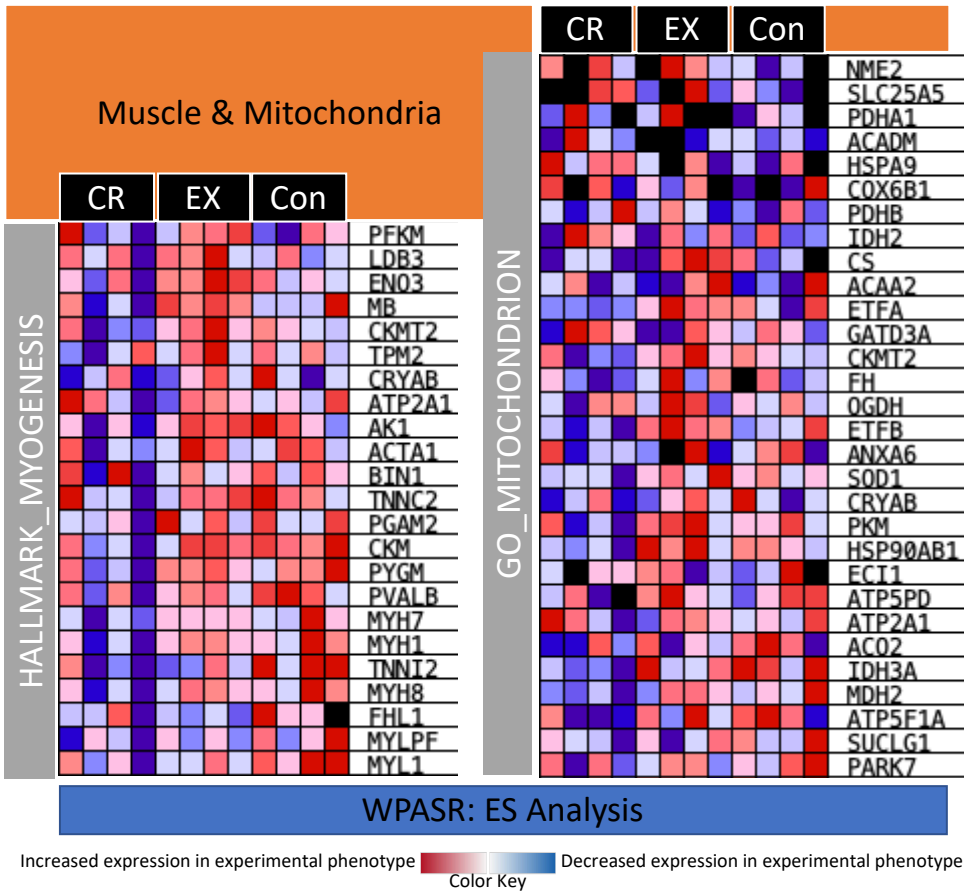

Figure 4-13. WPASR of mitochondria and muscle proteins. Enrichment score analysis show that while global WPASR of muscle proteins under CR is observed, mitochondria and muscle ontologies show a lower WPASR (true increase in half-lives). No obvious changes were observed under EX.

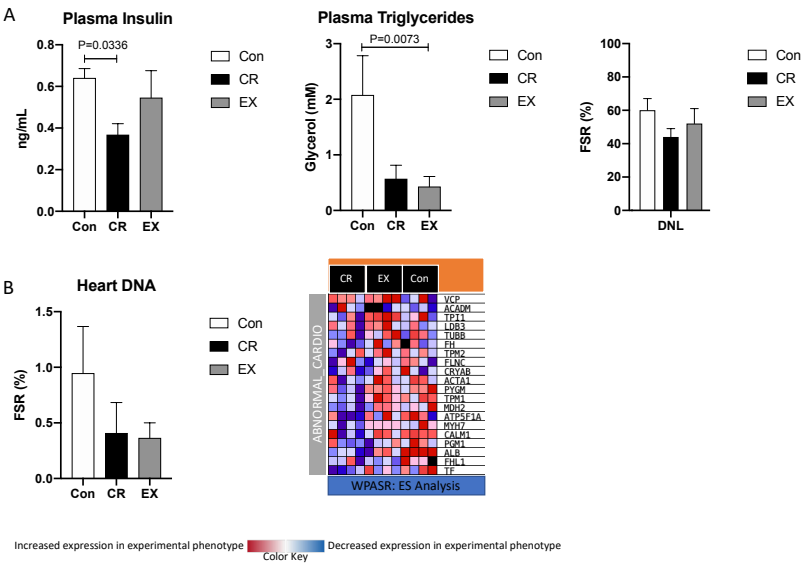

Figure 4-14. Other metrics evaluated. (A) Plasma from mice was used to determine insulin and triglyceride content. FSR of TG-palmitate (de novo lipogenesis) and TG-glycerol (all-source triglyceride replacement) were measured by GC-MS. **(B)** Enrichment score analysis of muscle WPASR revealed differences within groups towards abnormal cardio vasculature. Cell proliferation studies were therefore done by measuring heart DNA. The cell replacement rate marked by newly synthetized DNA for heart tissue were measured as FSR (%) values.

CHAPTER FIVE: Metformin Increases Hepatic Protein Half-lives in Mice

1. INTRODUCTION

CR is one of the oldest strategies known to promote health-span and increase lifespan in a wide array of animal models. The ability of CR to ameliorate the morbidity of various pathologies, including age-associated diseases has led to numerous scientific efforts to understand its mode of action in order to apply it towards human health. However, the current understanding behind the mechanisms of CR on health remains lacking, with many challenges complicating its application to higher organisms such as non-human primates [41,43,377]. In humans, this is particularly challenging as its adherence is poor [378] and with the concern that sustained CR may have undesirable consequences such as negative outcomes toward reproductive hormones that can lead to lower libido, loss of strength, and/or decreased quality of life [379]. This issues are compounded by the fact there are no long-term data on longevity and mortality available on the effects of CR in humans [379]. This has led to increased efforts to replicate the beneficial effects of CR through mimetic compounds with the ability to imitate the health-promoting and lifespan-extending effects of CR without the need for dietary restriction.

The ancient historian Herodotus talked of a society that lived up to one hundred and twenty years old and beyond. It was said that what gave them their exceptional longevity was their flower scented water [11], conceptualizing the idea that compounds hidden in nature can be key to the fountain of youth. Metformin, an anti-diabetic drug derived from the french lilac (*Galega officinalis*), has garnered considerable attention because it has been shown to extend the health and lifespan in mice [217]. Even though the exact mechanism by which metformin improves health span is not fully understood [380], cumulative evidences supports its role in modulating mitochondrial metabolism, extend life- and health span in mice [217], and induce autophagic flux in a manner similar to CR by targeting AMPK, mTOR, histone acetyltransferases, and sirtuins [54,380–382].

CR is also known to trigger a series of complex events, including activation of cellular stress response elements, induction of autophagy, adaptation to apoptosis, and alteration in hormonal balance [383]. Potential CR mimetics like metformin have been explored in hopes to identified important modulators of one or more of these complex events through one of a number of major signaling pathways known to be regulated under CR such as: I) insulin receptor signaling, II) mTOR/S6K signaling, and III) adenylate cyclase/protein kinase-A [384]. The current research on CR mimetics has explored numerous compounds including, but not limited to, 2-Deoxy-d-glucose (glycolytic inhibitor) [385], spermidine and triethylenetetramine (acetyltransferase inhibitor) [386,387], hydroxycitrate (AcCoA synthesis inhibitor) [386], polyphenols like resveratrol or their analogues (sirtuin activators) [105,386], and metformin (AMPK activator) [381,388]. This compounds all share some commonalities within the aforementioned signaling pathways such as their capacity to induce autophagy [9]. For example, mTOR and autophagy signaling share common pathways with that of CR, suggesting they both might share the capacity to maintain proteome homeostasis by balancing the synthesis and recycling of intracellular proteins [9]. In addition, CR mimetics like resveratrol have been shown to influence and increase autophagic flux in a manner similar to the CR-induced deacetylase activity of Sirt1 and other cellular signals in the absence of cytotoxicity [13,389].

While CR can be broadly defined as decreased caloric intake while maintaining proper nutrition, it is also a known activator of autophagy. Under CR and nutrient deprivation, the cell is believed to maintain homeostasis through catabolic adaptations such as autophagosome-lysosome biogenesis [390]. This adaptation is responsible for allowing the lysosome to dispose and recycle macromolecules and damaged organelles through the autophagy degradation processes [156]. While induction of autophagy occurs rapidly under nutrient deprivation, its inactivation can be caused by nutrient enrichment which increases the presence of amino acids and growth factors such as insulin [391]. The possible beneficial effects of CR-induced autophagy could be explained by its role in cell surveillance where autophagy functions as a housekeeping system to maintain proper cellular homeostasis under both normal physiology and pathologic conditions [156]. Another important aspect of autophagy is its role in the clearance of protein aggregates [391]. Studies of CR in young rats have shown autophagic-lysosomal system activation through expressions levels of LAMP1, p62, and LC3II:LC3I [392]. Furthermore, *in vitro* and *in vivo* studies were done to explore the role of CR-induced autophagy in alleviating amyloid burden and tau pathology in animal models of dementia [388]. Therefore, understanding how CR and its mimetics can induce autophagy under various conditions may have important implications in understanding their beneficial effects.

The demonstration that CR can extend the lifespan of many organisms has been a topic of great interest. As a highly metabolically active cellular process, autophagy is hypothesized plays a crucial role in regulating organism longevity [380]. This has led to the question of whether CR mimetics could potentially induce similar beneficial effects through autophagy. Metformin has many diverse benefits and has been tested in numerous phase 3 and 4 studies [393], even though the exact mechanism by which metformin improves heath is not fully understood [380]. Nevertheless, cumulative evidence supports its role in modulating mitochondrial metabolism, extending life- and health span in mice [217], and inducing autophagic flux in a manner similar to CR by targeting AMPK, mTOR, histone acetyltransferases, and sirtuins [54,380–382].

AMPK phosphorylation and activation by LKB1 occurs on the surface of lysosomes in response to starvation [394], and emerging evidence indicates that metformin has some favorable effects on health that are mediated through lysosomal regulation [380,394]. Indeed, alterations in AMPK signaling in response to metformin appear to require the lysosome. For example, metformin was shown to coordinate with mTORC1 and AMPK on purified lysosomes, while attenuating the age-related fitness decline (determined by measuring locomotion, neutral fat depots, and age pigments) through lysosome-dependent activation of AMPK in *C. elegans* [234]. In human subjects who underwent 12 weeks of metformin therapy, it was observed that pro-autophagy genes (ATG4D, ATG9B, p62, ULK1) were increased through blood leukocyte qPCR analysis [382]. In a study on the anti-myeloma effects of metformin in cell lines, it was observed that metformin inhibited their proliferation through cell viability assays, an effect associated with the induction of autophagy [395]. In another study using CD4+ T cells from old human subjects, autophagy indicators were quantified (eg. LC3II and p62 accumulation) and metformin was shown to improve all measures of autophagy in this group [396]. Other findings have suggested that metformin not only activates AMPK,

but also inactivates mTORC1 through the AXIN/LKB1-v-ATPase-Ragulator pathway [397].

The most selective form of lysosomal proteolysis is the chaperone-mediated autophagy (CMA), where individual peptides, recognized by a consensus motif, are translocated directly across the lysosomal membrane. Macroautophagy and CMA activity are maximally activated under stress conditions such as starvation, oxidative stress, or conditions leading to enhanced protein misfolding [398]. However, CMA is the only autophagic pathway that allows selective degradation of soluble proteins in lysosomes. Proteins targeted for degradation are carried to the lysosomal membrane by recognition of a targeting motif (a KFERQ-like motif), by a chaperone complex, consisting of heat shock cognate 70 kDa protein (HSC70) and its cochaperones, in the cytoplasm. Once at the lysosomal membrane, the protein interacts with a lysosomal receptor for this pathway, lysosomal associated membrane protein type 2A (LAMP-2A), and it is translocated across the membrane into the lysosomal lumen assisted by a lysosome resident chaperone [399]. CMA regulates the abundance of many disease-related proteins, with causative roles postulated in neoplasia, neurodegeneration, hepatosteatosis, and other pathologies relevant to human health and aging. At the lysosomal membrane, CMA is inhibited by Akt-dependent phosphorylation of the CMA regulator GFAP. The INS-PI3K-PDPK1 pathway regulates Akt, but its role in CMA is unclear. However, it has been reported that inhibition of PI3K activates CMA [400].

The autophagy activating kinase 1 (ULK1) complex plays a central role in the initiation stage of autophagy. However, the function of ULK1 in the late stage of autophagy is unknown. ULK1 is associated with autophagy initiation by promoting autophagosome–lysosome fusion. It has been reported that phosphorylation of ULK1 enhances its interaction with HSC70 and increases its degradation through CMA [401], where proteins harboring the KFERQ-like motif are unfolded and translocated across the lysosomal membrane directly as single molecules by an HSP7C (heat shock cognate 71 kDa protein) chaperone complex through a pore formed by LAMP-2A [402]. While the exact link between metformin action and lysosomes remains elusive, the hypothesis that its role as a CR mimetic providing longevity and healthy aging suggests the possibility that autophagy plays a vital role.

2. METHODS AND RESULTS

Here, we use a novel flux proteomics approach to explore the role of metformin (referred to here as Met) in hepatic proteome regulation and activation of autophagic pathways. We first compared the effects of Met with those of CR to test the hypothesis that Met is a CR mimetic by using protein half-lives across the global proteome as biomarkers of lifespan extension, as we have previously demonstrated CR, rapamycin administration and the Snell Dwarf mouse [7]. We also included a group administered SBI-0206965 (SBI), a small molecule inhibitor of ULK1 which is a key regulator of autophagy initiation [403].

In the experimental setup, **(Figure 5-1A)**, repeat experiments were divided into five groups (Control [Con] n=4-8; CR n=4-7; Met n=4-15; Met+CR n=4; Met+ULK1

inhibitor SBI n=3-7) were used with C57Bl/6J (6 weeks old) placed under CR (30%) and/or Met treatment (HED: 12-14mg/kg/day) in their drinking water **(Figure 5-1B)** for the duration of the experiment. Body weights **(Figure 5-1A)** were measured regularly throughout the experimental intervention and groups under CR had significantly less weight ($p<0.05$). Insulin **(Figure 5-1C)** was measured in plasma under fasting conditions and showed significant downregulation under CR ($p<0.04$) but not Met (p=n.s.). Glucose **(Figure 5-1D)** was measured in plasma and showed highly significant fall ($p<0.007$) under CR but not Met (p=n.s.).

We first took a comprehensive view of gene expression during CR at the length of our intervention. We used hepatic RNA to perform RNA-seq and performed gene sequence enrichment analysis **(Figure 5-2A)**, where we identified the major upregulated (1281 genes) and downregulated (2552 genes) ontological-enriched pathways. Data characterization was then performed using gene enrichment scores to define some of the major biological themes **(Figure 5-2B)** within an enrichment map including clusters of either up- or downregulated groups. Of note was significant upregulation of nitric oxide (NO) stimulated pathways which interacted with the plateau phase 4 and unblocking nmda.

A similar approach was done for gene expression during Met. We first took a comprehensive view of gene expression during Met. We used hepatic RNA to perform RNA-seq and performed gene sequence enrichment analysis **(Figure 5-3A)**, where we identified the major upregulated (2144 genes) and downregulated (752 genes) ontological-enriched pathways. Data characterization was then performed using gene enrichment scores to define some of the major biological themes **(Figure 5-3B)** within an enrichment map including clusters of either up- or downregulated groups. Of note was significant upregulation of binding proteins and a downregulation of cholesterol SREBP.

Following up on the observation of cholesterol biogenesis on the biological theme analysis. We performed ontological analysis of enriched pathways for both CR and Met **(Figure 5-4A through 5-4B)**. Reactome analysis showed significant (FDR<0.003) in cholesterol biosynthesis under CR **(Figure 5-4A)** and Hallmark cholesterol homeostasis **(Figure 5-4B)** at high significance (FDR<0.08). We then measured the fractional synthesis of cholesterol in both plasma and liver **(Figure 5-4C)** but we did not detect any significant changes. These results point out that mRNA levels often do not predict or correlate with metabolic fluxes through their cognate pathways.

We then measured the FSR (%) of liver proteins **(Figure 5-5A)** and observed a significant downregulation (longer half-lives) of proteins under CR under Met. Met and CR co-intervention did not differ from the results with either alone. We then analyzed the fold change of the proteins as compared to the control and quantified their binomial distribution of FSR values that were higher vs lower **(Figure 5-5B)**. CR had the most dramatic decrease in FSR with 92.3% of proteins downregulated (2-TAILED P<0.0001), with Met+CR showing 91.5% of proteins downregulated (2-TAILED P<0.0001) and Met treatment similarly slowing down the FSR of 78.9% of hepatic proteins (2-TAILED P<0.0001).

We performed enrichment analysis for both CR and Met **(Figure 5-6A through 5-4B)**. HP analysis reveals core enrichment of genes downregulated under all interventions in abnormal glucose homeostasis under CR **(Figure 5-6A)** and hallmark mTORC1 signaling **(Figure 5-6B)**. We also looked at proteins involved in autophagy **(Figure 5-6C)**. Of note was the increase in the half-lives of HSC70 which is involved in autophagy signaling.

Through free label quantitative proteomics, we then determined the change in protein pool size (abundances) in response to Met and CR. Using the pool size estimations for each protein and its corresponding FSR values as previously described in Chapter Four, we then determined the within-proteome absolute synthesis (WPAS) rates of hepatic proteins **(Figure 5-7A through 5-7C)** under Con, CR, Met and Met+CR. Under CR **(Figure 5-7A)**, all values but two were below their respective protein control for the 81 proteins that were identified. Met **(Figure 5-7B)** shared a similar pattern as CR where most proteins were downregulated, demonstrating that this antidiabetic drug has a potential CR mimetic by WPASR values. A similar pattern of downregulation was observed for the Met+CR group **(Figure 5-7C)**.

Activation of autophagy is a promising target of both CR and Met where the literature (discussed above) suggests that these interventions are potent activators. In agreement, our data point to a possible novel role of autophagy in the regulation of a particular subset of proteins resistant to this process. We therefore included a study group in which we inhibited the initiation of autophagy by administration of SBI-0206965 (SBI) [403]. Recently, the role of ULK1 in the fusion of the autophagosome to the lysosome was shown to be dependent on its phosphorylation state via the nutrient signal protein kinase C (PKC), which leads to ULK1 degradation by CMA. We administered Met as before, with the inclusion of an extra group where Met was combined with SBI. Body weights **(Figure 5-8A)** show the changes over time and the CR effect is observed early on; this Figure also points when SBI was administered IP. For the Met+SBI subgroup **(Figure 5-8A through 5-8D)**, we induced inhibition (n=7 mice, in two separate experiments) with SBI at the start of the labeling period for proteome turnover **(Figure 5-8A)**. We hypothesized that if there is activation of autophagy by Met, we could inhibit some of its effects by administration of a ULK1 inhibitor (**Figure 5-8B)**.

We first analyzed the hepatic proteome FSR values (**Figure 5-8C)** which show that under CR, as previously observed, most proteins had longer half-lives when compared to control. This pattern was reflected in the Met group. However, after inhibition of autophagy by SBI administration in the Met treatment group there was a more modest decrease in hepatic protein FSRs. When we analyzed the fold change of the FSR values compared to controls statistically **(Figure 5-10D)** by the binomial distribution test, CR had 80% decrease in protein FSR and Met had a 92% decrease in FSR values. However, while FSR values remained statistically significantly downregulated (longer half-lives) compared to controls, inhibition of autophagy with SBI through inhibition of ULK1 resulted in a 24% lower percent of proteins with reduced FSR values during metformin treatment (from 92% in Met, $p < 0.0000001$ to 68% in Met+SBI, $p = 0.00004$).

We then looked at the WPAS rates of all groups **(Figure 5-9A through 5-9B)**, observing that both CR and Met had a significant decrease in the WPAS turnover rate of most proteins when compared to Con. In contrast, several points in the Met+SBI group showed proteins with a higher turnover rate than Met alone. This reveals a potential role for measuring protein half-lives in assessing macroautophagy. We then hypothesized that during the labeling period we could see a signature of proteins whose replacement rate is influenced by the CMA signal sequence (KFERQ). We therefore set to explore how changes in protein half-lives could be influenced by the presence of this CMA signal sequence **(Figure 5-9B)** and found that 37% of the identified proteins were KFERQ-positive and 63% were KFERQ-negative.

To explore the role of autophagic targeting further, we looked at the fold change **(Figure 5-10A through 5-10C right side)** of the groups when compared to control in the context of proteins with a KFERQ positive or a KFERQ negative signal for CMA. In a global context, KFERQ positive proteins under CR **(Figure 5-10A)** had the greatest decrease in WPAS rates. Distribution analysis showed that the proteins with the greatest degree of change were also those within the longest period of turnover and were notably enriched for KFERQ-positive sequences. In the Met group **(Figure 5-10B)**, no pronounced patter was observed although longer-lived proteins tended to have the highest degree of change. However, after SBI administration in the Met group **(Figure 5-10C)** a fascinating observation was that fast-turnover proteins were uniquely upregulated for FSR (had shorter half-lives) in the KFERQ-positive group. The power of flux proteomics allowed us to detect changes in kinetically distinct subsets within the whole dataset.

3. CONCLUSION

Metformin has been used for over a half a century to treat type 2 diabetes. In humans, metformin enhances insulin sensitivity and suppresses gluconeogenesis but the molecular mechanisms that underlie its function remain unclear. It has been suggested that metformin acts as a CR mimetic, as both conditions are known to regulate many shared pathways. Using a novel flux proteomics approach to label newly synthetized proteins *in vivo*, we report here novel observations of the effects on proteome dynamics of metformin alone, in combination with CR or in combination with an autophagy inhibitor (SBI)

We demonstrate that metformin is a powerful CR mimetic that, like CR, slows down the FSR and WPAS (fractional and total synthesis) rates of hepatic proteins. We show, more specifically, that metformin significantly reduces the turnover rate of proteins in a signature that resembles CR. We then tested the effects of metformin within the context of lysosomal regulation through modulations of the lysosomal pathway to understand if autophagy could coordinate the half-lives of longer-lived proteins.

Within this context, we observed as a general effect that the half-lives of hepatic proteins were less prolonged by metformin treatment when autophagy was inhibited by SBI co-administration. This result suggests a possible role for autophagy in maintenance of proteins over a more non-specific response activation. Indeed, as more biology of autophagy is learnt, the mechanism appears to be regulated in an

increasingly nuanced manner. One such known regulatory mechanism for autophagy is CMA, where proteins with a KFERQ sequence are able to be targeted to the lysosome through a regulated process. Looking at a subset of proteins in our data set where we identified those with the longest lifespan (longest half-lives), we observed that the presence of the KFERQ specifically alters response of protein dynamics to Met treatment in more slowly turning over proteins. More broadly, our findings show that inhibition of autophagy does not slow down the replacement rate of all proteins in the setting of Met administration but accelerates replacement rates in longer-lived proteins that we measured. This is contrary to expectation, as autophagy is generally conceptualized as a general pathway for protein degradation and turnover. Our data for CMA-targeted proteins and SBI show that autophagy plays a role in maintenance of proteosome activity through the upkeep of KFERQ-positive proteins.

We also compare gene expression by RNA-Seq. We observed induction of important regulators of cell death such as a significant upregulation of the caspase recruitment domain (CARD) binding **(Figure 5-3B)**. In this regard, the modulatory roles of caspases are poorly understood. However, recent evidence has shown that in contrast to apoptosis, autophagy promotes cell survival by providing energy and nutrients through the lysosomal degradation of cytoplasmic constituents where caspases have been shown to directly interact with core autophagy proteins [404].

4. METHODS

Mice. Six-week old male C57Bl/6 mice (n=50) were purchased from Jackson labs (Jackson laboratory, Bar Harbor, ME), and were randomly divided into control group (n=12), CR under 30% restriction (n=11), metformin treated (n=16), metformin under CR (n=4), and metformin plus SBI administration (n=7). Animals not under CR were provided unrestricted access to the AIN-93M diet (Bio-Serv). Animals under CR were given 30% less food than the control group. Body weights and food intake were recorded approximately every 3-4 days during the duration of the experiment. Animals were labeled with $^{2}H_2O$ 4 days before sacrification.

Calorie Restriction. Male C57Bl/6J mice under CR were given 30% less food than the control every day between 12-1pm. Weight adjustments for diet were done weekly based on the amount of food the controls consumed.

Metformin Administration. Male C57Bl/6J mice under metformin administration were given USP grade Metformin (Sigma 1396309 USP) in their drinking water. Metformin was dissolved in the same water used for the whole colony at 1.5 mg/mL and sterile filtered through 0.22-μm disposable filters (Millipore, Millex-GV) before use. The solution was made fresh and given to mice in their drinking water bottles. Bottles with metformin were changed every 5 days for the duration of the experiment.

SBI-0206965 Administration. Male C57Bl/6J mice under metformin administration were given SBI-0206965 (Sigma SML1540) at 2 mg/kg body weight and injected into mice intraperitoneally (i.p.) as previously described [405].

Euthanasia. Animals were anesthetized with isoflurane and euthanized by cardiac puncture. All experiments were performed under the approval of the Institutional Animal Care and Use Committees of the University of California at Berkeley.

RNA-Sequencing. Total RNA was isolated from mouse livers using RNeasy Micro Kit from Qiagen (Hilden, Germany). RNA Quantity was determined using a Qubit (TM) fluorometric assay and quality was determined using Eukaryote Total RNA Pico (Agilent Bioanalyzer 2100). The library preparation and sequencing were done on a single lane (Illumina HiSeq4000) at 100bp pair-end (PE) reads and performed at the Vincent J. Coates Genomics Sequencing Laboratory at University of California (UC), Berkeley. The raw sequencing files were processed with CASAVA 1.8.2 (Illumina) to generate fastq files. We first obtained read quality reports by using the FastQC tool (http://www.bioinformatics.babraham.ac.uk/projects/fastqc/), which gave us overall high-quality scores. The fastq files were then uploaded onto the Galaxy project portal (https://usegalaxy.org/) [337]. The reads were then mapped to the mouse reference genome (mm10) using the Burrows-Wheeler Aligner (BWA) module. Differential gene expression of RNA-seq was determined using DESeq2 [338].

Measurement of ^2H enrichment in body water. Animals in each group were labeled with an intraperitoneal injection of 100% ^2H_2O saline (0.35mL/10 g body weight), and provided with 8% ^2H_2O drinking water for the remainder of the study to maintain body ^2H_2O enrichments of approximately 5%, as described previously [372]. Measurement of ^2H_2O enrichment in body water was done from whole blood samples using a Liquid Water Isotope Analyzer (Los Gatos Research, Mountain View, CA) after a 1:300 dilution and distillation as previously described [373].

Liver Protein Isolation and In-Gel Trypsin Digestion. Livers were harvested from mice at the time of euthanasia, and immediately snap frozen on liquid nitrogen until further analysis. Tissue protein was isolated by homogenization in RIPA buffer containing PhosStop phosphatase inhibitor cocktail (Roche, Indianapolis, IN), 1mM DTT, 7.5ug/mL leupeptin, 1ug/mL pepstatin, 2ug/mL aprotinin, 1mM PMSF in isopropanol, and 100nM nicotinamide using a TissueLyser (Qiagen, Germantown, MD), followed by centrifugation at 10,000g for 10 minutes at 4 ºC. The supernatant containing soluble proteins was used for the analysis. Protein from prepared homogenates was uniformly reduced by incubation in 10 mM DTT and SDS-PAGE sample loading buffer for 10 min at 70°C. The reduced samples were then alkylated by incubating in 15 mM iodoacetamide for 1 hour at room temperature in the dark. Samples were then trypsin digested at 37ºC (Trypsin Gold, Promega, Madison, WI). In each experiment, samples were analyzed by LC-MS/MS, corresponding to a molecular weight range of 20-80kDa.

LC/MS Analysis and Protein Turnover Calculations. Trypsin-digested peptides were analyzed on an Agilent 6520 QTOF (quadrupole time-of-flight) mass spectrometer with 1260 Chip Cube nano ESI source (Agilent Technologies, Santa Clara, CA). Peptides were separated chromatographically using a Polaris HR chip (Agilent #G4240-62030) consisting of a 360 nL enrichment column and a 0.075 x 150 mm analytical column, each packed with Polaris C18-A stationary phase with 3 µm particle size. Mobile phases were (A) 5% v/v acetonitrile and 0.1% formic acid in

deionized water and (B) 95% acetonitrile and 0.1% formic acid in deionized water. Peptides were eluted at a flow rate of 350 nL/min during a 18 min LC gradient (2%B at 0 min, 5%B at 0.5 min, 30%B at 10 min, 50%B at 13 min, 90%B at 13.1-18 min, 2%B at 18.1 min; Stop time: 32 min). Each sample was analyzed twice, once for protein/peptide identification in data-dependent MS/MS mode and once for peptide isotope analysis in MS-only mode. Acquisition parameters were: MS/MS acquisition rate = 6 Hz MS and 4 Hz MS/MS with up to 12 precursors per cycle, MS acquisition rate = 0.9 Hz, ionization mode = positive electrospray; capillary voltage = -1980 V; drying gas flow = 4 L/min; drying gas temperature = 290 °C; fragmentor = 170 V; skimmer = 65 V; maximum precursor per cycle = 20; scan range = 100-1700 m/z (MS), 50-1700 m/z (MS/MS); isolation width (MS/MS) = medium (~4 m/z); collision energy (V) = -4.8+3.6*(precursor m/z/100); active exclusion enabled (exclude after 1 spectrum, release after 0.12 min); charge state preference = 2, 3, >3 only, sorted by abundance; TIC target = 25,000; reference mass = 922.009798 m/z. Acquired MS/MS spectra were extracted and searched using Spectrum Mill Proteomics Workbench software (version B.04.00, Agilent Technologies, Santa Clara, CA) and a UniProtKB/Swiss-Prot mouse protein database (UniProt.org, release 2012_02). Data files were extracted with the following parameters: fixed modification = carbamidomethylation of cysteine, scans with same precursor mass merged by spectral similarity within tolerances (retention time +/- 10 sec, mass +/-1.4 m/z), precursor charge maximum z = 6, precursor minimum MS1 S/N = 10, and 12C precursor m/z assigned during extraction. Extracted files were searched with parameters: enzyme = trypsin, *Mus Musculus*, fixed modification = carbamidomethylation of cysteine, variable modifications = oxidized methionine + pyroglutamic acid + hydroxylation of proline, maximum missed cleavages = 2, minimum matched peak intensity = 30%, precursor mass tolerance = 10 ppm, product mass tolerance = 30 ppm, minimum detected peaks = 4, maximum precursor charge = 3. Search results were validated at the peptide and protein levels with a global false discovery rate of 1%. Proteins with scores greater than 11.0 were reported and a list of peptides with scores greater than 6 and scored peak intensities greater than 50% was exported from Spectrum Mill and condensed to a non-redundant peptide formula database using Excel. This database, containing peptide elemental composition, mass, and retention time was used to extract MS spectra (M0-M3) from corresponding MS-only acquisition files with the Find-by-Formula algorithm in Mass Hunter Qualitative Analysis software (version B.05.00, Agilent Technologies, Santa Clara, CA). MS spectra were extracted with parameters: EIC integration by Agile integrator, peak height > 10,000 counts, include spectra with average scans > 12% of peak height, no MS peak spectrum background, unbiased isotope model, isotope peak spacing tolerance = 0.0025 m/z plus 12.0 ppm, mass and retention time matches required, mass match tolerance = +/- 12 ppm, retention time match tolerance = +/- 0.8 min, charge states z = +2 to +4, chromatogram extraction = +/- 12 ppm (symmetric), EIC extraction limit around expected retention time = +/- 1.2 min. Details of FSR calculations and data filtering criteria were described previously [305,326]. Briefly, in-house software was developed to calculate peptide elemental composition and curve fit parameters for predicting isotope enrichments of peptides in newly synthesized proteins based on precursor body water enrichment (p) and the number (n) of amino acid C–H positions per peptide actively incorporating ^{1}H and ^{2}H from body water. Incorporation of ^{2}H into tryptic peptides decreases the relative proportion of M0 within the overall isotope envelope spanning M0-M3. Fractional

synthesis was calculated as the ratio of excess %M0 (EM_0) for each peptide compared to the maximal absolute EM_0 possible at the measured body water enrichment. Data handling was performed using Microsoft Excel templates, with input of precursor body water enrichment for each subject, to yield fractional replacement rate (FSR) data at the protein level. The kinetics data were filtered to exclude protein measurements with fewer than two peptide isotope measurements per protein. Following LC-MS/MS measurement of peptide spectra, we used five stringent selection criteria to remove low confidence kinetic data: (a) peptide signal intensity must be more than 30,000 counts, (b) RMS error for unlabeled peptide mass isotopomer abundance measurements must be less than 1.5% compared with natural abundance, (c) observation of the parent protein in at least 2 mice per experimental group, (d) a coefficient of variation of the one-phase exponential association curve fit less than 30%, and (e) an r^2 curve fit value greater than 0.7 **(Figure 4-1)**. Since all animals in the EX group were labeled for 3 days, the latter two curve-fit criteria were not applied.

Label Free Quantitative Proteomics. The signal intensities of unlabeled peptides were log2 transformed and mean centered to account for small variations in sample loading and instrument variability. A Pearson cross correlation matrix was then created as a visual quality control step in order to examine peptide-level intra-group and inter-group variability. Peptides were then rolled up into their parent proteins, using the top 30% most intense peptides. Proteins containing only a single peptide were eliminated from further analysis. A second Pearson cross correlation matrix was then created as a visual quality control step in order to examine protein-level intra-group and inter-group variability, followed by a heatmap examination of protein-level intensities. These signal intensities of the experimental groups were normalized against their control group means. All label free calculations, plots and analysis were performed using Inferno for Proteomics 1.0b (formerly known as DAnTE, developed and distributed by the *Pacific Northwest National Laboratory (PNNL).*

Calculation of Within Proteome Absolute Synthesis (WPAS) Rates. Protein FSR was calculated using the fractional synthesis values (f) according to a single pool. The label free normalized signal intensity quotient (Q) was calculated for each protein by correcting individual signal intensities against the control group mean. The WPAS rate is a quantitative metric that combines fractional synthesis and relative pool size changes. WPAS for a given protein was determined by multiplying the fractional synthesis rates and label free values together: WPAS=k*Q. Our calculation of WPAS rate of individual proteins represents the mass of newly synthesized proteins within a proteome.

Insulin. To determine glucose level, blood samples were taken by venipuncture. To quantify insulin level, plasma was obtained after ON fasting and spun at 14,000 rpm for 5 min to pellet blood cells and supernatant transferred to a fresh tube and placed on dry ice and stored at -80C until use. Insulin in plasma were measured by ELISA kits (Crystal Chem Inc., Downers Grove, IL) using manufactures instructions.

Cholesterol Biosynthesis. Mice under CR, Met and their control were measured for their liver and plasma cholesterol as previously described [406].

Statistics and Analysis. Reported rates and signifcance levels are based on a mixed model. Tests of the within ontological group treatment effects on FSR assess the difference between rates calculated from mean peptide counts from the control and experimental animals and correspond to tests on fixed effects coeffcients for treatment. Analyses were conducted using R (version 3.1.2). Data were analyzed using GraphPad Prism software (version 9.0) (La Jolla, CA, USA), InfernoRDN (https://omics.pnl.gov/software/infernordn) windows application (version 1.1), Gene set enrichment analysis, GSEA software, and Molecular Signature Database (MSigDB) [327] (http://www.broad.mit.edu/gsea/), and Real Statistics Resource Pack (http://www.real-statistics.com/free-download/real-statistics-resource-pack/) in Excel (version 16). KFERQ Sequence analysis was conducted using the KFERQ finder (version 0.8) considering for the output options the canonical standard motifs. CMA-targeting (KFERQ-like) targeting motifs were searched in mouse proteins in UniProt KFERQ-like motifs belonging to different classes based on their amino acid composition [407].

5. FIGURES

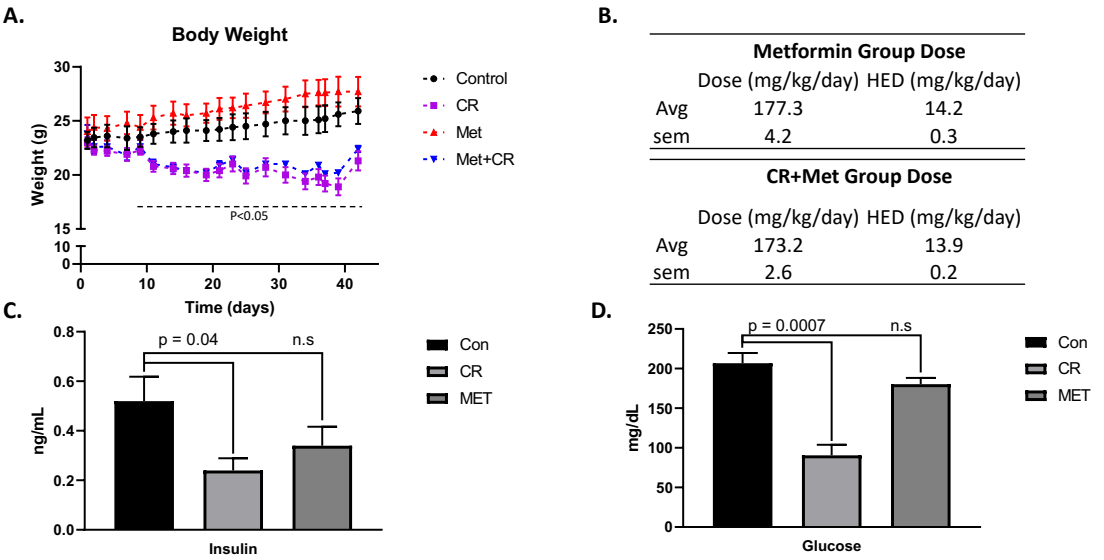

Figure 5-1. Experimental conditions. (A) C57Bl6/J mice (n=4 per group) at 6 weeks of age were single caged and their body weights tracked throughout the length of intervention. **(B)** Dose by factor method was used to estimate human equivalent dose (HED) to reflect the dose that in humans is anticipated to provide the same degree of effect as that observed in animals [408]. Met doses were calculated by HED for both Met and Met+CR groups and correspond to a dose of approximately 1,000 mg/day in a 70kg human subject, which is a low and common clinical dose in diabetic patients. **(C)** Plasma levels of insulin and **(D)** glucose. Data are represented as the mean ± s.e.m. $P \leq 0.05$ versus control mice (two-Sample assuming unequal variance followed t-test two tailed).

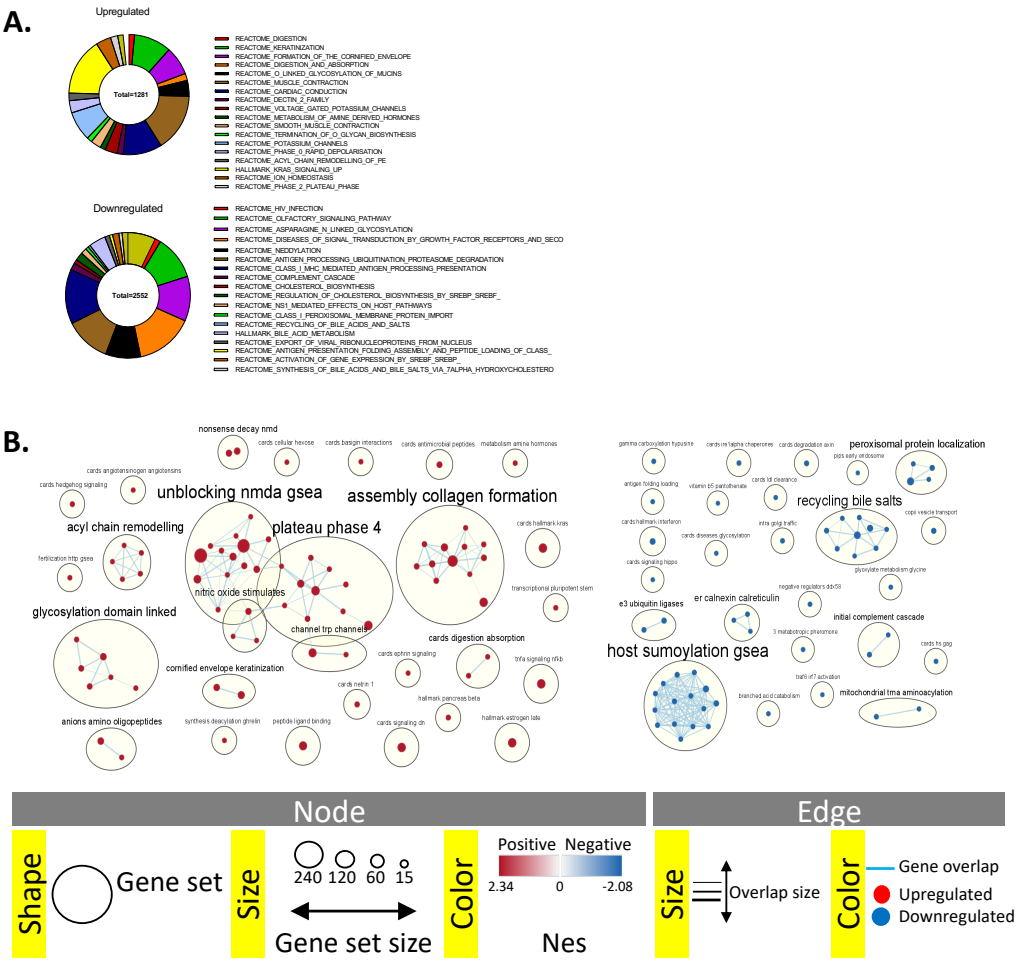

Figure 5-2. Gene sequence enrichment analysis. RNA-Seq experiment for CR group. **(A)** Top data sets significantly enriched at a FDR < 0.25. Ranked gene list correlation profile for FSR expressions showing the distribution of FSR between positive (CR group) and negative (Con group) correlation. Gene sets were counted by size and ordered by normalized enrichment score (*NES*). **(B)** Gene enrichment visualization of pathway networks under CR and clustered by function, where gene enrichment visualization of pathway networks under CR are represented by Blue dots as downregulated pathways, and red dots as upregulated pathways. (P-value Cutoff: 0.05, FDR Q-value Cutoff: 0.25)

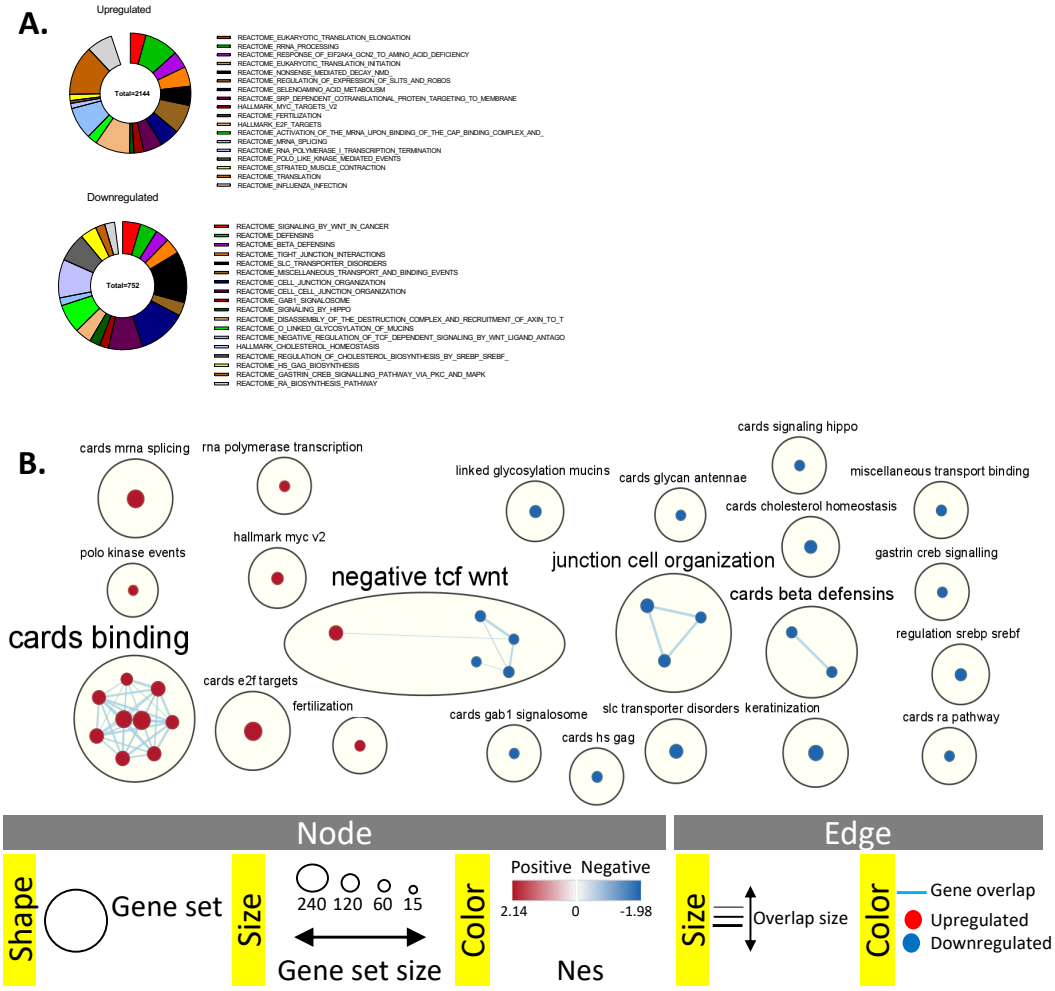

Figure 5-3. Gene sequence enrichment analysis. RNA-Seq experiment for Met group. **(A)** Top data sets significantly enriched at a FDR < 0.25. Ranked gene list correlation profile for FSR expressions showing the distribution of FSR between positive (CR group) and negative (Con group) correlation. Gene sets were counted by size and ordered by normalized enrichment score (*NES*). **(B)** Gene enrichment visualization of pathway networks under Met and clustered by function, where gene enrichment visualization of pathway networks under Met are represented by Blue dots as downregulated pathways, and red dots as upregulated pathways. (P-value Cutoff: 0.05, FDR Q-value Cutoff: 0.25)

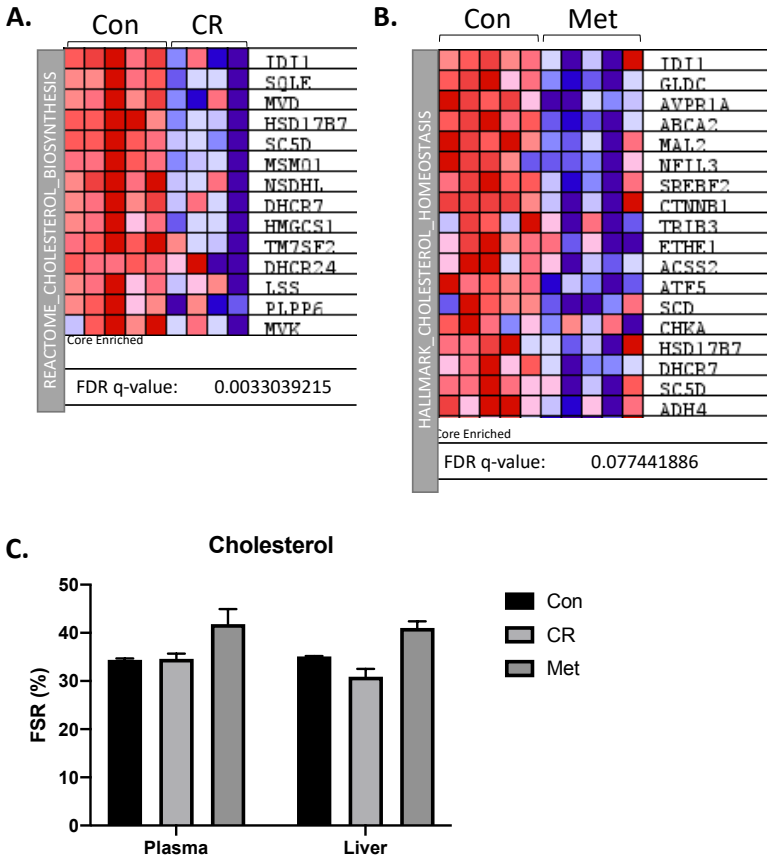

Figure 5-4. Effects of CR and Met on mRNA levels and metabolic fluxes through the cholesterol synthesis pathway. An expression data set sorted by correlation with phenotype through enrichment analysis (ES) **(A and B)** was used to compare the effects of intervention on liver gene expression by of ontological related pathways of cholesterol regulation. **(C)** The measurement of newly synthetized cholesterol was carried out in both plasma and liver.

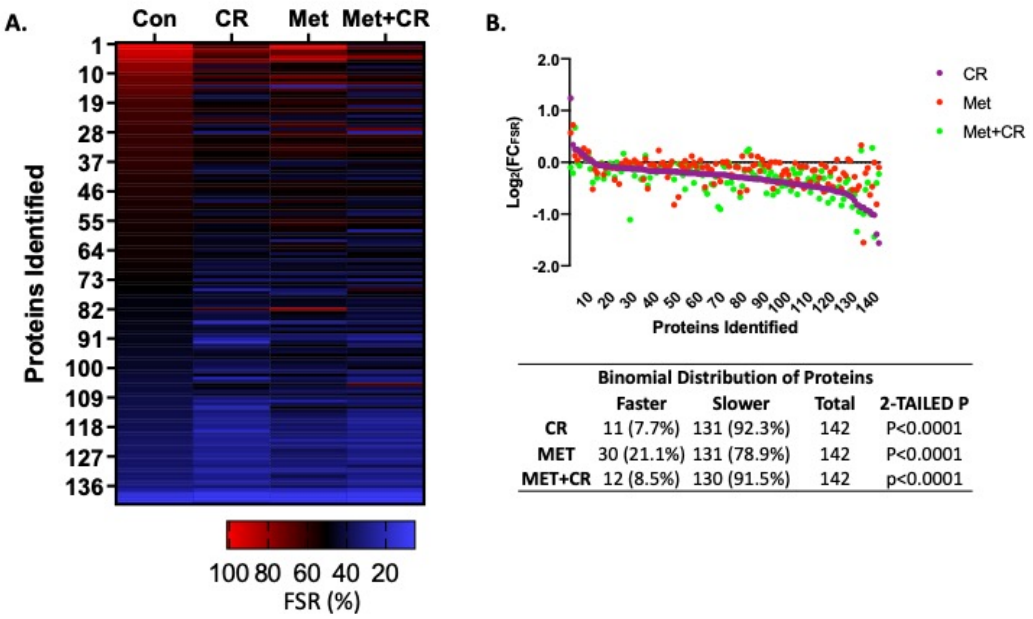

Binomial Distribution of Proteins

	Faster	Slower	Total	2-TAILED P
CR	11 (7.7%)	131 (92.3%)	142	P<0.0001
MET	30 (21.1%)	131 (78.9%)	142	P<0.0001
MET+CR	12 (8.5%)	130 (91.5%)	142	p<0.0001

Figure 5-5. Fractional synthesis rate (FSR) of hepatic proteins. (A) Heat map of FSR (%) after Met and/or CR interventions **(B)** Fold change of proteins compared to control represents the regulation of hepatic proteins after intervention. Proteins with either a faster FSR (shorter half-life) or slower FSR (prolonged half-life) were compared by binomial distribution and reveal a highly significant increase in the half-lives of hepatic proteins compared to control for CR, MET and Met+CR groups. Proteins compared (n =142) had kinetic data in all 4 groups. FSR is shown in the heat map as % replaced per day.

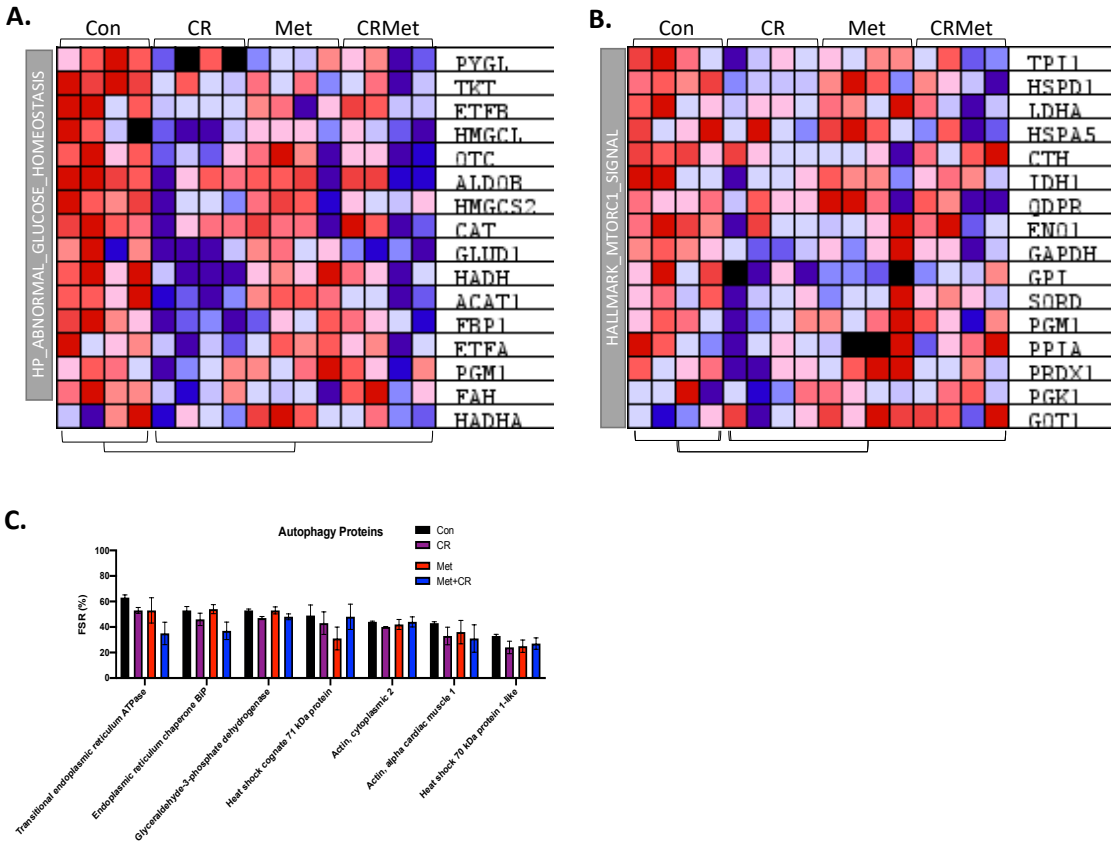

Figure 5-6. Analysis of enriched pathways for protein FSR measurement during Met and CR interventions. An expression data set sorted by correlation with phenotype through enrichment analysis (ES). **(A)** Metformin is a known glucose sensitizer. Here, we observed an increase in the protein half-lives under all experimental conditions was observed for regulation of glucose homeostasis. **(B)** CR is a known mTORC1 inhibitor. Here, mTROC1 signaling was noticeably decreased in all experimental conditions. **(C)** mTOR signaling is a central regulator of autophagy by modulating multiple aspects of the autophagy process. Here, analysis of protein FSR values (%) for autophagy-associated proteins detected in the liver is shown in bar graphs.

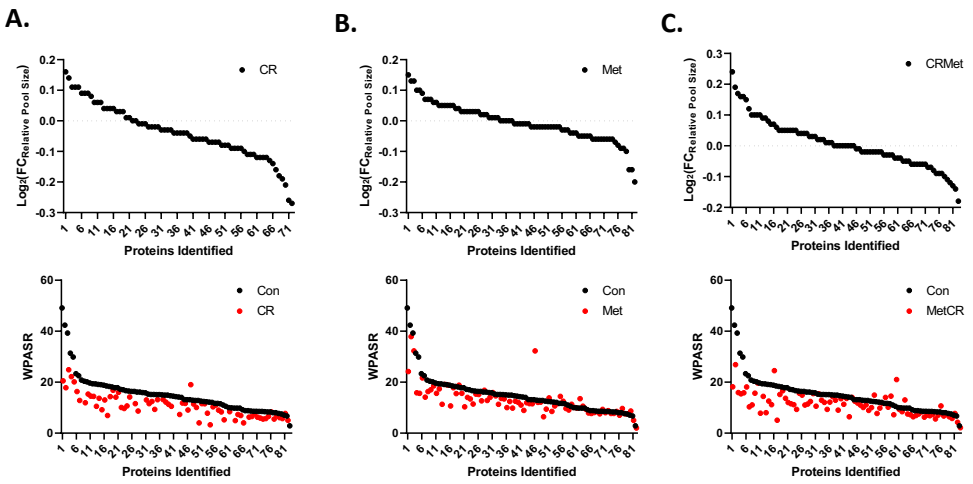

Figure 5-7. Effects of CR and Met on the WPAS rate. (A) Pool sizes (top) and FSR values were used to estimate the WPAS rate of hepatic proteins under CR. **(B)** Pool sizes (top) and FSR values were used to estimate the WPAS rate of hepatic proteins under Met. **(C)** Pool sizes (top) and FSR values were used to estimate the WPAS rate of hepatic proteins under CR and Met.

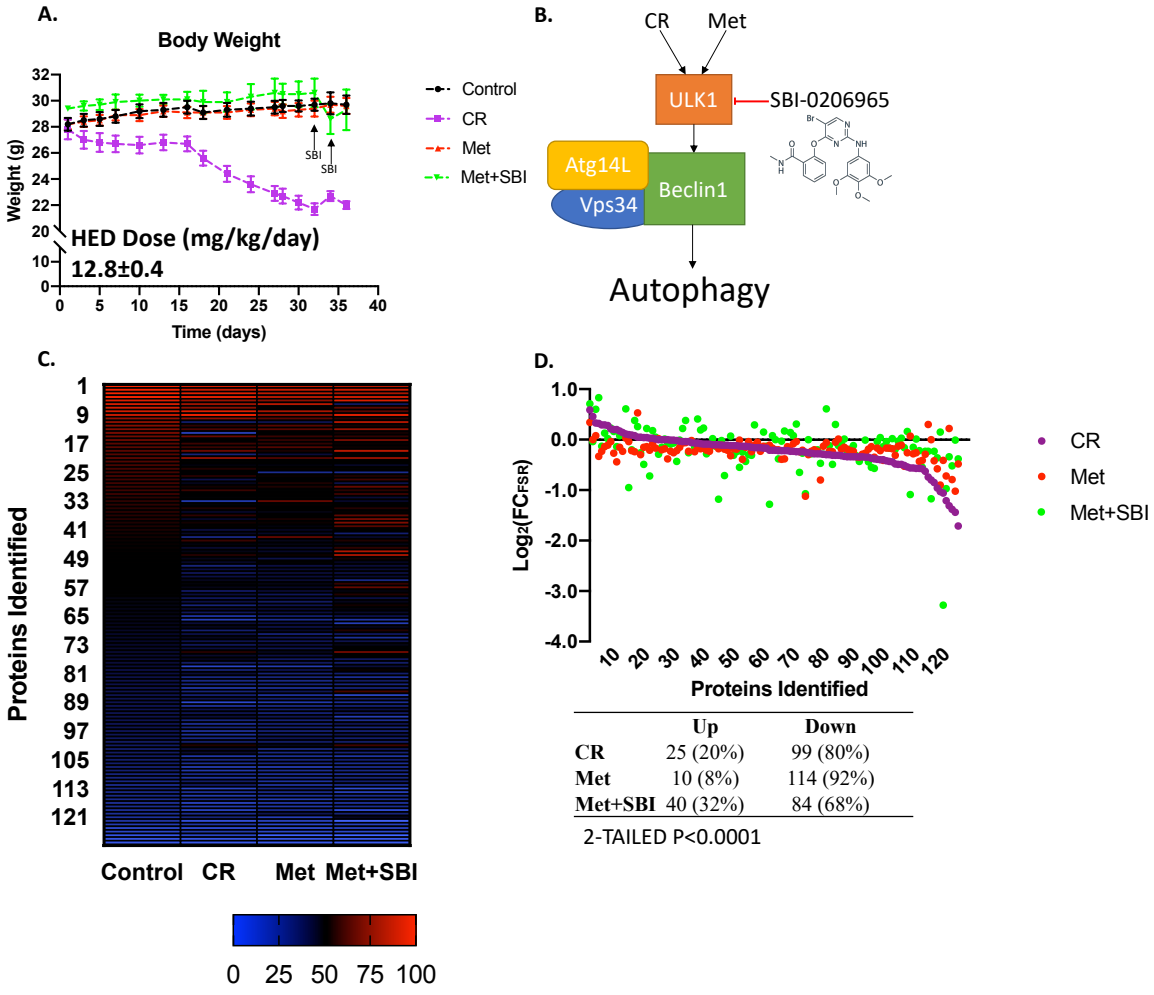

Figure 5-8. Effects of inhibition of autophagy in combination with Met treatment. **(A)** Body weights of the four experimental groups (Control; n=8, CR; n=7, Met; n=12, and Met+SBI; n=3). Met was given at a human equivalent of 12.8mg/kg/day. At the beginning of labeling (4 days before SAC; day 33), a subset of mice (n=3-7) was given SBI-0206965 every 2 days **(B)** by IP to inhibit ULK1 in order to inhibit autophagy. The proposed basis of autophagy inhibition by SBI-0206965 is represented in the figure [411]. CR and Met are known activators of autophagy through phosphorylation of ULK1. SBI-0206965 inhibits ULK1 directly and inhibits formation and activity of autophagosomes. **(C)** Heatmap of FSR (%) after CR, Met and Met+SBI interventions. **(D)** Fold Change of proteins compared to control represent the regulation of hepatic proteins after intervention. Table shows the fraction of proteins with kinetic data in all 4 groups that exhibited higher or lower FSRs than controls.

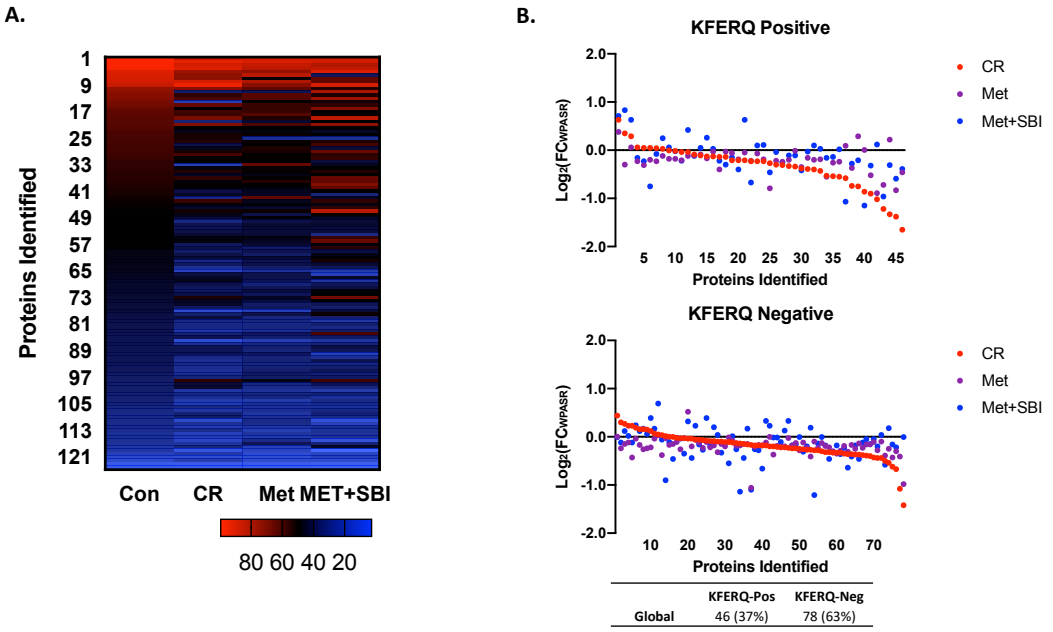

Figure 5-9. Effects of autophagy inhibition on WPAS rates of hepatic proteins under Met treatment. (A) WPAS rates are represented in by their expression in controls, from highest to lowest synthesis rates, as a heat map (FSR, % replaced per day). Each line represents an identified protein by LC/MS/MS and analysis. **(B)** Comparisons were then made for all proteins identified either with a KFERQ sequence or without a KFERQ sequence. The line of unity is from the control values for each protein. Table shows the relative fraction of proteins with the sequence and without the sequence.

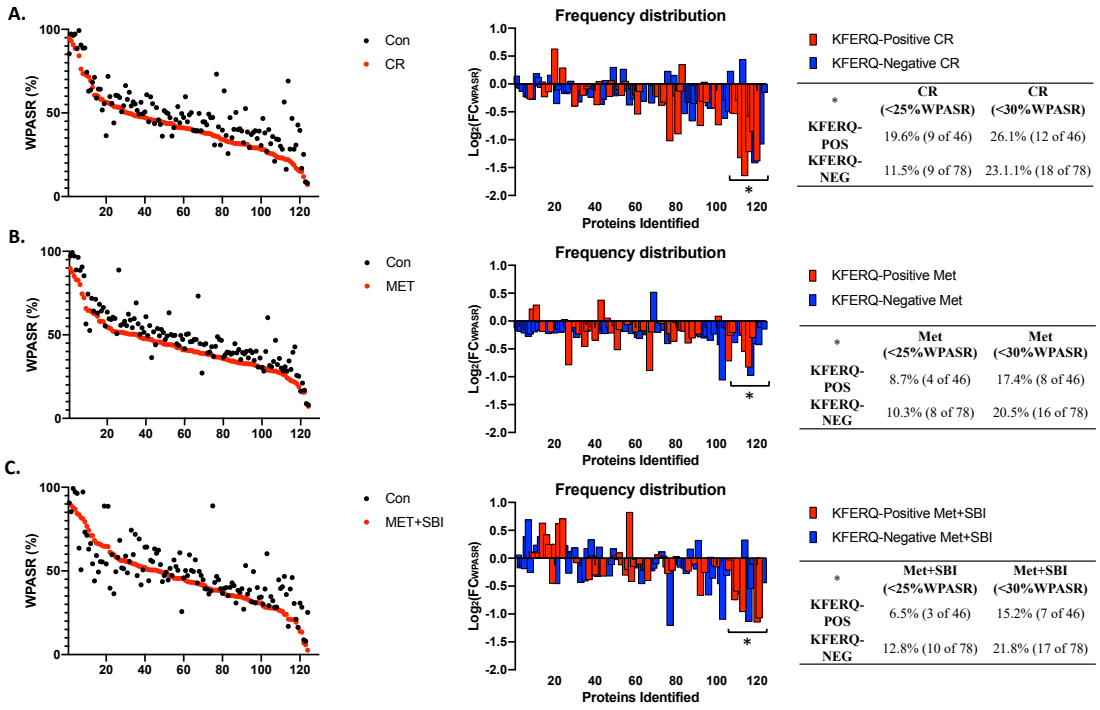

*	CR (<25%WPASR)	CR (<30%WPASR)
KFERQ-POS	19.6% (9 of 46)	26.1% (12 of 46)
KFERQ-NEG	11.5% (9 of 78)	23.1.1% (18 of 78)

*	Met (<25%WPASR)	Met (<30%WPASR)
KFERQ-POS	8.7% (4 of 46)	17.4% (8 of 46)
KFERQ-NEG	10.3% (8 of 78)	20.5% (16 of 78)

*	Met+SBI (<25%WPASR)	Met+SBI (<30%WPASR)
KFERQ-POS	6.5% (3 of 46)	15.2% (7 of 46)
KFERQ-NEG	12.8% (10 of 78)	21.8% (17 of 78)

Figure 5-10. Global analysis of proteins with lowest rate of WPAS by autophagic sequence presence. Dots (left) represent individual proteins identified by their WPAS rate for CR **(A)**, Met **(B)**, or Met+SBI **(C).** For each condition, the frequency distribution of the WPASR by fold change due to the intervention for proteins with or without the KFERQ sequence was plotted from highest turnover (left) to slowest turnover (right). From this distribution, a subset (represented by proteins whose WPASR fold change under treatment is < 25 or 30%) of the slowest turn-over proteins was noted to have the greatest degree of change. Table (inset) shows the percentage of proteins with or without the KFERQ sequence in correspondence with their total.

CHAPTER SIX: NO is Necessary for Proteome Regulation under CR

1. INTRODUCTION

CR has been linked to lifespan extension and preserved cellular homeostasis, conferring the organism with a wide array of beneficial effects. Many biological functions are modulated under CR but it is unknown how it regulates these metabolic processes. However, an interesting signature of CR is its modulation of protein translation, a fundamental and highly controlled process that can be stimulated or inhibited by amino acid levels. This regulation is controlled through intracellular signaling mechanisms (discussed in Chapter One) that affect several translation checkpoints, including the initiation factor activity of eIF2 and availability eIF4 through regulation of eIF2 guanosine exchange and 4E-BP1 binding activity, respectively. Increased amino acid levels can accelerate translation initiation, where the energy sensor mTORC1 mediates the phosphorylation of S6-K, promoting protein synthesis through the translation initiation factor eIF4B and the elongation regulator eEF2K. On the other hand, lack of essential amino acids leads to activation of eIF2 kinases such as GCN2 (EIF2AK4) that trap eIF2 in its inactive conformation and thus block translation [149,409,410].

It is clear that many biological functions are modulated under CR to prevent the deleterious effects of age-related diseases, but it is unknown how CR regulates these metabolic processes. Of the diverse pathways known to change under CR, many coalesce at the point of protein translation. Of interest here, based on meta-omics data **(Figure 5-2 and 6-1)**, the signaling molecule NO stands out due to its diminished bioavailability during aging being prevented under CR [411]. Of interest in this regard was a previous observation done in which NO mediated NMDA-induced persistent inhibition of protein synthesis through dephosphorylation of 4E-BP1[412]. NO is produced enzymatically in most cells and tissues by a family of enzymes known as NO synthase (NOS). A function of NO is through signal transductions, first observed in endothelial cells to relax vascular smooth muscle through activation of guanylate cyclase [413]. Since those initial observations, an extensive range of NO-based processed induced have been observed and linked to the expression of NOS enzymes involved in the production of NO. Endogenous NO is generated from arginine by three distinct calmodulin-dependent NOS enzymes. NOS from endothelial cells (eNOS) and neurons (nNOS) are both constitutively expressed enzymes, whose activities are stimulated by increases in intracellular calcium. Stress and immune function for NO are mediated by a calcium-independent inducible NOS (iNOS) [414,415]. Interestingly, expression of iNOS protein requires transcriptional activation, which is mediated by specific combinations of cytokines [415].

L-Arginine is the only endogenous nitrogen-containing substrate of NOS, and it thus governs the production of NO. iNOS is the only NOS enzyme not constitutively active, playing a fundamental role as mediator of inflammation and stress responses such as injury-induced insulin resistance in metabolically active tissues [416,417], and during nervous system development [418] as well as in disease states such as stroke, multiple sclerosis, Parkinson's disease, and HIV dementia [419,420]. The citrulline-NO-urea cycle **(Figure 6-2B)** is a recycling processes characterized by the synthesis of NO from arginine by either of the NOS enzymes using NADPH as a cofactor. Citrulline may be recycled back to arginine, using arginosuccinic acid as an intermediate. It has been shown that this pathway is a key response under CR in response to hypothermic

conditions. In this regard, several metabolites of the urea cycle are altered following CR in plasma and the hypothalamus [421]. In addition, under CR the most abundant proteins detected (reflected by the peptide n) belong to the citrulline-NO-urea cycling **(Figure 6-2A)**.

NO-mediated regulation of gene expression is known to involve activation of multiple serine (Ser)/threonine (Thr) kinases that phosphorylate eIF2 [412]. PERK, a Ser/Thr protein kinase that is a critical effector of the unfolded protein response, phosphorylates the alpha subunit of eIF2, leading to its inactivation and to a rapid reduction of translational initiation and repression of global protein synthesis [422]. In this regard, studies on stress response have revealed PERK and GCN2 as kinases able to phosphorylate eIF2 to inhibit protein synthesis, revealing NOS as the activation controller for these kinases during cellular damage [423]. This infers a further role for NO to be stimulated in parallel to CR and amino acid depletion through GCN2. Of note is that changes in cellular NO production are induced by the same stressors that stimulate autophagy (eg. starvation, CR, ER stress, mitochondria dysfunction, oxidative stress).

NO is also capable of inducing post-translational modifications in proteins. In this regard, the addition of a NO group to the thiol side chain of cysteine residues within proteins and peptides is known as S-nitrosylation (Cys-NO). This modification conveys a large part of the ubiquitous influence of NO on cellular signal transduction [414], and has been implicated in proteins that are components of at least two pro-autophagic pathways: JNK1/Bcl-2/Beclin 1, where NO negatively regulates JNK1 [424], and IKKb/AMPK/mTORC1 [425].

Animal studies have revealed NO as a central regulator of energy metabolism and body composition [426]. NO bioavailability is decreased in animal models of diet-induced obesity [427] and in obese and insulin-resistant patients [428], and increasing NO output has remarkable effects on obesity and insulin resistance [428,429]. On the other hand, CR has been linked to decreased systolic blood pressure through an increase in serum NO bioavailability [430]. In this regard, CR was able to prevent systolic blood pressure rises in specific by improving the NO effect on smooth muscle and morphological changes in the aorta of rats [431]. In the absence of NOS (eg. eNOS−/−), the outcome of heart failure is more sever in mice was more severe, and the protective effects of CR are not observed to exert cardioprotection without this fundamental enzyme [432]. Indeed, the physiological effects of CR are numerous. As a versatile gas biomolecule that increase blood flow, transmit nerve signals, and regulate immune function, it is also able to prolong life in *C. Elegans* by up to 15% through its modulation of *hsf1* and *daf16* .[433]

In short, NO is a free radical that mediates several biological functions. NO accomplishes its functional diversity through various mechanisms such as protein cysteine residue modifications to form Cys-NO, impacting protein function, stability, and location. Pathological conditions are often associated with overproduction of NO, a condition called nitrosative stress, and result in inappropriate S-nitrosylation of proteins, leading to dysfunction and pathological phenotypes. As a response to the overproduction of NO, cells respond by inhibiting eIF2 to slow down protein synthesis.

iNOS is the only NOS enzyme not constitutively active, playing instead a fundamental role as mediator of inflammation and stress responses such as injury-induced insulin resistance in metabolically active tissues like liver [416,417]. It also has been implicated in the biology of CR, such as in an RNA-Seq analysis of enrichment networks **(Figure 6-1)**, where we show it interacts with 'plateau phase 4' and 'unblocking nmda' clusters. However, the exact mode of action between NO and CR is not known [421].

Accordingly, we examined here the physiological and biological effects of CR in NO deficient (NO-) mice (iNOS knockout [434–436]) or aminoguanidine [AG] supplemented mice [437]) using the genetic background animals as controls (C57Bl/6J).

2. METHODS AND RESULTS

Exploring the role of CR on NO-related proteins **(Figure 6-2A)**, we observed that the half-lives of several enzymes involved in the cycling and generation of citrulline were globally increased. We therefore considered the functional role of these enzymes in the context of NOS regulation of NO production **(Figure 6-2B)** and asked whether there is an important role for NO in regulation of proteome fluxes, particularly in the hepatic response of proteome fluxes to CR.

We used an experimental design workflow **(Figure 6-3A)** in which various measurements were carried out throughout the length of CR intervention. We tested the metabolic adaptation of mice in the absence of NO under CR before mice reached either 10 or 22 weeks under CR. We also measured physiological and behavioral performance and tested their insulin sensitivity within those timepoints. Before time of sacrification, we labeled the mice for 4-5 days with $^{2}H_2O$. After tissue collection we performed a series of analysis on the tandem mass spectrometer to study their proteome fractional synthesis flux. Comparison of body weights **(Figure 6-3B)**, measured at regular intervals, showed significant body weight shifts between Con and CR during the first week of intervention. After seven weeks of CR, we observed a significant shift in body weights between Con and NO- mice. This pattern repeated after ten weeks of intervention between CR and NO-CR where the NO- mice were significantly heavier than CR. Measurements of their food consumption showed no significant changes in their food usage.

Behavioral and performance tests were done at ten and twenty-two weeks, marked by significant body weight shifts. At 10 weeks **(Figure 6-4A)**, we saw how wire-hang tests were performed poorly in the NO- group compared to control, while CR elucidated the best performance under both CR and NO-CR conditions. CageTOP tests revealed a similar performance deficit only under the NO- group, with both CR groups performing perfectly. Treadmill exhaustion test showed a non-significant trend in which the NO- group performed poorly ($p=0.06$) compared to control and both CR interventions performed better through the assessment of distance (m) run on a treadmill. Finally, the inverted pole test is used to assess the time it takes the mouse to turn around and climb down of a pole. The task involves both mental and physical coordination to execute properly and is scored accordingly, with the lower the score the less favorable the performance was executed. In here, we observed NO- mice

trending (p=0.06) towards a poor outcome. CR on the other hand performed the best, with NO-CR mice having no significant improvements compared to Con.

At 22 weeks **(Figure 6-4B)** of intervention we saw wire-hang testing performed decreased in the NO- group only. CageTOP test showed a significant decrease in performance under NO-. The treadmill exhaustion test showed no changes within the *ad lib* groups, and time to exhaustion increased significantly under CR for both groups. Finally, the inverted pole test showed a significant decrease in coordination and performance under NO- and an improvement under CR for both conditions.

Metrics of body composition were also done at 10 **(Figure 6-5A)** and 22 **(Figure 6-5B)** weeks of intervention. At 10 weeks of CR, mice underwent GTT after fasting, with significant increase in blood glucose levels for all timepoints tested except minute 15 in the NO group. CR performed better for all timepoints except during fasting. ITT test showed NO- having more blood glucose levels under fasting only. Comparison between CR and NO-CR showed a significant increase in all times measured under NO-CR. At 22 weeks of intervention, we saw under fasting conditions in a GTT experiment that NO-CR had higher blood glucose levels than CR. We also observed than NO- induced a prolongation of the uptake of glucose into cells at min 120, showing clear signs of insulin resistance. ITT testing showed no significant changes for any of the time points tested.

Metabolic cages (CLAMS) were used to test RER, HEAT, and movement scores (ZTOT, XTOT, XAMB) as metrics of energy usage and behavioral movement. At 10 weeks of intervention **(Figure 6-6A)**, CR mice had a significant preference for using carbs as an energy source, which was not observed in the NO-CR group which preferred the use of fats as energy source. CR under both conditions generated less heat. Metabolic cages analysis at 22 weeks of intervention **(Figure 6-6B)** showed a shift for NO- mice to use carbohydrates as energy sources in a manner similar to CR and NO-CR. However, we observed a significant increase in body heat generation which may implicate NO in energy usage and heat production.

To summarize, NO-CR mice exhibited worse functional performance, higher body weight, worse insulin sensitivity in comparison to CR wild-type mice.

Hepatic proteome analysis of protein fractional synthesis fluxes revealed a consistent pattern of higher global protein FSR rates in the absence of NO. At 10 weeks of CR **(Figure 6-7A)**, most proteins analyzed were increased in the NO- group (70% of proteins measured were upregulated), while under CR most proteins had a significant decrease in their turnover rate (81% of proteins were downregulated). The effect of CR was markedly blunted in NO-CR mice, with only 65% of hepatic proteins being downregulated in the NO-CR group. At 22 weeks of CR **(Figure 6-7B)**, the NO- group saw a similar increase in protein fractional synthesis rates (75% of proteins were upregulated), while under CR 75% of proteins were downregulated (increased protein half-lives). Of interest was that in the NO-CR group, the effects of CR were completely prevented, with 69% of the proteins analyzed actually upregulated. These week 22 findings revealed a time-dependent modulation in which CR is no longer able to slow proteome fluxes when iNOS is absent in the liver.

Gene sequence enrichment analysis of top changes in fractional synthesis rates was performed to understand ontological changes. Data sets analyzed were compared to 195 gene sets **(Figure 6-8A)**. Of this sets, 170 out of the 194 were downregulated under CR. Of significance (nominal $p < 0.01$) were sets belonging to mitochondria function, oxidative phosphorylation and abnormality of acid-base homeostasis. Comparing the enrichment of gene sets between NO-CR and CR was then done to understand the pathways regulated by CR when NO is available. Interestingly, 183 out of 195 gene sets analyzed were enriched in the NO-CR group. Of this, 12 sets were significantly enriched (nominal $p < 0.05$) and of note was that two sets were involved in mitochondria. Therefore, we isolated liver mitochondria **(Figure 6-8B)** by sucrose gradient ultracentrifugation and generated a large set of mitochondria protein FSRs. These proteins were then analyzed by core enrichment and saw that while CR downregulated (increased the half-lives) of most liver mitochondrial matrix proteins, NO-CR showed significantly higher FSRs for these proteins when compared to CR.

Of the 195 gene sets analyzed and compared between NO- and Con, 157 were upregulated under NO-. Significantly enriched sets (nominal $p < 0.05$) showed significance in pathways involved in amino acid metabolism **(Figure 6-9A).** Though not significant, we also observed a core enrichment of proteins in the liver involved in adipogenesis. Therefore, based on our observations of increased body weight, and insulin resistance, we analyzed the FSR of white adipose tissue proteins **(Figure 6-9B).** In the NO- group, there was no noticeable effect of the kinetic rate of adipose tissue (WAT) proteins (47% were upregulated). However, it has been reported in the past that disruption of iNOS can improve tissue inflammation and fibrosis in an *ob* mouse model [438]. Under CR and NO-CR, 64% of proteins had a significant decrease in synthesis rates.

An important regulator of iNOS in the liver is the peroxisome. Indeed, in hepatocytes the peroxisome is considered a site of iNOS localization [439], whose association exists as a pool believed to be involved in protective mechanisms [440]. Therefore, we performed sucrose gradient ultracentrifugation in liver samples to obtain a peroxisomal enriched fraction. We analyzed these proteins by LC/MS/MS **(Figure 6-10)** and observed that after 4 days of labeling, CR upregulated 77.3% of the peroxisomal proteins measured ($p = 0.004$). NO did not have an influence on the expression of peroxisomal proteins demonstrating CR as the unique modulator of proteins from the peroxisome. Because huge amounts of ROS are generated during oxidative reactions carried out in peroxisomes, we then looked at liver protein carbonylation as a marker for protein oxidation that can be promoted by ROS [441]. We observed a dramatic increase of carbonylated amino acid side chains in the absence of NO- in both conditions. We further tested the level of ubiquitination and observed a slight increase in ubiquitination in the absence of NO-.

Lastly, we validated these observations with a shorter CR intervention of 6 weeks. In this experiment, we also included a group of mice lacking nNOS and control groups in which we gave the mice either NO donors or pharmaceutical inhibitors of NOS.

Establishing the baseline for this experiment **(Figure 6-11)**, we labeled mice for 4 days with $^{2}H_2O$ after which we isolated livers to study their protein flux rates. We observed a repeat pattern of our previous observations, where NO- leads to a significant increase in protein FSRs (67% of proteins were upregulated; $p<0.001$). Similarly, CR led to a 73.7% decrease ($p<0.001$) in protein turnover rates that was blunted by the absence of NO (56% of proteins were downregulated in NO-CR; $p=0.1$).

We then gave mice AG **(Figure 6-12)** as a pharmaceutical inhibitor of NOS that is highly specific for iNOS [437,442]. We observed that in the hepatic proteome, AG increased the FSR of 74% of proteins under *ad lib* conditions, a similar finding as our previous observations in the genetic knockout mice. Furthermore, while CR decreased the turnover rate (data from **Figure 6-11**) in 74% of hepatic proteins, AG given to CR mice altered their FSR values to an even split of 50%:50%, lower vs higher.

To understand whether we could rescue the effects of CR in NO- animals, we gave to genetic NO- mice an NO therapeutic drug, Molsidomine (Mols), that is metabolized in the liver where it is converted by esterases to the active metabolite, SIN-1, which then releases NO [443,444]. The half-life of Mols in plasma is 1-2 hours. In this experiment **(Figure 6-13)** Mols was given at a dose of 120mg/L based on a study on klotho-hypomorphic mice [445] in which this dose was enough to reverse vascular calcification. However this dose was roughly 10 times higher than in another study reporting similar effects in enhanced atherosclerotic plaque stability in ApoE deficient mice [443]. We observed that in the absence of NO-, Mols was capable of eliciting similar effects as CR, with 70% of proteins downregulated. This stood in contrast with NO- where 67% of proteins were upregulated. Under NO-CR, when Mols was added, 82% of proteins were downregulated (similar to CR alone).

Because Mols is a drug used to treat myocardial dysfunction (angina pectoris) [446], we then looked at the effects of NO on proteome turnover in the heart **(Figure 6-14A through 6-14B)**. In the NO- group, a similar signature was repeated as in the liver, with 82% of proteins being upregulated when compared to control. Under CR, however, we did not observe the same signature as in the liver and saw little if any effect on heart proteome turnover (59% of the proteins being upregulated). In the NO-CR group, we observed a similar effect as in NO- alone, with an upregulation of 70% of cardiac proteins. In comparison, Mols was able to bring NO- mice back to a baseline (56% of proteins being downregulated). This observation was also repeated in the NO-CR group after Mols administration where only 58% of proteins were downregulated.

Looking at the effects of NO in brain, we used nNO- mice **(Figure 6-15)**. The first observation from this group of mice was that they had a significant reduction in body weights **(Figure 6-15A)** reflecting that of the CR group. While these mice (n=3) were *ad lib* their phenotype led them to consume less food putting them on a self-imposed CR regimen of ~22% **(Figure 6-15B)** over the course of the experiment. Analyzing their brain proteome dynamics, we observed that 69% of the proteins analyzed were downregulated, showing that CR is able to regulate the proteome in a similar fashion to liver (but not heart). As we had established earlier, these mice were under a CR

state, so when we analyzed their total brain proteome, we were surprised to observe no changes (46% of proteins were downregulated). To verify that these mice were indeed under a CR state, we looked at their liver proteome and observed that, in the liver, they had a 67% downregulation of FSRs **(Figure 6-16)**. Comparing this group with the NO- group (where the iNOS enzyme was KO) demonstrate its CR condition.

We conclude that NOS and CR have a fundamental interplay in the production of NO that has implications for global proteome dynamics **(Figure 6-17).** Physiologically, NO appears to be necessary for the slowing effects of CR on global protein turnover in the liver. It will be of interest to ask whether the effects on life-span extension parallel these effects on lobal protein turnover.

3. CONCLUSION

There is an interesting paradox in arginine metabolism, where intracellular levels of arginine far surpass the K_M of the NOS enzymes, and yet, when exogenous arginine is added into the system more NO is produced [447,448]. It is interesting to conceptualize how this unique family of enzymes can regulate NO production under different levels of amino acid (eg. arginine and citrulline) availability. CR offers a point of context in this regard, as less amino acids are consumed under such energy restricted conditions, leading to a slowdown of protein synthesis. Yet in the absence of NOS, protein synthesis rates are significantly increased even under CR. Here, we tackle this intriguing paradox to elucidate the functional role of NO interventions that influence turnover rates of the global proteome as well as altering lifespan in living animals [433].

We conclude through meta-omics, genetic, and pharmacological approaches that NO plays a fundamental role in the regulation of protein turnover. We have consistently shown that CR leads to reduced synthesis (increased half-lives of most hepatic proteins. Indeed, CR and other lifespan extension interventions such as rapamycin treatment have been associated with the preservation of cellular homeostasis, conferring the organism with a wide array of beneficial effects. As discussed earlier, many biological functions are modulated under CR in which NO appears to play a singular role as a regulator of CR-linked pathways that ultimately regulate proteostasis.

The physiological and biological effects of NO on mice demonstrate a unique state in which this signaling molecule regulates body composition, behavior and physical performance. These changes are a unique reflection of the dictating biology of CR, where NO appears to be necessary for the preservation of protein half-lives. Indeed, the use LC/MS/MS to measure the replacement rate of proteins *in vivo* shows a dynamic and constant role for NO to maintain protein homeostasis. In NO- mice, a significant number of proteins undergo replacement, and this effect is exacerbated under CR, whose effect was observed to be dramatically inhibited in NO- mice.

In short, we demonstrate for the first time a fundamental role for NO production in maintenance of the proteome in liver, heart and brain (but not WAT). In tissues that are also affected by CR, NO plays an indispensable role in maintaining the half-lives increases of most hepatic and brain proteins analyzed. We observed this pattern of regulation throughout various lengths of intervention (eg. 6, 10, 22 weeks of CR) in

genetic iNOS knockout mouse models and with pharmacological interventions where AG duplicated the effects observed in the knockout mice. In addition, in the absence of iNOS, we could rescue the effects of CR by giving Mols as a NO donor.

4. METHODS

Mice. Six- to eight-week-old male C57Bl/6J control mice (n=48) and B6.129P2-*Nos2tm1Lau* /J transgenic mice (NO-) (Stock no: 002609) were purchased from Jackson labs (Jackson laboratory, Bar Harbor, ME). Mice and were randomly divided into control group (n=29), CR under 30% restriction (n=19), *ad lib* NO- (n=20), NO-CR (n=17). Animals not under CR were provided unrestricted access to the AIN-93M diet (Bio-Serv). Animals under CR were given 30% less food than the control group. Body weights and food intake were recorded approximately every 3-4 days during the duration of the experiment. Animals were labeled with $^{2}H_2O$ 4-5 days before sacrification.

Calorie Restriction. Male C57Bl/6J mice under CR and NO- under CR were given 30% less food than their respective *ad lib* groups every day between 12-1pm. Weight adjustments for diet were done weekly based on the amount of food their controls consumed.

AG administration. AG was administered to mice as previously described [449]. In short, AG was purchased from Sigma (No. 19266598). AG was dissolved in the same drinking water used for the animal colony at 2mg/mL and sterile filtered through a 0.22-µm disposable filters (Millipore, Millex-GV) before administration. The solution was made fresh and given to mice in their drinking water bottles daily. Bottles with AG were changed every day for the duration of the experiment.

Mols Administration. Mols was administered to mice as previously described [445]. In short, Mols was purchased from Sigma (No. M2901). Mols was dissolved in the same drinking water used for the animal colony at 120mg/L and sterile filtered through a 0.22-µm disposable filters (Millipore, Millex-GV) before administration. The solution was made fresh and given to mice in their drinking water bottles daily. Bottles with Mols were changed every day for the duration of the experiment.

Euthanasia. Animals were anesthetized with isoflurane and euthanized by cardiac puncture. All experiments were performed under the approval of the Institutional Animal Care and Use Committees of the University of California at Berkeley.

RNA-Sequencing. Total RNA was isolated from mouse livers using RNeasy Micro Kit from Qiagen (Hilden, Germany). RNA Quantity was determined using a Qubit (TM) fluorometric assay and quality was determined using Eukaryote Total RNA Pico (Agilent Bioanalyzer 2100). The library preparation and sequencing were done on a single lane (Illumina HiSeq4000) at 100bp pair-end (PE) reads and performed at the Vincent J. Coates Genomics Sequencing Laboratory at University of California (UC), Berkeley. The raw sequencing files were processed with CASAVA 1.8.2 (Illumina) to generate fastq files. We first obtained read quality reports by using the FastQC tool (http://www.bioinformatics.babraham.ac.uk/projects/fastqc/), which gave us overall

high-quality scores. The fastq files were then uploaded onto the Galaxy project portal (https://usegalaxy.org/) [337]. The reads were then mapped to the mouse reference genome (mm10) using the Burrows-Wheeler Aligner (BWA) module. Differential gene expression of RNA-seq was determined using DESeq2 [338].

Measurement of ^2H enrichment in body water. Animals in each group were labeled with an intraperitoneal injection of 100% ^2H_2O saline (0.35mL/10 g body weight), and provided with 8% 2H2O drinking water for the remainder of the study to maintain body ^2H_2O enrichments of approximately 5%, as described previously [372]. Measurement of ^2H_2O enrichment in body water was done from whole blood samples using a Liquid Water Isotope Analyzer (Los Gatos Research, Mountain View, CA) after a 1:300 dilution and distillation as previously described [373].

Tissue Protein Isolation and In-Gel Trypsin Digestion. Livers, brains, hearts and WAT were harvested from mice at the time of euthanasia, and immediately snap frozen on liquid nitrogen until further analysis. Tissue protein was isolated by homogenization in RIPA buffer containing PhosStop phosphatase inhibitor cocktail (Roche, Indianapolis, IN), 1mM DTT, 7.5ug/mL leupeptin, 1ug/mL pepstatin, 2ug/mL aprotinin, 1mM PMSF in isopropanol, and 100nM nicotinamide using a TissueLyser (Qiagen, Germantown, MD), followed by centrifugation at 10,000g for 10 minutes at 4 ^oC. The supernatant containing soluble proteins was used for the analysis. Protein from prepared homogenates was uniformly reduced by incubation in 10 mM DTT and SDS-PAGE sample loading buffer for 10 min at 70°C. The reduced samples were then alkylated by incubating in 15 mM iodoacetamide for 1 hour at room temperature in the dark. Samples were then trypsin digested at 37^oC (Trypsin Gold, Promega, Madison, WI). In each experiment, samples were analyzed by LC-MS/MS, corresponding to a molecular weight range of 20-80kDa.

LC/MS Analysis and Protein Turnover Calculations. Trypsin-digested peptides were analyzed on an Agilent 6520 QTOF (quadrupole time-of-flight) mass spectrometer with 1260 Chip Cube nano ESI source (Agilent Technologies, Santa Clara, CA). Peptides were separated chromatographically using a Polaris HR chip (Agilent #G4240-62030) consisting of a 360 nL enrichment column and a 0.075 x 150 mm analytical column, each packed with Polaris C18-A stationary phase with 3 µm particle size. Mobile phases were (A) 5% v/v acetonitrile and 0.1% formic acid in deionized water and (B) 95% acetonitrile and 0.1% formic acid in deionized water. Peptides were eluted at a flow rate of 350 nL/min during a 18 min LC gradient (2%B at 0 min, 5%B at 0.5 min, 30%B at 10 min, 50%B at 13 min, 90%B at 13.1-18 min, 2%B at 18.1 min; Stop time: 32 min). Each sample was analyzed twice, once for protein/peptide identification in data-dependent MS/MS mode and once for peptide isotope analysis in MS-only mode. Acquisition parameters were: MS/MS acquisition rate = 6 Hz MS and 4 Hz MS/MS with up to 12 precursors per cycle, MS acquisition rate = 0.9 Hz, ionization mode = positive electrospray; capillary voltage = -1980 V; drying gas flow = 4 L/min; drying gas temperature = 290 °C; fragmentor = 170 V; skimmer = 65 V; maximum precursor per cycle = 20; scan range = 100-1700 m/z (MS), 50-1700 m/z (MS/MS); isolation width (MS/MS) = medium (~4 m/z); collision energy (V) = -4.8+3.6*(precursor m/z/100); active exclusion enabled (exclude after 1 spectrum, release after 0.12 min); charge state preference = 2, 3, >3 only, sorted by

abundance; TIC target = 25,000; reference mass = 922.009798 m/z. Acquired MS/MS spectra were extracted and searched using Spectrum Mill Proteomics Workbench software (version B.04.00, Agilent Technologies, Santa Clara, CA) and a UniProtKB/Swiss-Prot mouse protein database (UniProt.org, release 2012_02). Data files were extracted with the following parameters: fixed modification = carbamidomethylation of cysteine, scans with same precursor mass merged by spectral similarity within tolerances (retention time +/- 10 sec, mass +/-1.4 m/z), precursor charge maximum z = 6, precursor minimum MS1 S/N = 10, and 12C precursor m/z assigned during extraction. Extracted files were searched with parameters: enzyme = trypsin, *Mus Musculus*, fixed modification = carbamidomethylation of cysteine, variable modifications = oxidized methionine + pyroglutamic acid + hydroxylation of proline, maximum missed cleavages = 2, minimum matched peak intensity = 30%, precursor mass tolerance = 10 ppm, product mass tolerance = 30 ppm, minimum detected peaks = 4, maximum precursor charge = 3. Search results were validated at the peptide and protein levels with a global false discovery rate of 1%. Proteins with scores greater than 11.0 were reported and a list of peptides with scores greater than 6 and scored peak intensities greater than 50% was exported from Spectrum Mill and condensed to a non-redundant peptide formula database using Excel. This database, containing peptide elemental composition, mass, and retention time was used to extract MS spectra (M0-M3) from corresponding MS-only acquisition files with the Find-by-Formula algorithm in Mass Hunter Qualitative Analysis software (version B.05.00, Agilent Technologies, Santa Clara, CA). MS spectra were extracted with parameters: EIC integration by Agile integrator, peak height > 10,000 counts, include spectra with average scans > 12% of peak height, no MS peak spectrum background, unbiased isotope model, isotope peak spacing tolerance = 0.0025 m/z plus 12.0 ppm, mass and retention time matches required, mass match tolerance = +/- 12 ppm, retention time match tolerance = +/- 0.8 min, charge states z = +2 to +4, chromatogram extraction = +/- 12 ppm (symmetric), EIC extraction limit around expected retention time = +/- 1.2 min. Details of FSR calculations and data filtering criteria were described previously [305,326]. Briefly, in-house software was developed to calculate peptide elemental composition and curve fit parameters for predicting isotope enrichments of peptides in newly synthesized proteins based on precursor body water enrichment (p) and the number (n) of amino acid C–H positions per peptide actively incorporating ^{1}H and ^{2}H from body water. Incorporation of ^{2}H into tryptic peptides decreases the relative proportion of M0 within the overall isotope envelope spanning M0-M3. Fractional synthesis was calculated as the ratio of excess %M0 (EM_0) for each peptide compared to the maximal absolute EM_0 possible at the measured body water enrichment. Data handling was performed using Microsoft Excel templates, with input of precursor body water enrichment for each subject, to yield fractional replacement rate (FSR) data at the protein level. The kinetics data were filtered to exclude protein measurements with fewer than two peptide isotope measurements per protein. Following LC-MS/MS measurement of peptide spectra, we used five stringent selection criteria to remove low confidence kinetic data: (a) peptide signal intensity must be more than 30,000 counts, (b) RMS error for unlabeled peptide mass isotopomer abundance measurements must be less than 1.5% compared with natural abundance, (c) observation of the parent protein in at least 2 mice per experimental group, (d) a coefficient of variation of the one-phase exponential association curve fit less than 30%, and (e) an r^2 curve fit value greater than 0.7.

Statistics and Analysis. Reported rates and signifcance levels are based on a mixed model. Tests of the within ontological group treatment effects on FSR assess the difference between rates calculated from mean peptide counts from the control and experimental animals and correspond to tests on fixed effects coeffcients for treatment. Analyses were conducted using R (version 3.1.2). Data were analyzed using GraphPad Prism software (version 9.0) (La Jolla, CA, USA), InfernoRDN (https://omics.pnl.gov/software/infernordn) windows application (version 1.1), Gene set enrichment analysis, GSEA software, and Molecular Signature Database (MSigDB) [327] (http://www.broad.mit.edu/gsea/), and Real Statistics Resource Pack (http://www.real-statistics.com/free-download/real-statistics-resource-pack/) in Excel (version 16).

5. FIGURES

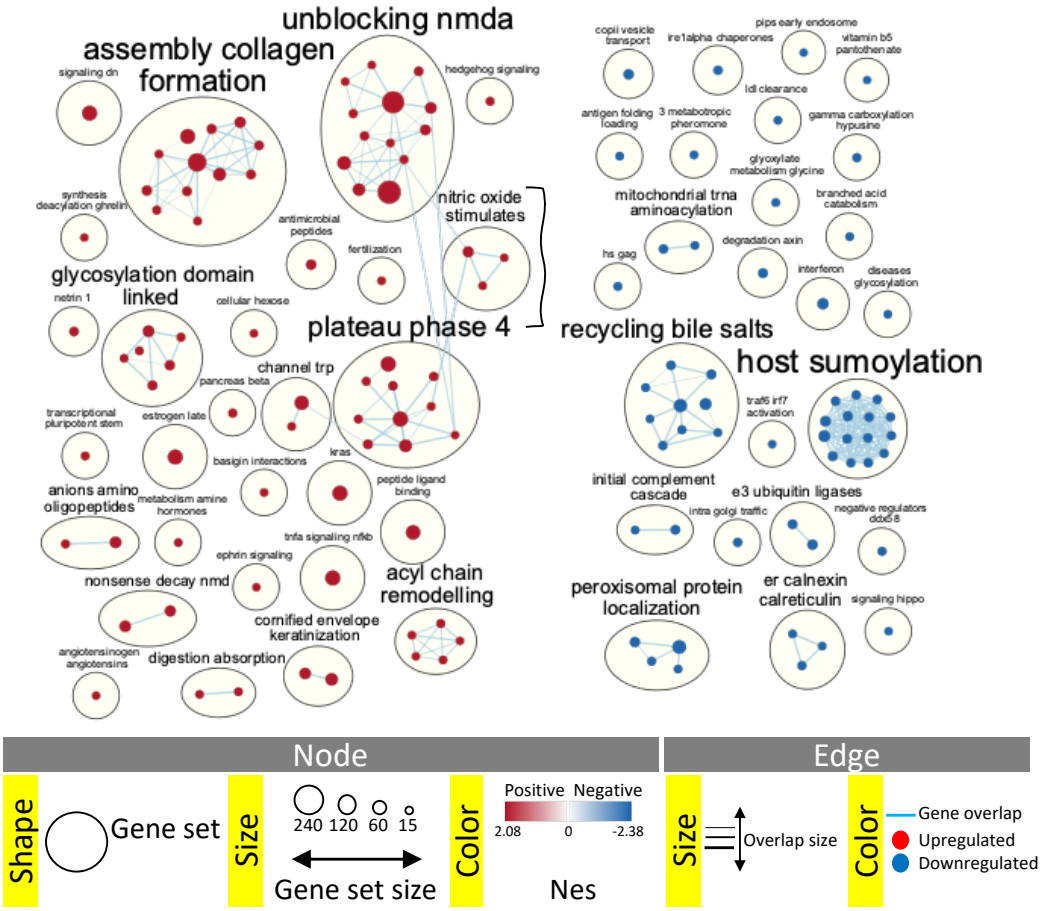

Figure 6-1. Gene sequence enrichment analysis. RNA-Seq experiment for CR group. Figure represents data sets significantly enriched at an FDR < 0.25. Ranked gene list correlation profile for FSR expressions showing the distribution of gene expression sets normalized enrichment score (*NES*). Gene enrichment visualization was performed with networks under CR and clustered by function. Genes are represented by Blue dots as downregulated pathways, and red dots as upregulated pathways under CR. Line represent the only enrichment cluster that overlaps with other clusters.

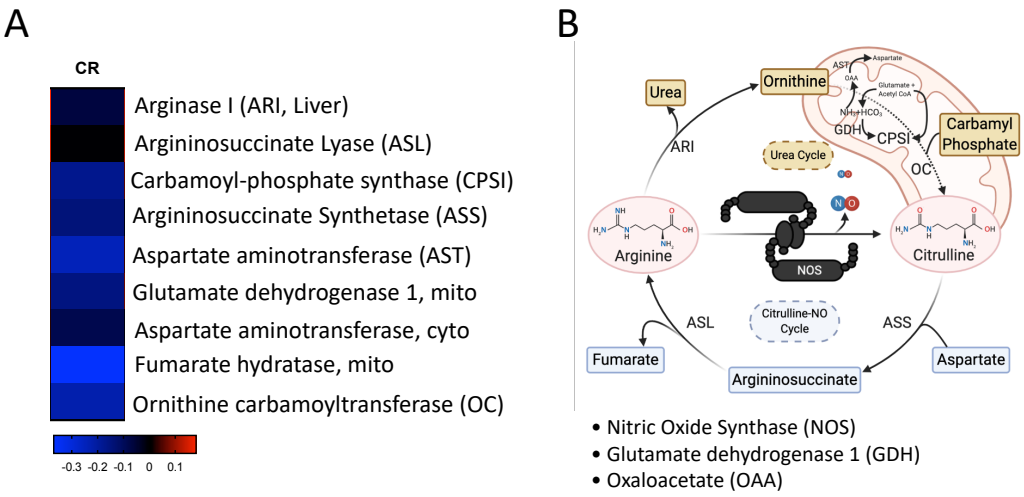

Figure 6-2. Generation of NO under CR. Representation of proteins involved in the generation of NO. **(A)** Heatmap represents the fold change of proteins involved in the generation of NO under CR. **(B)** Schematic of the process by which the cells generate NO. In the diagram, arginine is converted intro citrulline by the enzyme NOS, producing NO as a byproduct of the conversion. Two pathways are also represented; Blue outlines the Citrulline-NO recycling process by which citrulline is converted by into arginine. Red; Urea Cycle by which wasted ammonia from amino acid catabolism is eliminated through their conversion to urea.

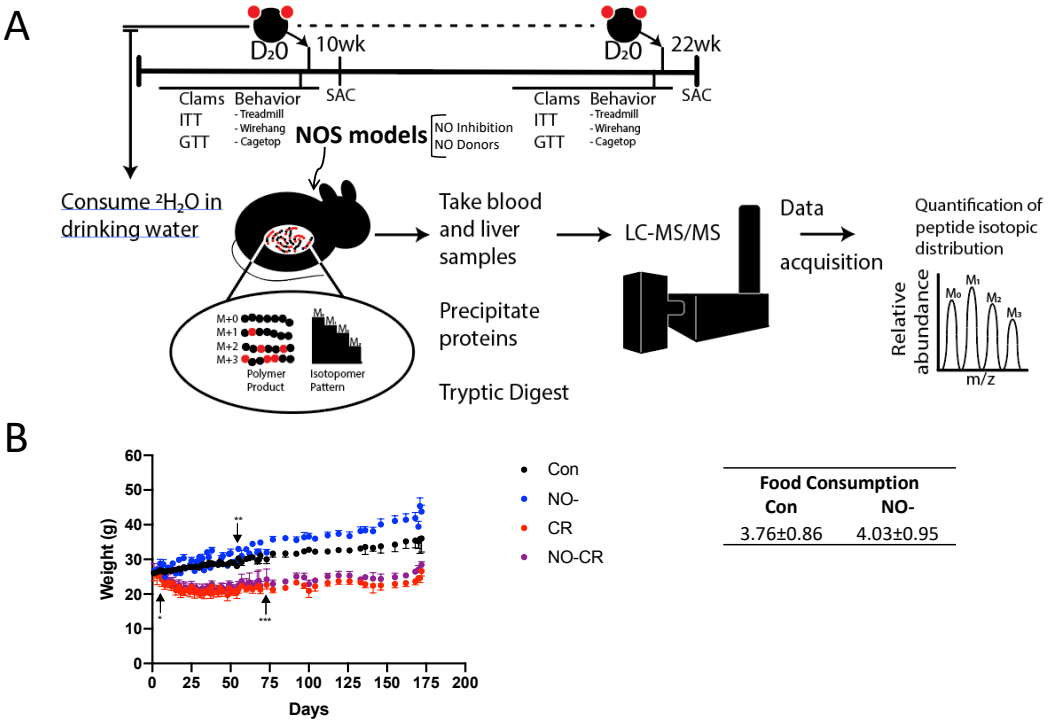

Figure 6-3. Experimental design and model. (A) Mouse experimental workflow: at the beginning of CR, mice underwent a series of non-invasive tests to assess their behavioral markers. Mice underwent two lengths of experimentation at 10 and 22 weeks of age. Before SAC, mice were labeled with $^{2}H_2O$ for 4 days. Schematic represents labeling concept and tissue processing approach. **(B)** NO- mice (n=37) and their control C57Bl6/J mice (n=48), starting at 6-8 weeks of age, were randomly divided into four groups: I) Con *adlib* (n=29), NO- *adlib* (n=20), CR (n=19), NO- CR (n=17). Mice were single caged, and their body weights and food consumption measured throughout the length of intervention. Significance starts where indicated by the arrow; ***p<0.05 between Con and CR, **p<0.05 between Con and NO-, and ***p<0.05 between CR and NO-CR.**

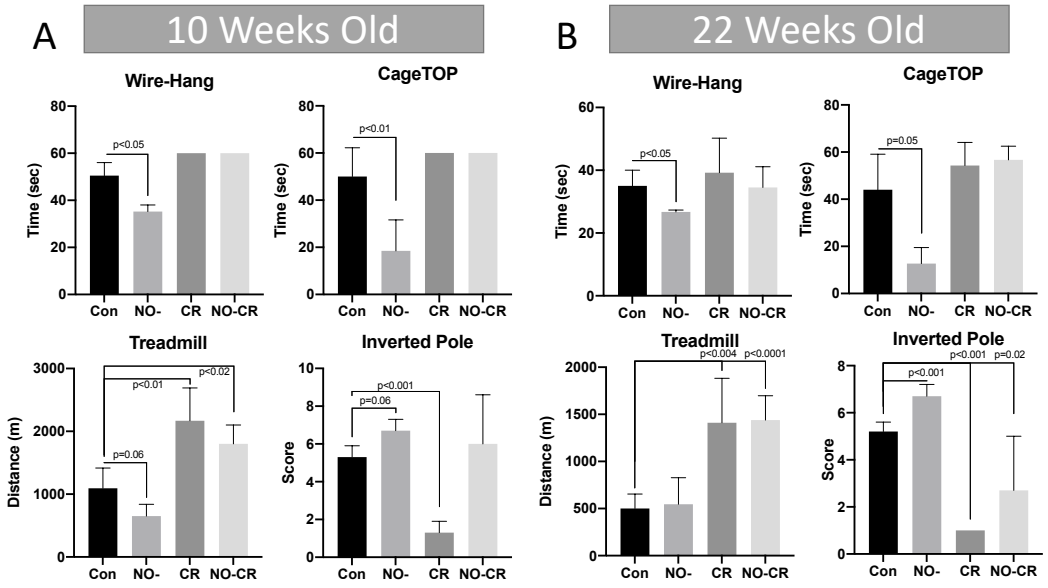

Figure 6-4. Behavioral and performance metrics. Physical and behavioral tests performed on mice at 10 **(A)** or 22 **(B)** weeks of intervention. Treadmill exercise was done to exhaustion. Cage-Top and Wire-hang were executed for up to 60 seconds. Pole-test assessing motor function was scored by time required to turn downward. Significance assessed by student t-test.

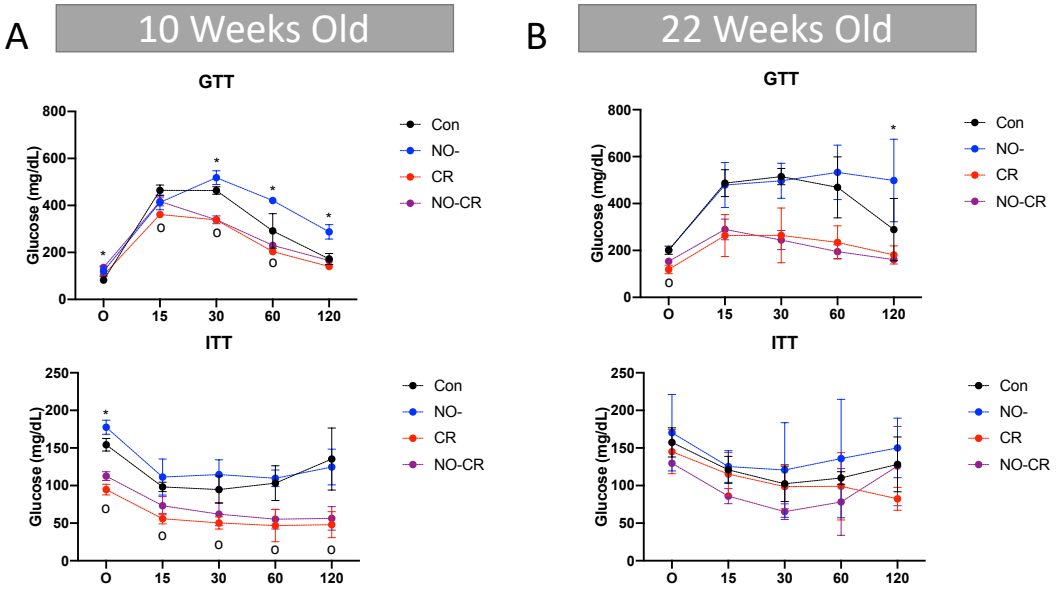

Figure 6-5. Insulin and Glucose Tolerance Tests. ITT and GTT were performed under fasting conditions for 10 **(A)** or 22 **(B)** weeks of intervention. The levels of glucose in blood of mice fasted for 6 hours were measured in a time course after IP insulin injection (ITT) in all groups (n=3-4 per group). Plasma levels of glucose after intraperitoneal glucose load (GTT) from mice fasted ON (n=3-4 per group) (*$p<0.05$ between Con and NO-, °$p<0.05$ between CR and NO-CR).

A 10 Weeks Old

	RER	HEAT	ZTOT	XTOT	XAMB
Con	1.04 ± 0.017	0.27 ± 0.007	129.0 ± 43.0	495.6 ± 63.7	262.3 ± 41.1
NO-	1.01 ± 0.028	0.29 ± 0.012	109.0 ± 8.6	471.6 ± 51.3	238.2 ± 28.2
CR	***0.95 ± 0.008**	***0.19 ± 0.010**	222.9 ± 47.5	755.0 ± 69.5	453.9 ± 52.8
NO-CR	***1.00 ± 0.013**	***0.19 ± 0.013**	97.5 ± 31.5	429.3 ± 66.0	231.1 ± 44.2

B 22 Weeks Old

	RER	HEAT	ZTOT	XTOT	XAMB
Con	0.97 ± 0.025	0.43 ± 0.013	109.5 ± 38.1	476.0 ± 81.7	213.2 ± 55.2
NO-	***0.91 ± 0.030**	***0.48 ± 0.012**	97.9 ± 15.0	432.3 ± 73.6	184.3 ± 27.0
CR	***0.91 ± 0.014**	***0.32 ± 0.012**	76.8 ± 19.1	431.5 ± 56.9	200.8 ± 40.5
NO-CR	***0.90 ± 0.010**	***0.33 ± 0.013**	157.5 ± 61.4	644.4 ± 77.9	288.3 ± 58.0

* p<0.05, Student T-test

Figure 6-6. CLAMS assessment of mice. Metabolic assessment was performed in metabolic cages before 10 **(A)** or 22 **(B)** weeks of intervention. Metabolic Cages were used to assess the RER, HEAT, and movement scores of mice (12 total, *n=4* per group). Animals were placed on a CLAMS system and their metrics were taken for 3 nights (dark) and 2 days (light). Dark and Light values were averaged together (*p<0.05 to Con).

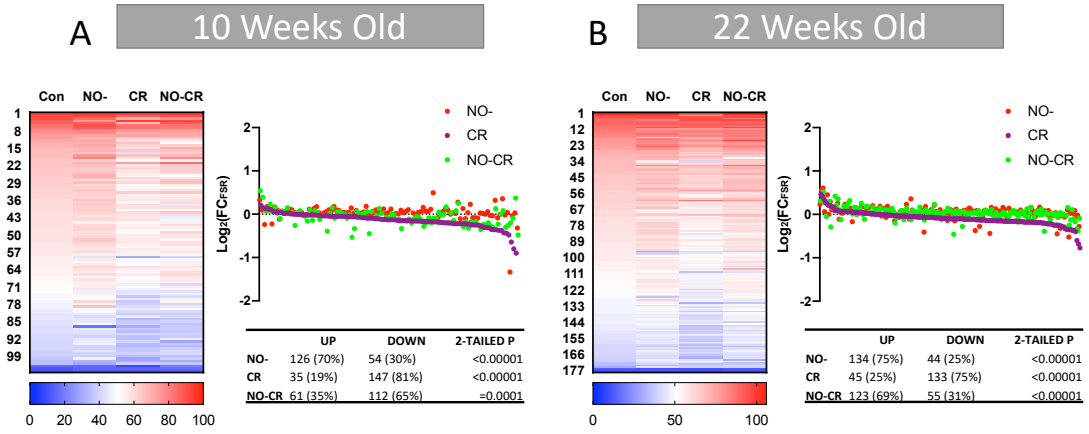

Figure 6-7. Effects of NO and CR on hepatic proteome FSR. FSR values were obtained for the liver proteome at weeks 10 **(A)** or 22 **(B)** of intervention for Con, CR, NO- and NO-CR**.** Heatmap representing the FSR of proteins. Dots along the line represent identified proteins sorted from highest FSR to lowest FSR on the CR group by the fold change to control. Comparisons are done for all groups. Table represents the binomial distribution of proteins with an increased FSR (upregulated, UP), or decreased (downregulated, Down).

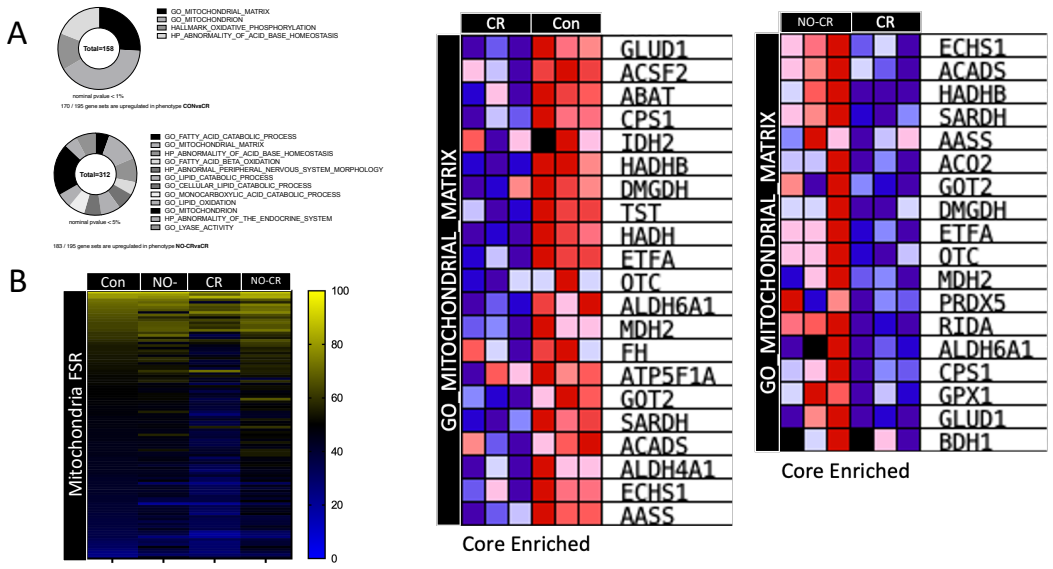

Figure 6-8. Protein enrichment analysis of hepatic proteome FSR. This data represents the sequence enrichment analysis by gene expression profiling. **(A)** 170 out of 195 datasets tested were enriched in the CR group and are represented as a fraction of the total number of genes included in each dataset. Of these, 4 datasets were significantly enriched at a nominal $p < 0.01$. In addition, 183 out of 195 datasets were upregulated in the NO-CR group compared to CR. Of these, 12 datasets were significantly enriched at a nominal $p < 0.05$. **(B)**. Mitochondria proteins were observed to be highly regulated among the significant ontologies analyzed by enrichment analysis. Liver samples were therefore prepared for mitochondria isolation and analyzed by LC/MS/MS for FSR. **(C)** Core enriched proteins under ontological pathways significantly regulated in our experimental groups.

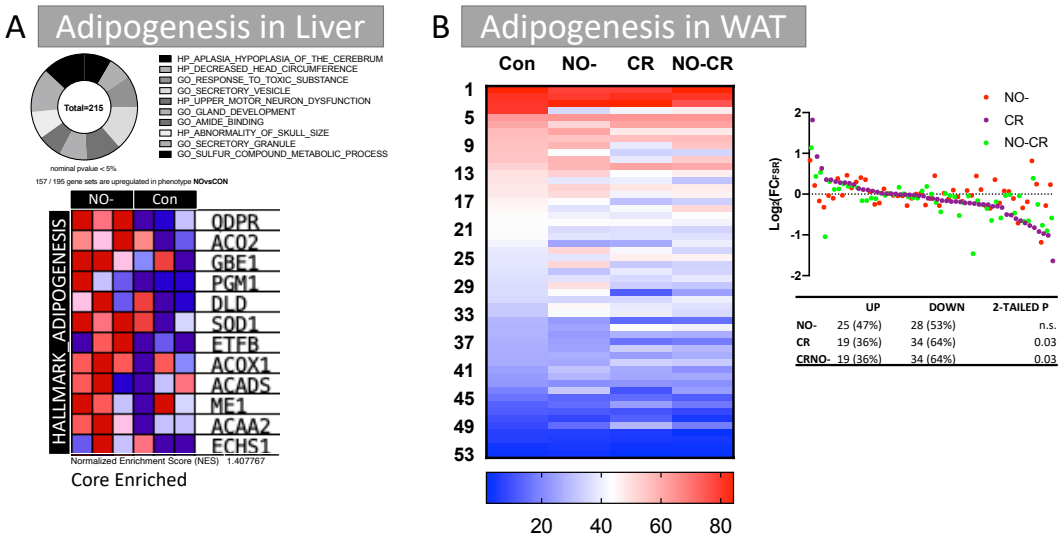

Figure 6-9. Analysis of white adipose proteome FSR. (A) Enriched pathways within the NO- group compared to Con are represented by nominal p<0.05. Hallmark Adipogenesis was identified as one of the 157 out of 195 gene sets upregulated under NO- (NES:1.4). Core enriched proteins are represented in a heat map. To test if NO plays a role in adipogenesis in WAT, FSR were then calculated **(B)** where the heatmap represents the FSR of adipose proteins. Dots along the line represent identified proteins sorted from highest FSR to lowest FSR on the CR group by the fold change to control. Comparisons are done for all groups. Table represents the binomial distribution of proteins with an increased FSR (upregulated, UP), or decreased (downregulated, Down).

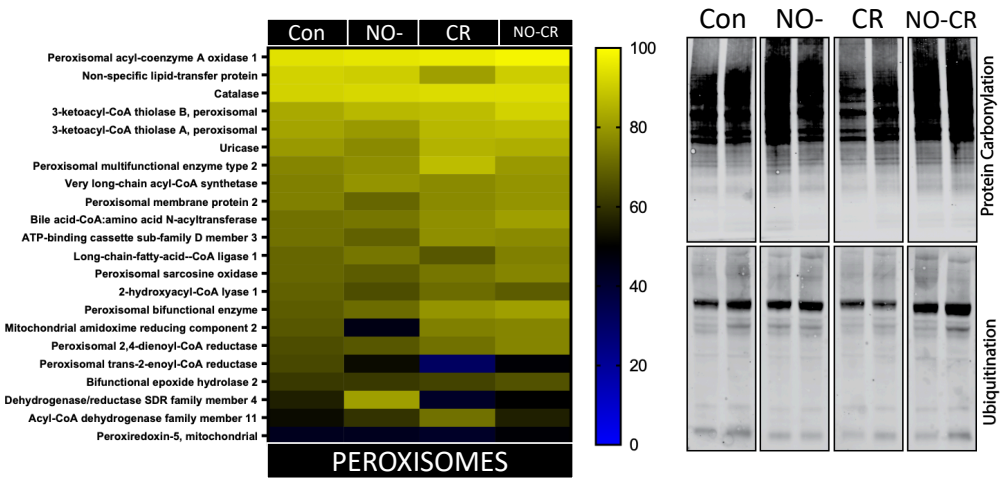

	UP	Down	2-TAILED P
NO-	54.5% (n=12)	54.5% (n=10)	0.523
CR	77.3% (n=17)	22.7% (n=5)	0.004
NO-CR	81.8% (n=18)	18.2 (n=4)	0.001

Figure 6-10. Analysis of peroxisomal proteins in liver under CR and NO. To test if NO plays a role in peroxisome biogenesis, peroxisomes were isolated from liver samples by gradient ultracentrifugation and the fraction was analyzed by LC/MS/MS for peroxisomal proteins. The heatmap represents the FSR of liver peroxisomes. The western blots represent expression of protein carbonylation or ubiquitination in total liver lysate.

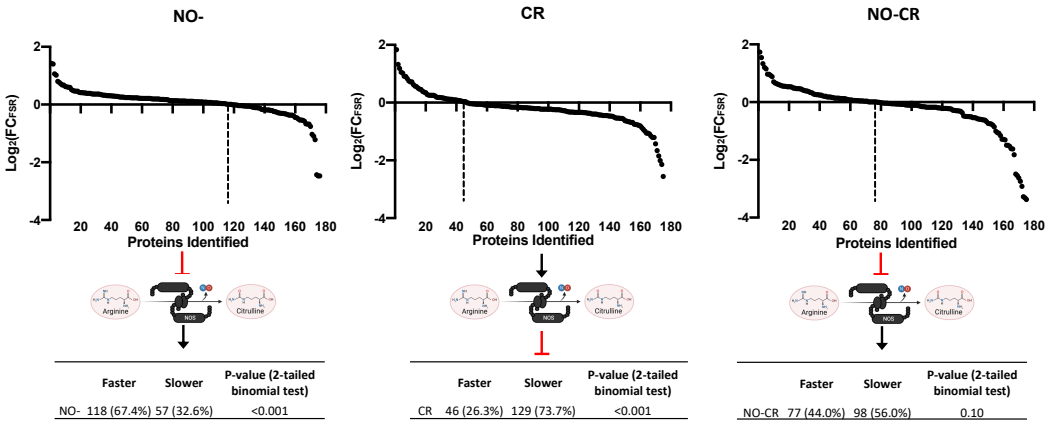

Figure 6-11. Validation of FSR results for six weeks of intervention. FSR values for hepatic proteins was assessed. Data represents the fold change between the group to control. Data is represented by either inhibiting or allowing the activity of NOS. Table represents the binomial distribution of proteins by either increased or decreased FSR values compared to control.

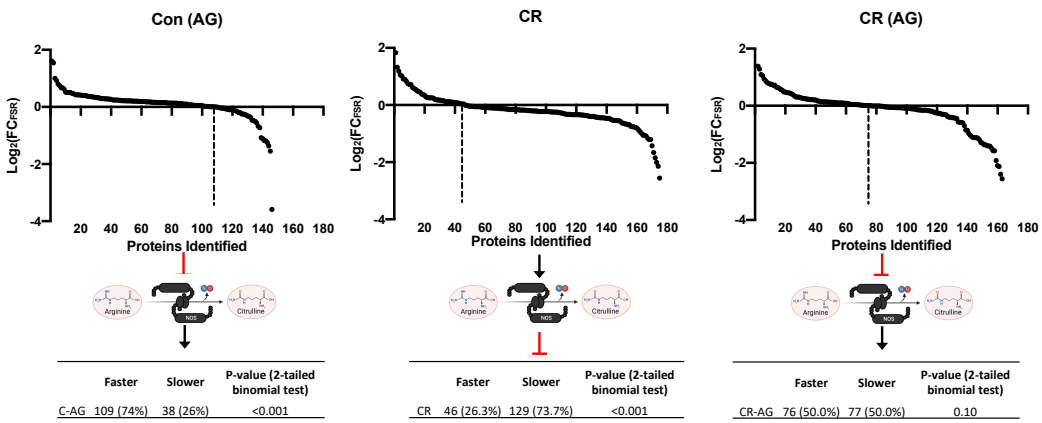

Figure 6-12. AG reverses the effects of CR. AG is a selective inhibitor of NOS enzymes. Here, mice were given AG in the drinking water for the same length of intervention as CR (6 weeks). FSR values for hepatic proteins measured in all 4 groups were compared. Data represent the fold change between the group to controls. Data are represented by either inhibiting or allowing the activity of NOS. Table represents the binomial distribution of proteins by either increased or decreased FSR values compared to controls.

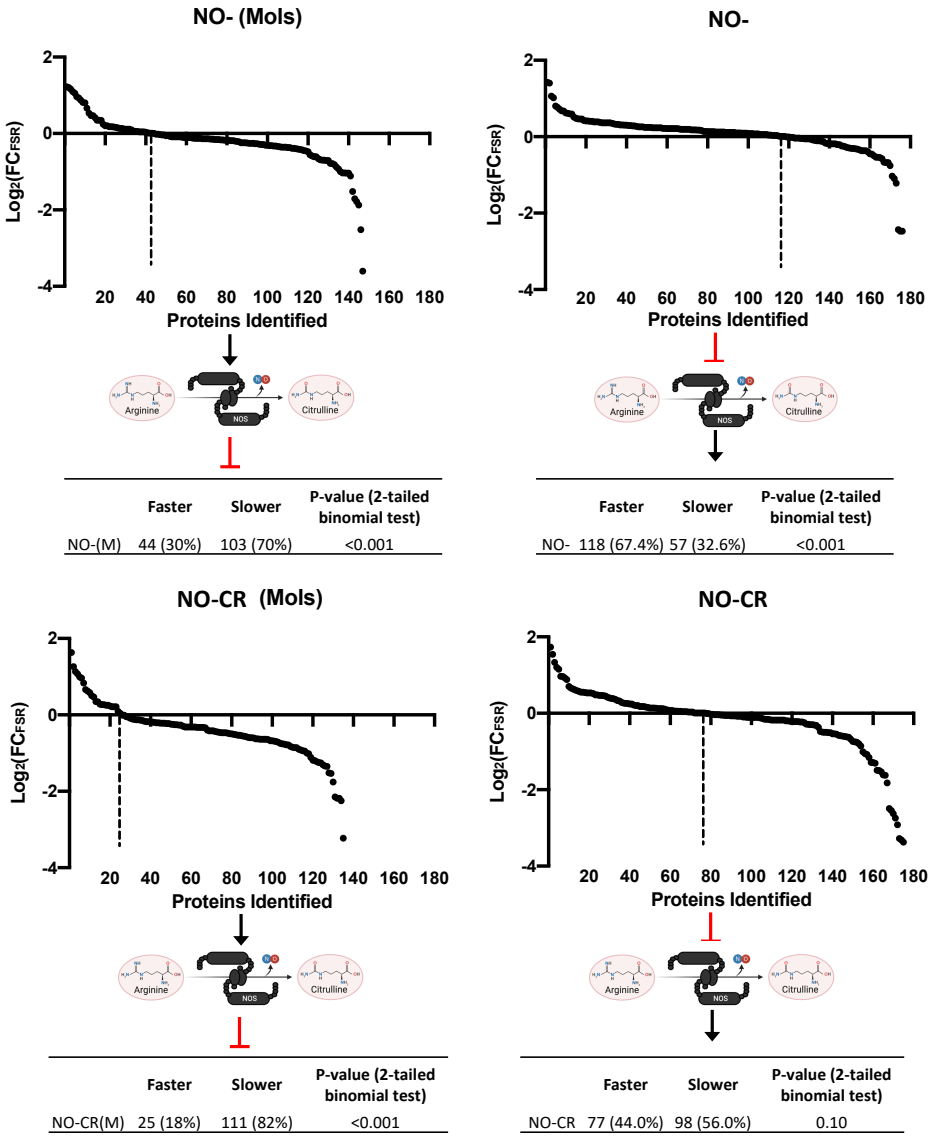

Figure 6-13. Mols rescues the effects of CR on proteome regulation in NO- mice. Mols is a potent donor of NO metabolized in the liver. Here, NO- mice were given Mols in the drinking water for the same length of intervention as CR (6 weeks). FSR values for hepatic proteins were assessed. Data represents the fold change between the group to control. Data are represented by either inhibiting or allowing the activity of NOS. Table represents the binomial distribution of proteins by either increased or decreased FSR values compared to control.

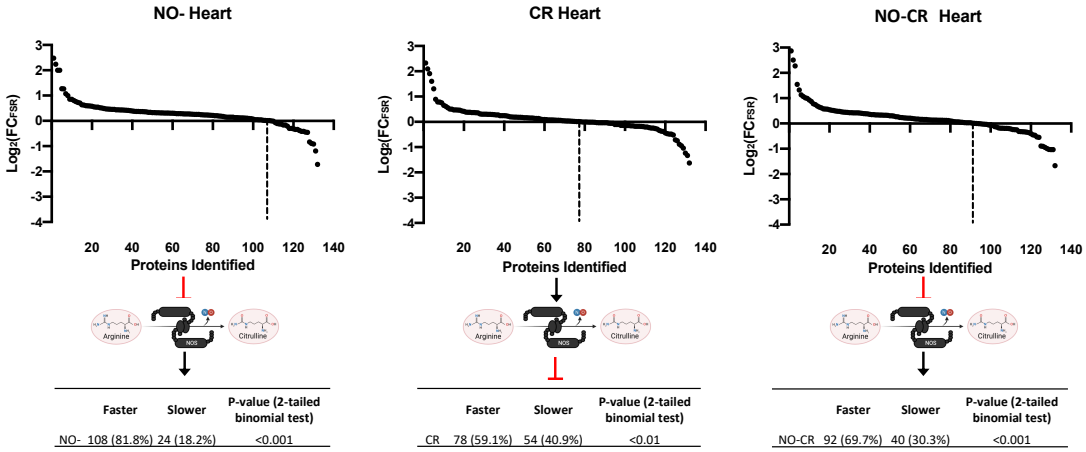

Figure 6-14A. Effect of NO on the heart proteome. FSR values for cardiac proteins were assessed. Data represents the fold change between the group to control. Data is represented by either inhibiting or allowing the activity of NOS. Table represents the binomial distribution of proteins by either increased or decreased FSR values compared to control.

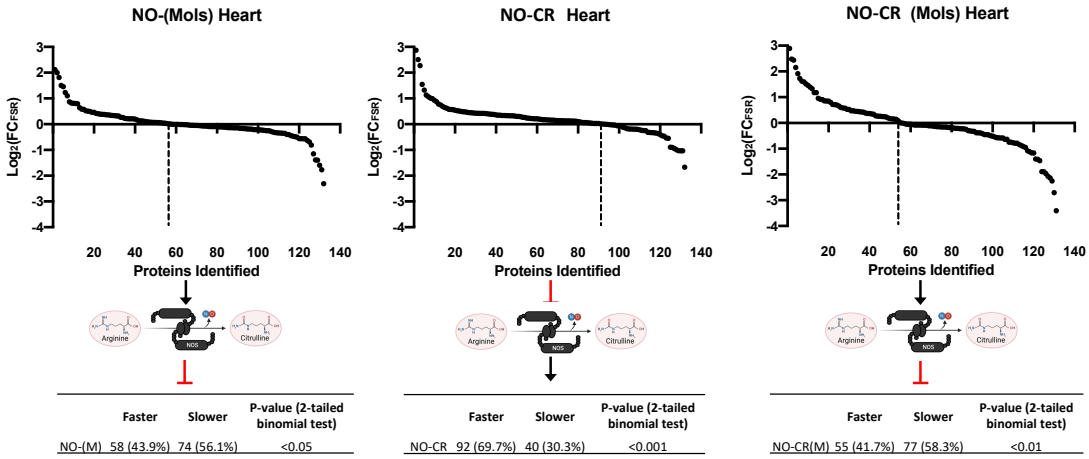

Figure 6-14B. Mols rescues the effects of CR on heart proteome regulation. Here, NO- mice were given Mols in the drinking water for the same length of intervention as CR (6 weeks). FSR values for cardiac proteins were assessed. Data represent the fold change between the group to control. Data are represented by either inhibiting or allowing the activity of NOS. Table shows the binomial distribution of proteins by either increased or decreased FSR values compared to control.

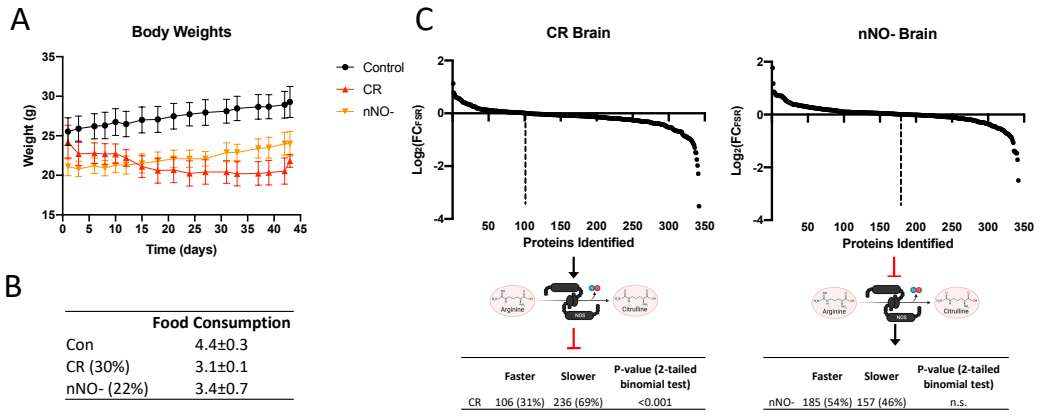

B

	Food Consumption
Con	4.4±0.3
CR (30%)	3.1±0.1
nNO- (22%)	3.4±0.7

Figure 6-15. nNO- mice exhibit a modest signature of CR. nNO- mice exhibit a modest CR under *adlib.* **(A)** Body weights of nNO- mice were measured for the duration of the experiment and show a decrease body weight compared to control. **(B)** Food consumption revealed that nNO- mice ate 22% less food than control placing them in a 22% CR diet. **(C)** Assessment of brain proteome reveal that in the absence of brain NOS enzyme, the effects of CR are blunted.

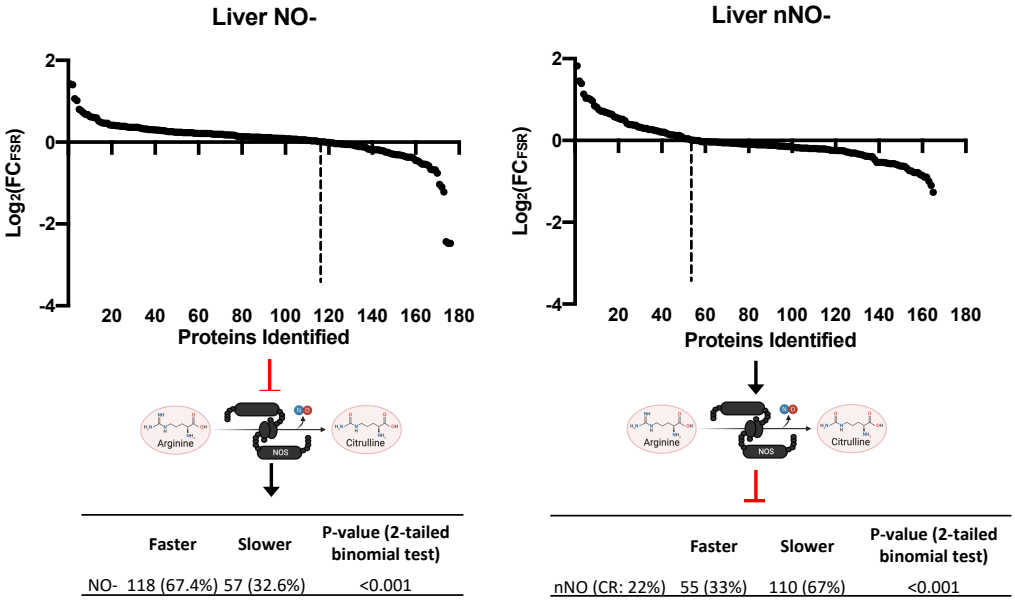

	Faster	Slower	P-value (2-tailed binomial test)
NO-	118 (67.4%)	57 (32.6%)	<0.001

	Faster	Slower	P-value (2-tailed binomial test)
nNO (CR: 22%)	55 (33%)	110 (67%)	<0.001

Figure 6-16. Moderate CR observed in nNO- mice slows down the hepatic FSR in nNO mice. nNO mice are under 22% CR. FSR values for hepatic proteins was assessed. Data represent the fold change between the group to control. Data are represented by either inhibiting or allowing the activity of NOS. Table represents the binomial distribution of proteins by either increased or decreased FSR values compared to control.

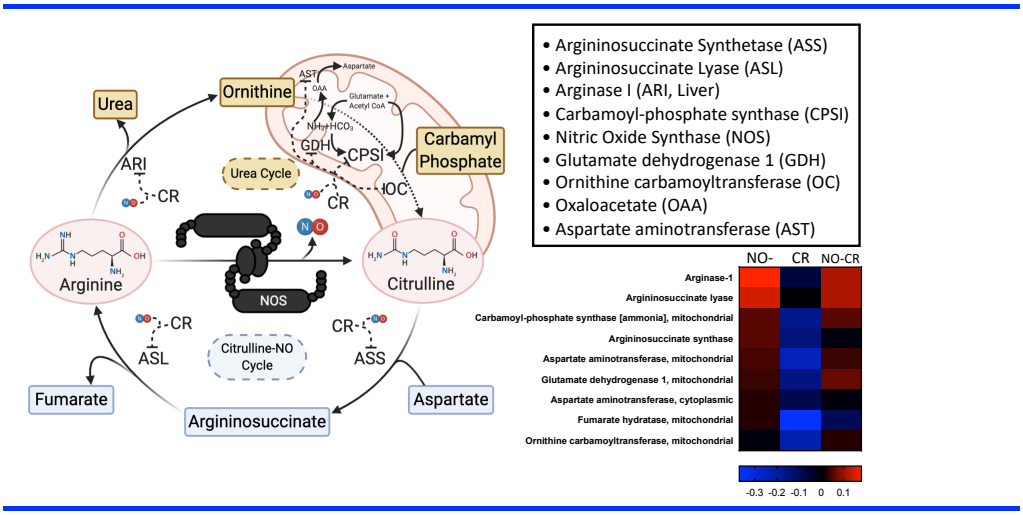

Figure 6-17. Summary of results. CR was observed to induce NO stimulating genes and increase the hepatic protein half-lives of proteins involved in the regulation of the Citrulline-NO-Urea cycles. In the absence of NOS, the half-lives of these proteins are dramatically decreased. Here, we suggest a role for NO in proteome regulation and the effects of CR on proteome flux response to modulations.

CHAPTER SEVEN: Conclusions

1. CHAPTERS SUMMARIZED

Dysregulation of cell metabolism is a primary signature of aging whose occurrence is unpredictable, steering the life of an organism towards abnormal function and ultimately death. CR is the only method currently known to effectively ameliorate the effects of aging. In Chapter One, I reviewed numerous paradigms and metabolic pathways common in aging, and how CR contributes to health and lifespan extension by altering the metabolism of aging. Chapter One also discusses various aspects of proteome regulation that reference to these metabolic adaptations, and the current therapeutic potential that have arisen from this research.

A large number of pathways linked to CR presented in Chapter One, from energy sensors to surveillance systems, act towards the maintenance of the proteome. Yet, their specific relations with the proteome still remain poorly defined. Deciphering the direct effect of CR on proteome homeostasis is critical in understanding the biological action that leads to lifespan extension. Dynamic proteomic technologies have arisen as a powerful strategy that enable the assessment of complex molecular fluxes. In Chapter Two I reviewed the dynamic basis of the synthesis and breakdown rate of molecules, and how this dynamic movement can be interconnected with proteomics to measure not just the concentration of a large number of individual proteins in a sample, but their kinetics.

In Chapter Three, I used a combination of non-radioactive stable isotope labeling with tandem mass spectrometry in mice to assess the complex mix of proteins composed of thousands of peptides in a CR time course. Looking at the liver proteome for the FSR of the identified proteins, I discovered discreet time period by which the half-lives of hepatic proteins become uniquely preserved.

In Chapter Four, I used forced treadmill exercise training, a well-established model for increasing mitochondrial biogenesis and compare it to CR. I observe that EX significantly increased the turnover rates (decreased the half-lives) of the majority of proteins involved muscle function like contractile fiber, cytoskeletal, glycolytic, and mitochondrial. I further observed increased cellular and mitochondrial protein abundances compared with control, suggesting an increase in absolute synthesis rates. In contrast, CR significantly reduced the turnover rates (increased the half-lives) of muscle contractile fiber, cytoskeletal, glycolytic, antioxidant and mitochondrial proteins, and increased abundances of cellular and mitochondrial proteins compared with control, linking the increase in concentrations of mitochondrial proteins to a reduction in catabolic rates rather than increasing synthesis rates.

In Chapter Five, I use metformin administration to assess the effects of this antidiabetic drug in proteome regulation. I demonstrate that metformin acts as a powerful CR mimetic by increasing the hepatic protein half-lives through a partial-but-significant involvement with the lysosomal degradation pathway. I further find a subset of long-lived proteins that require CMA for their maintenance.

In Chapter Six, I discover a never-before-seen role for NO in proteome regulation. Under CR, the absence of NO inhibits its regulatory role in increasing the hepatic

protein half-lives. I confirm through stringent genomic analysis that under CR, NO signaling is significantly upregulated and interacts with various clusters for proper cell function. I further confirm CR increases the half-lives of the main enzymes involved in the Citrulline-NO-Urea cycle involved in the recycling and maintenance of NOS. I further validate these effects in heart and brain tissues and in a time dependent manner.

Overall, the findings presented in Here show the utility of proteome dynamics in understanding the cellular mechanisms involved in the response to energy cell status, offering protein kinetics as a powerful approach for identifying novel mechanisms of action in the context of lifespan extension.

2. FINAL REMARKS

The ultimate aim of this dissertation was to present a current understanding of CR metabolism and its regulation of the proteome through proteome dynamics and apply this knowledge to further discover new CR mimetics like exercise and metformin administration and mechanisms of action like NO and autophagy. One of the largest challenges remaining in developing new therapies is that most of the approaches to study the proteome is through stasis; most proteins are seen in the context of a snapshot that does not reveal changes over time. Here, I have shown how, by coupling stable isotope labeling strategies, we can discover novel target pathways and proteins that were once considered unrelated to proteome function, including NO, to understand the pathogenesis of aging.

Using proteome dynamics approaches, I elucidate many previously unknown aspects of CR, from its time dependent effect in proteome regulation to the discovery CR mimetic markers in protein maintenance and the fundamental role of NO on CR and proteome regulation. Here, I shed light into how global modulation of the proteome can be a powerful biomarker of lifespan extension.

References

1. Smith, R. L., Soeters, M. R., Wüst, R. C. I. & Houtkooper, R. H. Metabolic Flexibility as an Adaptation to Energy Resources and Requirements in Health and Disease. *Endocr Rev* **39**, 489–517 (2018).
2. Balasubramanian, P., Howell, P. R. & Anderson, R. M. Aging and Caloric Restriction Research: A Biological Perspective With Translational Potential. *EBioMedicine* **21**, 37–44 (2017).
3. López-Lluch, G. & Navas, P. Calorie restriction as an intervention in ageing. *J Physiol* **594**, 2043–2060 (2016).
4. Handschin, C. Caloric restriction and exercise "mimetics": ready for prime time? *Pharmacol Res* **103**, 158–166 (2016).
5. Lee, S.-H. & Min, K.-J. Caloric restriction and its mimetics. *BMB Rep* **46**, 181–187 (2013).
6. Armandola, E. Caloric Restriction and Life Expectancy. *MedGenMed* **6**, (2004).
7. Thompson, A. C. S. *et al.* Reduced in vivo hepatic proteome replacement rates but not cell proliferation rates predict maximum lifespan extension in mice. *Aging Cell* **15**, 118–127 (2016).
8. Dai, D.-F. *et al.* Altered proteome turnover and remodeling by short-term caloric restriction or rapamycin rejuvenate the aging heart. *Aging Cell* **13**, 529–539 (2014).
9. Escobar, K. A., Cole, N. H., Mermier, C. M. & VanDusseldorp, T. A. Autophagy and aging: Maintaining the proteome through exercise and caloric restriction. *Aging Cell* **18**, e12876 (2019).
10. Sampaio-Marques, B., Burhans, W. C. & Ludovico, P. Longevity pathways and maintenance of the proteome: the role of autophagy and mitophagy during yeast ageing. *Microb Cell* **1**, 118–127.
11. Herodotus, G. R. *History of Herodotus: A New English Version*. (Murray, 1880).
12. Rous, P. THE INFLUENCE OF DIET ON TRANSPLANTED AND SPONTANEOUS MOUSE TUMORS. *J Exp Med* **20**, 433–451 (1914).
13. Ungvari, Z., Parrado-Fernandez, C., Csiszar, A. & de Cabo, R. Mechanisms underlying caloric restriction and life span regulation: implications for vascular aging. *Circ Res* **102**, 519–528 (2008).
14. Osborne, T. B., Mendel, L. B. & Ferry, E. L. THE EFFECT OF RETARDATION OF GROWTH UPON THE BREEDING PERIOD AND DURATION OF LIFE OF RATS. *Science (New York, N.Y.)* **45**, 294–295 (1917).
15. McCay, C. M., Crowell, M. F. & Maynard, L. A. The effect of retarded growth upon the length of life span and upon the ultimate body size. 1935. *Nutrition (Burbank, Los Angeles County, Calif.)* **5**, 155–171; discussion 172 (1989).
16. Davis, T. A., Bales, C. W. & Beauchene, R. E. Differential effects of dietary caloric and protein restriction in the aging rat. *Experimental Gerontology* **18**, 427–435 (1983).
17. Yu, B. P., Masoro, E. J. & McMahan, C. A. Nutritional influences on aging of Fischer 344 rats: I. Physical, metabolic, and longevity characteristics. *Journal of Gerontology* **40**, 657–670 (1985).
18. Weindruch, R. & Walford, R. L. Dietary restriction in mice beginning at 1 year of age: effect on life-span and spontaneous cancer incidence. *Science (New York, N.Y.)* **215**, 1415–1418 (1982).

19. Lin, S.-J., Defossez, P.-A. & Guarente, L. Requirement of NAD and SIR2 for Life-Span Extension by Calorie Restriction in Saccharomyces cerevisiae. *Science* **289**, 2126–2128 (2000).
20. Lin, S.-J. *et al.* Calorie restriction extends Saccharomyces cerevisiae lifespan by increasing respiration. *Nature* **418**, 344–348 (2002).
21. Kaeberlein, M., McVey, M. & Guarente, L. The SIR2/3/4 complex and SIR2 alone promote longevity in Saccharomyces cerevisiae by two different mechanisms. *Genes Dev* **13**, 2570–2580 (1999).
22. Leonov, A. *et al.* Caloric restriction extends yeast chronological lifespan via a mechanism linking cellular aging to cell cycle regulation, maintenance of a quiescent state, entry into a non-quiescent state and survival in the non-quiescent state. *Oncotarget* **8**, 69328–69350 (2017).
23. Smith, E. D. *et al.* Age- and calorie-independent life span extension from dietary restriction by bacterial deprivation in Caenorhabditis elegans. *BMC Dev Biol* **8**, 49 (2008).
24. Morselli, E. *et al.* Caloric restriction and resveratrol promote longevity through the Sirtuin-1-dependent induction of autophagy. *Cell Death Dis* **1**, e10 (2010).
25. Greer, E. L. & Brunet, A. Different dietary restriction regimens extend lifespan by both independent and overlapping genetic pathways in C. elegans. *Aging Cell* **8**, 113–127 (2009).
26. Dall, K. B. & Færgeman, N. J. Metabolic regulation of lifespan from a C. elegans perspective. *Genes Nutr* **14**, (2019).
27. David, J., Van Herrewege, J. & Fouillet, P. Quantitative under-feeding of Drosophila: effects on adult longevity and fecundity. *Experimental Gerontology* **6**, 249–257 (1971).
28. Piper, M. D. W. & Partridge, L. Dietary Restriction in Drosophila: Delayed Aging or Experimental Artefact? *PLoS Genet* **3**, (2007).
29. Tatar, M. Diet restriction in Drosophila melanogaster. Design and analysis. *Interdisciplinary Topics in Gerontology* **35**, 115–136 (2007).
30. Tatar, M., Post, S. & Yu, K. Nutrient control of Drosophila longevity. *Trends Endocrinol Metab* **25**, 509–517 (2014).
31. Staats, S. *et al.* Dietary Resveratrol Does Not Affect Life Span, Body Composition, Stress Response, and Longevity-Related Gene Expression in Drosophila melanogaster. *Int J Mol Sci* **19**, (2018).
32. Broughton, S. J. *et al.* Longer lifespan, altered metabolism, and stress resistance in Drosophila from ablation of cells making insulin-like ligands. *Proceedings of the National Academy of Sciences of the United States of America* **102**, 3105–3110 (2005).
33. Clancy, D. J. *et al.* Extension of life-span by loss of CHICO, a Drosophila insulin receptor substrate protein. *Science (New York, N.Y.)* **292**, 104–106 (2001).
34. Bjedov, I. *et al.* Mechanisms of Life Span Extension by Rapamycin in the Fruit Fly Drosophila melanogaster. *Cell Metab* **11**, 35–46 (2010).
35. Orr, W. C. & Sohal, R. S. Extension of life-span by overexpression of superoxide dismutase and catalase in Drosophila melanogaster. *Science (New York, N.Y.)* **263**, 1128–1130 (1994).
36. Taormina, G. *et al.* Longevity: Lesson from Model Organisms. *Genes (Basel)* **10**, (2019).
37. Huang, C.-W. *et al.* Tequila Regulates Insulin-Like Signaling and Extends Life Span in Drosophila melanogaster. *J Gerontol A Biol Sci Med Sci* **70**, 1461–1469 (2015).
38. Justice, M. J. & Dhillon, P. Using the mouse to model human disease: increasing validity and reproducibility. *Dis Model Mech* **9**, 101–103 (2016).

39. Perlman, R. L. Mouse models of human disease. *Evol Med Public Health* **2016**, 170–176 (2016).
40. Chinwalla, A. T. *et al.* Initial sequencing and comparative analysis of the mouse genome. *Nature* **420**, 520–562 (2002).
41. Colman, R. J. *et al.* Caloric restriction delays disease onset and mortality in rhesus monkeys. *Science* **325**, 201–204 (2009).
42. Colman, R. J. *et al.* Caloric restriction reduces age-related and all-cause mortality in rhesus monkeys. *Nat Commun* **5**, 3557 (2014).
43. Mattison, J. A. *et al.* Impact of caloric restriction on health and survival in rhesus monkeys: the NIA study. *Nature* **489**, (2012).
44. Pifferi, F. *et al.* Caloric restriction increases lifespan but affects brain integrity in grey mouse lemur primates. *Communications Biology* **1**, 1–8 (2018).
45. Redman, L. M. & Ravussin, E. Caloric Restriction in Humans: Impact on Physiological, Psychological, and Behavioral Outcomes. *Antioxid Redox Signal* **14**, 275–287 (2011).
46. Vallejo, E. A. [Hunger diet on alternate days in the nutrition of the aged]. *Prensa Med Argent* **44**, 119–120 (1957).
47. Das, S. K. *et al.* Low or moderate dietary energy restriction for long-term weight loss: what works best? *Obesity (Silver Spring)* **17**, 2019–2024 (2009).
48. Heilbronn, L. K. *et al.* Effect of 6-month calorie restriction on biomarkers of longevity, metabolic adaptation, and oxidative stress in overweight individuals: a randomized controlled trial. *JAMA* **295**, 1539–1548 (2006).
49. Weiss, E. P. *et al.* Improvements in glucose tolerance and insulin action induced by increasing energy expenditure or decreasing energy intake: a randomized controlled trial. *Am J Clin Nutr* **84**, 1033–1042 (2006).
50. Redman, L. M. *et al.* Metabolic Slowing and Reduced Oxidative Damage with Sustained Caloric Restriction Support the Rate of Living and Oxidative Damage Theories of Aging. *Cell Metabolism* **27**, 805-815.e4 (2018).
51. Willcox, D. C., Willcox, B. J., Hsueh, W.-C. & Suzuki, M. Genetic determinants of exceptional human longevity: insights from the Okinawa Centenarian Study. *Age (Dordr)* **28**, 313–332 (2006).
52. Kerr, G. *Okinawa: The History of an Island People*. (Tuttle Publishing, 2000).
53. Willcox, B. J. & Willcox, D. C. Caloric restriction, caloric restriction mimetics, and healthy aging in Okinawa: controversies and clinical implications. *Curr Opin Clin Nutr Metab Care* **17**, 51–58 (2014).
54. Madeo, F., Carmona-Gutierrez, D., Hofer, S. J. & Kroemer, G. Caloric Restriction Mimetics against Age-Associated Disease: Targets, Mechanisms, and Therapeutic Potential. *Cell Metabolism* **29**, 592–610 (2019).
55. Moatt, J. P., Nakagawa, S., Lagisz, M. & Walling, C. A. The effect of dietary restriction on reproduction: a meta-analytic perspective. *BMC Evol Biol* **16**, (2016).
56. Na, C., L, F., V, T. & J, N.-Ž. Calorie restriction induces reversible lymphopenia and lymphoid organ atrophy due to cell redistribution. *Geroscience* **40**, 279–291 (2018).
57. Martin, C. K. *et al.* Effect of Calorie Restriction on Mood, Quality of Life, Sleep, and Sexual Function in Healthy Nonobese Adults. *JAMA Intern Med* **176**, 743–752 (2016).
58. Weinert, B. T. & Timiras, P. S. Invited review: Theories of aging. *J Appl Physiol (1985)* **95**, 1706–1716 (2003).
59. Ivanova, D. G. & Yankova, T. M. The free radical theory of aging in search of a strategy for increasing life span. *Folia Med (Plovdiv)* **55**, 33–41 (2013).

60. Sanz, A. & Stefanatos, R. K. A. The mitochondrial free radical theory of aging: a critical view. *Curr Aging Sci* **1**, 10–21 (2008).
61. Harman, D. Aging: a theory based on free radical and radiation chemistry. *J Gerontol* **11**, 298–300 (1956).
62. Walsh, M. E., Shi, Y. & Van Remmen, H. The effects of dietary restriction on oxidative stress in rodents. *Free Radic Biol Med* **66**, 88–99 (2014).
63. Speakman, J. R. Body size, energy metabolism and lifespan. *J Exp Biol* **208**, 1717–1730 (2005).
64. Sung, H. J. *et al.* Ambient oxygen promotes tumorigenesis. *PLoS One* **6**, e19785 (2011).
65. Valko, M., Rhodes, C. J., Moncol, J., Izakovic, M. & Mazur, M. Free radicals, metals and antioxidants in oxidative stress-induced cancer. *Chem Biol Interact* **160**, 1–40 (2006).
66. Andersen, J. K. Oxidative stress in neurodegeneration: cause or consequence? *Nat Med* **10 Suppl**, S18-25 (2004).
67. Halliwell, B. Oxidative stress and neurodegeneration: where are we now? *J Neurochem* **97**, 1634–1658 (2006).
68. Dhalla, N. S., Temsah, R. M. & Netticadan, T. Role of oxidative stress in cardiovascular diseases. *J Hypertens* **18**, 655–673 (2000).
69. Griendling, K. K. & FitzGerald, G. A. Oxidative stress and cardiovascular injury: Part II: animal and human studies. *Circulation* **108**, 2034–2040 (2003).
70. Ceriello, A. & Motz, E. Is oxidative stress the pathogenic mechanism underlying insulin resistance, diabetes, and cardiovascular disease? The common soil hypothesis revisited. *Arterioscler Thromb Vasc Biol* **24**, 816–823 (2004).
71. Shinmura, K. Effects of caloric restriction on cardiac oxidative stress and mitochondrial bioenergetics: potential role of cardiac sirtuins. *Oxid Med Cell Longev* **2013**, 528935 (2013).
72. Gredilla, R. & Barja, G. Minireview: The Role of Oxidative Stress in Relation to Caloric Restriction and Longevity. *Endocrinology* **146**, 3713–3717 (2005).
73. Lambert, A. J. & Merry, B. J. Lack of Effect of Caloric Restriction on Bioenergetics and Reactive Oxygen Species Production in Intact Rat Hepatocytes. *J Gerontol A Biol Sci Med Sci* **60**, 175–180 (2005).
74. Lambert, A. J. & Merry, B. J. Effect of caloric restriction on mitochondrial reactive oxygen species production and bioenergetics: reversal by insulin. *Am J Physiol Regul Integr Comp Physiol* **286**, R71-79 (2004).
75. Minamiyama, Y. *et al.* Calorie restriction improves cardiovascular risk factors via reduction of mitochondrial reactive oxygen species in type II diabetic rats. *J Pharmacol Exp Ther* **320**, 535–543 (2007).
76. Gladyshev, V. N. The Free Radical Theory of Aging Is Dead. Long Live the Damage Theory! *Antioxid Redox Signal* **20**, 727–731 (2014).
77. Kowaltowski, A. J. Caloric restriction and redox state: Does this diet increase or decrease oxidant production? *Redox Report* **16**, 237–241 (2011).
78. Jin, K. Modern Biological Theories of Aging. *Aging Dis* **1**, 72–74 (2010).
79. Afanas'ev, I. Signaling and Damaging Functions of Free Radicals in Aging-Free Radical Theory, Hormesis, and TOR. *Aging Dis* **1**, 75–88 (2010).
80. Hayflick, L. & Moorhead, P. S. The serial cultivation of human diploid cell strains. *Exp Cell Res* **25**, 585–621 (1961).
81. von Zglinicki, T., Wan, T. & Miwa, S. Senescence in Post-Mitotic Cells: A Driver of Aging? *Antioxidants & Redox Signaling* (2020) doi:10.1089/ars.2020.8048.

82. Fontana, L., Nehme, J. & Demaria, M. Caloric restriction and cellular senescence. *Mech Ageing Dev* **176**, 19–23 (2018).
83. Dodig, S., Čepelak, I. & Pavić, I. Hallmarks of senescence and aging. *Biochem Med (Zagreb)* **29**, (2019).
84. Boniewska-Bernacka, E., Pańczyszyn, A. & Klinger, M. Telomeres and telomerase in risk assessment of cardiovascular diseases. *Exp Cell Res* 112361 (2020) doi:10.1016/j.yexcr.2020.112361.
85. Hayflick, L. THE LIMITED IN VITRO LIFETIME OF HUMAN DIPLOID CELL STRAINS. *Exp Cell Res* **37**, 614–636 (1965).
86. Marchionni, S., Sell, C. & Lorenzini, A. Development and Longevity: Cellular and Molecular Determinants – A Mini-Review. *Gerontology* **66**, 223–230 (2020).
87. Barnes, R. P., Fouquerel, E. & Opresko, P. L. The impact of oxidative DNA damage and stress on telomere homeostasis. *Mech Ageing Dev* **177**, 37–45 (2019).
88. Liu, Y., Bloom, S. I. & Donato, A. J. The role of senescence, telomere dysfunction and shelterin in vascular aging. *Microcirculation* **26**, e12487 (2019).
89. Prieur, A., Besnard, E., Babled, A. & Lemaitre, J.-M. p53 and p16 INK4A independent induction of senescence by chromatin-dependent alteration of S-phase progression. *Nature Communications* **2**, 473 (2011).
90. Campisi, J. & d'Adda di Fagagna, F. Cellular senescence: when bad things happen to good cells. *Nat Rev Mol Cell Biol* **8**, 729–740 (2007).
91. Jun, J.-I. & Lau, L. F. Cellular senescence controls fibrosis in wound healing. *Aging (Albany NY)* **2**, 627–631 (2010).
92. Arai, Y. *et al.* Inflammation, But Not Telomere Length, Predicts Successful Ageing at Extreme Old Age: A Longitudinal Study of Semi-supercentenarians. *EBioMedicine* **2**, 1549–1558 (2015).
93. Barnes, P. J. Mechanisms of development of multimorbidity in the elderly. *Eur Respir J* **45**, 790–806 (2015).
94. Kandoth, C. *et al.* Mutational landscape and significance across 12 major cancer types. *Nature* **502**, 333–339 (2013).
95. Inoue, K. & Fry, E. A. Aberrant expression of p16INK4a in human cancers – a new biomarker? *Cancer Rep Rev* **2**, (2018).
96. Mallakin, A. *et al.* Mutually exclusive inactivation of DMP1 and ARF/p53 in lung cancer. *Cancer Cell* **12**, 381–394 (2007).
97. Ahmed, T. *et al.* Calorie Restriction Enhances T-Cell–Mediated Immune Response in Adult Overweight Men and Women. *J Gerontol A Biol Sci Med Sci* **64A**, 1107–1113 (2009).
98. Wang, C. *et al.* Adult-onset, short-term dietary restriction reduces cell senescence in mice. *Aging (Albany NY)* **2**, 555–566 (2010).
99. Messaoudi, I. *et al.* Delay of T cell senescence by caloric restriction in aged long-lived nonhuman primates. *Proceedings of the National Academy of Sciences* **103**, 19448–19453 (2006).
100. Il'yasova, D. *et al.* Effects of 2 years of caloric restriction on oxidative status assessed by urinary F2-isoprostanes: The CALERIE 2 randomized clinical trial. *Aging Cell* **17**, (2018).
101. Yang, L. *et al.* Long-Term Calorie Restriction Enhances Cellular Quality-Control Processes in Human Skeletal Muscle. *Cell Reports* **14**, 422–428 (2016).

102. Meydani, S. N. *et al.* Long-term moderate calorie restriction inhibits inflammation without impairing cell-mediated immunity: a randomized controlled trial in non-obese humans. *Aging (Albany NY)* **8**, 1416–1431 (2016).
103. James, S. J., Muskhelishvili, L., Gaylor, D. W., Turturro, A. & Hart, R. Upregulation of apoptosis with dietary restriction: implications for carcinogenesis and aging. *Environ Health Perspect* **106**, 307–312 (1998).
104. Holt, P. R., Moss, S. F., Heydari, A. R. & Richardson, A. Diet Restriction Increases Apoptosis in the Gut of Aging Rats. *The Journals of Gerontology Series A: Biological Sciences and Medical Sciences* **53A**, B168–B172 (1998).
105. Yessenkyzy, A. *et al.* Polyphenols as Caloric-Restriction Mimetics and Autophagy Inducers in Aging Research. *Nutrients* **12**, (2020).
106. Childs, B. G., Baker, D. J., Kirkland, J. L., Campisi, J. & van Deursen, J. M. Senescence and apoptosis: dueling or complementary cell fates? *EMBO Rep* **15**, 1139–1153 (2014).
107. Franco, R. & Cidlowski, J. A. Apoptosis and glutathione: beyond an antioxidant. *Cell Death & Differentiation* **16**, 1303–1314 (2009).
108. Tower, J. Programmed cell death in aging. *Ageing Res Rev* **23**, 90–100 (2015).
109. Warner, H. R. Aging and regulation of apoptosis. *Curr Top Cell Regul* **35**, 107–121 (1997).
110. Li, Y. Z., Li, C. J., Pinto, A. V. & Pardee, A. B. Release of mitochondrial cytochrome C in both apoptosis and necrosis induced by beta-lapachone in human carcinoma cells. *Mol Med* **5**, 232–239 (1999).
111. Ortega, A. L., Mena, S. & Estrela, J. M. Glutathione in Cancer Cell Death. *Cancers (Basel)* **3**, 1285–1310 (2011).
112. Desideri, E., Ciccarone, F. & Ciriolo, M. R. Targeting Glutathione Metabolism: Partner in Crime in Anticancer Therapy. *Nutrients* **11**, (2019).
113. Alt, E. U. *et al.* Aging alters tissue resident mesenchymal stem cell properties. *Stem Cell Res* **8**, 215–225 (2012).
114. Wilson, A., Shehadeh, L. A., Yu, H. & Webster, K. A. Age-related molecular genetic changes of murine bone marrow mesenchymal stem cells. *BMC Genomics* **11**, 229 (2010).
115. Selman, C. *et al.* Short-term caloric restriction and regulatory proteins of apoptosis in heart, skeletal muscle and kidney of Fischer 344 rats. *Biogerontology* **4**, 141–147 (2003).
116. Lee, J. H. *et al.* Suppression of apoptosis by calorie restriction in aged kidney. *Experimental Gerontology* **39**, 1361–1368 (2004).
117. Almeida, A. J. P. O. de, Ribeiro, T. P. & Medeiros, I. A. de. Aging: Molecular Pathways and Implications on the Cardiovascular System. *Oxidative Medicine and Cellular Longevity* vol. 2017 e7941563 https://www.hindawi.com/journals/omcl/2017/7941563/ (2017).
118. Barzilai, N., Huffman, D. M., Muzumdar, R. H. & Bartke, A. The Critical Role of Metabolic Pathways in Aging. *Diabetes* **61**, 1315–1322 (2012).
119. Newgard, C. B. & Pessin, J. E. Recent Progress in Metabolic Signaling Pathways Regulating Aging and Life Span. *J Gerontol A Biol Sci Med Sci* **69**, S21–S27 (2014).
120. Roubenoff, R. Catabolism of aging: is it an inflammatory process? *Curr Opin Clin Nutr Metab Care* **6**, 295–299 (2003).
121. Weir, H. J. *et al.* Dietary Restriction and AMPK Increase Lifespan via Mitochondrial Network and Peroxisome Remodeling. *Cell Metabolism* **26**, 884-896.e5 (2017).

122. Herzig, S. & Shaw, R. J. AMPK: guardian of metabolism and mitochondrial homeostasis. *Nature Reviews Molecular Cell Biology* **19**, 121–135 (2018).
123. Shackelford, D. B. & Shaw, R. J. The LKB1–AMPK pathway: metabolism and growth control in tumour suppression. *Nature Reviews Cancer* **9**, 563–575 (2009).
124. Hudson, E. R. *et al.* A novel domain in AMP-activated protein kinase causes glycogen storage bodies similar to those seen in hereditary cardiac arrhythmias. *Curr Biol* **13**, 861–866 (2003).
125. Chen, K., Kobayashi, S., Xu, X., Viollet, B. & Liang, Q. AMP activated protein kinase is indispensable for myocardial adaptation to caloric restriction in mice. *PLoS One* **8**, e59682 (2013).
126. Cantó, C. & Auwerx, J. Calorie restriction: is AMPK a key sensor and effector? *Physiology (Bethesda)* **26**, 214–224 (2011).
127. Sinnett, S. E. & Brenman, J. E. The Role of AMPK in Drosophila melanogaster. *Exp Suppl* **107**, 389–401 (2016).
128. Funakoshi, M. *et al.* A gain-of-function screen identifies wdb and lkb1 as lifespan-extending genes in Drosophila. *Biochem Biophys Res Commun* **405**, 667–672 (2011).
129. Stenesen, D. *et al.* Adenosine nucleotide biosynthesis and AMPK regulate adult life span and mediate the longevity benefit of caloric restriction in flies. *Cell Metab* **17**, 101–112 (2013).
130. Garcia, D. & Shaw, R. J. AMPK: Mechanisms of Cellular Energy Sensing and Restoration of Metabolic Balance. *Mol Cell* **66**, 789–800 (2017).
131. Dong, D. *et al.* Alleviation of senescence and epithelial-mesenchymal transition in aging kidney by short-term caloric restriction and caloric restriction mimetics via modulation of AMPK/mTOR signaling. *Oncotarget* **8**, 16109–16121 (2017).
132. BonDurant, L. D. & Potthoff, M. J. Fibroblast Growth Factor 21: A Versatile Regulator of Metabolic Homeostasis. *Annu Rev Nutr* **38**, 173–196 (2018).
133. Kuhla, A. *et al.* Lifelong caloric restriction reprograms hepatic fat metabolism in mice. *J Gerontol A Biol Sci Med Sci* **69**, 915–922 (2014).
134. Ornitz, D. M. & Marie, P. J. Fibroblast growth factor signaling in skeletal development and disease. *Genes Dev* **29**, 1463–1486 (2015).
135. Cyphert, H. A., Alonge, K. M., Ippagunta, S. M. & Hillgartner, F. B. Glucagon stimulates hepatic FGF21 secretion through a PKA- and EPAC-dependent posttranscriptional mechanism. *PLoS One* **9**, e94996 (2014).
136. Dutchak, P. A. *et al.* Fibroblast Growth Factor-21 Regulates PPARγ Activity and the Antidiabetic Actions of Thiazolidinediones. *Cell* **148**, 556–567 (2012).
137. Lundåsen, T. *et al.* PPARalpha is a key regulator of hepatic FGF21. *Biochem Biophys Res Commun* **360**, 437–440 (2007).
138. Rühlmann, C. *et al.* Long-term caloric restriction in ApoE-deficient mice results in neuroprotection via Fgf21-induced AMPK/mTOR pathway. *Aging (Albany NY)* **8**, 2777–2789 (2016).
139. Dossou, A. S. & Basu, A. The Emerging Roles of mTORC1 in Macromanaging Autophagy. *Cancers (Basel)* **11**, (2019).
140. Zhu, Z. *et al.* Balancing mTOR Signaling and Autophagy in the Treatment of Parkinson's Disease. *Int J Mol Sci* **20**, (2019).
141. Hemmings, B. A. & Restuccia, D. F. PI3K-PKB/Akt Pathway. *Cold Spring Harb Perspect Biol* **4**, (2012).

142. Hopkins, B. D., Goncalves, M. D. & Cantley, L. C. Insulin–PI3K signalling: an evolutionarily insulated metabolic driver of cancer. *Nature Reviews Endocrinology* **16**, 276–283 (2020).
143. Hirschey, M. D. *et al.* Dysregulated metabolism contributes to oncogenesis. *Semin Cancer Biol* **35 Suppl**, S129–S150 (2015).
144. Deprez, J., Vertommen, D., Alessi, D. R., Hue, L. & Rider, M. H. Phosphorylation and activation of heart 6-phosphofructo-2-kinase by protein kinase B and other protein kinases of the insulin signaling cascades. *J Biol Chem* **272**, 17269–17275 (1997).
145. Rathmell, J. C. *et al.* Akt-Directed Glucose Metabolism Can Prevent Bax Conformation Change and Promote Growth Factor-Independent Survival. *Mol Cell Biol* **23**, 7315–7328 (2003).
146. Gottlieb, E. & Tomlinson, I. P. M. Mitochondrial tumour suppressors: a genetic and biochemical update. *Nat Rev Cancer* **5**, 857–866 (2005).
147. Czech, M. P. PIP2 and PIP3: Complex Roles at the Cell Surface. *Cell* **100**, 603–606 (2000).
148. Mercken, E. M. *et al.* Calorie restriction in humans inhibits the PI3K/AKT pathway and induces a younger transcription profile. *Aging Cell* **12**, 645–651 (2013).
149. Woodcock, H. V. *et al.* The mTORC1/4E-BP1 axis represents a critical signaling node during fibrogenesis. *Nature Communications* **10**, 6 (2019).
150. Beauchamp, E. M. & Platanias, L. C. The evolution of the TOR pathway and its role in cancer. *Oncogene* **32**, 3923–3932 (2013).
151. Engelman, J. A. Targeting PI3K signalling in cancer: opportunities, challenges and limitations. *Nat Rev Cancer* **9**, 550–562 (2009).
152. Duszka, K., Gregor, A., Guillou, H., König, J. & Wahli, W. Peroxisome Proliferator-Activated Receptors and Caloric Restriction—Common Pathways Affecting Metabolism, Health, and Longevity. *Cells* **9**, (2020).
153. Huang, J. & Manning, B. D. The TSC1-TSC2 complex: a molecular switchboard controlling cell growth. *Biochem J* **412**, 179–190 (2008).
154. Porta, C., Paglino, C. & Mosca, A. Targeting PI3K/Akt/mTOR Signaling in Cancer. *Front Oncol* **4**, (2014).
155. Hay, N. Interplay between FOXO, TOR, and Akt. *Biochim Biophys Acta* **1813**, 1965–1970 (2011).
156. Chung, K. W. & Chung, H. Y. The Effects of Calorie Restriction on Autophagy: Role on Aging Intervention. *Nutrients* **11**, (2019).
157. Chen, C.-N., Liao, Y.-H., Tsai, S.-C. & Thompson, L. V. Age-dependent effects of caloric restriction on mTOR and ubiquitin-proteasome pathways in skeletal muscles. *GeroScience* **41**, 871–880 (2019).
158. Ma, L. *et al.* Effect of caloric restriction on the SIRT1/mTOR signaling pathways in senile mice. *Brain Research Bulletin* **116**, 67–72 (2015).
159. Yang, F. *et al.* mTOR and autophagy in normal brain aging and caloric restriction ameliorating age-related cognition deficits. *Behav Brain Res* **264**, 82–90 (2014).
160. Cantó, C. & Auwerx, J. Caloric restriction, SIRT1 and longevity. *Trends Endocrinol Metab* **20**, 325–331 (2009).
161. Zheng, Q. *et al.* Inhibition of AMPK accentuates prolonged caloric restriction-induced change in cardiac contractile function through disruption of compensatory autophagy. *Biochimica et Biophysica Acta (BBA) - Molecular Basis of Disease* **1852**, 332–342 (2015).

162. Wang, P. *et al.* Loss of AMP-Activated Protein Kinase-α2 Impairs the Insulin-Sensitizing Effect of Calorie Restriction in Skeletal Muscle. *Diabetes* **61**, 1051–1061 (2012).
163. Ma, L., Wang, R., Wang, H., Zhang, Y. & Zhao, Z. Long-term caloric restriction activates the myocardial SIRT1/ AMPK/PGC-1α pathway in C57BL/6J male mice. *Food & Nutrition Research* (2020) doi:10.29219/fnr.v64.3668.
164. Bayliss, J. A. *et al.* Ghrelin-AMPK Signaling Mediates the Neuroprotective Effects of Calorie Restriction in Parkinson's Disease. *J. Neurosci.* **36**, 3049–3063 (2016).
165. Rogers, N. H. *et al.* Metabolic Benefit of Chronic Caloric Restriction and Activation of Hypothalamic AGRP/NPY Neurons in Male Mice Is Independent of Ghrelin. *Endocrinology* **157**, 1430–1442 (2016).
166. Darici, S. *et al.* Targeting PI3K/Akt/mTOR in AML: Rationale and Clinical Evidence. *J Clin Med* **9**, (2020).
167. Showkat, M., Beigh, M. A. & Andrabi, K. I. mTOR Signaling in Protein Translation Regulation: Implications in Cancer Genesis and Therapeutic Interventions. *Mol Biol Int* **2014**, (2014).
168. Xie, J., Wang, X. & Proud, C. G. mTOR inhibitors in cancer therapy. *F1000Res* **5**, (2016).
169. Vézina, C., Kudelski, A. & Sehgal, S. N. RAPAMYCIN (AY-22, 989), A NEW ANTIFUNGAL ANTIBIOTIC I. TAXONOMY OF THE PRODUCING STREPTOMYCETE AND ISOLATION OF THE ACTIVE PRINCIPLE. *J. Antibiot.* **28**, 721–726 (1975).
170. Saxton, R. A. & Sabatini, D. M. mTOR Signaling in Growth, Metabolism, and Disease. *Cell* **168**, 960–976 (2017).
171. Sills, A. M., Artavia, J. M., DeRosa, B. D., Ross, C. N. & Salmon, A. B. Long-term treatment with the mTOR inhibitor rapamycin has minor effect on clinical laboratory markers in middle-aged marmosets. *Am J Primatol* **81**, e22927 (2019).
172. Kallijärvi, J. & Fellman, V. Rapamycin – "One size does not fit all". *EBioMedicine* **42**, 30–31 (2019).
173. Kahan, B. D. Sirolimus: a comprehensive review. *Expert Opin Pharmacother* **2**, 1903–1917 (2001).
174. Kwitkowski, V. E. *et al.* FDA Approval Summary: Temsirolimus as Treatment for Advanced Renal Cell Carcinoma. *Oncologist* **15**, 428–435 (2010).
175. Lee, L., Ito, T. & Jensen, R. T. Everolimus in treatment of neuroendocrine tumors: efficacy, side-effects, resistance and factors affecting its place in the treatment sequence. *Expert Opin Pharmacother* **19**, 909–928 (2018).
176. Chen, G., Ding, X.-F., Bouamar, H., Pressley, K. & Sun, L.-Z. Everolimus induces G1 cell cycle arrest through autophagy-mediated protein degradation of cyclin D1 in breast cancer cells. *Am J Physiol Cell Physiol* **317**, C244–C252 (2019).
177. Hu, Y. *et al.* Torin2 inhibits the EGFR-TKI resistant Non-Small Lung Cancer cell proliferation through negative feedback regulation of Akt/mTOR signaling. *J Cancer* **11**, 5746–5757 (2020).
178. Li, J., Kim, S. G. & Blenis, J. Rapamycin: one drug, many effects. *Cell Metab* **19**, 373–379 (2014).
179. Papadopoli, D. *et al.* mTOR as a central regulator of lifespan and aging. *F1000Res* **8**, (2019).
180. Fabrizio, P., Pozza, F., Pletcher, S. D., Gendron, C. M. & Longo, V. D. Regulation of longevity and stress resistance by Sch9 in yeast. *Science* **292**, 288–290 (2001).

181. Jia, K., Chen, D. & Riddle, D. L. The TOR pathway interacts with the insulin signaling pathway to regulate C. elegans larval development, metabolism and life span. *Development* **131**, 3897–3906 (2004).
182. Vellai, T. *et al.* Genetics: influence of TOR kinase on lifespan in C. elegans. *Nature* **426**, 620 (2003).
183. Choi, K.-M. *et al.* Caloric Restriction and Rapamycin Differentially Alter Energy Metabolism in Yeast. *J Gerontol A Biol Sci Med Sci* **73**, 29–38 (2017).
184. Kafri, M., Metzl-Raz, E., Jona, G. & Barkai, N. The Cost of Protein Production. *Cell Rep* **14**, 22–31 (2015).
185. Dougherty, S. E., Maduka, A. O., Inada, T. & Silva, G. M. Expanding Role of Ubiquitin in Translational Control. *Int J Mol Sci* **21**, (2020).
186. Hertz, R. *et al.* Proteomic Identification of S-Nitrosylated Proteins in the Parasite Entamoeba histolytica by Resin-Assisted Capture: Insights into the Regulation of the Gal/GalNAc Lectin by Nitric Oxide. *PLoS One* **9**, (2014).
187. Pierrat, O. A., Mikitova, V., Bush, M. S., Browning, K. S. & Doonan, J. H. Control of protein translation by phosphorylation of the mRNA 5'-cap-binding complex. *Biochem Soc Trans* **35**, 1634–1637 (2007).
188. Alirezaei, M. *et al.* Short-term fasting induces profound neuronal autophagy. *Autophagy* **6**, 702–710 (2010).
189. Karunadharma, P. P. *et al.* Subacute calorie restriction and rapamycin discordantly alter mouse liver proteome homeostasis and reverse aging effects. *Aging Cell* **14**, 547–557 (2015).
190. Buttgereit, F. & Brand, M. D. A hierarchy of ATP-consuming processes in mammalian cells. *Biochem J* **312**, 163–167 (1995).
191. Russell, J. B. & Cook, G. M. Energetics of bacterial growth: balance of anabolic and catabolic reactions. *Microbiol Rev* **59**, 48–62 (1995).
192. Li, G.-W., Burkhardt, D., Gross, C. & Weissman, J. S. Quantifying absolute protein synthesis rates reveals principles underlying allocation of cellular resources. *Cell* **157**, 624–635 (2014).
193. Miller, B. F. *et al.* Calorie Restriction Does Not Increase Short-term or Long-term Protein Synthesis. *J Gerontol A Biol Sci Med Sci* **68**, 530–538 (2013).
194. Bruss, M. D., Thompson, A. C. S., Aggarwal, I., Khambatta, C. F. & Hellerstein, M. K. The effects of physiological adaptations to calorie restriction on global cell proliferation rates. *Am J Physiol Endocrinol Metab* **300**, E735-745 (2011).
195. Hsieh, E. A., Chai, C. M. & Hellerstein, M. K. Effects of caloric restriction on cell proliferation in several tissues in mice: role of intermittent feeding. *American Journal of Physiology-Endocrinology and Metabolism* **288**, E965–E972 (2005).
196. Iwasaki, S. & Ingolia, N. T. The Growing Toolbox for Protein Synthesis Studies. *Trends in Biochemical Sciences* **42**, 612–624 (2017).
197. Dermit, M., Dodel, M. & Mardakheh, F. K. Methods for monitoring and measurement of protein translation in time and space. *Mol. BioSyst.* **13**, 2477–2488 (2017).
198. Chassé, H., Boulben, S., Costache, V., Cormier, P. & Morales, J. Analysis of translation using polysome profiling. *Nucleic Acids Res* **45**, e15 (2017).
199. Makwana, K., Gosai, N., Poe, A. & Kondratov, R. V. Calorie restriction reprograms diurnal rhythms in protein translation to regulate metabolism. *The FASEB Journal* **33**, 4473–4489 (2019).

200. Rollins, J. A., Shaffer, D., Snow, S. S., Kapahi, P. & Rogers, A. N. Dietary restriction induces posttranscriptional regulation of longevity genes. *Life Sci Alliance* **2**, (2019).
201. Vaklavas, C., Blume, S. W. & Grizzle, W. E. Translational Dysregulation in Cancer: Molecular Insights and Potential Clinical Applications in Biomarker Development. *Front Oncol* **7**, (2017).
202. Laham-Karam, N., Pinto, G. P., Poso, A. & Kokkonen, P. Transcription and Translation Inhibitors in Cancer Treatment. *Front Chem* **8**, (2020).
203. Malina, A., Mills, J. R. & Pelletier, J. Emerging Therapeutics Targeting mRNA Translation. *Cold Spring Harb Perspect Biol* **4**, (2012).
204. Nisoli, E. *et al.* Calorie restriction promotes mitochondrial biogenesis by inducing the expression of eNOS. *Science* **310**, 314–317 (2005).
205. Guarente, L. Sirtuins in aging and disease. *Cold Spring Harb Symp Quant Biol* **72**, 483–488 (2007).
206. Courtney, K. D., Corcoran, R. B. & Engelman, J. A. The PI3K Pathway As Drug Target in Human Cancer. *J Clin Oncol* **28**, 1075–1083 (2010).
207. Egerman, M. A. & Glass, D. J. Signaling pathways controlling skeletal muscle mass. *Critical Reviews in Biochemistry and Molecular Biology* **49**, 59–68 (2014).
208. Frame, S. & Cohen, P. GSK3 takes centre stage more than 20 years after its discovery. *Biochem J* **359**, 1–16 (2001).
209. Baird, T. D. & Wek, R. C. Eukaryotic Initiation Factor 2 Phosphorylation and Translational Control in Metabolism. *Adv Nutr* **3**, 307–321 (2012).
210. Martin-Rincon, M. *et al.* Protein synthesis signaling in skeletal muscle is refractory to whey protein ingestion during a severe energy deficit evoked by prolonged exercise and caloric restriction. *International Journal of Obesity* **43**, 872–882 (2019).
211. Dennis, P. P. In vivo stability, maturation and relative differential synthesis rates of individual ribosomal proteins in Escherichia coli B/r. *J Mol Biol* **88**, 25–41 (1974).
212. Lemaux, P. G., Herendeen, S. L., Bloch, P. L. & Neidhardt, F. C. Transient rates of synthesis of individual polypeptides in E. coli following temperature shifts. *Cell* **13**, 427–434 (1978).
213. Schwanhäusser, B., Gossen, M., Dittmar, G. & Selbach, M. Global analysis of cellular protein translation by pulsed SILAC. *Proteomics* **9**, 205–209 (2009).
214. Selbach, M. *et al.* Widespread changes in protein synthesis induced by microRNAs. *Nature* **455**, 58–63 (2008).
215. Wood, S. H. *et al.* Transcriptome analysis in calorie-restricted rats implicates epigenetic and post-translational mechanisms in neuroprotection and aging. *Genome Biol* **16**, (2015).
216. Ma, S. *et al.* Caloric Restriction Reprograms the Single-Cell Transcriptional Landscape of Rattus Norvegicus Aging. *Cell* **180**, 984-1001.e22 (2020).
217. Martin-Montalvo, A. *et al.* Metformin improves healthspan and lifespan in mice. *Nature Communications* **4**, 2192 (2013).
218. Rattan, S. I. S. Rationale and methods of discovering hormetins as drugs for healthy ageing. *Expert Opin Drug Discov* **7**, 439–448 (2012).
219. Mercken, E. M., Carboneau, B. A., Krzysik-Walker, S. M. & de Cabo, R. Of Mice and Men: The Benefits of Caloric Restriction, Exercise, and Mimetics. *Ageing Res Rev* **11**, 390–398 (2012).
220. Mohar, D. S. & Malik, S. The Sirtuin System: The Holy Grail of Resveratrol? *J Clin Exp Cardiolog* **3**, (2012).

221. Naiman, S. & Cohen, H. Y. The Contentious History of Sirtuin Debates. *Rambam Maimonides Med J* **3**, (2012).
222. Zhang, C.-S. *et al.* The Lysosomal v-ATPase-Ragulator Complex Is a Common Activator for AMPK and mTORC1, Acting as a Switch between Catabolism and Anabolism. *Cell Metabolism* **20**, 526–540 (2014).
223. El-Mir, M. Y. *et al.* Dimethylbiguanide inhibits cell respiration via an indirect effect targeted on the respiratory chain complex I. *J Biol Chem* **275**, 223–228 (2000).
224. Kasznicki, J., Sliwinska, A. & Drzewoski, J. Metformin in cancer prevention and therapy. *Ann Transl Med* **2**, (2014).
225. Cuyàs, E. *et al.* Metformin Is a Direct SIRT1-Activating Compound: Computational Modeling and Experimental Validation. *Front. Endocrinol.* **9**, (2018).
226. Kalender, A. *et al.* Metformin, Independent of AMPK, Inhibits mTORC1 In a Rag GTPase-Dependent Manner. *Cell Metab* **11**, 390–401 (2010).
227. Fontaine, E. Metformin-Induced Mitochondrial Complex I Inhibition: Facts, Uncertainties, and Consequences. *Front Endocrinol (Lausanne)* **9**, (2018).
228. Wu, Y. *et al.* SIRT3 aggravates metformin-induced energy stress and apoptosis in ovarian cancer cells. *Exp Cell Res* **367**, 137–149 (2018).
229. Clare, C. E., Brassington, A. H., Kwong, W. Y. & Sinclair, K. D. One-Carbon Metabolism: Linking Nutritional Biochemistry to Epigenetic Programming of Long-Term Development. *Annual Review of Animal Biosciences* **7**, 263–287 (2019).
230. Luciano-Mateo, F. *et al.* Nutrients in Energy and One-Carbon Metabolism: Learning from Metformin Users. *Nutrients* **9**, (2017).
231. Cuyàs, E. *et al.* Metformin regulates global DNA methylation via mitochondrial one-carbon metabolism. *Oncogene* **37**, 963–970 (2018).
232. Howell, J. J. *et al.* Metformin Inhibits Hepatic mTORC1 Signaling via Dose-Dependent Mechanisms Involving AMPK and the TSC Complex. *Cell Metabolism* **25**, 463–471 (2017).
233. Utami, K. H. *et al.* Elevated de novo protein synthesis in FMRP-deficient human neurons and its correction by metformin treatment. *Molecular Autism* **11**, 41 (2020).
234. Chen, J. *et al.* Metformin extends C. elegans lifespan through lysosomal pathway. *eLife* **6**, (2017).
235. Reimers, C. D., Knapp, G. & Reimers, A. K. Does Physical Activity Increase Life Expectancy? A Review of the Literature. *J Aging Res* **2012**, (2012).
236. Weihrauch, M. & Handschin, C. Pharmacological targeting of exercise adaptations in skeletal muscle: Benefits and pitfalls. *Biochem Pharmacol* **147**, 211–220 (2018).
237. López-Lluch, G. *et al.* Calorie restriction induces mitochondrial biogenesis and bioenergetic efficiency. *Proc. Natl. Acad. Sci. U.S.A.* **103**, 1768–1773 (2006).
238. Peterson, C. M., Johannsen, D. L. & Ravussin, E. Skeletal Muscle Mitochondria and Aging: A Review. *Journal of Aging Research* **2012**, (2012).
239. Hood, D. A., Uguccioni, G., Vainshtein, A. & D'souza, D. Mechanisms of exercise-induced mitochondrial biogenesis in skeletal muscle: implications for health and disease. *Compr Physiol* **1**, 1119–1134 (2011).
240. Larson-Meyer, D. E. *et al.* Effect of Calorie Restriction With or Without Exercise on Insulin Sensitivity, β-Cell Function, Fat Cell Size, and Ectopic Lipid in Overweight Subjects. *Dia Care* **29**, 1337–1344 (2006).
241. Fontana, L., Meyer, T. E., Klein, S. & Holloszy, J. O. Long-term calorie restriction is highly effective in reducing the risk for atherosclerosis in humans. *Proc. Natl. Acad. Sci. U.S.A.* **101**, 6659–6663 (2004).

242. Picca, A. *et al.* Aging and calorie restriction oppositely affect mitochondrial biogenesis through TFAM binding at both origins of mitochondrial DNA replication in rat liver. *PLoS ONE* **8**, e74644 (2013).
243. Holloszy, J. O. Biochemical adaptations in muscle. Effects of exercise on mitochondrial oxygen uptake and respiratory enzyme activity in skeletal muscle. *J. Biol. Chem.* **242**, 2278–2282 (1967).
244. Masoro, E. J. Caloric restriction and aging: an update. *Exp. Gerontol.* **35**, 299–305 (2000).
245. Menshikova, E. V. *et al.* Effects of exercise on mitochondrial content and function in aging human skeletal muscle. *J. Gerontol. A Biol. Sci. Med. Sci.* **61**, 534–540 (2006).
246. Baar, K. *et al.* Adaptations of skeletal muscle to exercise: rapid increase in the transcriptional coactivator PGC-1. *FASEB J.* **16**, 1879–1886 (2002).
247. Booth F. W., Baldwin K. M. Muscle plasticity: energy demanding and supply processes. in *Handbook of Physiology, Sect. 12: Exercise Regulation and Integration of Multiple Systems* 1075–1123 (Oxford University Press).
248. Holloszy, J. O. & Coyle, E. F. Adaptations of skeletal muscle to endurance exercise and their metabolic consequences. *J Appl Physiol* **56**, 831–838 (1984).
249. Sevits, K. J. *et al.* Total daily energy expenditure is increased following a single bout of sprint interval training. *Physiol Rep* **1**, e00131 (2013).
250. Bartfai, T. & Conti, B. Molecules affecting hypothalamic control of core body temperature in response to calorie intake. *Front Genet* **3**, 184 (2012).
251. Anderson, R. M., Shanmuganayagam, D. & Weindruch, R. Caloric restriction and aging: studies in mice and monkeys. *Toxicol Pathol* **37**, 47–51 (2009).
252. Guarente, L. Calorie restriction and SIR2 genes--towards a mechanism. *Mech. Ageing Dev.* **126**, 923–928 (2005).
253. Houthoofd, K. & Vanfleteren, J. R. The longevity effect of dietary restriction in Caenorhabditis elegans. *Exp. Gerontol.* **41**, 1026–1031 (2006).
254. Partridge, L., Piper, M. D. W. & Mair, W. Dietary restriction in Drosophila. *Mech. Ageing Dev.* **126**, 938–950 (2005).
255. Ramsey, J. J., Harper, M. E. & Weindruch, R. Restriction of energy intake, energy expenditure, and aging. *Free Radic. Biol. Med.* **29**, 946–968 (2000).
256. Colman, R. J. *et al.* Caloric Restriction Delays Disease Onset and Mortality in Rhesus Monkeys. *Science* **325**, 201–204 (2009).
257. Das, S. K. *et al.* Long-term effects of 2 energy-restricted diets differing in glycemic load on dietary adherence, body composition, and metabolism in CALERIE: a 1-y randomized controlled trial. *The American Journal of Clinical Nutrition* **85**, 1023–1030 (2007).
258. Mattison, J. A., Roth, G. S., Lane, M. A. & Ingram, D. K. Dietary restriction in aging nonhuman primates. *Interdiscip Top Gerontol* **35**, 137–158 (2007).
259. López-Torres, M. & Barja, G. [Calorie restriction, oxidative stress and longevity]. *Rev Esp Geriatr Gerontol* **43**, 252–260 (2008).
260. Sohal, R. S. & Weindruch, R. Oxidative stress, caloric restriction, and aging. *Science* **273**, 59–63 (1996).
261. Little, J. P., Safdar, A., Wilkin, G. P., Tarnopolsky, M. A. & Gibala, M. J. A practical model of low-volume high-intensity interval training induces mitochondrial biogenesis in human skeletal muscle: potential mechanisms. *J. Physiol. (Lond.)* **588**, 1011–1022 (2010).

262. Little, J. P., Safdar, A., Bishop, D., Tarnopolsky, M. A. & Gibala, M. J. An acute bout of high-intensity interval training increases the nuclear abundance of PGC-1α and activates mitochondrial biogenesis in human skeletal muscle. *Am. J. Physiol. Regul. Integr. Comp. Physiol.* **300**, R1303-1310 (2011).
263. Little, J. P., Safdar, A., Benton, C. R. & Wright, D. C. Skeletal muscle and beyond: the role of exercise as a mediator of systemic mitochondrial biogenesis. *Appl Physiol Nutr Metab* **36**, 598–607 (2011).
264. Konopka, A. R., Suer, M. K., Wolff, C. A. & Harber, M. P. Markers of Human Skeletal Muscle Mitochondrial Biogenesis and Quality Control: Effects of Age and Aerobic Exercise Training. *J. Gerontol. A Biol. Sci. Med. Sci.* (2013) doi:10.1093/gerona/glt107.
265. Hood, D. A. Mechanisms of exercise-induced mitochondrial biogenesis in skeletal muscle. *Appl Physiol Nutr Metab* **34**, 465–472 (2009).
266. Holloszy, J. O. Regulation of mitochondrial biogenesis and GLUT4 expression by exercise. *Compr Physiol* **1**, 921–940 (2011).
267. Nisoli, E. *et al.* Calorie restriction promotes mitochondrial biogenesis by inducing the expression of eNOS. *Science* **310**, 314–317 (2005).
268. Barazzoni, R. *et al.* Moderate caloric restriction, but not physiological hyperleptinemia per se, enhances mitochondrial oxidative capacity in rat liver and skeletal muscle--tissue-specific impact on tissue triglyceride content and AKT activation. *Endocrinology* **146**, 2098–2106 (2005).
269. Cerqueira, F. M., Laurindo, F. R. M. & Kowaltowski, A. J. Mild mitochondrial uncoupling and calorie restriction increase fasting eNOS, akt and mitochondrial biogenesis. *PLoS ONE* **6**, e18433 (2011).
270. Civitarese, A. E. *et al.* Calorie Restriction Increases Muscle Mitochondrial Biogenesis in Healthy Humans. *PLoS Med* **4**, e76 (2007).
271. Hancock, C. R., Han, D.-H., Higashida, K., Kim, S. H. & Holloszy, J. O. Does calorie restriction induce mitochondrial biogenesis? A reevaluation. *The FASEB Journal* **25**, 785–791 (2011).
272. Sreekumar, R. *et al.* Effects of caloric restriction on mitochondrial function and gene transcripts in rat muscle. *Am. J. Physiol. Endocrinol. Metab.* **283**, E38-43 (2002).
273. Lanza, I. R. *et al.* Chronic caloric restriction preserves mitochondrial function in senescence without increasing mitochondrial biogenesis. *Cell Metab.* **16**, 777–788 (2012).
274. Johnson, J. S. *et al.* Evaluation of 16S rRNA gene sequencing for species and strain-level microbiome analysis. *Nature Communications* **10**, 5029 (2019).
275. Janda, J. M. & Abbott, S. L. 16S rRNA Gene Sequencing for Bacterial Identification in the Diagnostic Laboratory: Pluses, Perils, and Pitfalls. *Journal of Clinical Microbiology* **45**, 2761–2764 (2007).
276. Woo, P. C. Y., Lau, S. K. P., Teng, J. L. L., Tse, H. & Yuen, K.-Y. Then and now: use of 16S rDNA gene sequencing for bacterial identification and discovery of novel bacteria in clinical microbiology laboratories. *Clinical Microbiology and Infection* **14**, 908–934 (2008).
277. Peker, N. *et al.* A Comparison of Three Different Bioinformatics Analyses of the 16S–23S rRNA Encoding Region for Bacterial Identification. *Front. Microbiol.* **10**, (2019).

278. Zhang, S., Hu, Z. & Wang, H. Metagenomic analysis exhibited the co-metabolism of polycyclic aromatic hydrocarbons by bacterial community from estuarine sediment. *Environ Int* **129**, 308–319 (2019).
279. Li, F., Hitch, T. C. A., Chen, Y., Creevey, C. J. & Guan, L. L. Comparative metagenomic and metatranscriptomic analyses reveal the breed effect on the rumen microbiome and its associations with feed efficiency in beef cattle. *Microbiome* **7**, 6 (2019).
280. Shakya, M., Lo, C.-C. & Chain, P. S. G. Advances and Challenges in Metatranscriptomic Analysis. *Front. Genet.* **10**, (2019).
281. Turnbaugh, P. J. *et al.* A core gut microbiome in obese and lean twins. *Nature* **457**, 480–484 (2009).
282. Turnbaugh, P. J. *et al.* An obesity-associated gut microbiome with increased capacity for energy harvest. *Nature* **444**, 1027–1031 (2006).
283. Koren, O. *et al.* Host Remodeling of the Gut Microbiome and Metabolic Changes during Pregnancy. *Cell* **150**, 470–480 (2012).
284. Fabbiano, S. *et al.* Functional Gut Microbiota Remodeling Contributes to the Caloric Restriction-Induced Metabolic Improvements. *Cell Metabolism* **28**, 907-921.e7 (2018).
285. Zhang, C. *et al.* Structural modulation of gut microbiota in life-long calorie-restricted mice. *Nat Commun* **4**, 2163 (2013).
286. Fraumene, C. *et al.* Caloric restriction promotes rapid expansion and long-lasting increase of *Lactobacillus* in the rat fecal microbiota. *Gut Microbes* **9**, 104–114 (2018).
287. Cani, P. D. *et al.* Metabolic Endotoxemia Initiates Obesity and Insulin Resistance. *Diabetes* **56**, 1761–1772 (2007).
288. Zheng, X., Wang, S. & Jia, W. Calorie restriction and its impact on gut microbial composition and global metabolism. *Front. Med.* **12**, 634–644 (2018).
289. Touchefeu, Y. *et al.* Systematic review: the role of the gut microbiota in chemotherapy- or radiation-induced gastrointestinal mucositis - current evidence and potential clinical applications. *Aliment Pharmacol Ther* **40**, 409–421 (2014).
290. Liu, T. *et al.* A More Robust Gut Microbiota in Calorie-Restricted Mice Is Associated with Attenuated Intestinal Injury Caused by the Chemotherapy Drug Cyclophosphamide. *mBio* **10**, (2019).
291. Tang, Z.-Z. *et al.* Multi-Omic Analysis of the Microbiome and Metabolome in Healthy Subjects Reveals Microbiome-Dependent Relationships Between Diet and Metabolites. *Front. Genet.* **10**, (2019).
292. Collet, T.-H. *et al.* A Metabolomic Signature of Acute Caloric Restriction. *J Clin Endocrinol Metab* **102**, 4486–4495 (2017).
293. Rezzi, S. *et al.* Metabolic shifts due to long-term caloric restriction revealed in nonhuman primates. *Exp Gerontol* **44**, 356–362 (2009).
294. Wang, Y. *et al.* Metabonomic investigations of aging and caloric restriction in a life-long dog study. *J Proteome Res* **6**, 1846–1854 (2007).
295. Tanca, A. *et al.* Caloric restriction promotes functional changes involving short-chain fatty acid biosynthesis in the rat gut microbiota. *Sci Rep* **8**, (2018).
296. McCullough, L. D. *et al.* Pharmacological inhibition of AMP-activated protein kinase provides neuroprotection in stroke. *J Biol Chem* **280**, 20493–20502 (2005).
297. Viollet, B. *et al.* AMPK inhibition in health and disease. *Crit Rev Biochem Mol Biol* **45**, 276–295 (2010).
298. Dintzis, H. M. ASSEMBLY OF THE PEPTIDE CHAINS OF HEMOGLOBIN*. *Proc Natl Acad Sci U S A* **47**, 247–261 (1961).

299. Eastman, G., Smircich, P. & Sotelo-Silveira, J. R. Following Ribosome Footprints to Understand Translation at a Genome Wide Level. *Computational and Structural Biotechnology Journal* **16**, 167–176 (2018).
300. Castelo-Szekely, V., Arpat, A. B., Janich, P. & Gatfield, D. Translational contributions to tissue specificity in rhythmic and constitutive gene expression. *Genome Biology* **18**, 116 (2017).
301. Schafer, S. *et al.* Translational regulation shapes the molecular landscape of complex disease phenotypes. *Nature Communications* **6**, 7200 (2015).
302. Rosman, K. J. R. & Taylor, P. D. P. Isotopic compositions of the elements 1997 (Technical Report). *Pure and Applied Chemistry* **70**, 217–235 (1998).
303. Eisenacher, M. *et al.* Find Pairs: The Module for Protein Quantification of the PeakQuant Software Suite. *OMICS* **16**, 457–467 (2012).
304. Alves, G., Ogurtsov, A. Y. & Yu, Y.-K. Molecular Isotopic Distribution Analysis (MIDAs) with Adjustable Mass Accuracy. *J Am Soc Mass Spectrom* **25**, 57–70 (2014).
305. Holmes, W. E., Angel, T. E., Li, K. W. & Hellerstein, M. K. Dynamic Proteomics: In Vivo Proteome-Wide Measurement of Protein Kinetics Using Metabolic Labeling. *Methods Enzymol* **561**, 219–276 (2015).
306. Hellerstein, M. K. & Neese, R. A. Mass isotopomer distribution analysis: a technique for measuring biosynthesis and turnover of polymers. *Am J Physiol* **263**, E988-1001 (1992).
307. Ahmed, Z. *et al.* Software LS-MIDA for efficient mass isotopomer distribution analysis in metabolic modelling. *BMC Bioinformatics* **14**, 218 (2013).
308. Mitchell, S. J. *et al.* Effects of Sex, Strain, and Energy Intake on Hallmarks of Aging in Mice. *Cell Metab* **23**, 1093–1112 (2016).
309. Wang, S., Lai, X., Deng, Y. & Song, Y. Correlation between mouse age and human age in anti-tumor research: Significance and method establishment. *Life Sciences* **242**, 117242 (2020).
310. Zhang, L. *et al.* Timing of Calorie Restriction in Mice Impacts Host Metabolic Phenotype with Correlative Changes in Gut Microbiota. *mSystems* **4**, (2019).
311. Weindruch, R. & Sohal, R. S. Caloric Intake and Aging. *N Engl J Med* **337**, 986–994 (1997).
312. Weindruch, R., Walford, R. L., Fligiel, S. & Guthrie, D. The retardation of aging in mice by dietary restriction: longevity, cancer, immunity and lifetime energy intake. *The Journal of Nutrition* **116**, 641–654 (1986).
313. Nichenametla, S. N., Mattocks, D. A. L., Midya, V. & Shneyder, J. Differential effects of sulfur amino acid-restricted and low-calorie diets on gut microbiome profile and bile acid composition in male C57BL6/J mice. *J Gerontol A Biol Sci Med Sci* (2020) doi:10.1093/gerona/glaa270.
314. Levine, M. *et al.* A rat epigenetic clock recapitulates phenotypic aging and co-localizes with heterochromatin. *eLife* **9**, e59201 (2020).
315. Acosta-Rodríguez, V. A., de Groot, M. H. M., Rijo-Ferreira, F., Green, C. B. & Takahashi, J. S. Mice Under Caloric Restriction Self-Impose a Temporal Restriction of Food Intake as Revealed by an Automated Feeder System. *Cell Metab* **26**, 267-277.e2 (2017).
316. Robertson, L. T. & Mitchell, J. R. Benefits of short-term dietary restriction in mammals. *Experimental gerontology* **48**, 1043 (2013).
317. Mahoney, L. B., Denny, C. A. & Seyfried, T. N. Caloric restriction in C57BL/6J mice mimics therapeutic fasting in humans. *Lipids Health Dis* **5**, 13 (2006).

318. Mitchell, J. R. *et al.* Short-term dietary restriction and fasting precondition against ischemia reperfusion injury in mice. *Aging Cell* **9**, 40–53 (2010).
319. Kim, C. H. *et al.* Short-term calorie restriction ameliorates genomewide, age-related alterations in DNA methylation. *Aging Cell* **15**, 1074–1081 (2016).
320. Ke, Z., Firsanov, D., Spencer, B., Seluanov, A. & Gorbunova, V. Short-term calorie restriction enhances DNA repair by non-homologous end joining in mice. *npj Aging and Mechanisms of Disease* **6**, 1–3 (2020).
321. Dommerholt, M. B., Dionne, D. A., Hutchinson, D. F., Kruit, J. K. & Johnson, J. D. Metabolic effects of short-term caloric restriction in mice with reduced insulin gene dosage. *J Endocrinol* **237**, 59–71 (2018).
322. Boldrin, L. *et al.* The effect of calorie restriction on mouse skeletal muscle is sex, strain and time-dependent. *Scientific Reports* **7**, 5160 (2017).
323. Cameron, K. M., Miwa, S., Walker, C. & von Zglinicki, T. Male mice retain a metabolic memory of improved glucose tolerance induced during adult onset, short-term dietary restriction. *Longev Healthspan* **1**, 3 (2012).
324. Vaughan, K. L. *et al.* Caloric Restriction Study Design Limitations in Rodent and Nonhuman Primate Studies. *J Gerontol A Biol Sci Med Sci* **73**, 48–53 (2018).
325. Mitchell, S. E. *et al.* The effects of graded levels of calorie restriction: III. Impact of short term calorie and protein restriction on mean daily body temperature and torpor use in the C57BL/6 mouse. *Oncotarget* **6**, 18314–18337 (2015).
326. Price, J. C. *et al.* The effect of long term calorie restriction on in vivo hepatic proteostatis: a novel combination of dynamic and quantitative proteomics. *Mol Cell Proteomics* **11**, 1801–1814 (2012).
327. Subramanian, A. *et al.* Gene set enrichment analysis: a knowledge-based approach for interpreting genome-wide expression profiles. *Proc Natl Acad Sci U S A* **102**, 15545–15550 (2005).
328. Paone, A. *et al.* SHMT1 knockdown induces apoptosis in lung cancer cells by causing uracil misincorporation. *Cell Death & Disease* **5**, e1525–e1525 (2014).
329. Swindell, W. R. Genes and gene expression modules associated with caloric restriction and aging in the laboratory mouse. *BMC Genomics* **10**, 585 (2009).
330. Tong, M., Jun, T., Nie, Y., Hao, J. & Fan, D. The Role of the Slit/Robo Signaling Pathway. *J Cancer* **10**, 2694–2705 (2019).
331. Zhou, Y. *et al.* Metascape provides a biologist-oriented resource for the analysis of systems-level datasets. *Nat Commun* **10**, 1523 (2019).
332. Ingram, D. K. & de Cabo, R. Calorie Restriction in Rodents: Caveats to Consider. *Ageing Res Rev* **39**, 15–28 (2017).
333. Pal, R. & Bhattacharya, A. Modelling Protein Synthesis as A Biomarker in Fragile X Syndrome Patient-Derived Cells. *Brain Sci* **9**, (2019).
334. Xiao, L., Wang, Y. C., Li, W. S. & Du, Y. The role of mTOR and phospho-p70S6K in pathogenesis and progression of gastric carcinomas: an immunohistochemical study on tissue microarray. *J Exp Clin Cancer Res* **28**, 152 (2009).
335. DRUMMOND, M. J., GLYNN, E. L., LUJAN, H. L., DICARLO, S. E. & RASMUSSEN, B. B. GENE AND PROTEIN EXPRESSION ASSOCIATED WITH PROTEIN SYNTHESIS AND BREAKDOWN IN PARAPLEGIC SKELETAL MUSCLE. *Muscle Nerve* **37**, 505–513 (2008).
336. Liu, Y., Beyer, A. & Aebersold, R. On the Dependency of Cellular Protein Levels on mRNA Abundance. *Cell* **165**, 535–550 (2016).

337. Goecks, J., Nekrutenko, A., Taylor, J. & Galaxy Team. Galaxy: a comprehensive approach for supporting accessible, reproducible, and transparent computational research in the life sciences. *Genome Biol* **11**, R86 (2010).
338. Love, M. I., Huber, W. & Anders, S. Moderated estimation of fold change and dispersion for RNA-seq data with DESeq2. *Genome Biology* **15**, (2014).
339. Opalach, K., Rangaraju, S., Madorsky, I., Leeuwenburgh, C. & Notterpek, L. Lifelong Calorie Restriction Alleviates Age-Related Oxidative Damage in Peripheral Nerves. *Rejuvenation Res* **13**, 65–74 (2010).
340. Valdez, G. *et al.* Attenuation of age-related changes in mouse neuromuscular synapses by caloric restriction and exercise. *Proc Natl Acad Sci U S A* **107**, 14863–14868 (2010).
341. García-Matas, S. *et al.* In vitro caloric restriction induces protective genes and functional rejuvenation in senescent SAMP8 astrocytes. *Aging Cell* **14**, 334–344 (2015).
342. Carvalho, A., Rea, I. M., Parimon, T. & Cusack, B. J. Physical activity and cognitive function in individuals over 60 years of age: a systematic review. *Clin Interv Aging* **9**, 661–682 (2014).
343. Hord, J. M., Botchlett, R. & Lawler, J. M. Age-related alterations in the sarcolemmal environment are attenuated by lifelong caloric restriction and voluntary exercise. *Exp Gerontol* **83**, 148–157 (2016).
344. Belaya, I. *et al.* Long-Term Exercise Protects against Cellular Stresses in Aged Mice. *Oxidative Medicine and Cellular Longevity* **2018**, 1–10 (2018).
345. Holloszy, J. O. Mortality rate and longevity of food-restricted exercising male rats: a reevaluation. *J Appl Physiol (1985)* **82**, 399–403 (1997).
346. Menshikova, E. V. *et al.* Effects of Exercise on Mitochondrial Content and Function in Aging Human Skeletal Muscle. *J Gerontol A Biol Sci Med Sci* **61**, 534–540 (2006).
347. Popov, D. V. *et al.* Effect of aerobic training on baseline expression of signaling and respiratory proteins in human skeletal muscle. *Physiol Rep* **6**, (2018).
348. Pellegrin, M. *et al.* Impact of aerobic exercise type on blood flow, muscle energy metabolism, and mitochondrial biogenesis in experimental lower extremity artery disease. *Scientific Reports* **10**, 14048 (2020).
349. Flatt, J. P. Body composition, respiratory quotient, and weight maintenance. *Am. J. Clin. Nutr.* **62**, 1107S-1117S (1995).
350. Hancock, C. R., Han, D.-H., Higashida, K., Kim, S. H. & Holloszy, J. O. Does calorie restriction induce mitochondrial biogenesis? A reevaluation. *FASEB J.* **25**, 785–791 (2011).
351. López-Lluch, G. *et al.* Calorie restriction induces mitochondrial biogenesis and bioenergetic efficiency. *Proc Natl Acad Sci U S A* **103**, 1768–1773 (2006).
352. Wahid, A. *et al.* Quantifying the Association Between Physical Activity and Cardiovascular Disease and Diabetes: A Systematic Review and Meta-Analysis. *J Am Heart Assoc* **5**, (2016).
353. Patel, H. *et al.* Aerobic vs anaerobic exercise training effects on the cardiovascular system. *World J Cardiol* **9**, 134–138 (2017).
354. Feng, R. *et al.* A systematic comparison of exercise training protocols on animal models of cardiovascular capacity. *Life Sci* **217**, 128–140 (2019).
355. Villella, M. & Villella, A. Exercise and cardiovascular diseases. *Kidney Blood Press Res* **39**, 147–153 (2014).
356. Caruso, F. R. *et al.* Hemodynamic and metabolic response during dynamic and resistance exercise in different intensities: a cross-sectional study on implications of

intensity on safety and symptoms in patients with coronary disease. *Am J Cardiovasc Dis* **6**, 36–45 (2016).
357. Dougherty, J. P., Springer, D. A. & Gershengorn, M. C. The Treadmill Fatigue Test: A Simple, High-throughput Assay of Fatigue-like Behavior for the Mouse. *J Vis Exp* (2016) doi:10.3791/54052.
358. Shankaran, M. *et al.* Circulating protein synthesis rates reveal skeletal muscle proteome dynamics. *J Clin Invest* **126**, 288–302 (2016).
359. Miller, B. F., Robinson, M. M., Bruss, M. D., Hellerstein, M. & Hamilton, K. L. A comprehensive assessment of mitochondrial protein synthesis and cellular proliferation with age and caloric restriction. *Aging Cell* **11**, 150–161 (2012).
360. Yang, J.-S. *et al.* Spatial and functional organization of mitochondrial protein network. *Scientific Reports* **3**, 1403 (2013).
361. Huang, D. W., Sherman, B. T. & Lempicki, R. A. Bioinformatics enrichment tools: paths toward the comprehensive functional analysis of large gene lists. *Nucleic Acids Res* **37**, 1–13 (2009).
362. Huang, D. W., Sherman, B. T. & Lempicki, R. A. Systematic and integrative analysis of large gene lists using DAVID bioinformatics resources. *Nature Protocols* **4**, 44–57 (2009).
363. Price, J. C., Guan, S., Burlingame, A., Prusiner, S. B. & Ghaemmaghami, S. Analysis of proteome dynamics in the mouse brain. *PNAS* **107**, 14508–14513 (2010).
364. Stead, C. A. *et al.* Fractional Synthesis Rates of Individual Proteins in Rat Soleus and Plantaris Muscles. *Proteomes* **8**, (2020).
365. Doherty, M. K., Whitehead, C., McCormack, H., Gaskell, S. J. & Beynon, R. J. Proteome dynamics in complex organisms: using stable isotopes to monitor individual protein turnover rates. *Proteomics* **5**, 522–533 (2005).
366. Rocha, J. S., Bonkowski, M. S., de França, L. R. & Bartke, A. Effects of mild calorie restriction on reproduction, plasma parameters and hepatic gene expression in mice with altered GH/IGF-I axis. *Mech. Ageing Dev.* **128**, 317–331 (2007).
367. Heilbronn, L. K. *et al.* Effect of 6-month calorie restriction on biomarkers of longevity, metabolic adaptation, and oxidative stress in overweight individuals: a randomized controlled trial. *JAMA* **295**, 1539–1548 (2006).
368. Weiss, E. P. & Holloszy, J. O. Improvements in body composition, glucose tolerance, and insulin action induced by increasing energy expenditure or decreasing energy intake. *J. Nutr.* **137**, 1087–1090 (2007).
369. Wing, R. R. *et al.* Caloric Restriction Per Se Is a Significant Factor in Improvements in Glycemic Control and Insulin Sensitivity During Weight Loss in Obese NIDDM Patients. *Dia Care* **17**, 30–36 (1994).
370. Crescenzo, R. *et al.* Mitochondrial energetics in liver and skeletal muscle after energy restriction in young rats. *Br. J. Nutr.* **108**, 655–665 (2012).
371. Pignatti, C., D'Adamo, S., Stefanelli, C., Flamigni, F. & Cetrullo, S. Nutrients and Pathways that Regulate Health Span and Life Span. *Geriatrics (Basel)* **5**, (2020).
372. Neese, R. A. *et al.* Measurement in vivo of proliferation rates of slow turnover cells by 2H2O labeling of the deoxyribose moiety of DNA. *Proc. Natl. Acad. Sci. U.S.A.* **99**, 15345–15350 (2002).
373. Beysen, C. *et al.* Effect of bile acid sequestrants on glucose metabolism, hepatic de novo lipogenesis, and cholesterol and bile acid kinetics in type 2 diabetes: a randomised controlled study. *Diabetologia* **55**, 432–442 (2012).

374. Turner, S. M. *et al.* Measurement of TG synthesis and turnover in vivo by 2H2O incorporation into the glycerol moiety and application of MIDA. *Am J Physiol Endocrinol Metab* **285**, E790-803 (2003).
375. Huang, D. W., Sherman, B. T. & Lempicki, R. A. Systematic and integrative analysis of large gene lists using DAVID bioinformatics resources. *Nat Protoc* **4**, 44–57 (2009).
376. Huang, D. W., Sherman, B. T. & Lempicki, R. A. Bioinformatics enrichment tools: paths toward the comprehensive functional analysis of large gene lists. *Nucleic Acids Res.* **37**, 1–13 (2009).
377. Mattison, J. A. *et al.* Caloric restriction improves health and survival of rhesus monkeys. *Nature Communications* **8**, 14063 (2017).
378. Martinez-Lopez, N. *et al.* System-wide Benefits of Intermeal Fasting by Autophagy. *Cell Metabolism* **26**, 856-871.e5 (2017).
379. Dorling, J. L. *et al.* Effects of caloric restriction on human physiological, psychological, and behavioral outcomes: highlights from CALERIE phase 2. *Nutrition Reviews* nuaa085 (2020) doi:10.1093/nutrit/nuaa085.
380. Gabandé-Rodríguez, E., Gómez de Las Heras, M. M. & Mittelbrunn, M. Control of Inflammation by Calorie Restriction Mimetics: On the Crossroad of Autophagy and Mitochondria. *Cells* **9**, (2019).
381. Abdellatif, M., Sedej, S., Carmona-Gutierrez, D., Madeo, F. & Kroemer, G. Autophagy in Cardiovascular Aging. *Circulation Research* **123**, 803–824 (2018).
382. Pro-autophagy, anti-aging effects of metformin in patients with prediabetes - Virtual Meeting | EASD. https://www.easd.org/virtualmeeting/home.html#!resources/pro-autophagy-anti-aging-effects-of-metformin-in-patients-with-prediabetes-dbdab403-ffee-49df-8c75-3685dc36e55e.
383. Golbidi, S. *et al.* Health Benefits of Fasting and Caloric Restriction. *Current Diabetes Reports* **17**, 123 (2017).
384. Santos, J., Leitão-Correia, F., Sousa, M. J. & Leão, C. Dietary Restriction and Nutrient Balance in Aging. *Oxidative Medicine and Cellular Longevity* vol. 2016 e4010357 https://www.hindawi.com/journals/omcl/2016/4010357/ (2015).
385. Kumar, R., Saraswat, K. & Rizvi, S. I. 2 -Deoxy - d-glucose at chronic low dose acts as a caloric restriction mimetic through a mitohormetic induction of ROS in the brain of accelerated senescence model of rat. *Arch Gerontol Geriatr* **90**, 104133 (2020).
386. Pietrocola, F., Castoldi, F., Madeo, F. & Kroemer, G. Triethylenetetramine (trientine): a caloric restriction mimetic with a new mode of action. *Autophagy* **16**, 1534–1536 (2020).
387. Singh, S. *et al.* Spermidine, a caloric restriction mimetic, provides neuroprotection against normal and D-galactose-induced oxidative stress and apoptosis through activation of autophagy in male rats during aging. *Biogerontology* (2020) doi:10.1007/s10522-020-09900-z.
388. Yang, Y. & Zhang, L. The effects of caloric restriction and its mimetics in Alzheimer's disease through autophagy pathways. *Food Funct* **11**, 1211–1224 (2020).
389. Kepp, O., Chen, G., Carmona-Gutierrez, D., Madeo, F. & Kroemer, G. A discovery platform for the identification of caloric restriction mimetics with broad health-improving effects. *Autophagy* **16**, 188–189 (2020).
390. Wang, C. *et al.* Small-molecule TFEB pathway agonists that ameliorate metabolic syndrome in mice and extend C. elegans lifespan. *Nat Commun* **8**, 2270 (2017).

391. van Niekerk, G., du Toit, A., Loos, B. & Engelbrecht, A.-M. Nutrient excess and autophagic deficiency: explaining metabolic diseases in obesity. *Metabolism: Clinical and Experimental* **82**, 14–21 (2018).
392. Andrianova, N. V. *et al.* Resemblance and differences in dietary restriction nephroprotective mechanisms in young and old rats. *Aging (Albany NY)* **12**, (2020).
393. Nasri, H. & Rafieian-Kopaei, M. Metformin: Current knowledge. *J Res Med Sci* **19**, 658–664 (2014).
394. Soukas, A. A., Hao, H. & Wu, L. Metformin as Anti-Aging Therapy: Is It for Everyone? *Trends Endocrinol Metab* **30**, 745–755 (2019).
395. Wang, Y. *et al.* Metformin induces autophagy and G0/G1 phase cell cycle arrest in myeloma by targeting the AMPK/mTORC1 and mTORC2 pathways. *Journal of Experimental & Clinical Cancer Research* **37**, 63 (2018).
396. Bharath, L. P. *et al.* Metformin Enhances Autophagy and Normalizes Mitochondrial Function to Alleviate Aging-Associated Inflammation. *Cell Metabolism* **32**, 44-55.e6 (2020).
397. Zhang, C.-S. *et al.* Metformin Activates AMPK through the Lysosomal Pathway. *Cell Metabolism* **24**, 521–522 (2016).
398. Kaushik, S., Massey, A. C., Mizushima, N. & Cuervo, A. M. Constitutive Activation of Chaperone-mediated Autophagy in Cells with Impaired Macroautophagy. *MBoC* **19**, 2179–2192 (2008).
399. Massey, A. C., Zhang, C. & Cuervo, A. M. Chaperone-mediated autophagy in aging and disease. *Curr Top Dev Biol* **73**, 205–235 (2006).
400. Endicott, S. J., Ziemba, Z. J., Beckmann, L. J., Boynton, D. N. & Miller, R. A. Inhibition of class I PI3K enhances chaperone-mediated autophagy. *J Cell Biol* **219**, (2020).
401. Wang, C. *et al.* Phosphorylation of ULK1 affects autophagosome fusion and links chaperone-mediated autophagy to macroautophagy. *Nature Communications* **9**, 3492 (2018).
402. Papinski, D. & Kraft, C. Regulation of Autophagy By Signaling Through the Atg1/ULK1 Complex. *Journal of Molecular Biology* **428**, 1725–1741 (2016).
403. Ren, H. *et al.* Design, Synthesis, and Characterization of an Orally Active Dual-Specific ULK1/2 Autophagy Inhibitor that Synergizes with the PARP Inhibitor Olaparib for the Treatment of Triple-Negative Breast Cancer. *J Med Chem* (2020) doi:10.1021/acs.jmedchem.0c00873.
404. Tsapras, P. & Nezis, I. P. Caspase involvement in autophagy. *Cell Death & Differentiation* **24**, 1369–1379 (2017).
405. Yamamoto, S. *et al.* Autophagy Differentially Regulates Insulin Production and Insulin Sensitivity. *Cell Rep* **23**, 3286–3299 (2018).
406. Buono, M. D., Jones, P. J. H., Beaumier, L. & Wykes, L. J. Comparison of deuterium incorporation and mass isotopomer distribution analysis for measurement of human cholesterol biosynthesis. 8.
407. Kirchner, P. *et al.* Proteome-wide analysis of chaperone-mediated autophagy targeting motifs. *PLOS Biology* **17**, e3000301 (2019).
408. Nair, A. B. & Jacob, S. A simple practice guide for dose conversion between animals and human. *J Basic Clin Pharm* **7**, 27–31 (2016).
409. Zid, B. M. *et al.* 4E-BP extends lifespan upon dietary restriction by enhancing mitochondrial activity in Drosophila. *Cell* **139**, 149–160 (2009).

410. Bhandari, B. K. *et al.* Insulin regulation of protein translation repressor 4E-BP1, an eIF4E-binding protein, in renal epithelial cells. *Kidney Int* **59**, 866–875 (2001).
411. Donato, A. J. *et al.* Life-long caloric restriction reduces oxidative stress and preserves nitric oxide bioavailability and function in arteries of old mice. *Aging Cell* **12**, 772–783 (2013).
412. Petegnief, V., Font-Nieves, M., Martín, M. E., Salinas, M. & Planas, A. M. Nitric oxide mediates NMDA-induced persistent inhibition of protein synthesis through dephosphorylation of eukaryotic initiation factor 4E-binding protein 1 and eukaryotic initiation factor 4G proteolysis. *Biochem J* **411**, 667–677 (2008).
413. Murad, F. Cyclic guanosine monophosphate as a mediator of vasodilation. *J Clin Invest* **78**, 1–5 (1986).
414. Hess, D. T., Matsumoto, A., Kim, S.-O., Marshall, H. E. & Stamler, J. S. Protein S - nitrosylation: purview and parameters. *Nature Reviews Molecular Cell Biology* **6**, 150–166 (2005).
415. Bredt, D. S. Endogenous nitric oxide synthesis: biological functions and pathophysiology. *Free Radic Res* **31**, 577–596 (1999).
416. Sugita, M. *et al.* Inducible nitric oxide synthase deficiency ameliorates skeletal muscle insulin resistance but does not alter unexpected lower blood glucose levels after burn injury in C57BL/6 mice. *Metabolism* **61**, 127–136 (2012).
417. Guo, Y. *et al.* Inducible nitric oxide synthase contributes to insulin resistance and cardiac dysfunction after burn injury in mice. *Life Sci* **239**, 116912 (2019).
418. Esplugues, J. V. NO as a signalling molecule in the nervous system. *Br J Pharmacol* **135**, 1079–1095 (2002).
419. Blond, D., Raoul, H., Le Grand, R. & Dormont, D. Nitric Oxide Synthesis Enhances Human Immunodeficiency Virus Replication in Primary Human Macrophages. *J Virol* **74**, 8904–8912 (2000).
420. Torre, D., Pugliese, A. & Speranza, F. Role of nitric oxide in HIV-1 infection: friend or foe? *Lancet Infect Dis* **2**, 273–280 (2002).
421. Guijas, C. *et al.* Metabolic adaptation to calorie restriction. *Sci. Signal.* **13**, eabb2490 (2020).
422. Teske, B. F. *et al.* The eIF2 kinase PERK and the integrated stress response facilitate activation of ATF6 during endoplasmic reticulum stress. *Mol Biol Cell* **22**, 4390–4405 (2011).
423. Wang, L., Liu, Y. & Wu, S. The roles of nitric oxide synthase and eIF2alpha kinases in regulation of cell cycle upon UVB-irradiation. *Cell Cycle* **9**, 38–42 (2010).
424. Park, H.-S., Mo, J.-S. & Choi, E.-J. Nitric oxide inhibits an interaction between JNK1 and c-Jun through nitrosylation. *Biochem Biophys Res Commun* **351**, 281–286 (2006).
425. Zhang, Y. *et al.* S-nitrosylation of the Peroxiredoxin-2 promotes S-nitrosoglutathione-mediated lung cancer cells apoptosis via AMPK-SIRT1 pathway. *Cell Death Dis* **10**, 329 (2019).
426. Noronha, B. T., Li, J.-M., Wheatcroft, S. B., Shah, A. M. & Kearney, M. T. Inducible nitric oxide synthase has divergent effects on vascular and metabolic function in obesity. *Diabetes* **54**, 1082–1089 (2005).
427. Yu, Y., Park, S. J. & Beyak, M. J. Inducible nitric oxide synthase-derived nitric oxide reduces vagal satiety signalling in obese mice. *J Physiol* **597**, 1487–1502 (2019).
428. Sansbury, B. E. & Hill, B. G. Anti-obesogenic role of endothelial nitric oxide synthase. *Vitam Horm* **96**, 323–346 (2014).

429. Wu, G. & Meininger, C. J. Nitric oxide and vascular insulin resistance. *Biofactors* **35**, 21–27 (2009).
430. Sharifi, A. M. *et al.* Effect of caloric restriction on nitric oxide production, ACE activity, and blood pressure regulation in rats. *Acta Physiol Hung* **95**, 55–63 (2008).
431. Lino, A. D. de S. *et al.* Resistance training and caloric restriction prevent systolic blood pressure rise by improving the nitric oxide effect on smooth muscle and morphological changes in the aorta of ovariectomized rats. *PLoS One* **13**, e0201843 (2018).
432. Shinmura, K. *et al.* Indispensable role of endothelial nitric oxide synthase in caloric restriction-induced cardioprotection against ischemia-reperfusion injury. *American Journal of Physiology-Heart and Circulatory Physiology* **308**, H894–H903 (2015).
433. Gusarov, I. *et al.* Bacterial nitric oxide extends the lifespan of C. elegans. *Cell* **152**, 818–830 (2013).
434. Cummings, K. L. & Tarleton, R. L. Inducible nitric oxide synthase is not essential for control of Trypanosoma cruzi infection in mice. *Infect Immun* **72**, 4081–4089 (2004).
435. Auharek, S. A., Lara, N. L. M., Avelar, G. F., Sharpe, R. M. & França, L. R. Effects of inducible nitric oxide synthase (iNOS) deficiency in mice on Sertoli cell proliferation and perinatal testis development. *Int J Androl* **35**, 741–751 (2012).
436. dos Santos, C. C. *et al.* Sepsis-induced myocardial depression is associated with transcriptional changes in energy metabolism and contractile related genes: a physiological and gene expression-based approach. *Crit Care Med* **38**, 894–902 (2010).
437. Corbett, J. A. *et al.* Aminoguanidine, a novel inhibitor of nitric oxide formation, prevents diabetic vascular dysfunction. *Diabetes* **41**, 552–556 (1992).
438. Becerril, S. *et al.* Targeted disruption of the iNOS gene improves adipose tissue inflammation and fibrosis in leptin-deficient ob/ob mice: role of tenascin C. *International Journal of Obesity* **42**, 1458–1470 (2018).
439. Stolz, D. B. *et al.* Peroxisomal localization of inducible nitric oxide synthase in hepatocytes. *Hepatology* **36**, 81–93 (2002).
440. Loughran, P. A. *et al.* Monomeric inducible nitric oxide synthase localizes to peroxisomes in hepatocytes. *PNAS* **102**, 13837–13842 (2005).
441. Suzuki, Y. J., Carini, M. & Butterfield, D. A. Protein Carbonylation. *Antioxid Redox Signal* **12**, 323–325 (2010).
442. Corbett, null & McDaniel, null. The Use of Aminoguanidine, a Selective iNOS Inhibitor, to Evaluate the Role of Nitric Oxide in the Development of Autoimmune Diabetes. *Methods* **10**, 21–30 (1996).
443. Roth, L. *et al.* Nitric oxide donor molsidomine favors features of atherosclerotic plaque stability and reduces myocardial infarction in mice. *Vascul Pharmacol* **118–119**, 106561 (2019).
444. Schrör, K., Förster, S., Woditsch, I. & Schröder, H. Generation of NO from molsidomine (SIN-1) in vitro and its relationship to changes in coronary vessel tone. *J Cardiovasc Pharmacol* **14 Suppl 11**, S29-34 (1989).
445. Alesutan, I. *et al.* Augmentation of phosphate-induced osteo-/chondrogenic transformation of vascular smooth muscle cells by homoarginine. *Cardiovasc Res* **110**, 408–418 (2016).
446. Rudolph, W. & Dirschinger, J. Effectiveness of molsidomine in the long-term treatment of exertional angina pectoris and chronic congestive heart failure. *Am Heart J* **109**, 670–674 (1985).

447. Rochette, L. *et al.* Nitric oxide synthase inhibition and oxidative stress in cardiovascular diseases: possible therapeutic targets? *Pharmacol Ther* **140**, 239–257 (2013).
448. Nakaki, T. & Hishikawa, K. [The arginine paradox]. *Nihon Yakurigaku Zasshi* **119**, 7–14 (2002).
449. Mohamad, N. A. *et al.* Aminoguanidine impedes human pancreatic tumor growth and metastasis development in nude mice. *World J Gastroenterol* **15**, 1065–1071 (2009).